

THE OPTICAL PUMPING OF

LIQUID ACTIVE MEDIA

by

Colin Osborne Allingham

being a thesis submitted to the University of London in  
candidature for the degree of Philosophiae Doctor.

Department of Physics  
Royal Holloway College  
University of London

1976

R. H. C.	LIBRARY
CLASS	TBF
No	Alli
AUG. No	132,975
DATE ACQ	Oct '76

ProQuest Number: 10097407

All rights reserved

INFORMATION TO ALL USERS

The quality of this reproduction is dependent upon the quality of the copy submitted.

In the unlikely event that the author did not send a complete manuscript and there are missing pages, these will be noted. Also, if material had to be removed, a note will indicate the deletion.



ProQuest 10097407

Published by ProQuest LLC(2016). Copyright of the Dissertation is held by the Author.

All rights reserved.

This work is protected against unauthorized copying under Title 17, United States Code.  
Microform Edition © ProQuest LLC.

ProQuest LLC  
789 East Eisenhower Parkway  
P.O. Box 1346  
Ann Arbor, MI 48106-1346

## SUMMARY

The excitation of liquids to produce optical amplification depends on a number of factors associated with the molecular properties and the intra molecular structure of liquids. The most important factors determining the efficiency of the activation process are the lifetimes of the states which decay to produce laser transitions and the various mechanisms by which the excitation may be by-passed, for example, by the excitation of triplet states of dyes.

In a given column of excited liquid, the optical gain of the column will depend on the population inversion, the column length and the reflectivities of the mirrors defining the optical cavity. The latter mirror reflectivity may be enhanced by non linear optical processes in the liquid in the course of which hypersonic waves may be stimulated, or a stationary wave of thermal origin may be brought into existence which could introduce a periodicity of refractive index into the column.

The purpose of this investigation is to design and develop a very fast flashlamp pumped dye laser system which will have an active lasing time period  $<100$  ns so that triplet state population and any major thermal effects become less important. The design parameters for ultrafast ultra violet lights sources are also investigated.

The first part of the thesis considers the criteria required for the efficient optical excitation of a liquid and describes the design and construction of fast light sources. The properties of strip line pulsers are considered in detail, and the results from a series of prototype devices are evaluated. These include specially designed coaxial flash lamps as well as the usual linear type. Preliminary experiments and problems associated with achieving lasing output from rhodamine 6G are discussed.

	<u>PAGE No</u>
History of the lightning	8
How lightning is produced	10
Lightning bolts	14
The gods did not reveal, from the beginning,	16
All things to us, but in the course of time	31
Through seeking we may learn and know things better,	40
But as for certain truth, no man has known it,	
Nor shall he know it, neither of the gods	
Nor yet of all the things of which I speak,	
For even if by chance he were to utter	49
The final truth, he would himself not know it:	50
For all is but a woven web of guesses.	52

CHAPTER III

Xenophanes (~600 BC)

3.1	Introduction	62
3.2	The Blumlein system	63
3.3	False performance for Blumlein systems driving matched and mismatched resistance loads	66
3.4	Modified Blumlein pulser	71
3.5	Matching the Blumlein to the load	73
3.6	The multi-channel spark gap	75
3.7	DC and pulse charging of the Blumlein	85



## CHAPTER I

Page No.

### LIQUID LASERS

1.1	Historical Introduction	8
1.2	General problems in achieving laser action in liquids	10
1.3	Organic liquid laser	14
1.4	Properties of organic dyes	16
1.5	Oscillation condition for dye lasers	31
1.6	Rate equations for dye lasers	40

## CHAPTER II

### FLASHLAMP SYSTEMS

2.1	Introduction	49
2.2	An analysis of the discharge mechanism in a flash lamp	50
2.3	Design of flash lamp and circuitry for a dye laser	58

## CHAPTER III

### THE ELECTRICAL DRIVING SYSTEM

3.1	Introduction	62
3.2	The Blumlein system	62
3.3	Pulse performance for Blumlein systems driving matched and mismatched resistance loads	66
3.4	Modified Blumlein pulser	71
3.5	Matching the Blumlein to the load	73
3.6	The multi-channel spark gap	78
3.7	DC and pulse charging of the Blumlein	88

CHAPTER IV

Page No.

DESIGN OF APPARATUS USED IN EXPERIMENTS

4.1	General description of linear and coaxial flashlamps	94
4.2	Experimental arrangements used for altering the gases and pressures within the flashlamps	96
4.3	Coupling of flashlamps to the Blumlein pulser	96
4.4	Description of the gas cell and its coupling to the Blumlein pulser	99
4.5	Various dye cells used for different flashlamps and cavities	99

CHAPTER V

FLASHLAMP CHARACTERISTICS

5.1	Introduction	107
5.2	Analysis of results from prototype pulser	108
5.3	Analysis of light output from flashlamps used in the different Blumlein pulsers	112
	(a) Pulse shapes obtained with a linear flashtube	112
	(b) Pulse shapes obtained with a coaxial flashtube	117
5.4	Flashlamp output in the wavelength range 3000-4000 Å compared with unrestricted spectral output	123
5.5	Analysis of a short linear flashtube in the 24 feet system	133
5.6	Analysis of a short coaxial flashlamp in the 24 feet system	136
5.7	Comparison of the output intensities from differing flashlamps	140
5.8	Discharge mechanisms for fast coaxial flashlamps	157

<u>CHAPTER VI</u>		<u>Page No.</u>
<u>PREIONISATION</u>		
6.1	Gas breakdown at radio frequencies	160
6.2	Continuous radio frequency excitation of a flashlamp	161
6.3	Limitations of continuous radio frequency preionisation	165
6.4	Pulsed preionisation of a flashlamp	165
6.5	The effect of continuous preionisation on a linear flashlamp output characteristics	168
6.6	The effect of pulsed keep alive on flashlamp output characteristics	176
6.7	The effect of pulsed keep alive on laser output	181
 <u>CHAPTER VII</u>		
<u>SPECTRAL ANALYSIS</u>		
7.1	Introduction	183
7.2	Experimental results	186
 <u>CHAPTER VIII</u>		
<u>THE NITROGEN LASER</u>		
8.1	Introduction	202
8.2	The inversion criterion	203
8.3	Dependence of laser power density on various parameters	206
8.4	Calculating the optimum $\frac{E}{P}$ values	209
8.5	Experimental results	209
8.6	Resonator configurations for laser pumped dye lasers.	211

CHAPTER IX

Page No.

ORGANIC DYE EMISSION

9.1	Introduction	216
9.2	Experimental arrangement	222
8.3	Flashtube coupling to the active media	224
9.4	Lasing action from RH6G in methanol	225
9.5	Discussion	228
	CONCLUSIONS	232

Appendix I	The Beer-Lambert Absorption Law	234
Appendix II	Oxygen quenching of triplet states	235
Appendix III(a)	Properties of the stripline	237
	(b) Reflection coefficients and standing waves	244
Appendix IV	The Stefan-Boltzmann Law	247
Appendix V	Spectroscopic Notation	248
REFERENCES		250
ACKNOWLEDGEMENTS		257

## CHAPTER 1

### LIQUID LASERS

#### 1.1 Historical Introduction

The use of stimulated emission for microwave amplification was proposed during the early 1950's independently by Weber and Townes in the USA and by Basov and Prokhorov in the Soviet Union. During 1954 Townes<sup>(1)</sup> completed the construction of the first microwave amplifier, or maser. Ever since this time there have been speculations concerning the possibility of extending this principle to amplification and generation in the optical region (see Schalow et al 1958<sup>(2)</sup>, for example). A great deal of analytical work preceded the successful construction of the first light amplifier, or laser, by Maiman<sup>(3)(4)</sup> in 1960. There was also considerable speculation both in the United States and in the Soviet Union about the creation of a state of negative absorption in gases. In 1959 Javan et al.<sup>(5)</sup> explored the effectiveness of electron excitation and exchange of excitation as a means of producing negative absorption and this led to the development of the helium neon laser in 1960. Subsequently, Basov<sup>(6)</sup> and his co-workers carried out a mathematical analysis of the conditions under which the exchange of excitation in a mixture of different gases leads to negative absorption. This work<sup>(6)</sup> was published in 1960 and before the end of the year Sorokin<sup>(7)(8)(9)</sup> and Stephenson announced the operation of a four level solid laser. Many such lasers were discovered during the following two years. Essentially all rare earth metals were found to be suitable laser materials when incorporated in certain crystals.

Intensive speculation about the use of semiconductors as laser materials began about 1959. Basov published many calculations concerning the possibility of utilising a variety of processes in semiconductors for

the purpose of light amplification. Significant theoretical contributions were also made by Lax and several French investigators. Then in 1962, three groups Hall et al<sup>(10)</sup>, Nathen et al<sup>(11)</sup> and Quist et al<sup>(12)</sup> working independently succeeded almost simultaneously in obtaining stimulated emission from p-n junctions of Ga As.

As soon as the five lines of the helium neon laser in the 1.1-1.2  $\mu\text{m}$  region became known, a search started for other gaseous lines. However it was a further two years before other lines were found. During 1962 the discovery of gaseous lasers began like an avalanche. By mid 1964 over 500 lines of the Noble gases alone had been observed in stimulated emission, and several new methods utilising ions, atoms and molecules of other elements had been discovered for exciting laser oscillations.

Although the initial successes in the laser field were achieved with solids and gases, liquid laser systems combine some important advantages of solid-state and gas laser systems in addition to some unique properties of their own. The first liquid laser system used metallo-organic systems, namely rare earth chelates. In 1963, two groups Wolf et al<sup>(13)</sup> and Lempicki et al<sup>(14)</sup> simultaneously reported successful operation of europium chelate lasers. An important inorganic laser system namely neodymium in selenium oxychloride ( $\text{Nd}^{3+}$  in  $\text{SeO Cl}_2$ ) was reported in 1966 by Lempicki and Heller<sup>(15)</sup>, and  $\text{Nd}^{3+}$  in  $\text{PO Cl}_3$  in 1968 by Schimitschek<sup>(16)</sup>. Another very important class of liquid lasers is the organic dye lasers. The earliest published suggestions that organic materials could be used as active media seem to be those of Brock et al<sup>(17)</sup> and Rautian and Sobelmann<sup>(18)</sup> who proposed in 1961 that triplet state phosphorescence could serve as the basis for an organic laser. In 1964, Stockman et al<sup>(19)</sup> discussed a laser process based upon singlet state fluorescence and



Stockman<sup>(20)</sup> described early results in the experimental effort to realise a dye laser using the dye perylene excited by a fast powerful flashlamp. The first unambiguously successful effort to produce stimulated emission from organic molecules, however, was reported in 1966 by Sorokin<sup>(21)</sup><sup>(22)</sup> and co-workers. These authors used a giant pulse ruby laser to excite solutions of the dyes chloro aluminium phthalocyanine (CAP) and 3,3'-diethyl thiadicarbocyanine (DTTC) iodide in an optical cavity, an arrangement referred to as the "laser pumped laser". Similar results were obtained independently by Schafer et al<sup>(23)</sup> and also by Spaeth et al<sup>(24)</sup> using several cyanine dyes with structures similar to DTTC. Based upon the laser pumped laser results, Sorokin et al<sup>(25)</sup> suggested that flashlamp excitation of a dye laser should also be possible and estimated the flash lamp requirements. A suitable flashlamp was constructed and laser emission from solutions of several dyes of the xanthene class was reported by Sorokin and Lankard<sup>(26)</sup> in 1967. Shortly thereafter, similar results were reported independently by Schmidt and Schafer<sup>(27)</sup>. Flashlamp excited dye lasers have since been studied in many laboratories.

## 1.2 General problems in achieving laser action in liquids

Liquid laser research was split into two broad categories, the organic liquid laser based on solutions of purely organic compounds and inorganic liquid laser based on solutions of rare earth ions in aprotic solvents.

It became evident that the poor performance of inorganic liquid lasers was not due to the change of the index of refraction due to pumping because it is known that there exists liquids whose optical performance on heating is as good as with solids. Investigations on the behaviour of trivalent neodymium in aqueous solutions had shown quenching rates of the

luminescent level to be  $10^8 \text{ s}^{-1}$ . It is obvious that such a high rate of quenching of the luminescent level would not allow sufficient population to build up for stimulated emission to occur in solutions containing water. Further studies on the radiationless relaxation rates have shed more light into the problem of the quenching of the fluorescence in liquids. It was already known from the work of Hutchinson and Magnum<sup>(30)</sup> that replacement of the hydrogen atoms by deuterium in the molecules of naphthalene leads to a decrease in the rate of radiationless relaxation. Subsequent experiments have indicated that the presence of hydrogen atoms was intimately connected with the quenching of fluorescence in the solutions<sup>(31)</sup>: Finally Heller<sup>(32)</sup> was able to show that the main factor responsible for the quenching of the fluorescence of rare earth ions in solutions was the hydroxyl group. The experimental work involved had shown that the rate of radiationless relaxation depends strongly on the energy of the acceptor vibrations. This result was to be expected since it is well known that the closer the matching of the energy a donor can donate to the energy an acceptor can accept, the faster the rate of energy transfer becomes. High vibrational energies, therefore, increase the overlap between the vibrational levels and the electronic levels of the excited atoms. Considering that the vibrational energy of the hydroxyl group is  $3600 \text{ cm}^{-1}$  (energies denoted in this way are in units of  $hc$ ) and that the separation between the lowest electronically excited level and the highest vibrational level of the ground state of neodymium is  $5300 \text{ cm}^{-1}$ , (Figure 1.1) we see the reason for the fast quenching rate of the neodymium luminescence in aqueous solutions.

Thus solvents with light atoms and consequently high vibrational energies will quench fluorescence and therefore are not suitable for liquid lasers. Solutions with heavy atoms should therefore be used to dissolve



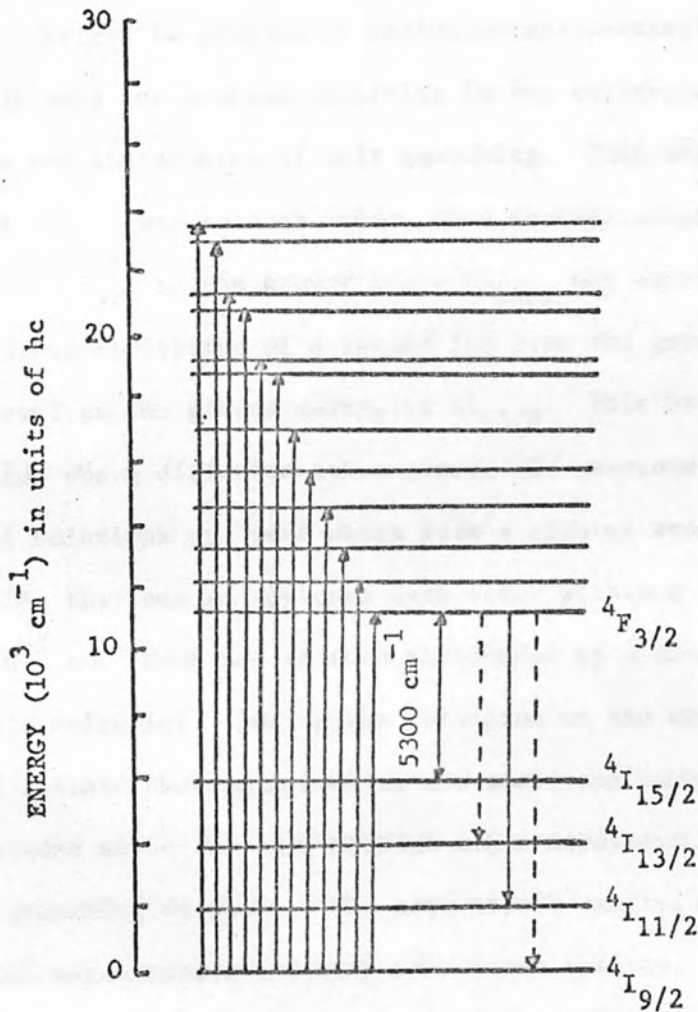


FIGURE 1.1: ENERGY LEVEL SCHEME FOR IONIC NEODYMIUM

the active ions. The other requirement is that a solvent must have a high dielectric constant in order to dissolve ionic compounds. Selenium oxychloride was the first such solvent to be used. Its highest vibrational energy is  $955 \text{ cm}^{-1}$  which is small compared with  $5300 \text{ cm}^{-1}$  of the de-excitation energy of trivalent neodymium. Its dielectric constant is 46.

After the problem of radiationless relaxation had been solved, there was only one problem remaining in the achievement of good liquid lasers and this was the problem of self quenching. This occurs when neodymium ions are very close to each other, then de-excitation of an ion in the metastable  $4F_{3/2}$  to the ground state  $4I_{15/2}$  may occur, with the simultaneous excitation of a second ion from the ground state  $4I_{9/2}$  to the upper level of the ground multiplet  $4I_{15/2}$ . This becomes even more serious in liquids where diffusion takes place. To overcome self quenching, chemical solutions are used which form a cluster around each ion thus preventing the ions to approach each other within a distance less than  $1.5 \times 10^{-7} \text{ cm}$ . Each ion is then surrounded by a shell made up by the solvent's molecules. During the formation of the chemical systems it must be made certain that anions which are small and have high charge densities are excluded since they may attract other neodymium ions and bring them within quenching distance. The same effect can result from the presence of anions which coordinate with rare earth cations. The presence of these ions may well result in precipitation or polymerization<sup>(33)</sup>.

Inorganic liquid lasers can now be prepared which have all the adequate properties for laser action. An excellent account of inorganic laser performance may be found in Andreou's thesis<sup>(34)</sup>. He used a double flashlamp arrangement for optically pumping  $\text{Nd}^{+3}$  in solutions of  $\text{SeO Cl}_2$  (selenium oxychloride) and  $\text{POCl}_3$  (phosphor oxychloride).

The achievement of laser action with organic compounds came when it was realised that the main problem initially was the accumulation of excited molecules from the first excited level of the singlet state to the triplet state by fast radiationless transitions. Thus the triplet state acts as a heat sink for the excited molecules. Triplet transitions may occur in which the fluorescence emission is reabsorbed, thus prohibiting laser action. To overcome this difficulty, organic dyes were first pumped with Q-switched ruby lasers which provided a high intensity in a sufficiently short time, thus overcoming the effects of the fast radiationless relaxation to the triplet state. Flashlamps with sufficiently short rise times have been developed to overcome the effects of the triplet state<sup>(26)</sup>. More recently quenching of the triplet state has been achieved with the aid of other substances in the laser solution.

This and other effects will be discussed more fully in the following thesis.

The main advantage of an organic laser as compared to an inorganic laser is its wide range of tunability<sup>(29)</sup>.

### 1.3 Organic liquid lasers

The efficient luminescence exhibited by many organic compounds makes their use as laser materials attractive and this possibility was considered early in laser research. Initial experiments produced disappointing results, however, and interest waned. Then since 1966, the production of coherent, visible radiation by fluorescent organic dyes in solution has been demonstrated. The device based upon this phenomenon is called the dye laser.

Dye laser systems combine many of the advantages of solid state and gas laser systems<sup>(35)</sup>. In addition they have some unique properties which open up new fields of laser applications. The gain of a dye solution is much greater than that obtainable from a gas and is comparable

to the gain of solid state materials. This is due to the same high concentration of active molecules in dyes as in solid state materials. The use of a liquid active medium simplifies the problem of obtaining high optical quality which is not susceptible to the irreversible radiation damage of high power solid state lasers. The temperature dependence of the refractive index is usually much greater in liquids than in solids, necessitating a careful control of temperature gradients in the laser liquid to avoid scattering losses which arise from the change of refractive index,<sup>(29) (36)</sup> but once this is achieved, a beam spread similar to that of gas lasers can be obtained.

The unlimited range of organic laser substances can be fully exploited only in laser systems using liquid solutions of these substances. Gas lasers using organic molecules do not seem to exist so far.\* The most probable reason is that relatively few organic substances with electronic transitions between near UV and near IR are able to withstand the temperature needed to bring a sufficient number of molecules into the gas phase. In addition, most of these show a rapid decrease of the quantum efficiency of luminescence with rising temperature. Organic crystals, on the other hand, are unsuitable as laser media because they are soft, of limited optical quality, and generally difficult to fabricate<sup>(35)</sup>.

The chief disadvantage of the more conventional laser systems is that laser action can be achieved at only a very limited number of wavelengths. However, tunability is essential in an increasing number of applications, for instance in excited state spectroscopy, in the study of

---

\* After the preparation of this manuscript, lasing action from a dye vapour pumped by a pulse nitrogen laser was reported<sup>(147) (151)</sup>.

optical frequency stark shifts, and in self induced transparency to name only a few. Non linear optical methods such as frequency mixing or stimulated Raman scattering can be used to multiply the number of discrete wavelengths at which intense coherent light can be generated. For continuous tuning, parametric oscillators, are at first sight, very appealing but the practical difficulties of making these into powerful, reliable and convenient devices are considerable.

The organic dye solution laser is at the present time the most versatile continuously tunable source of coherent light. Individual dyes have broad fluorescence bands several tens of nanometers wide<sup>(37)</sup>, and, as shown in Figure 1.2, different dyes can be found with bands almost anywhere in the range 340-1170 nm. Fine tuning<sup>(38)</sup> can be achieved by inserting a frequency selective element into the optical cavity, and coarse tuning simply by changing the dye.

#### 1.4 Properties of organic dyes

Conjugated double bonds are a common property of all organic molecules that can be used as active media in liquid lasers. The generic term "dye" may be used for substances containing double bonds. Nevertheless these substances do not necessarily absorb in the visible part of the spectrum although the basic mechanism responsible for light absorption is the same for all these substances including the dyes in the usual sense of the word. Substances without conjugated double bonds usually absorb at wavelengths shorter than 200 nm, corresponding to a photon energy of 150 kcal/mole. Since this energy is higher than the dissociation energy of most chemical bonds, photo-chemical decomposition competes effectively with radiative deactivation. This is one of the reasons these substances are not very likely to exhibit laser action in solution.



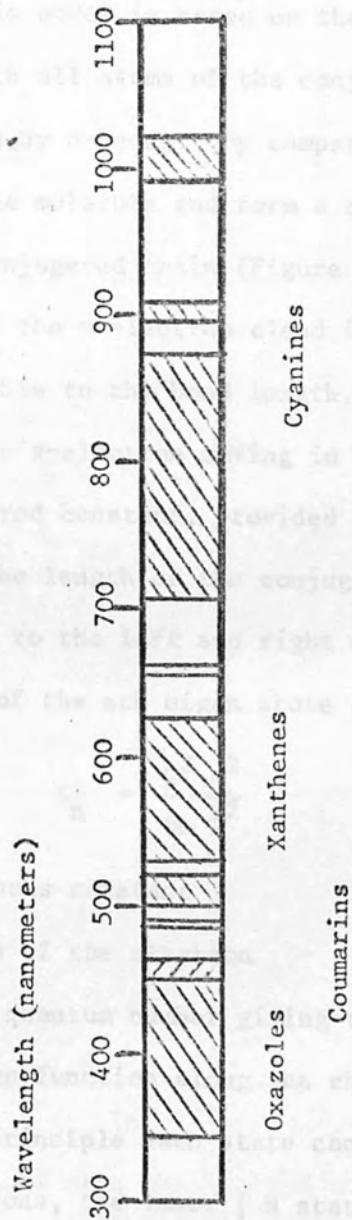


FIGURE 1.2: THE MAIN OPERATING SPECTRAL REGIONS OF DIFFERENT DYE LASERS

The light absorption of dyes can easily be understood on a semi-quantitative basis using a highly simplified quantum mechanical model, such as the free electron gas model. (From Kuhn<sup>(39)</sup> 1958 as described by Schafer<sup>(35)</sup> 1972). This model is based on the fact that dye molecules are essentially planar, with all atoms of the conjugated chain lying in a common plane and linked by  $\sigma$ -bonds. By comparison the  $\pi$ -electrons have a node in the plane of the molecule and form a charge cloud above and below this plane along the conjugated chain (Figure 1.3). The center of the upper and lower lobe of the  $\pi$ -electron cloud is at a distance from the molecular plane comparable to the bond length. Hence the electrostatic potential for any single  $\pi$ -electron moving in the field of the rest of the molecule can be considered constant, provided all bond lengths and atoms are the same. Assume the length of the conjugated (unbranched) chain which extends one bond length to the left and right end beyond the terminal atoms is  $L$ . Then the energy of the  $n$ th eigen state of this electron is given by

$$E_n = \frac{h^2 n^2}{8m L^2}$$

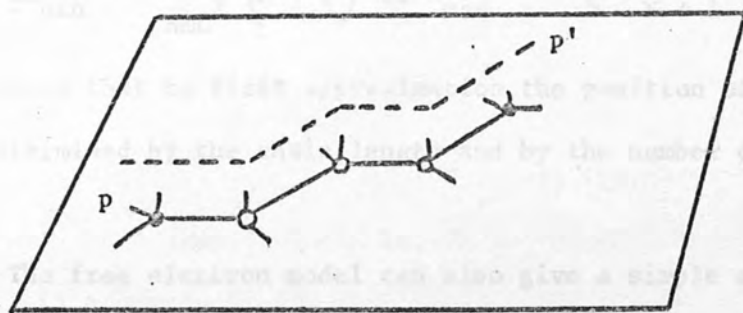
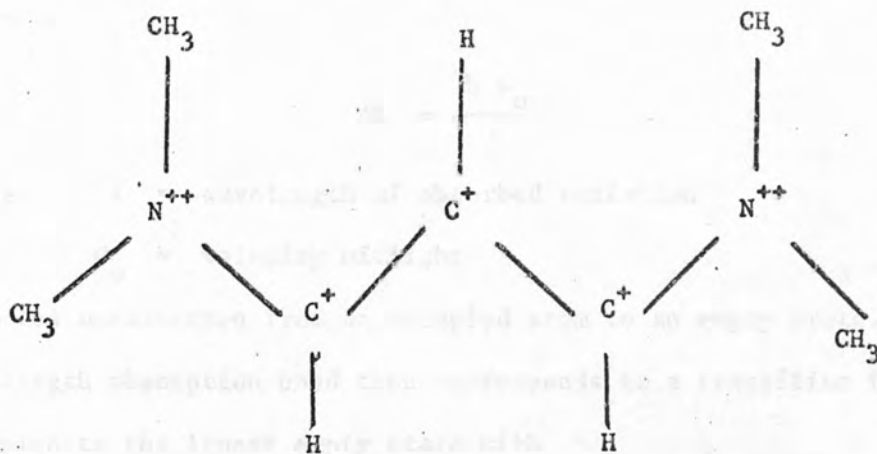
where

$h$  = Plancks constant

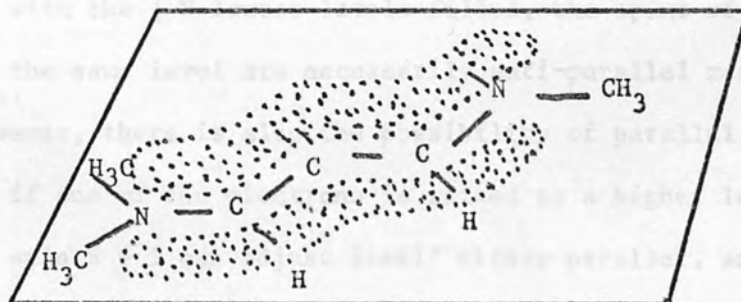
$m$  = mass of the electron

$n$  = the quantum number giving the number of modes of the eigen function along the chain.

According to the Pauli principle each state can be occupied by two electrons. This if we have  $N$  electrons, the lower  $\frac{1}{2} N$  states are filled with two electrons each while all higher states are empty (provided  $N$  is an even number; this is usually the case for stable molecules since only radicals possess an unpaired electron). The absorption of one photon of energy



(a)



(b)

- (a) Molecular skeleton of a cyanine dye and zig-zag path p-p' of a  $\pi$ -electron moving along the conjugated chain.
- (b) Charge cloud of the  $\pi$ -electron gas extending above and below the molecular plane.

FIGURE 1.3



$$\Delta E = \frac{h C_0}{\lambda}$$

where  $\lambda$  = wavelength of absorbed radiation

$C_0$  = velocity of light

promotes one electron from an occupied atom to an empty state. The longest wavelength absorption band then corresponds to a transition from the highest occupied to the lowest empty state with

$$\Delta E_{\min} = \frac{h^2}{8mL^2} (N + 1) \quad \text{or} \quad \lambda_{\max} = \frac{8mC_0}{h} \frac{L^2}{N + 1}$$

This indicates that to first approximation the position of the absorption band is determined by the chain length and by the number of  $\pi$ -electrons,  $N$ , only.

The free electron model can also give a simple explanation for another important property of the energy levels of organic dyes, namely the position of the triplet levels in relation to the singlet levels. In the ground state of the dye molecule, which in the free electron model is the state with the  $\frac{1}{2} N$  lowest levels filled, the spins of two electrons occupying the same level are necessarily anti-parallel resulting in zero spin. However, there is also the possibility of parallel arrangement of the spins if one of the electrons is raised to a higher level. The resulting spin  $S = 1$  can adjust itself either parallel, anti-parallel or orthogonal with respect to an external magnetic field. The parallel arrangement of the spins of the two most energetic electrons gives a triplet state of the same energy as the singlet state with zero spin within the framework of one electron functions. The Dirac formulation of the Pauli exclusion principle states that the total wavefunction including the spin function must be anti-symmetric with respect to the

exchange of any two electrons. In the two electron case considered this means that the following four antisymmetrical product wave functions can be used. Here spin  $+\frac{1}{2}$  is described by the spin function  $\alpha$ , spin  $-\frac{1}{2}$  by the spin function  $\beta$  and electron correlations are neglected for the moment.

$$\begin{aligned}\psi_s &= \{\psi_m(1) \psi_n(2) + \psi_n(1) \psi_m(2)\} \{\alpha(1) \beta(2) - \alpha(2) \beta(1)\} \\ \psi_{t,+1} &= \{\psi_m(1) \psi_n(2) - \psi_n(1) \psi_m(2)\} \{\alpha(1) \alpha(2)\} \\ \psi_{t,0} &= \{\psi_m(1) \psi_n(2) - \psi_n(1) \psi_m(2)\} \{\alpha(1) \beta(2) + \alpha(2) \beta(1)\} \\ \psi_{t,-1} &= \{\psi_m(1) \psi_n(2) - \psi_n(1) \psi_m(2)\} \{\beta(1) \beta(2)\}\end{aligned}$$

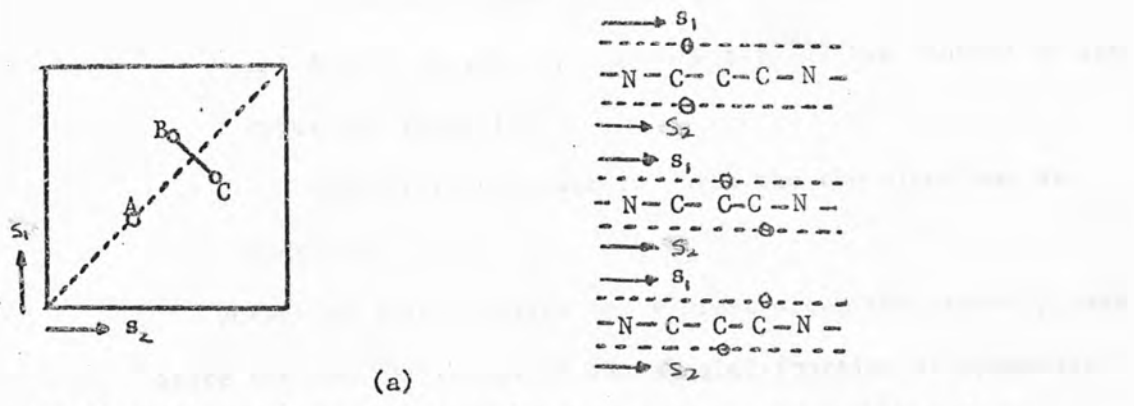
Here  $\psi_s$  is the singlet,  $\psi_{t,+1}$ ,  $\psi_{t,-1}$ ,  $\psi_{t,0}$  are the three triplet wave functions and the argument 1 or 2 refers to electron No. 1 or No. 2.

Because of the symmetry of the spin factor, the spatial factor of these functions is symmetric for the singlet wavefunction and anti symmetric for the triplet wavefunctions. The spatial factors of one-dimensional two-electron functions can be interpreted in terms of two-dimensional one-electron functions:

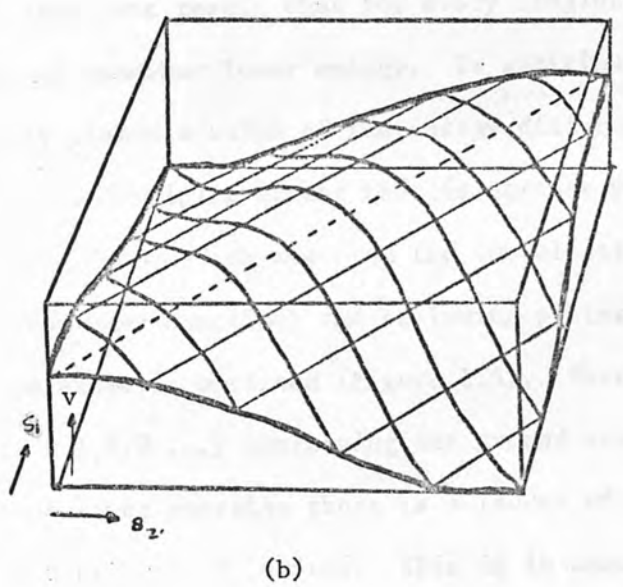
$$\begin{aligned}\psi_{m,n}(S_1, S_2) + \psi_{n,m}(S_1, S_2) &\text{ for the singlet case and} \\ \psi_{m,n}(S_1, S_2) - \psi_{n,m}(S_1, S_2) &\text{ for the triplet case}\end{aligned}$$

Here  $S_1, S_2$  are coordinates which extend along the conjugated chain in the upper and lower lobe of the  $\pi$ -electron cloud, respectively (Figure 1.4). For every configuration of the two electrons we can give the repulsion energy of the two electrons

$$V = \frac{\epsilon_0^2}{Dr} = \frac{\epsilon_0^2}{D \left[ (S_1 - S_2)^2 + d^2 \right]^{\frac{1}{2}}}$$



(a) Three configurations of a two electron system. The three points A, B, C in the cartesian coordinate system on the left belong to the three two-electron configurations pictured on the right.



(b) Potential energy  $v(s_1, s_2)$  of the two electron system.

FIGURE 1.4

where  $r$  = the distance between the two electrons

$d = 1.2 \text{ \AA}$  units being the distance between the centres of the upper and lower lobe

$D$  = the dielectric constant in which the two electrons are embedded.

The potential energy relief has a crest along the symmetry axis  $S_1 = S_2$ . Since the spatial factor of the singlet function is symmetric with respect to this axis, it must have anti nodes there. By contrast, the antisymmetrical spatial factor of the triplet wave functions has a nodal line along  $S_1 = S_2$ . Consequently the mean potential energy of the electrons in the singlet state with quantum numbers  $n, m$  is higher than that in the triplet state with the same quantum number. This crude model gives the most important result that for every singlet state there exists a triplet state of somewhat lower energy. In addition the numerical calculation usually yields a value of the energy difference between corresponding singlet and triplet states that is correct within a factor of two or three.

Proceeding now from the two electron wave function to the  $N$ -electron wave function; the following picture of the eigen state of the dye molecule is obtained (Figure 1.5). There is a ladder of singlet states  $S_i$  ( $i = 1, 2, 3 \dots$ ) containing the ground state,  $S_0$ . Somewhat displaced towards lower energies there is a ladder of triplet states  $T_i$  ( $i = 1, 2, 3 \dots$ ) No triplet level  $T_0$  exists. This is in accordance with the Pauli exclusion principle. The longest wavelength absorption is from  $S_0$  to  $S_1$ , the next absorption band from  $S_0$  to  $S_2$  etc. By contrast, the absorption from  $S_0$  to  $T_i$  is strongly forbidden and is not observed to occur to a significant extent. This does not mean that triplet states are unpopulated, however, since an alternative non radiative path to populate triplets via  $S_2$  or  $S_1$  exists and this will be discussed more fully later.

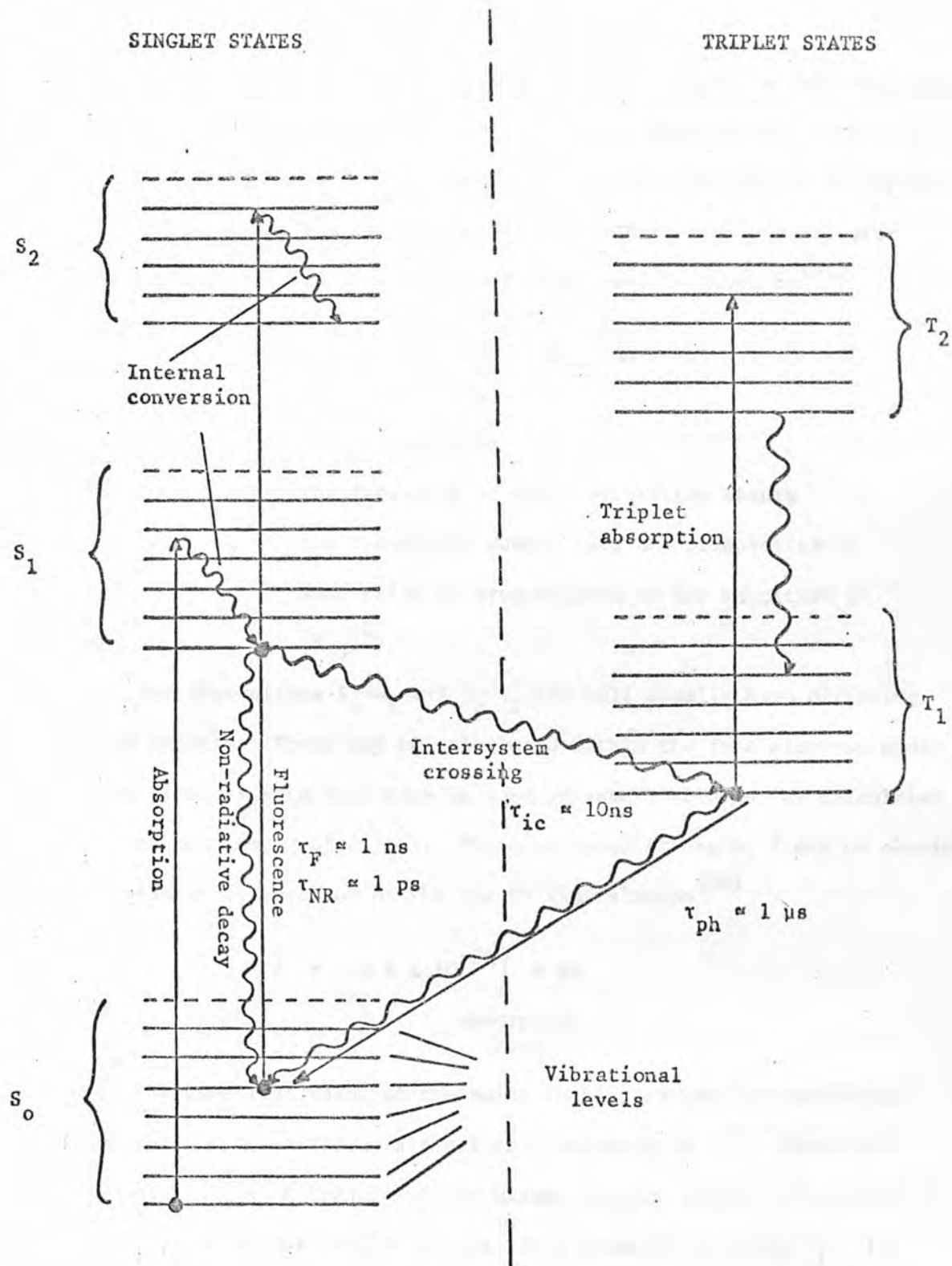


FIGURE 1.5: A SCHEMATIC ENERGY LEVEL DIAGRAM OF A TYPICAL DYE MOLECULE

A quantity often used in relation to intensities is the oscillator strength,  $f$ . Classically, the oscillator strength measures the effective number of electrons whose oscillations give rise to a particular absorption or emission band. The quantum mechanical counterpart of the oscillator strength for the transition from state 1 to state 2 is given by<sup>(41)</sup>

$$f_{12} = \frac{8\pi C_o \nu m_o}{3h e_o^2} |R_{12}|^2$$

where  $m_o$  = mass of electron

$\nu$  = the frequency at which absorption occurs

$R_{12}$  = the transition moment (and the probability of absorption is proportional to the magnitude of  $|R_{12}|^2$ ).

The absorptions  $S_o \rightarrow S_1$  and  $S_o \rightarrow S_2$  etc will usually have differing transition moments. These may be calculated within the free electron model even in its simplest form and there is good agreement between the calculated and observed oscillator strengths. The oscillator strength,  $f$  may be obtained from the absorption spectrum of the dye by the relation<sup>(35)</sup>

$$f = 14.4 \times 10^{-20} \int_{\text{absorption band}} \epsilon \, d\nu$$

Here  $\epsilon$  is the numerical value of the molar decadic extinction coefficient (measured in  $l/cm \text{ mole}$ ) and  $\nu$  is the light frequency in  $s^{-1}$ . There is also the possibility of transitions to higher singlet states for a molecule in state  $S_1$  or to higher triplet states for a molecule in state  $T_1$ . In fact, these  $S_1 \rightarrow S_i$  and  $T_1 \rightarrow T_i$  transitions play an important role in dye lasers.



The above picture of the absorptive electronic transitions in a dye molecule has to be modified slightly to include the effect of superimposed vibrations, rotations and external forces due to the solvent molecules. In fact, every vibronic sub-level of every electronic state, including the ground state, has superimposed on it a ladder of rotationally excited sub-levels. These are extremely broadened due to the frequent collisions with solvent molecules which hinder the rotational movement. This finally leads to a quasi-continuum of states superimposed on every electronic level.

Absorption and fluorescence spectra for a dye such as rhodamine 6G are shown in Figure 1.6. The ratio of the areas under the fluorescence and absorption curves is the fraction of the number of excited molecules in  $S_1$  which return to  $S_0$  by fluorescence and is known as the fluorescence quantum efficiency. The red shift of the fluorescence peak arises to some extent from self absorption<sup>(37)</sup>. In many dyes, however, the primary cause is the Franck-Condon Effect which causes absorption from the lowest vibrational level of  $S_0$  to take place preferentially to a higher vibrational level of  $S_1$  and similarly fluorescence from a low vibrational level of  $S_1$  to take place preferentially to a higher vibrational level of  $S_0$ . A semi classical argument is helpful for understanding the Franck-Condon Principle. Consider a diatomic molecule with inter-nuclear distance  $R$ . Now suppose that a transition occurs between two electronic states having different equilibrium values of  $R$ . Since the change in the electron configuration takes place in a time  $\sim 10^{-15}$  s which is at least a hundred times shorter than the typical time required for the nuclei to reach their new equilibrium separation, vibration about the new value of  $R$  would be expected. Quantum mechanically, this corresponds to the molecule being left in a

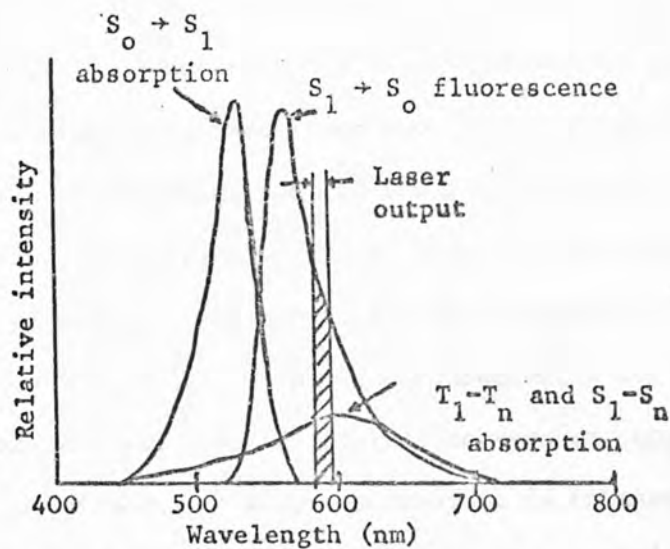


FIGURE 1.6: ABSORPTION AND FLUORESCENCE SPECTRA OF RHODAMINE 6G.

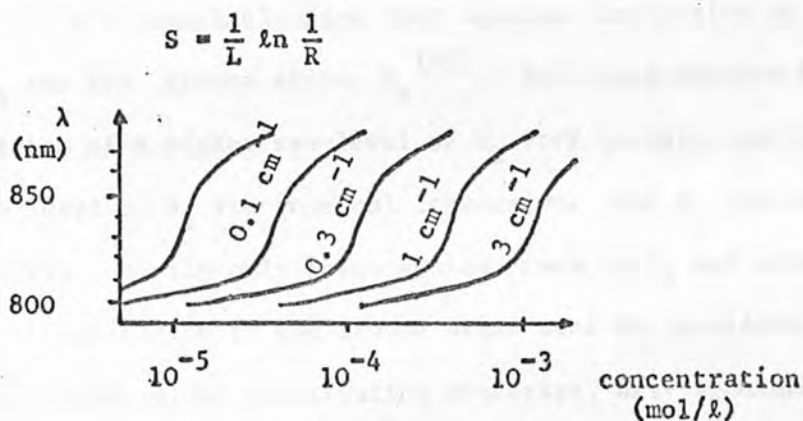


FIGURE 1.7: PLOT OF CALCULATED LASER WAVELENGTH VS CONCENTRATION OF THE LASER DYE, WITH  $S$  AS A PARAMETER.

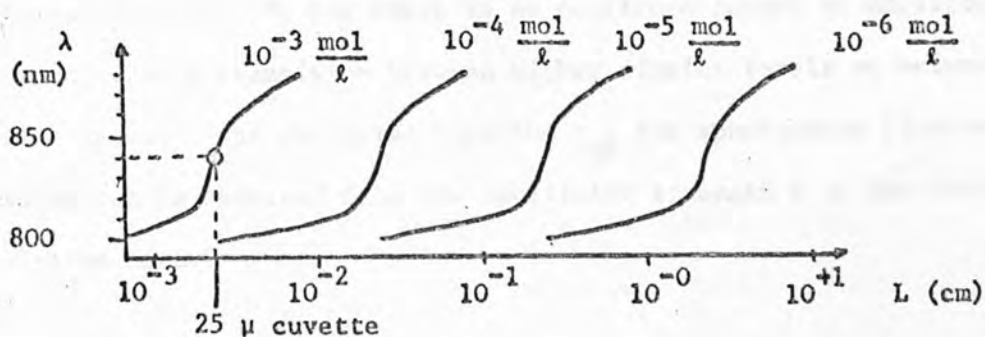


FIGURE 1.8: PLOT OF LASER WAVELENGTH VS ACTIVE LENGTH OF THE LASER CUVETTE, WITH CONCENTRATION OF DYE SOLUTION AS A PARAMETER



higher vibrational state of the new electronic level. The situation in a multi atomic molecule is entirely analogous although obviously more complex.

If a radiationless transition and the subsequent approach to equilibrium takes place among levels of the same multiplicity, the process is termed "internal conversion". If the radiationless transition is between levels of different multiplicity, it is termed inter-system crossing. The latter involves a change in spin and consequently its probability is usually much smaller than that of internal conversion, typically by six or more orders of magnitude. Intersystem crossing is enhanced by perturbations like enhanced spin orbit coupling in dye molecules containing heavy atoms, or by neighbouring molecules containing such atoms.

It is a remarkable fact that internal conversion is not effective between  $S_1$  and the ground state,  $S_0$  <sup>(35)</sup>. Thus molecules excited to higher singlet states of a higher sub-level of  $S_1$  very quickly come down to the lowest sub-level of  $S_1$  via internal conversion. For  $S_1$  internal conversion is so slow that usually only inter-system cross to  $T_1$  and subsequent radiative recombination to the ground state need be considered. In the absence of radiationless deactivation processes, only spontaneous and stimulated emission may lead to the relaxation of excited molecules. The emission from a singlet level to the ground state is generally termed "fluorescence", and that from a triplet level to the ground state "phosphorescence". So far there is no confirmed report of emission resulting from a transition between higher singlet levels or between higher triplet levels. The radiative lifetime  $\tau_{rf}$  for spontaneous fluorescence emission can be obtained from the oscillator strength  $f$  of the corresponding absorption band.

$$\frac{1}{\tau_{rf}} = \left( \frac{8\pi^2 \mu^2 e_o^2}{m_o C_o} \right) \tilde{\nu}^2 f$$

where  $\mu$  = refractive index of the solution

$e_o$  = the charge of the electron

$m_o$  = the mass of the electron

$C_o$  = velocity of light

$\tilde{\nu}$  = the wave number of the centre of the absorption band

This relation is valid if the half width of the emission band is small and its position not shifted significantly from that of the absorption band. Since the  $f$  values of the transition are near unity in most dyes, the radiative lifetime  $\tau_{rf}$  is typically of the order of a few nanoseconds. Generally, however, the fluorescence spectrum is broad and shows considerable Stokes shift. In this case the radiative lifetime can be computed with the aid of the following relation (Strickler and Berg<sup>(42)</sup> 1962)

$$\frac{1}{\tau_{rf}} = 2.88 \times 10^{-9} \mu^2 \frac{\int F(\tilde{\nu}) d\tilde{\nu}}{\int \tilde{\nu}^{-3} F(\tilde{\nu}) d\tilde{\nu}} \int \epsilon(\tilde{\nu}) d\tilde{\nu} \frac{\text{cm mole}}{\text{sec}}$$

longest  
wavelength  
absorption band

where  $F(\tilde{\nu}) = dq/d\tilde{\nu}$  is the fluorescence spectrum (in quanta per wave number) and  $\epsilon(\tilde{\nu})$  is the molecular decadic extinction coefficient as defined by Beer's law of absorption:

$$\log_{10} \left( \frac{I}{I_o} \right) = \epsilon cd$$

Here  $I_o$  is the intensity of light entering,  $I$  that of light leaving a layer of absorbing solution containing  $C$  mole/litre of absorbing species and having effective width of  $d$  centimeters. The radiative lifetime  $\tau_{rf}$  can be related to the observed fluorescence lifetime  $\tau_f$  through

$$\tau_f = \eta_f \tau_{rf}$$

where

$$\eta_f = \frac{\frac{1}{\tau_{rf}}}{\frac{1}{\tau_{rf}} + K_{S,T} + K_{S,S_0}}$$

is the quantum yield of fluorescence, ie the ratio of the radiative to the total transition rate to the groundstate. The total rate is the sum of radiative and the non radiative rates via intersystem crossing  $K_{S,T}$  and via internal conversion  $K_{S,S_0}$ . In principle one should be able to estimate the radiative lifetime  $\tau_{rp}$  of the phosphorescence from the lowest triplet state on the basis of the  $S_0 \rightarrow T_1$  absorption. Since this transition is spin forbidden, however, it is very hard to detect. It is normally completely obscured by absorption due to impurities. The phosphorescence radiative lifetime can be obtained from the quantum yield of phosphorescence,  $\eta_p$  and the observed phosphorescence lifetime  $\tau_p$ , as in the fluorescence case

$$\tau_p = \eta_p \tau_{rp}$$

As expected for spin forbidden transitions, it is extremely long, ranging from milliseconds to several seconds for molecules with small spin orbit coupling. Consequently, even relatively slow processes can lead to radiationless deactivation in liquid solution. Note that  $\eta_p$  is the true quantum yield of phosphorescence. It is defined as the ratio of the phosphorescence rate to the total rate of radiative and radiationless deactivation.

$$\eta_p = \frac{\frac{1}{\tau_{rp}}}{\frac{1}{\tau_{rp}} + K_{T,S_0}}$$

By comparison, very often one quotes the apparent quantum yield of phosphorescence  $\eta_p^+$ , which relates the rate of phosphorescence emission to the rate of light absorption. The relation between the two is

$$\eta_p^+ = \eta_p \eta_T$$

Here  $\eta_T$  = triplet formation efficiency, ie the ratio of the intersystem crossing rate  $K_{S,T}$  to the total rate of deactivation of the fluorescent level

$$\eta_T = \frac{K_{S,T}}{\frac{1}{\tau_{rf}} + K_{S,T} + K_{S,S_0}}$$

Energy can also be removed from the lowest singlet and triplet states (resulting in a lower quantum yield of fluorescence and phosphorescence respectively) by a long range radiationless energy transfer to some other dye molecule. For this to happen the absorption band of the latter, the "acceptor" molecule, must overlap the fluorescence of phosphorescence band of the former "sensitizer" molecule. The so-called critical distance, at which the quantum yield is reduced by a factor of two can reach values of 100 Å for the case of singlet-singlet energy transfer. For details of these and some other processes resulting in "delayed fluorescence" which are less important in the present context, see Parker<sup>(43)</sup> 1968.

### 1.5 Oscillation condition for dye lasers

There are two possibilities, at least in principle, to use an organic solution as active medium in a laser. One may utilise either the fluorescence or the phosphorescence emission. At first sight the long lifetime of the triplet state makes use of the phosphorescence more attractive. On the other hand, due to the highly forbidden transition a

very high concentration of the active species is required to obtain an amplification factor large enough to overcome the inevitable cavity losses. In fact, for many dyes the concentration would be higher than the solubility of these dyes in any solvent. As a further unfavourable property of these systems, losses due to triplet - triplet absorption occur with high probability. It must be remembered that triplet-triplet absorption bands are generally very broad and diffuse and the probability for overlapping the phosphorescence band is high. Due to these difficulties no lasing using the phosphorescence of a dye has been reported so far (a preliminary report Morantz et al<sup>(44), (45)</sup> 1962, 1963 was evidently in error). The possibility cannot be excluded, however, that further study of phosphorescence and triplet-triplet absorption in molecules of different types of chemical constitution might eventually lead to a workable system.

If the fluorescence band of a dye solution is utilised in a dye laser, the allowed transition from the lower sublevel of the first excited singlet state to some higher sublevel of the ground state will give a high amplification factor even at low dye concentration. The main complication in these systems is the existence of the lower lying triplet states. The intersystem crossing rate to the lowest triplet state is high enough in most molecules to reduce the quantum yield of fluorescence to values substantially below one. Firstly this reduces the population of the excited singlet state, and hence the amplification factor. Secondly, it enhances the triplet-triplet absorption losses by increasing the population of the lowest triplet state. Assume a light flux density which slowly rises to a level  $P$  (quanta  $s^{-1} cm^{-2}$ ) a total molecular absorbing cross section  $\sigma$  (cm<sup>2</sup>), a quantum yield  $\eta_T$  of triplet formation, populations of the triplet and ground state of  $N_T$  and  $N_0$  (cm<sup>-3</sup>) respectively and, neglecting



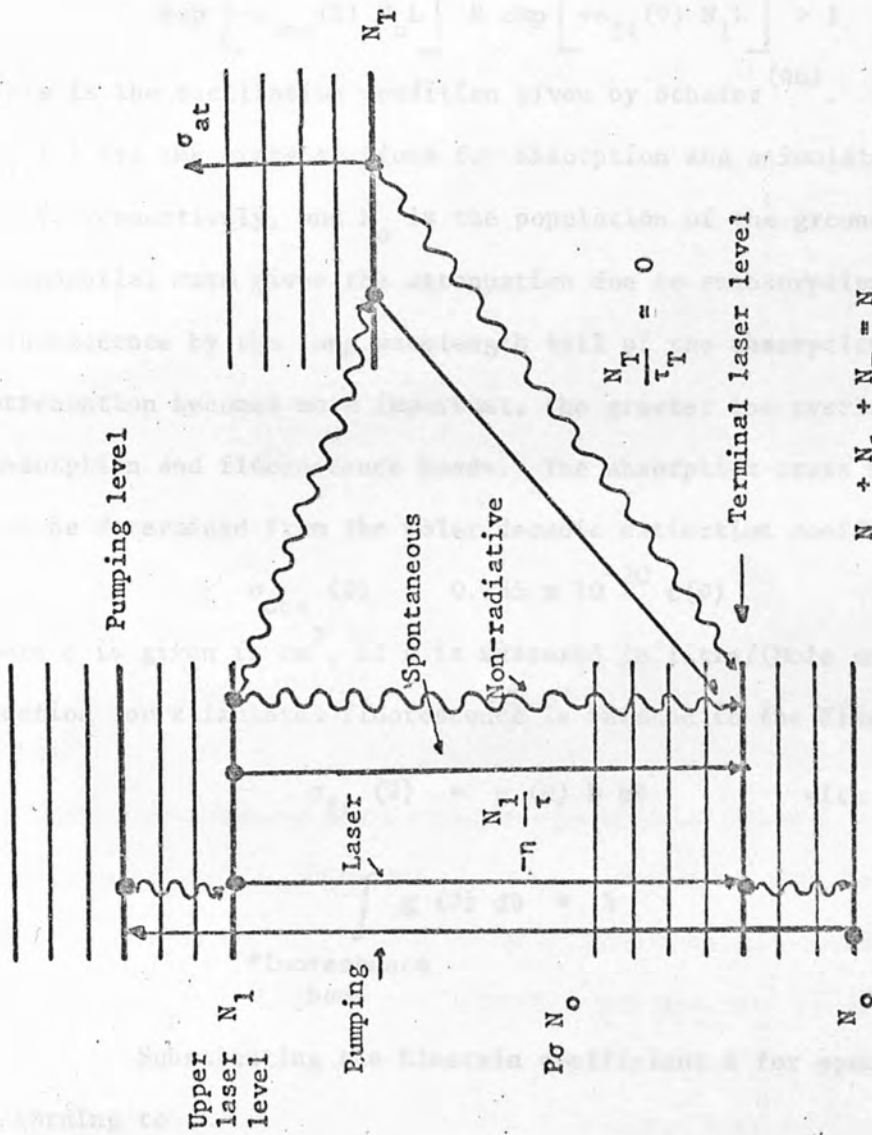
the small population of the excited singlet state, total concentration of dye molecules of  $N = N_0 + N_T$ . Then a steady state is reached, when the triplet formation and deactivation rates are equal.

$$P\sigma N_0 \eta_T = \frac{N_T}{\tau_T}$$

Hence the fraction of molecules in the triplet state is given by

$$\frac{N_T}{N} = \frac{P\sigma \eta_T \tau_T}{(1 + P\sigma \eta_T \tau_T)}$$

Assuming some typical values for a dye,  $\sigma = 10^{-16} \text{ cm}^2$ ,  $\eta_T = 0.1$  (corresponding to a 90% quantum yield of fluorescence), and  $\tau_T = 10^{-4} \text{ s}$ , the power to maintain half of the molecules in the triplet state is  $P_{\frac{1}{2}} = 10^{21} \text{ quanta s}^{-1} \text{ cm}^{-2}$ , or an irradiation of only  $\frac{1}{2} \text{ kW cm}^{-2}$  in the visible part of the spectrum, which is a lot less than the threshold pump power. Hence a slowly rising pump light pulse would transfer most of the molecules to the triplet state and deplete the ground state accordingly. On the other hand, the population of the triplet level can be held arbitrarily small, if the pumping light flux density rises fast enough, ie if it reaches threshold in a time  $t_r$  small compared to the reciprocal of the intersystem crossing rate,  $t_r \ll 1/k_{S,T}$ . Here  $t_r$  is the rise time of the pump light power, during which it rises from zero to the threshold level. For a typical value of  $k_{S,T} = 10^7 \text{ s}^{-1}$ , the risetime should be less than 100 ns. This is easily achieved, for example with a giant pulse laser as pump light source since giant pump lasers usually have risetimes of 5-20 ns. In such laser pumped dye laser systems one may neglect all triplet effects to a first approximation.



Energy level diagrams of a dye molecule with indication of transitions and terms considered in the calculation of the excited singlet population  $N_1$ .

FIGURE 1.9a

In its simplest form a dye laser consists of a cuvette of length  $L$  (cm) with dye solution of concentration  $N$  ( $\text{cm}^{-3}$ ) and two parallel end windows carrying a reflective layer each of reflectivity  $R$  for the laser resonator. With  $N_1$  molecules/ $\text{cm}^3$  excited to the first singlet state, the dye laser will start oscillating at a wave number  $\tilde{\nu}$ , if the overall gain there is equal to or greater than one:

$$\exp \left[ -\sigma_{\text{abs}}(\tilde{\nu}) N_0 L \right] R \exp \left[ +\sigma_{\text{fl}}(\tilde{\nu}) N_1 L \right] > 1.$$

This is the oscillation condition given by Schafer<sup>(46)</sup>. Here  $\sigma_{\text{abs}}(\tilde{\nu})$  and  $\sigma_{\text{fl}}(\tilde{\nu})$  are the cross sections for absorption and stimulated fluorescence at  $\tilde{\nu}$ , respectively, and  $N_0$  is the population of the ground state. The first exponential term gives the attenuation due to reabsorption of the fluorescence by the long wavelength tail of the absorption band. The attenuation becomes more important, the greater the overlap between the absorption and fluorescence bands. The absorption cross section  $\sigma_{\text{abs}}(\tilde{\nu})$  can be determined from the molar decadic extinction coefficient  $\epsilon(\tilde{\nu})$  by

$$\sigma_{\text{abs}}(\tilde{\nu}) = 0.385 \times 10^{-20} \epsilon(\tilde{\nu})$$

Here  $\sigma$  is given in  $\text{cm}^2$ , if  $\epsilon$  is measured in litre/(Mole cm). The cross section for stimulated fluorescence is related to the Einstein coefficient  $B$

$$\sigma_{\text{fl}}(\tilde{\nu}) = g(\tilde{\nu}) B h \tilde{\nu} \quad \text{with}$$

$$\int_{\text{fluorescence band}} g(\tilde{\nu}) d\tilde{\nu} = 1$$

Substituting the Einstein coefficient  $A$  for spontaneous emission according to

$$B = \frac{1}{8\pi\tilde{\nu}^2} A \frac{1}{h\tilde{\nu}}$$



and realising that  $g(\tilde{\nu})A$  is proportional to the number of fluorescence quanta per wave number interval,  $dN_{fl}/d\tilde{\nu}$ , one obtains

$$\sigma_{fl}(\tilde{\nu}) = \text{const} \frac{1}{\tilde{\nu}^2} \frac{dN_{fl}}{d\tilde{\nu}}$$

Since the fluorescence band is usually a mirror image of the absorption band, the maximum values of the cross sections in absorption and emission may be set equal

$$\sigma_{fl \text{ max}} = \sigma_{\text{abs max}}$$

Taking the logarithm of the oscillation condition and rearranging leads to a form of the oscillation condition which facilitates a discussion of the influence of the various parameters:

$$\frac{\frac{S}{N} + \sigma_{\text{abs}}(\tilde{\nu})}{\sigma_{fl}(\tilde{\nu}) + \sigma_{\text{abs}}(\tilde{\nu})} < \gamma(\tilde{\nu})$$

where

$$S = \left(\frac{1}{L}\right) \ln\left(\frac{1}{R}\right) \quad \text{and} \quad \gamma(\tilde{\nu}) = \frac{N_1}{N}$$

The constant  $S$  on the left hand side of the equation only contains parameters of the resonator, i.e. the active length  $L$  and reflectivity  $R$ . Other types of losses, like scattering, diffraction etc, may be accounted for by an effective reflectivity,  $R_{\text{eff}}$ . The value  $\gamma(\tilde{\nu})$  is the minimum fraction of the molecules that must be raised to the first singlet state to reach the threshold of oscillation. One may then calculate the function  $\gamma(\tilde{\nu})$  from the absorption and fluorescence spectra for any concentration  $N$  of the dye and value  $S$  of the cavity. In this way one finds the frequency for the minimum of this function. Laser oscillations will start at this frequency if the pump light raises the population of  $S_1$  to a level

corresponding to the value  $\gamma(\bar{\nu})$ . Since always  $N_1/N < 1$  a necessary condition is  $(S/N) < \sigma_{fl}$ , which allows a quick estimate of the feasibility of laser action for a given resonator and dye concentration. Another interesting feature of equation (1.1) is that  $S$  and  $1/N$  enter as a product. This means that a tenfold increase in concentration, for instance, will have the same effect as a tenfold increase in length or as an increase of the reflectivity of the mirrors eg from 90% to 99%. It is worth noticing that an increase in concentration shifts the minimum of  $\gamma(\bar{\nu})$  towards the red. Figure 1.7 is a plot of the laser wavelength  $\lambda$  (ie the wavelength where the minimum of  $\gamma(\bar{\nu})$  occurs) versus the concentration with  $S$  a fixed parameter, reproduced from Shafer's<sup>(28)</sup> work. Similarly Figure 1.8 shows the laser wavelength versus the active length  $L$  of the cuvette with dye solution, with the concentration of the dye as a parameter. Both figures apply to the dye 3,3' diethylthiatricarbocyanine. These diagrams demonstrate the wide tunable range of dye lasers by changing the concentration of the dye solution, or length, or  $Q$  of the resonating cavity. They also show the high gain which permits the use of extremely small active lengths.

The absorbed power density  $W$  necessary to maintain a fraction  $\gamma$  of the molecular concentration  $N$  in the excited state is

$$W = \frac{\gamma N h C_o \bar{\nu}_{\text{pump}}}{\tau_f}$$

and power flux

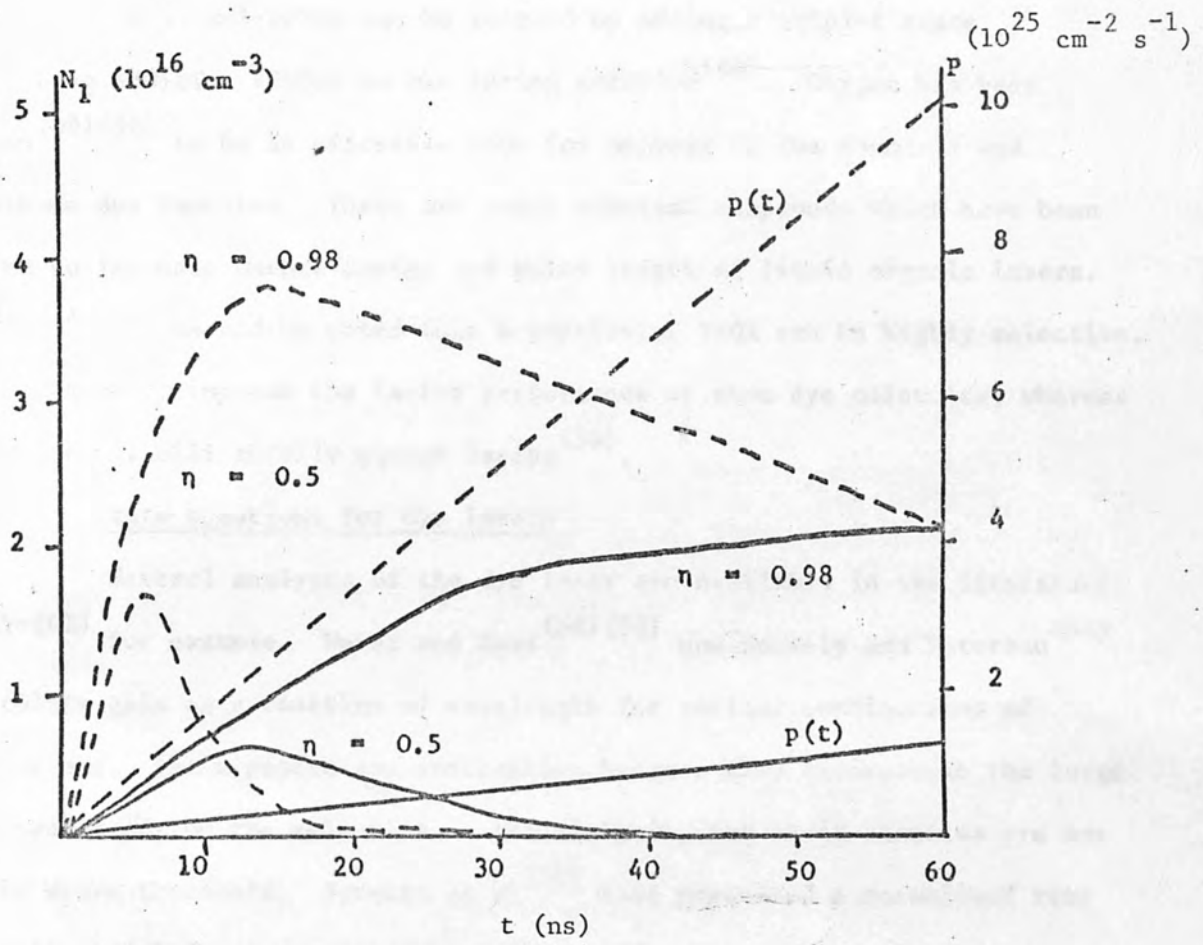
$$P = \frac{W}{N\sigma} = \frac{\gamma h C_o \bar{\nu}_{\text{pump}}}{\tau_f \sigma}$$

where  $\bar{\nu}_{\text{pump}}$  is the wave number of the absorbed pump radiation.

In the above derivation of the oscillation condition and concentration dependence on the laser wavelength, broad band reflectors have

been assumed. In the case of flashlamp pumped dye lasers, triplet effects become important because of the long rise time or duration of the pump light pulse. Figure 1.9b shows the time dependence of the population density  $N_1$  in the excited singlet state (Schmidt et al<sup>(47)</sup>). The solid curve applies to a slowly rising, and the broken curve to a fast rising pump light pulse. Both are computed for two different values of the quantum yield of fluorescence  $\eta_f$ . It is assumed that there is no direct radiationless internal conversion between the first excited singlet and the ground state, so that a fraction  $\rho = 1 - \eta_f$  of excited molecules in the singlet state make an intersystem crossing to the triplet state. It is further assumed that the triplet state has a very long lifetime compared to the singlet state. It is seen that there is a maximum in the excited singlet state population density  $N_1$ . It is higher for a faster rise of the pump light and for a higher quantum yield of fluorescence. Despite the continuing rise of the pump light intensity,  $N_1$  falls to a low value after passing through the maximum, since the ground state becomes depleted and virtually all of the molecules accumulate in the triplet state. It should be pointed out that this behaviour occurs with spontaneous fluorescence of an optically thin layer of dye solution. This type of behaviour would remain practically unaltered when stimulated emission is taken into account. Thus a dye laser may be pumped above the threshold by a fast rising light source. On the other hand, the necessary population density in the excited singlet state may not be achieved with a slowly rising light source, even if the asymptotic pump level is the same for both cases.

The accumulation of molecules in the triplet state gives rise to a further loss mechanism not previously discussed. The triplet absorption spectra very often extend into the region of fluorescence emission. This



Result of analogue computer calculations for  $N_1$  for high (0.98) and lower (0.5) quantum yield of fluorescence both for the case of low (solid lines) and high (dotted lines) rate of pump light intensity.

FIGURE 1.9b

gives rise to absorption which transfers the molecules into higher excited triplet states. Thus they lead to losses that often are higher than the gain of the laser and eventually prevent laser emission. However, the accumulation of molecules can be reduced by adding a triplet state quenching additive (TSQA) to the lasing solution<sup>(48)</sup>. Oxygen has been shown<sup>(49) (50)</sup> to be an effective TSQA for members of the coumarin and xanthene dye families. There are other chemical compounds which have been found to increase output energy and pulse length of liquid organic lasers.<sup>(48) (51)</sup>. It should be noted that a particular TSQA can be highly selective, it can greatly improve the lasing performance of some dye molecules, whereas in others it will totally quench lasing<sup>(50)</sup>.

#### 1.6 Rate equations for dye lasers

Several analyses of the dye laser are available in the literature<sup>(52)-(62)</sup> for example. Weber and Bass<sup>(52) (53)</sup> and Snavely and Peterson<sup>(54)</sup> calculate gain as a function of wavelength for various combinations of parameters. These papers are interesting because they incorporate the large spectral bands of the molecules in the analysis, but their theories are not valid above threshold. Sorokin et al<sup>(56)</sup> have presented a normalised rate equation model for a single wavelength dye laser pumped above threshold by a Gaussian shaped flash lamp pulse. However, they assumed the triplet lifetime was long with respect to the half width of the pumping flashlamp. Snavely<sup>(55)</sup>, Keller<sup>(61)</sup> and Huth and Kagan<sup>(57)</sup> considered triplet losses which are important when the pumping source is not very fast, along with the effect of triplet quenching processes. The dye laser model by Huth and Kagan<sup>(57)</sup> will be considered in more detail.

In order to write a set of rate equations that model the dye laser, Huth et al simplified the energy level diagram (Figure 1.5) to that



shown in Figure 1.10. The states shown on the left are the singlet states and depict the 4-level nature of the dye laser. The triplet states are on the right hand portion of the diagram.

The two relevant vibronic levels in the ground singlet state are assumed to be in thermal equilibrium, and the populations are in Boltzmann distribution. This is taken into account by the factors  $\alpha$  and  $\beta$  which sum to unity and have the proper exponential ratio to one another (60).

$$\beta = \frac{\exp(-\Delta E/kT)}{1 + \exp(-\Delta E/kT)}$$

where  $\Delta E$  is the energy between the vibronic levels.

The population density of the ground state is labelled  $N_0$ . It is assumed that optical pumping takes place between the ground state and the level with population density  $N_2$ . The molecules then undergo non radiative transitions to the upper lasing level with population  $N_1$ .

Molecules in the triplet manifold decay non radiatively to the lowest triplet state which has population  $N_T$  and is metastable because of selection rules for transitions to the ground state. Radiative decay to the ground state can be observed as phosphorescence but usually has a very long lifetime. Non radiative decay is much more likely and is caused by a number of possible quenching mechanisms. As mentioned earlier oxygen dissolved in solution is a very efficient quencher and is undoubtedly the most important mechanism.

The rate equations for dye lasers whose energy levels are shown in Figure 1.10 are given below:

$$\frac{dN_2}{dt} = \sigma_{ss} v q_p \left[ \alpha N_0 - N_2 \right] - K' N_2 \quad \dots (1.6.1)$$



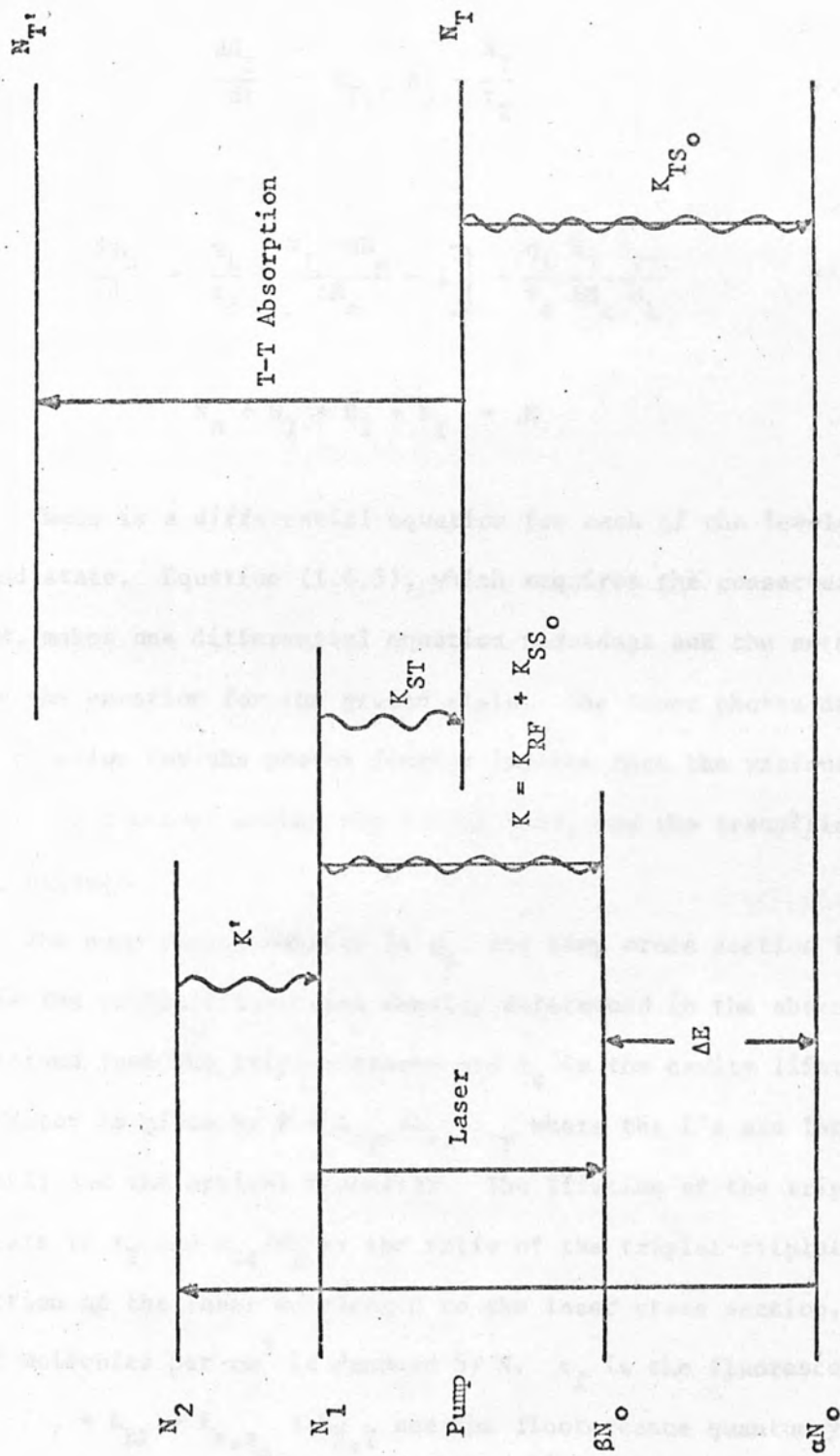


FIGURE 1.10: ENERGY LEVEL DIAGRAM USED TO MODEL THE ORGANIC DYE LASER

$$\frac{dN_1}{dt} = K' N_2 - \frac{q_L}{\tau_c F \Delta N_c} \left[ N_1 - \beta N_0 \right] - \frac{N_1}{\tau_f} \quad \dots (1.6.2)$$

$$\frac{dN_T}{dt} = K_{S,T} N_1 - \frac{N_T}{\tau_T} \quad \dots (1.6.3)$$

$$\frac{dq_L}{dt} = \frac{q_L}{\tau_c} \left[ \frac{N_1 - \beta N_0}{\Delta N_c} - 1 \right] - \frac{q_L}{\tau_c} \frac{N_T \sigma_{TT}}{\Delta N_c \sigma_L} \quad \dots (1.6.4)$$

$$N_0 + N_1 + N_2 + N_T = N \quad \dots (1.6.5)$$

There is a differential equation for each of the levels except the ground state. Equation (1.6.5), which requires the conservation of molecules, makes one differential equation redundant and the authors choose to ignore the equation for the ground state. The laser photon density is  $q_L$ . The equation for the photon density implies that the various parameters are relatively constant across the lasing band, and the transition is homogeneously broadened.

The pump photon density is  $q_p$ , the pump cross section is  $\sigma_{ss}$  and  $\Delta N_c$  is the critical inversion density determined in the absence of losses derived from the triplet states and  $\tau_c$  is the cavity lifetime. A filling factor is given by  $F = L_{\text{dye}}/L_{\text{cavity}}$  where the L's are lengths of the dye cell and the optical resonator. The lifetime of the triplet metastable state is  $\tau_T$  and  $\sigma_{TT}/\sigma_L$  is the ratio of the triplet-triplet absorption cross section at the laser wavelength to the laser cross section. The total number of molecules per  $\text{cm}^3$  is denoted by  $N$ .  $\tau_f$  is the fluorescence lifetime and  $1/\tau_f = K_{RF} + K_{s,s_0} + K_{S,T}$  and the fluorescence quantum yield is

$$\eta_F = \frac{K_{RF}}{K_{RF} + K_{S,S_0} + K_{ST}}$$

One can identify most of the terms in the equations by inspection of Figure 1.10.

The last term in (1.6.3) accounts for the decay of the triplet metastable state and the last term in (1.6.4) represents the optical loss introduced by excited state absorption in the triplet manifold.

The power output from the mathematical model can be computed from

$$P_o = \frac{\text{Energy stored in cavity}}{\text{Coupling lifetime}} \quad \dots (1.6.6)$$

where the "coupling lifetime" refers to a cavity lifetime that includes only those coupling or loss mechanisms that contribute to the useful output. Since the coupling is normally accomplished with partially reflecting mirrors, the lifetime can be calculated from

$$\tau_c = \frac{L_{\text{cavity}}}{v} \frac{\sqrt{\rho}}{1-\rho} \quad \dots (1.6.7)$$

In this equation,  $v$  is the speed of light and  $\rho$  is the geometrical mean of the two mirror reflectivities, ie  $\rho = (R_1 R_2)^{\frac{1}{2}}$ . In terms of the variables, the output power is therefore

$$P_o = \frac{h \nu q_L L_{\text{cav}} A_{\text{cav}}}{\lambda_L \tau_c}$$

with  $A_{\text{cav}}$  equal to the laser cross sectional area.

Relating the pump power to the variables in the model is more difficult because of the lack of precise knowledge of spectral and geometrical coupling factors in actual laboratory devices.

It is useful to consider the steady-state solutions or quasi-steady-state solutions of (1.6.1)→(1.6.5). If the time derivatives are set to zero and the resulting algebraic equations are solved under the assumption that  $K' \gg \sigma_{ss} V q_p$ , the following expression for  $q_L$  is obtained:

$$q_L = \frac{F \Delta N_c \left( \frac{\tau_c}{\tau_f} \right) \left( \beta + \frac{\Delta N_c}{N} \right)}{\Delta N_c / N + \beta \xi} \left[ \left\{ \frac{(1 - \xi) \sigma_{ss} V q_p}{\left( \frac{\tau_c}{\tau_f} \right) \left( \beta + \frac{\Delta N_c}{N} \right)} \right\} - 1 \right] \quad \dots (1.6.8)$$

where 
$$\xi = \frac{\Delta N_c}{N} + K_{S,T} \tau_T \left( \frac{\Delta N_c}{N} + \frac{\sigma_{TT}}{\sigma_L} \right) \quad \dots (1.6.9)$$

In most cases of interest, the constant  $\xi$  can be further simplified to the approximate value

$$\xi = K_{ST} \tau_T \left( \frac{\sigma_{TT}}{\sigma_L} \right) \quad \dots (1.6.10)$$

Equation (1.6.8) is valid only above threshold. Note that the first term in the square brackets must be positive and greater than unity to produce laser emission. This term can never satisfy these requirements unless the positive definite constant  $\xi$  has a value less than one. Thus, steady state operation of a dye laser is possible only if  $\xi < 1$ . The fact that a steady-state solution can exist contradicts the earlier analyses of dye lasers and leads to the possibility of cw operation<sup>(49)</sup> which has been experimentally achieved.<sup>(63)</sup>

Laser operation when  $\xi > 1$  is not precluded, but the result given above indicate that the solutions are transient in nature. In fact, when  $\xi > 1$ , one can show that a critical risetime for the flashlamp does exist by following the reasoning of Sorokin et al<sup>(56)</sup>.

The effects of dissolved oxygen can be included in the rate equations. Some molecules can quench the fluorescence and phosphorescence of organic compounds. Dissolved oxygen arising from contact with the atmosphere is an effective quencher, and the quenching reaction is diffusion controlled. In normal dye laser situations, oxygen quenching is the dominant process for relaxation of the triplet metastable state, and the triplet lifetime  $\tau_T$  can be written

$$\tau_T = \frac{1}{K_{O_2} (O_2)}$$

where  $K_{O_2}$  is the rate constant and  $(O_2)$  is the molar concentration of dissolved oxygen. (See Appendix II).

Oxygen can also quench the excited singlet state, by increasing the intersystem crossing.

Thus the intersystem rate becomes

$$K_{S,T} = K_{ST}^o + \eta K_{O_2} (O_2)$$

with  $\eta$  equal to the ratio of the singlet quenching rate constant to the triplet rate constant.

To apply the model presented above, one must know a value of the triplet decay time at dye concentrations that are typical for laser applications. Stockman has observed decay times between 90 and 120 ns for Rh 6G in methanol which compare favourably with the authors results showing experimental values of triplet lifetimes in air equilibrated solutions to be approximately  $10^{-7}$  s.

Another important piece of information is given by Huth and Kagan<sup>(57)</sup>. This is the saturation intensity of rhodamine 6G. The saturation intensity is the circulating power density in the laser necessary to reduce the population inversion to one half its small signal value. It is also an indication of the power level necessary for the lasing process to compete favourably with spontaneous emission.

The output power of the laser is related to the saturation intensity  $I_{\text{sat}}$  by the following equation.

$$P_{\text{out}} = I_{\text{sat}} A \frac{(1-\rho)}{\rho} \left( V F \tau_c g_0 - 1 \right) \quad \dots (1.6.11)$$

where  $\rho = (R_1 R_2)^{\frac{1}{2}}$ ,  $A$  is the area, and  $g_0$  is the unsaturated small signal gain coefficient. The output energy for a laser with 21.5 J input was 55 mJ and the base width of the pulse was approximately 5  $\mu\text{s}$ . If one makes a triangular approximation for the pulse shape, the peak output power is  $2.2 \times 10^4$  W. The other parameter values necessary to evaluate the saturation intensity are as follows:  $g_0 = 0.22 \text{ cm}^{-1}$ ,  $\rho = (0.65 \times 1)^{\frac{1}{2}} = 0.806$ ,  $F = 0.133$ ,  $\tau_c = 3 \times 10^{-9}$  s and  $A = 0.1 \text{ cm}^2$ . Upon substitution of these values into (1.6.11) we obtain  $I_{\text{sat}} = 6.2 \times 10^5 \text{ W/cm}^2$ .

An alternate expression for the saturation intensity is

$$I_{\text{sat}} = \frac{\hbar \omega}{\tau_f \sigma_L} \quad \dots (1.6.12)$$

The fluorescence lifetime for rhodamine 6G is approximately 5.5 ns, and the laser cross section at 5900 Å is given as  $1.06 \times 10^{-16} \text{ cm}^2$ . Substitution into (1.6.12) yields  $I_{\text{sat}} = 5.8 \times 10^5 \text{ W/cm}^2$ . To place this number in perspective, one may compare this result with the saturation intensities of other laser materials. In a transverse flow CO<sub>2</sub> laser,  $I_{\text{sat}} = .246 \text{ W/cm}^2$ <sup>(64)</sup> and in Nd:YAG,  $I_{\text{sat}} = 720 \text{ W/cm}^2$ ,<sup>(65)</sup>. The saturation



intensity for rhodamine 6G is three orders of magnitude larger than those of the other materials, which implies that very large pump rates are required for efficient operation.

The excitation of dye lasers with the laser light for use in laser systems has been growing rapidly since the late 1960s. This is due to the discovery of the dye laser by R. G. Barr and R. W. Hellwarth in 1968. This laser was the first to operate at a wavelength longer than the visible spectrum and to have a pulse duration as short as that of the dye laser. This for the first time eliminated the need for a separate excitation source for the dye laser. The excitation of dye lasers requires a much higher pump rate than, for example, ruby or neodymium as was shown in the last chapter. For the shorter wavelength regions the excitation becomes even more important because the noise, or loss due to spontaneous emission in a system is proportional to the cube of the laser frequency.

The effect of inhomogeneities in the gain medium will be discussed in detail in the next chapter. A small inhomogeneity in the gain medium will cause a decrease in the laser output and an increase in the noise. In order to obtain a high quality laser beam, it is necessary to use a laser with a high gain medium. The gain medium must be excited to a high energy state. The excitation of the gain medium is done by the pump laser. The pump laser must have a high pump rate and a high pulse rate. The pump laser must also have a high pulse rate and a high pulse rate. The pump laser must also have a high pulse rate and a high pulse rate. The pump laser must also have a high pulse rate and a high pulse rate.

## CHAPTER II

### FLASHLAMP SYSTEMS

#### 2.1 Introduction

The generation of flashtubes with fast rise times for use in laser excitation and various other fields of photon physics has been growing rapidly over the last decade, especially since the invention of the dye laser. In the following period many workers reported laser action over a broad wavelength range using the same flashtube as the exciting source of radiation along with various dyes. This for the first time eliminated the bandwidth limitation connected with the usual type of gas and solid state lasers. However, the excitation of dye lasers require a much faster optical pumping system than, for example, ruby or neodymium as was seen in the last chapter. For the shorter wavelength regions fast rising flashtubes become even more important because the noise, or loss due to spontaneous emission in a system is proportional to the cube of the laser emission frequency.

The effect of inductance on the peak intensity and duration of the radiation from a spark discharge is very significant. An increase in inductance causes a decrease in peak intensity and an increase in duration and so, in order to obtain more intense flashes a great deal of work has been directed towards developing systems of very low inductance.

In the design of a flashlamp pumped dye laser it is important to choose the appropriate flashlamp. A determining factor is the rise-time requirement of the specific dye or class of dyes to be used. So far the fastest risetimes (70 ns) were achieved with capillary air sparks fed by transmission line storage<sup>(77)(78)</sup>. Another type with a very fast rise-time is a low inductance coaxial lamp first developed for flash photolysis work by Claesson and Lindquist<sup>(79)</sup> in 1958. It was successfully used later by Sorokin and Lankard<sup>(80)</sup>, and Schmidt and Schäfer<sup>(47)</sup>, for dye

laser pumping. An improved version of this lamp<sup>(81)</sup> uses a spark gap in series with the lamp, so that a voltage much higher than the breakdown voltage of the lamp can be used. Risetimes of 150 ns using a 0.05  $\mu$ F capacitor were achieved from this lamp.

## 2.2 An analysis of the discharge mechanism in a flashtube

When a capacitor is discharged through a flashtube a highly conducting path is formed. The formation of this path can be divided into several stages:-

- (a) The initial build up of the space charge during which the development of the current is accelerated.
- (b) A cathode fall is formed which supplies the electrons for the remainder of the zone.
- (c) An ionisation wave from the anode to the cathode producing a further rise in current.
- (d) The final stage in which the discharge consists of the cathode fall and an associated plasma in which there is little ionisation.

The breakdown of a gas between two electrodes is dependent on their being one or more electrons between the electrodes. The gas becomes a good conductor via the plasma column formed between the electrodes. The change from insulator to conductor was explained by Townsend<sup>(68)</sup> in his theory of gas breakdown. He proposed that the breakdown was caused by the ionisation of gas atoms by collisions with electrons and positive ions and the production of secondary processes: photoionisation of gas atoms, photo emission from the cathode, positive ion bombardment of the cathode etc. When an electron is released from an atom in the gas, for example by cosmic radiation, it is accelerated towards the anode. If it is sufficiently energetic it can ionise neutral gas atoms by collision and

thereby produce another electron and a positive ion. Due to its comparatively large mass the ion is only slowly accelerated towards the cathode, whereas the two electrons continue towards the anode and cause further ionisation by collision, and an electron avalanche is formed.

Ionisation need not occur when an electron collides with an atom, even if the electron has sufficient energy - the electron may raise the atom to an excited state which returns to the ground state by radiating. These photons emitted may ionise other gas atoms or cause photo-emission from the cathode. The electrons from these secondary processes are accelerated towards the anode and in turn generate electron avalanches. The current  $i$  flowing in such a discharge is given by<sup>(69)</sup>

$$i = \frac{i_0 e^{\alpha x}}{1 - \gamma (e^{\alpha x} - 1)} \quad \dots (1)$$

where  $i_0$  is the current due to external radiation

$\alpha$  is the first Townsend coefficient relating to ionisation by electron collision.

$\gamma$  is the second Townsend coefficient relating to all secondary producing processes and

$x$  is the electrode separation

If the voltage gradient between the electrodes is high enough

$\gamma(e^{\alpha x} - 1) \rightarrow 1$  and  $i$  becomes infinite. At this point the gas is considered to have broken down and this condition is known as Townsend's sparking criterion ie

$$\gamma (e^{\alpha x} - 1) = 1 \quad \dots (2)$$

The voltage at which this criterion is satisfied varies with pressure  $p$  as both  $\alpha$  and  $\gamma$  vary with pressure and voltage but are constant for constant  $E/p$  at a given  $p$  (where  $E$  is the electric field across the electrodes)

At breakdown  $\gamma e^{\alpha x} \gg 1$  so the criterion can be rewritten as

$$\gamma e^{\alpha x} = 1 \quad \dots (3)$$

This criterion has been interpreted by Loeb<sup>(70)</sup> as follows:

(a) For  $\gamma e^{\alpha x} < 1$  the discharge follows equation (1) and the current is not self sustaining, being dependent on external radiation to supply  $i_0$ .

(b) For  $\gamma e^{\alpha x} = 1$  as a result of each avalanche due to one electron there is one new electron formed due to the secondary processes. Thus the discharge is just self sustaining and independent of  $i_0$ . However, it does not carry increasingly large currents. This is the threshold for breakdown.

(c) For  $\gamma e^{\alpha x} > 1$ , on average, each avalanche gives rise to more than one electron so that the discharge grows and is able to carry large currents.

The Townsend theory is found to apply well for low gas pressures and small electrode separations ie the product  $px$  is small. However, if the product becomes too large then as Rogowski<sup>(71)</sup> showed, the time of formation of a spark is less than that predicted by the Townsend theory. The observed formation time being of the order of the transit time of an electron between the electrodes as opposed to the predicted formation time of the order of the transit time of an ion. Raether<sup>(72)</sup> and Meek<sup>(73)</sup> independently produced a new theory to account for the mechanism in operation when the product  $px$  is large. The new theory depends on the formation of a "streamer" between the electrodes. Although this theory is inadequate to explain all phenomenon it is able to explain observations of streamers from the anode - in direct conflict with the Townsend theory.



Consider an electron produced near the cathode of a gap across which a uniform electric field is applied, of high enough potential to cause breakdown. The electron is accelerated towards the anode and causes an avalanche to form. The electrons formed are accelerated much more quickly than the positive ions formed due to their mass, so that by the time the electrons have reached the anode the ions have hardly moved. This means that there is a cone of positive ions left spreading out from the cathode due to the cumulative ionisation in the avalanche causing the ion concentration to be greatest at the anode end of the cone.

Not all the collisions between electrons and atoms produce ionisation, some of the collisions produce excited atoms. These excited atoms emit photons which may produce secondary electrons near the base of the cone which give rise to small avalanches. If the field due to positive ions in the cone is large enough then even the small avalanches are deviated into the main avalanche region leaving behind positive ions which extend the region of high ion density. Thus the space charge and its associated field are enhanced down to the apex of the original cone. The field distortion causes more secondary avalanches to be attached to the main avalanche nearer the cathode, thus further increasing the ion concentration. This process continues down the column of gas between the electrodes so that eventually a channel of highly ionised gas - the streamer, is set up between the anode and cathode. This streamer is the starting point from which a spark channel may grow. If the space charge field was not strong enough then the secondary avalanches would not be deviated enough to join the main avalanche and form a streamer as just described, but breakdown would still occur as a series of avalanches.



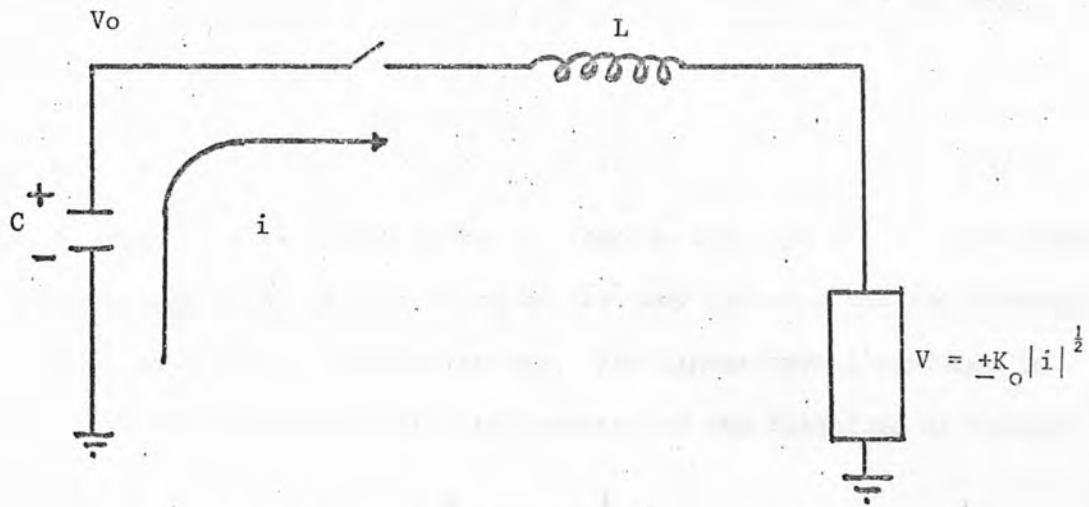


FIGURE 2.1: FLASHLAMP CIRCUIT

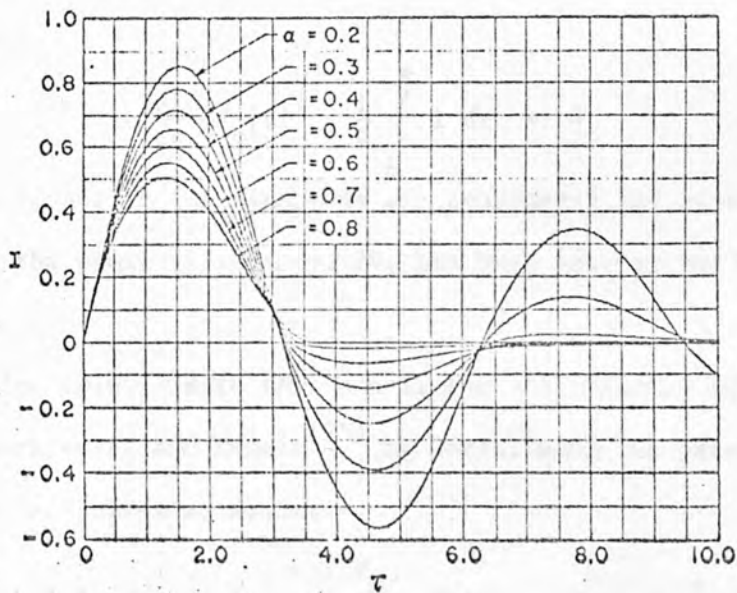


FIGURE 2.2: NORMALISED CURRENT VS NORMALISED TIME FOR VARIOUS VALUES OF THE DAMPING PARAMETERS  $\alpha$

It has been shown by Goncz<sup>(74)</sup> that the V-i characteristic of a flashlamp for the high current region can, under certain circumstances, be represented as

$$V = \pm K_0 |i|^{\frac{1}{2}} \quad \text{volts} \quad \dots (1)$$

where the sign of v is chosen to be the same as the sign for i - see Figure 2.1. The parameter  $K_0$  is a function of the lamp geometry and the pressure and type of gas used to sustain the arc. For linear type flashlamps it can be shown that  $K_0$  scales with the geometry of the flashlamp as follows<sup>(75)</sup>

$$K_0 = k \frac{\ell}{d} \text{ ohm amp}^{\frac{1}{2}}$$

where  $k$  is only a function of the type and pressure of gas  
 $\ell$  is the length of the lamp in centimetres and  
 $d$  is the bore diameter in cms.

The non linear differential equation describing the loop voltage of a single mesh flashlamp discharge circuit like the one shown in Figure 2.1 is

$$L \frac{di}{dt} \pm K_0 |i|^{\frac{1}{2}} + \frac{1}{C} \int_0^t i \, d\tau = V_0 \quad \dots (2.1)$$

where only losses in the flashlamp are considered and also the term containing the ohmic resistance,  $iR$ , has been ignored for the present discussion.

The solutions to this non linear differential equation have been given by Markiewicz and Emmett<sup>(75)</sup> by normalising the parameters in the circuit in the following manner:-

$$z_0 = \sqrt{\frac{L}{C}} \quad (a), \quad i = \frac{I V_0}{z_0} \quad (b), \quad \tau = \frac{t}{T} \quad (c)$$

$$T = \sqrt{LC} \quad (d), \quad \alpha = \frac{k\ell}{d} \frac{1}{(V_0 z_0)^{\frac{1}{2}}} \quad (e), \quad p = P_N \frac{V_0^2}{z_0} \quad (f)$$

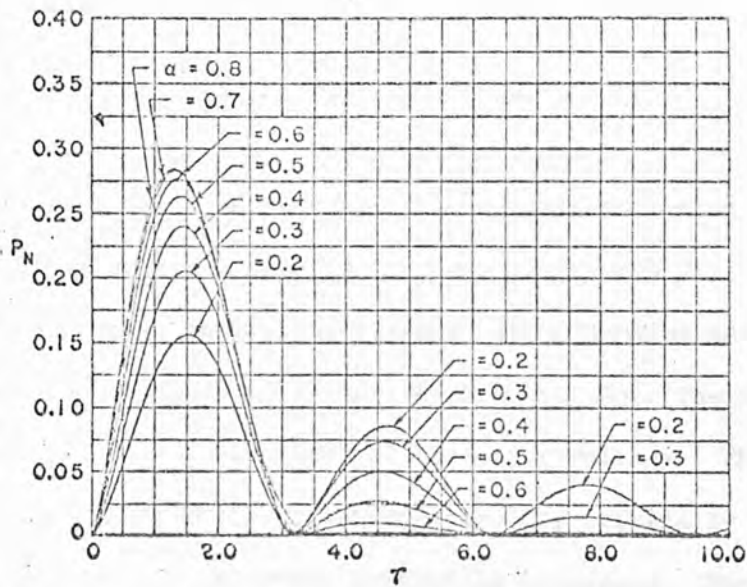


FIGURE 2.3: NORMALISED POWER VS NORMALISED TIME FOR VARIOUS VALUES OF THE DAMPING PARAMETERS  $\alpha$

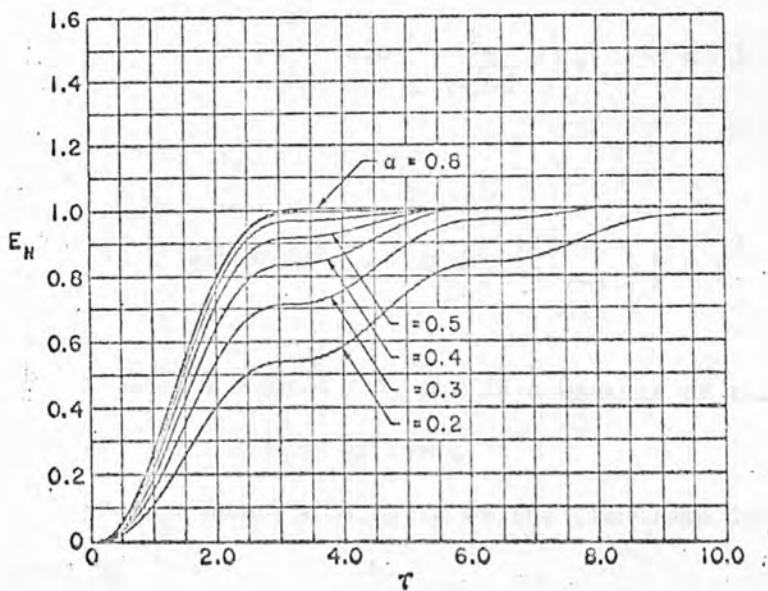


FIGURE 2.4: NORMALISED ENERGY VS NORMALISED TIME FOR VARIOUS VALUES OF DAMPING PARAMETERS  $\alpha$

and  $e = E_n \left( \frac{1}{2} C V_o^2 \right)$  (g) one obtains the relation

$$\frac{dI}{d\tau} + \alpha |I|^{\frac{1}{2}} + \frac{1}{\tau} \int_0^{\tau} I d\tau = 1$$

The solutions to this equation for the normalised current, normalised power and normalised energy transfer are shown in Figures 2.2, 2.3, 2.4. These solutions are given for various values of the damping parameter  $\alpha$ , and are shown as a function of the normalised time  $\tau$ . Note the damping parameter,  $\alpha$ , is dependent on  $V_o$ , the initial capacitor voltage. This is consistent with the experience that a discharge circuit, critically damped at one voltage, begins to ring as the voltage is increased. The power dissipated by the flashlamp as a function of time is given in Figure 2.3. The first half cycle of the function can be approximated quite well by <sup>(76)</sup>

$$p(\tau) = P_N(\alpha) \sin\left(\frac{\tau}{3} \pi\right), \tau \leq 3$$

or in unnormalised parameters

$$p(t) = P(\alpha) \frac{V_o^2}{Z_o} \sin\left(\frac{t}{3\sqrt{LC}} \pi\right), \quad t \leq 3\sqrt{LC}$$

$P(\alpha)$  is defined such that

$$\int_0^{3\sqrt{LC}} p(t') dt' = E_n \left( (\tau, \alpha) \Big|_{\tau=3} \right) \frac{1}{2} C V_o^2$$

where  $E_n(\tau)$  is shown in Figure 2.4, and is a measure of the energy transfer to the flashlamp as a function of time.

The average power dissipated by the flashlamp during the first cycle is given by

$$P_{av} = 0.638 P(\alpha) \frac{V_o^2}{Z_o}$$

Thus to maximise the average power (or peak power), neglecting other constraints, the initial capacitor voltage should be as large as possible and the circuit impedance  $z_o = \sqrt{L/C}$  should be as small as possible.

For the case  $t \ll 3\sqrt{LC}$  we obtain

$$p(t) \approx \frac{\pi}{3} P(\alpha) \frac{V_o^2}{L} t$$

This equation shows that for the maximum rate of rise of pump power,  $V_o^2$  and  $P(\alpha)$  should be large and the inductance of the system small. However, the self inductance of a flashlamp is proportional to its length, and its ability to dissipate energy is also proportional to its length. Consequently one cannot arbitrarily increase  $V_o$ , and with it the total energy dissipated by the lamp, and also decrease  $L$ , which decreases the ability of the lamp to withstand this energy. These relations must be optimised subject to additional restraints.

### 2.3 Design of flashlamp and circuitry for a dye laser

The design of the flashlamp and circuitry for a dye laser is greatly dependent upon whether or not the dye is subject to triplet state quenching. If that is not a problem, for the greatest peak laser power, one must achieve as high a peak pump power as possible. If the triplet state does quench the laser output, it will be advantageous to sacrifice high peak power to get a faster rate of rise.

An empirical relation which appears to describe the functional behaviour of a flashlamp explosion limit is <sup>(76)</sup>:

$$E_x = a \ell d (LC)^{\frac{1}{4}}$$

where  $\ell$  is the arc length in cms

$d$  is the diameter in cms

$L$  and  $C$  are the total inductance and capacity of the circuit and

a is a constant about  $6.8 \times 10^4 \text{ J cm}^{-2} \text{ s}^{-\frac{1}{2}}$ , which is found by measuring the explosion energy of any lamp. This equation determines the energy which, when dissipated in time  $3\sqrt{LC}$ , will explode one half of the flashlamps tested. It appears this relation holds very well for pulse length greater than  $10 \mu\text{s}$  and to be conservative for discharge times of  $1\text{-}2 \mu\text{s}$  in duration. The dependence of the explosion energy on the length of the discharge is particularly important. If one doubles the length of the discharge, the inductance increases approximately by a factor of two, which increases the risetime by a factor  $\sqrt{2}$ , while the energy which can be dissipated by the lamp doubles. It appears, therefore, that one can increase the pumping power output by  $\sqrt{2}$  by doubling the length of the lamp.

The authors<sup>(75)</sup> show that the peak power is

$$P_{\max} = P(\alpha) \frac{V_o^2}{Z_o} \approx \text{const} \frac{V_o^{3/2} \alpha^{5/6}}{\sqrt{L}}$$

indicating that for the highest power one should use as high a voltage as possible and choose a large value of  $\alpha$ .

The effect of a constant resistive circuit loss will produce an extra  $R_i$  term in the non linear differential equation for the circuit (equation 2.(1)). Markiewicz and Emmett<sup>(75)</sup> disregarded this term having showed that in any well designed circuit the pulse shape will deviate little from the case where the flashlamp is the only lossy element. They gave the limitations of equation 2.(1), the V-i characteristic of a linear xenon flashlamp, as being the neglect of two major lamp phenomenon - hysteresis in the V-i characteristic and the period during arc formation.

For any pulse length, there is always a small amount of hysteresis in the V-i characteristic, although it is not a problem for pulse durations from  $150 \mu\text{s}$  to  $4 \text{ ms}$ . It does, however, become noticeable for long pulses



(>5 ms), as the arc tends to remove material from the electrodes and walls, thus producing different arc characteristics. Hysteresis thus encountered during long pulses produces 10 to 20% deviation from 2.(1) although this is not usually sufficient to necessitate circuit redesign.

Hysteresis is a problem for short pulses where a major portion of the pulse time is spent in the transition of the discharge time from a small filament or streamer to an arc that fills the entire discharge volume available. For small lamps (diameter of discharge column  $d = 1-5$  mm) this time is of the order of 5 to 30  $\mu$ s. For larger lamps ( $d = 10-20$  mm) this might be as long as 50-125  $\mu$ s. For total pulse widths comparable to these numbers, the preceding analysis serves only as a good starting point for design. During the period of arc formation, either or both of the arc inductance  $L_a(t)$  and its time derivative  $L'_a(t)$  become important. (Assume  $L_a(t) = L_a$  at  $t = 0$  and  $L_a(t) = 0$  when the arc has reached the walls of the tube). The non linear differential equation showing dependence on these terms is

$$L \frac{di}{dt} + \frac{d}{dt} (L_a(t) i) \pm K_o |i|^{\frac{1}{2}} + \frac{1}{C} \int_0^t i dt = V_o$$

which can be expanded as

$$\left[ L + L_a(t) \right] \frac{di}{dt} + \left[ K_o + |i|^{\frac{1}{2}} \frac{d L_a(t)}{dt} \right] |i|^{\frac{1}{2}} + \frac{1}{C} \int_0^t i dt = V_o$$

In short pulse systems, where the total discharge circuit inductance is kept as small as possible, the inductance of the arc is important, and is usually included as the value of the full sized arc. However, initially it is larger due to the extremely small filament size. During the growth of the arc  $d L_a(t)/dt$  is a negative number. At high current, therefore, the term  $|i|^{\frac{1}{2}} d L_a(t)/dt$  can be quite significant. In fact, it is quite

usual in high power microsecond pulse systems to observe a negative voltage drop across the lamp during the first portion of the pulse. (A positive drop being the  $iR$  drop with respect to current direction). The measure of damping is  $\alpha = K_0 / (V_0 Z_0)^{1/2}$ . During arc formation  $Z > Z_0$  and also  $K$  can be  $< K_0$ . Both of these effects tend to produce a pulse that is more under damped than would be expected.

## CHAPTER III

### THE ELECTRICAL DRIVING SYSTEM

#### 3.1 Introduction

Very fast discharge systems have been successfully applied to  $H_2$ ,  $N_2$  and Ne high gain lasers. The excitation of a self terminating superradiant gas laser required the production of a discharge with a high current density established with an extremely fast initial rise. These systems consist of an energy storage unit, a pulse forming network and a laser tube. The components of the system are interdependent and several design combinations may be found in the literature. The more recent systems involve the successful application of modified Blumlein circuits for high gain  $H_2$ ,  $N_2$  and Ne pulsed lasers<sup>(82-86)</sup>.

The system used for the present work was a modified Blumlein circuit not previously used. It formed the driving circuit for both linear and coaxial flashtubes and a gas cell. The flashlamps were used to excite an organic dye but could have also been used for exciting a ruby rod for example, or as a flashlight for flash photolysis. The gas cell was used in conjunction with  $N_2$  to produce a superradiant laser operating at  $3371 \text{ \AA}$ .

#### 3.2 The Blumlein system

The Blumlein system<sup>(86)</sup>, patented under the heading "Improvements in or relating to apparatus for generating electrical impulses", by Alan Dower Blumlein, consists of capacitors and inductors constituting an artificial transmission line which is charged, and then shorted to obtain a pulse of length equal to the propagation time of the discharge wave down the line. The original generator was designed to drive a magnetron for use in radar.

Figure 3.1 shows a schematic diagram of the pulse generator originally used. The circuit is arranged so that a positive voltage developed across the transformer, 6, from ac supply causes current to flow

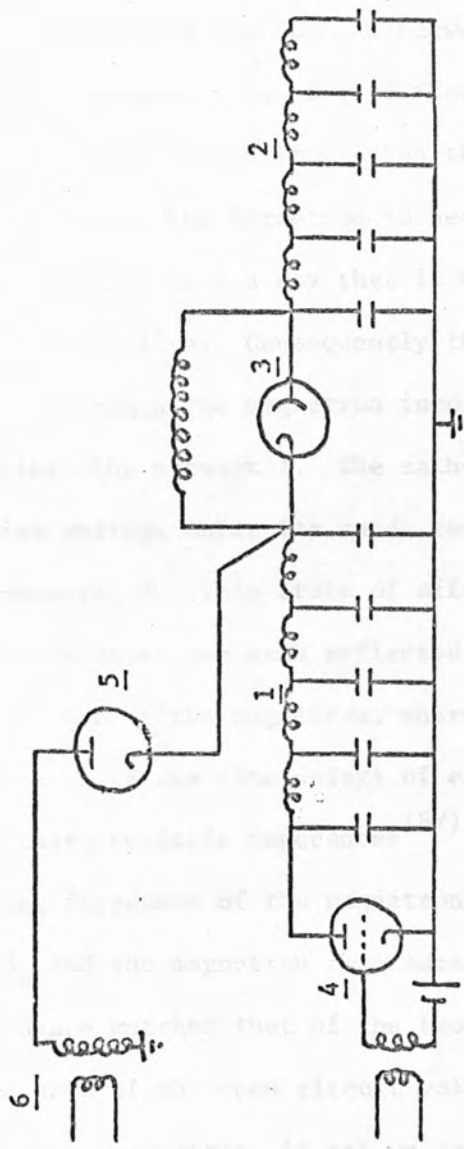


FIGURE 3.1: SCHEMATIC DIAGRAM OF ORIGINAL PULSE GENERATOR

through the diode, 5, which charges the capacitors in the two time delay networks 1 and 2. After the capacitors have been charged and the voltage across the transformer has become negative to render the diode non conducting a trigger pulse is applied to the grid of the thyatron, 4. The trigger pulse causes the anode impedance to fall to a very low value enabling the voltage across the left hand side of the network to fall rapidly to zero. This falling voltage propagates as a wave from the left hand side of the network towards the right. When it reaches the magnetron (3) it is reflected in reversed sense causing the magnetron to become conducting, since the magnetron is connected in such a way that it will only absorb energy when the voltage becomes negative. Consequently the original voltage drop is partly transmitted through the magnetron into the network, 2, and partly reflected back into the network 1. The cathode of the magnetron is thus held at a negative voltage while its anode remains positive due to the voltage on the network, 2. This state of affairs persists until the transmitted and reflected waves are each reflected at the respective ends of the network and return to the magnetron, whereupon the voltage across the magnetron collapses. If the time delays of each of the networks are made equal and their characteristic impedances<sup>(87)</sup> are arranged to be equal to half the operating impedance of the magnetron, (ie each arm of the network with impedance  $Z_0$  and the magnetron impedance  $2Z_0$ ), then as it draws current its impedance matches that of the two networks in series. Consequently one half of the open circuit voltage which would be developed in the absence of the magnetron, is set up across the magnetron. Thus, with this arrangement the voltage developed across the magnetron is doubled and becomes substantially equal to that which each of the networks were charged. In other words, if each arm of the network was charged to a voltage  $V$ , after being triggered a voltage of magnitude  $2V$  will be developed

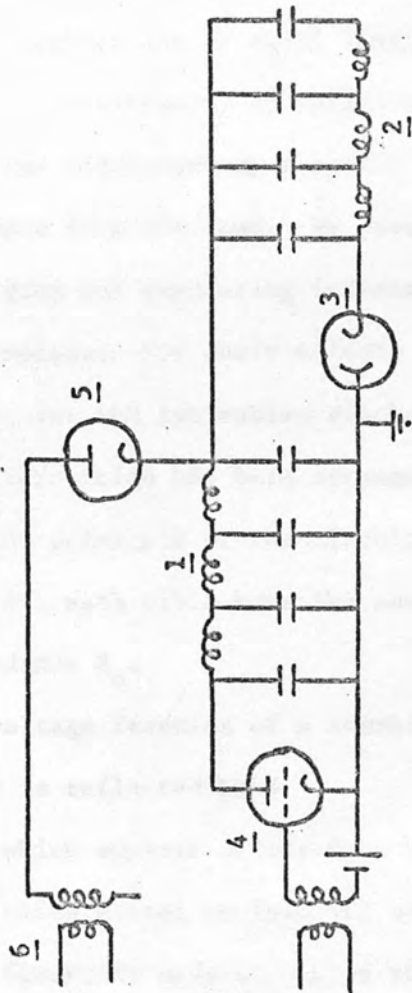


FIGURE 3.2: SCHEMATIC DIAGRAM OF ORIGINAL PULSE GENERATOR WITH MAGNETRON CATHODE EARTHED



across the magnetron until it starts conducting whereupon the voltage will fall to  $V$ . It should be noted here that the magnetron could be transferred from the high voltage line to the earthed line of the network (so that the anode of the magnetron is earthed, as shown in Figure 3.2).

### 3.3 Pulse performance when discharging two cables in Blumlein connection into a mismatched resistance load

A practical form of the original Blumlein circuit<sup>(88)</sup> is shown in Figure 3.3. Both coaxial cables are of equal length and impedance and are connected so that the load is virtually in series with them. The cables are charged in parallel and discharged by a switch placed directly across one cable at the end remote from the load. We assume that the cables are ideal, and that the charging and separating inductance and damping circuits have sufficiently high impedance for their effects to be ignored. In order to simplify the analysis, let the two cables discharge into a linear resistance load in a circuit which has been arranged as shown Figure 3.4. This in no way affects the principle of the circuit<sup>(88)</sup>. Let both cables be charged to a voltage  $+E$ , each cable have the same transit time  $T$ , and the same characteristic impedance  $Z_0$ .

Let (i) the voltage fraction of a travelling wave approaching  $R$  which is reflected be  $\beta$

(ii) that which appears across  $R$  be  $\gamma$

(iii) that which passes on into the other cable be  $\delta$

Then applying Kirchoffs Laws it can be shown in this case

$$\beta = \frac{R}{R + 2Z_0} \quad \gamma = + \frac{2R}{R + 2Z_0} \quad \delta = \frac{2Z_0}{R + 2Z_0} \quad \dots (1)$$

(if  $\gamma$  is considered positive for a wave approaching from the left, it must be negative for a wave approaching from the right).

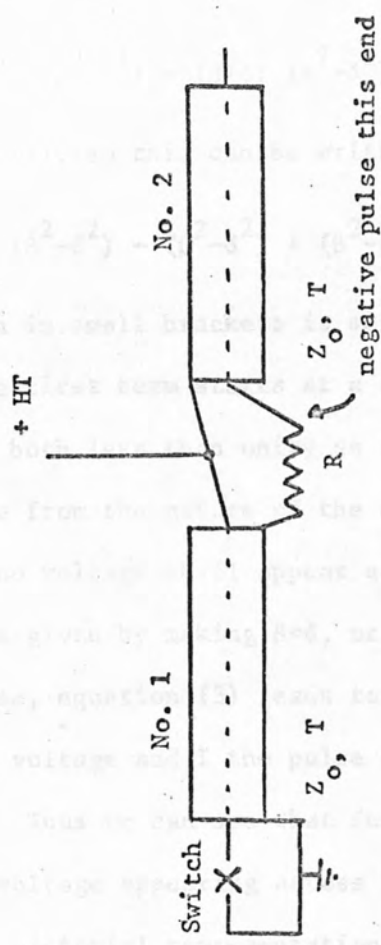


FIGURE 3.3: BLUMLEIN CONNECTION OF TWO CABLES IN A PRACTICAL FORM

A wave approaching the right hand or open end of cable 2 is reflected with coefficient +1 for voltage and -1 for current, and a wave approaching the left hand spark gap closed end of number 1 cable is reflected with the coefficient -1 for voltage and +1 for current (see Appendix III). The initial travelling wave which starts from the switch has voltage amplitude -E and by reference to a time lattice diagram (Figure 3.4) of the type due to L V Bewley, it can be seen that the voltage V appearing across the load is given by

$$V = -E\gamma \left[ 1 - (\beta+\delta) + (\beta^2-\delta^2) - (\beta+\delta)(\beta^2-\delta^2) + (\beta^2-\delta^2)^2 + \dots \right] \dots (2)$$

But  $\beta+\delta = 1$  (from (1)), so this can be written

$$V = -E\gamma \left[ (1)-(1) + (\beta^2-\delta^2) - (\beta^2-\delta^2) + (\beta^2-\delta^2)^2 - (\beta^2-\delta^2)^2 + \dots \right] \dots (3)$$

where each expression in small brackets is separated from the one before it by a time  $2T$ , and the first term starts at a time  $T$  after the switch first closes.  $\beta$  and  $\delta$  are both less than unity so the series converges, or is damped, as it must be from the nature of the circuit. The special matched load condition that no voltage shall appear across R, after the first rectangular pulse, is given by making  $\beta=\delta$ , or  $R = 2Z_0$  (from (1) and (3)). During the first pulse, equation (3) leads to the relationship  $2E = V + 2Z_0I$ , where V is the pulse voltage and I the pulse current. (Equation obtained by substituting for  $\gamma$ ). Thus we can see that for no current flowing through the load, the pulse voltage appearing across the load is equal to twice the charging voltage. A pictorial representation of Blumlein circuit action with a matched load is given in Figure 3.5. It shows a space/time picture of voltage and current conditions when two cables in Blumlein connection are discharged into a matched resistance load.

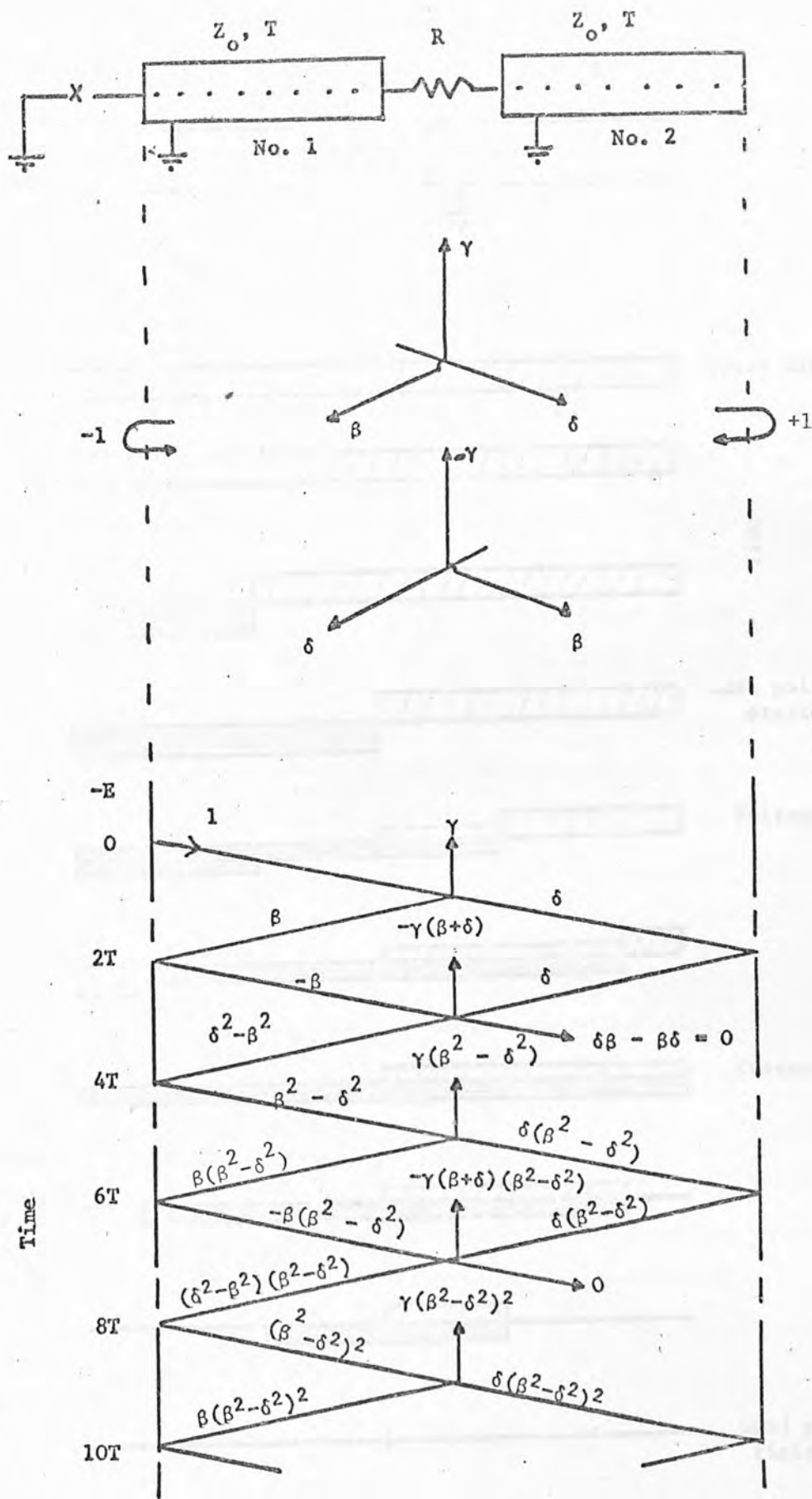


FIGURE 3.4: LATTICE DIAGRAM OF DISCHARGE OF BLUMLEIN CABLE CIRCUIT INTO RESISTANCE LOAD

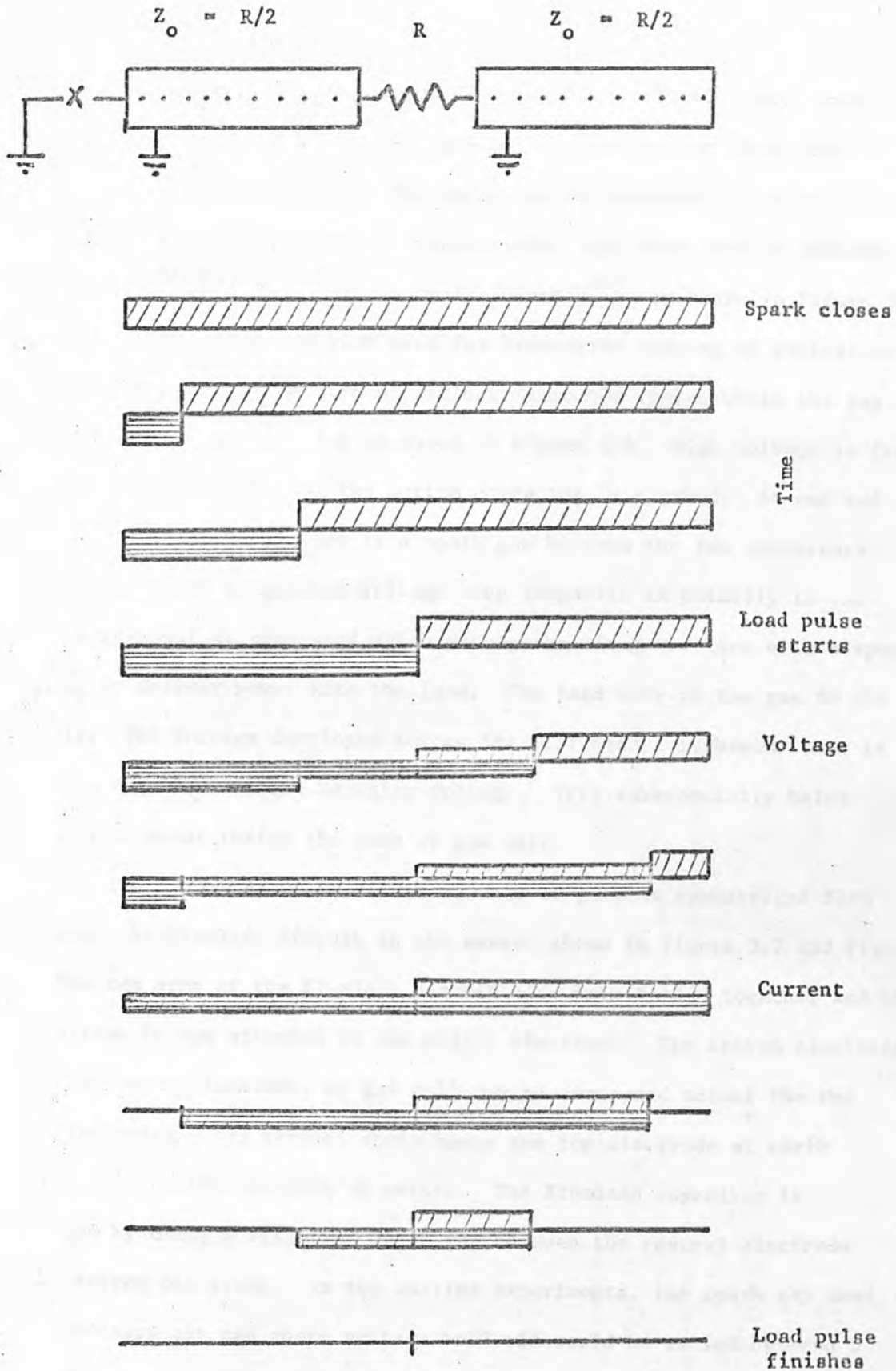


FIGURE 3.5: A SPACE/TIME PICTURE OF VOLTAGE AND CURRENT CONDITIONS WHEN TWO CABLES IN BLUMLEIN CONNECTION ARE DISCHARGED INTO A MATCHED RESISTANCE LOAD

### 3.4 Modified Blumlein pulser

The energy storing capacitor used in the following experiment is a specially designed strip line type of Blumlein pulser where the transmission lines are made of thin metal sheets insulated by solid dielectric. Blumlein pulsers of various types have been used by workers in the past<sup>(89)(82)(83)(84)</sup> and a typical system<sup>(82)</sup> is shown in Figure 3.6. Generally, this system has been used for transverse pumping or excitation of a gas confined by some form of dielectric to the region where the gap is cut into the top conductor as shown in Figure 3.6. High voltage is fed into the top conductor, and the bottom conductor is earthed. At one end of the system, usually, there is a spark gap between the two conductors. When the spark gap triggers a voltage step (opposite in polarity to the charging voltage) is generated which propagates along the line with a speed of  $C/\sqrt{\epsilon_r}$  to deliver power into the load. The load here is the gas in the gas cell. The voltage developed across the cell before it breaks down is twice the magnitude of the charging voltage. This substantially helps breakdown to occur inside the tube or gas cell.

The system shown in Figure 3.6 may be given a symmetrical form by folding the Blumlein circuit in the manner shown in Figure 3.7 and Figure 3.8. The two arms of the Blumlein circuit have been folded together and the high voltage is now attached to the middle electrode. The bottom electrode is earthed and a flashtube, or gas cell may be connected across the two outer electrodes. The bleeder chain keeps the top electrode at earth potential during the charging up period. The Blumlein capacitor is discharged by using a triggered spark gap between the central electrode and the bottom electrode. In the earlier experiments, the spark gap used was an ordinary air gap where voltage hold off could be varied between 5 and 15 kV. For the later experiments a triggered and pressurised multi-



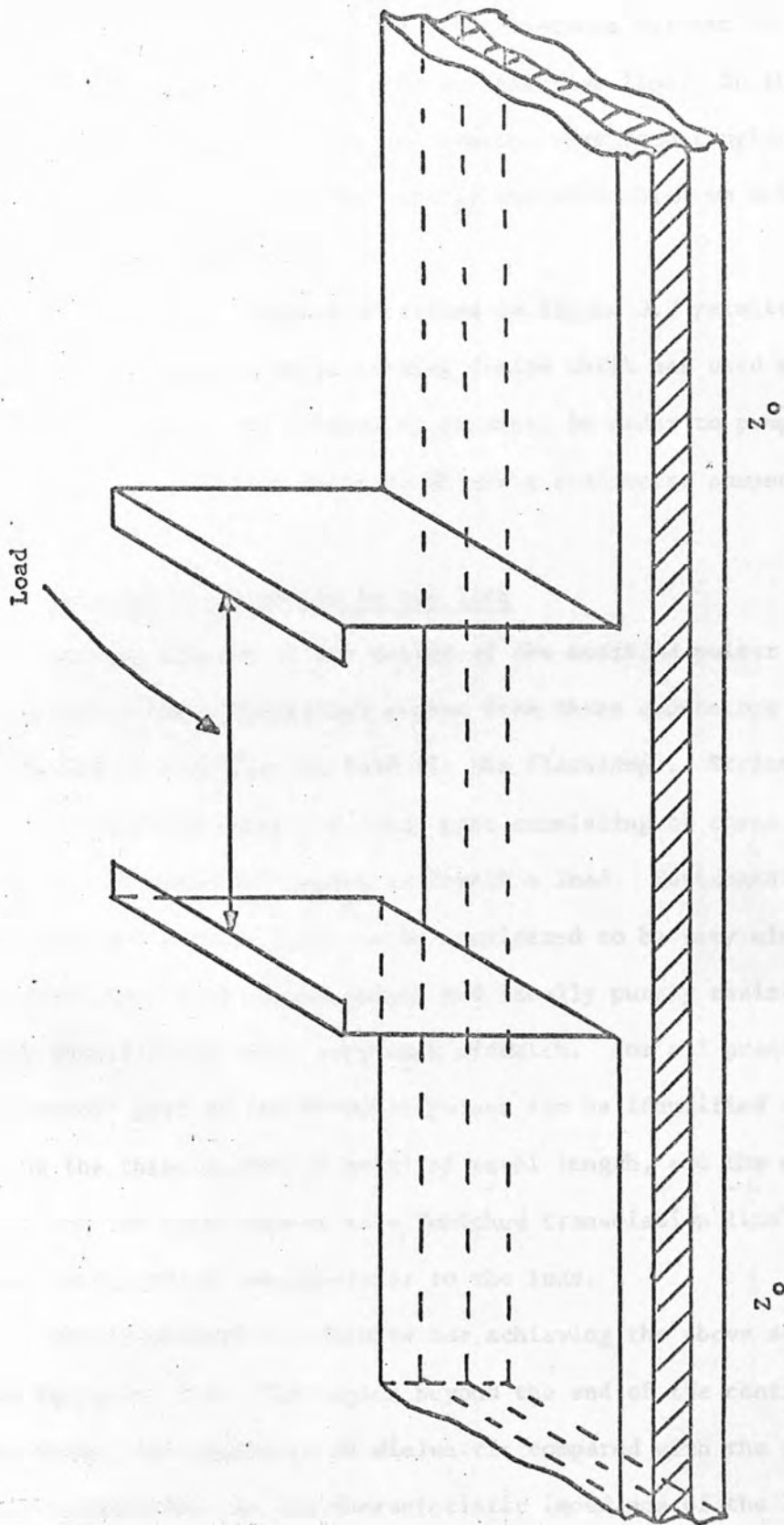


FIGURE 3.6: MODIFIED BLUMLEIN (Small and Ashari)

channel spark gap was used. The amount of energy that is stored in this system for a given voltage and for a fixed distance between the two conductors depends on the area of the transmission line. In the work reported here four slightly different systems were used ranging from a prototype low energy one to a high energy one with which we achieved lasing action from Rh 6G in methanol.

The modified Blumlein described in Figure 3.7 permitted the construction of a compact pulse forming device which was used with slight adaptations, with linear and coaxial flashlamps, in order to pump an organic dye, and with a gas cell in order to obtain a transverse pumped nitrogen laser.

### 3.5 Matching the Blumlein to the load

Looking closely at the design of the modified pulser shown in Figure 3.7 indicates a transition region from three conductors to two conductors before reaching the load (ie the flashlamp). Strictly speaking to the Blumlein pulse generator (that part consisting of three conductors), the extended two conductor region is itself a load. Fortunately, by simple careful construction this load can be considered to be very closely matched to the output impedance of the pulser and ideally purely resistive. Therefore this should not produce very much mismatch. For all practical purposes, the "generator" part of the Blumlein pulser can be identified as the part containing the three sheets of metal of equal length, and the extended region of the two outer sheets as a "matched transmission line" to carry the power delivered by the generator to the load.

The constructional details for achieving the above state of affairs is shown in Figure 3.8. The region beyond the end of the centre conductor contains double the thickness of dielectric compared with the gap between the other conductors. As the characteristic impedance of the line can be

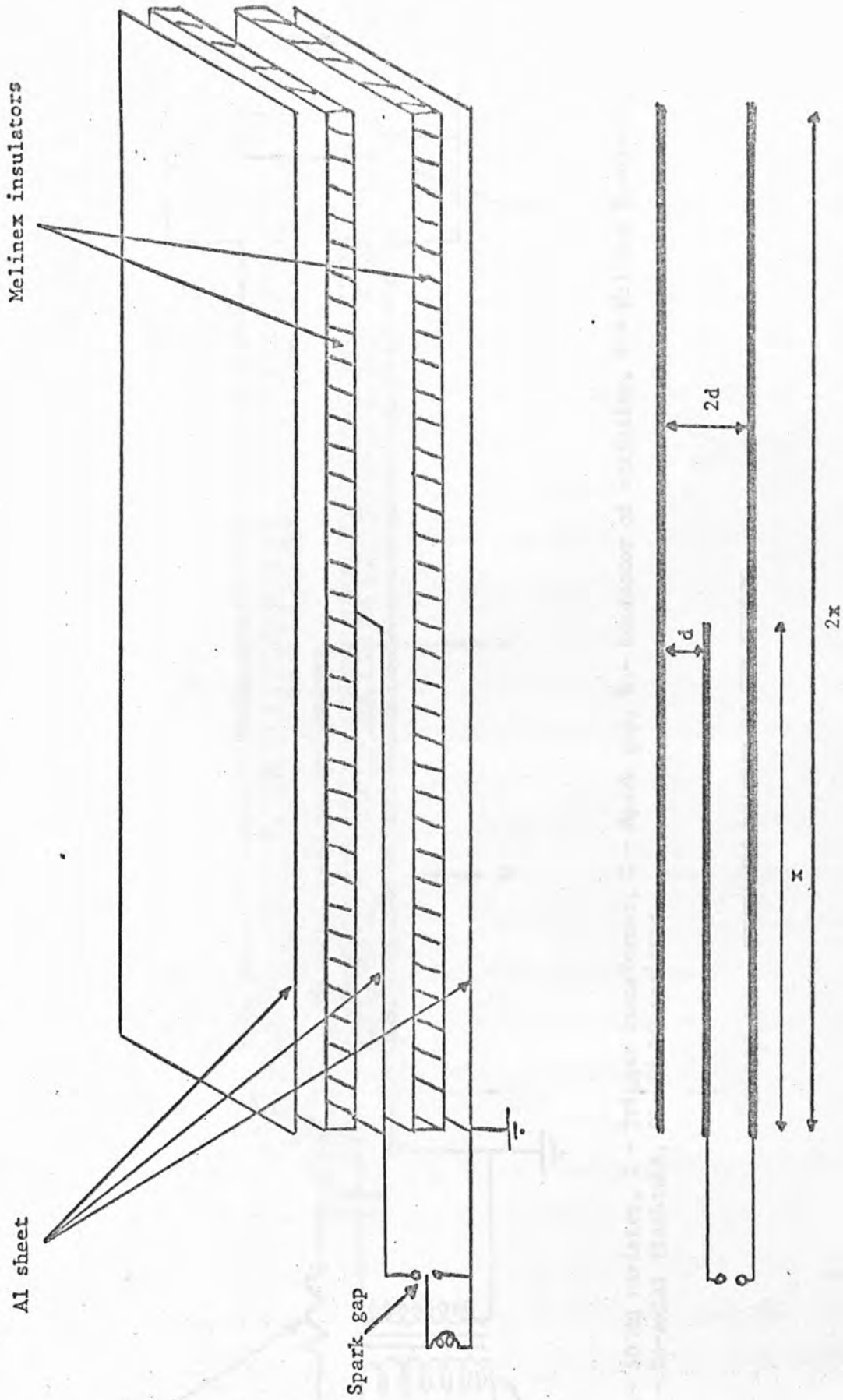
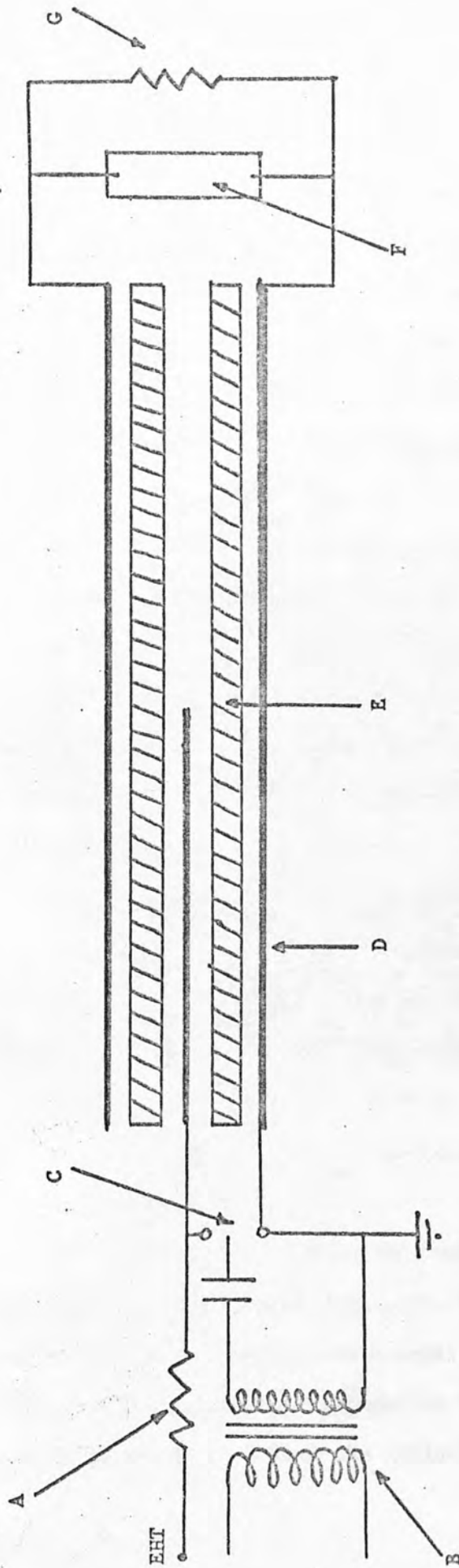


FIGURE 3.7: MODIFIED BLUMLEIN (our design)

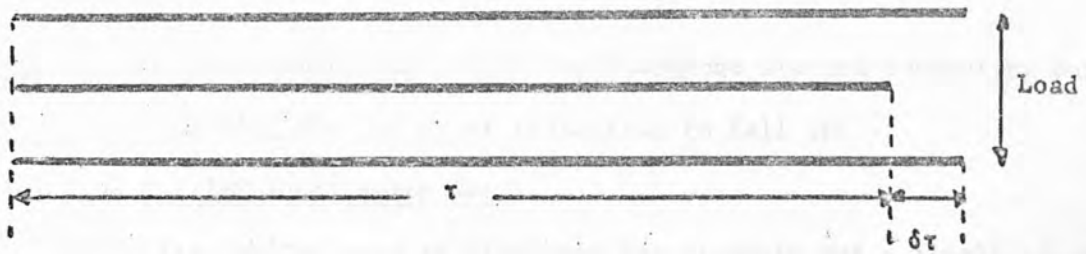


A - 50 MΩ resistor, B - Trigger transformer, C - Spark gap, D - Conductor of stripline, E - Melinex insulator, F - Co-axial flashtube, G - 25 kΩ resistor.

FIGURE 3.8: SCHEMATIC DIAGRAM OF THE SYSTEM

written  $Z_0 = 377 / \epsilon_{rel}^{1/2} (d/\omega)$  ohms where  $\epsilon_{rel}$  is the relative permittivity of the dielectric,  $d$  is the thickness of the dielectric and  $\omega$  the width of the conductor then we see that by increasing  $d$  to  $2d$  (as we have done in the extended two conductor region) we have increased the characteristic impedance from  $Z_0$  to  $2Z_0$ . Work carried out involved the use of a Blumlein pulser with the central conductor nearly the same length as the other two conductors, and the centre conductor only half the length of the other two conductors. As the loads we used were never matched to the transmission line there existed reflected pulses. The effect of the differing transmission line length to generator length on the separation of electrical pulses delivered to the load is explained with the aid of figure 3.9. In Figure 3.9 the centre conductor is almost the same length as the outer two conductors. In this diagram, let the transit time of the voltage pulse from the spark gap where it was initiated, to the end of the middle conductor be  $\tau$ . This can be regarded as a Blumlein generator driving a matched load and will yield a rectangular pulse of duration  $2\tau$  as was shown earlier. The transmission line for this system is very short and the transit time of the voltage pulse between the generator and the load (flashlamp for example) is considerably smaller and will be denoted  $\delta\tau$ . For such an example, Figure 3.9 shows the time scales involved for the initial and first reflected electrical pulse being delivered to the load from the initiation of the spark gap. As can be seen, the reflected pulse closely follows the initial pulse.

Referring to Figure 3.10, where the length of the generator is the same as the length of the transmission line, we can see that the initial and reflected pulse are separated by a time equal to the duration of the electrical pulse. This is useful for separating the fast from the slow processes in a gas discharge. In fact the reflected pulse would not have a



S G Breakdown

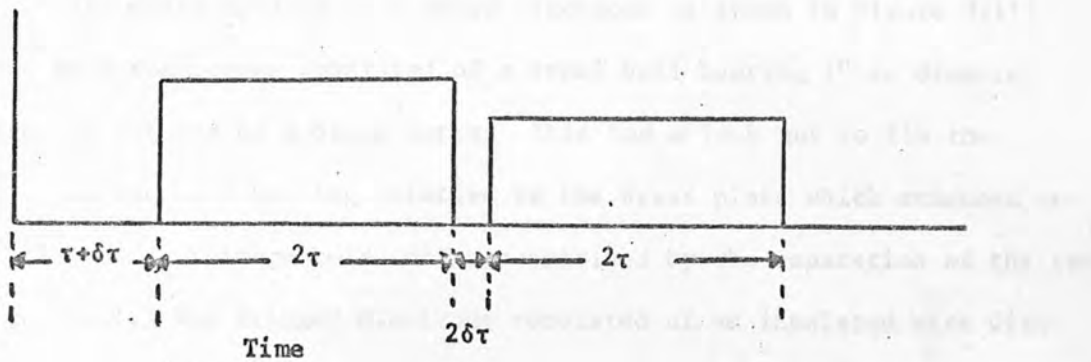
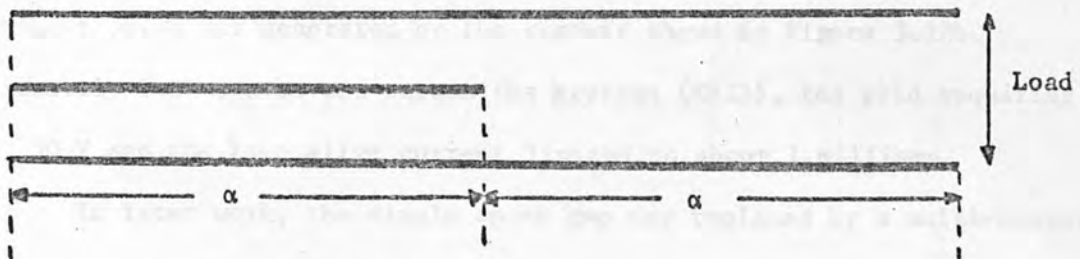


FIGURE 3.9: SCHEMATIC DIAGRAM SHOWING SEPARATION OF INITIAL AND REFLECTED ELECTRICAL PULSE ACROSS THE LOAD FOR THE SYSTEM WITH 3 CONDUCTORS ALMOST THE SAME LENGTH.



S G Breakdown

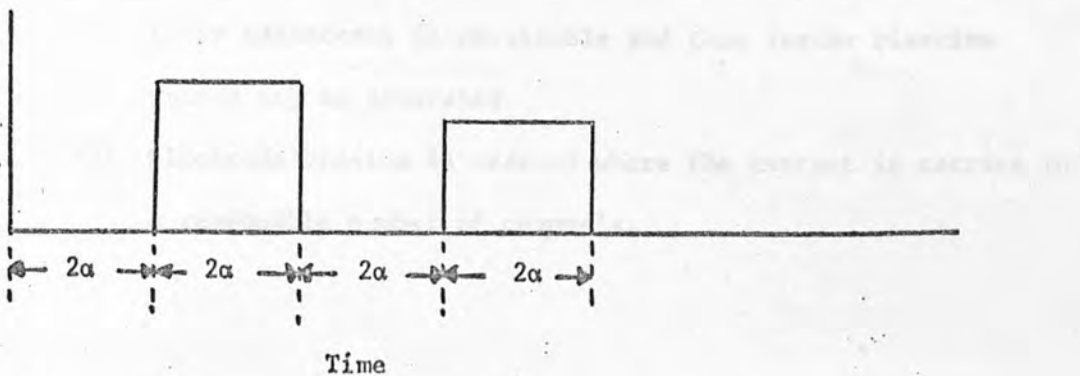


FIGURE 3.10: SCHEMATIC DIAGRAM SHOWING SEPARATION OF INITIAL AND REFLECTED PULSE ACROSS THE LOAD FOR THE SYSTEM WITH THE CENTRE CONDUCTOR HALF THE LENGTH OF THE OUTER CONDUCTORS.



rectangular shape but would tail off if the flashtube started conducting during the first pulse causing the amount of reflection to fall off.

### 3.6 The Multi-Channel Spark Gap

The first switch used to discharge the Blumlein was a single spark gap operating at atmospheric pressure in air triggered by a fast rising high voltage pulse applied to a third electrode as shown in Figure 3(11). The two main electrodes consisted of a steel ball bearing  $\frac{1}{4}$ " in diameter soldered to the end of a brass screw. This had a lock nut to fix the position of the ball bearing relative to the brass plate which attached to the strip line. Voltage hold off was obtained by the separation of the two ball bearings. The trigger electrode consisted of an insulated wire with an uninsulated pointed end. This was passed down the centre of the earth side electrode which had been drilled out as shown in Figure 3.11. The electronic driving units for the system are shown in Figures 3.12 and 3.12b. The centre conductor of the Blumlein pulser was charged through a current limiting resistance ( $\sim 1 \text{ M}\Omega$ ) by a Brandenburg high voltage power supply. The trigger pulse was generated by the circuit shown in Figure 3.12b. Approximately 5 kV can be put across the krytron (KN22), the grid requiring about 750 V and the keep alive current limited to about 1 milliamp.

In later work, the single spark gap was replaced by a multi-channel spark gap where voltage hold off was adjusted by differences in pressure within the gap. The main advantages of a multi-channel spark gap are<sup>(90)</sup>

- (1) Lower inductance is obtainable and thus faster risetime pulses may be generated.
- (2) Electrode erosion is reduced where the current is carried in a reasonable number of channels.

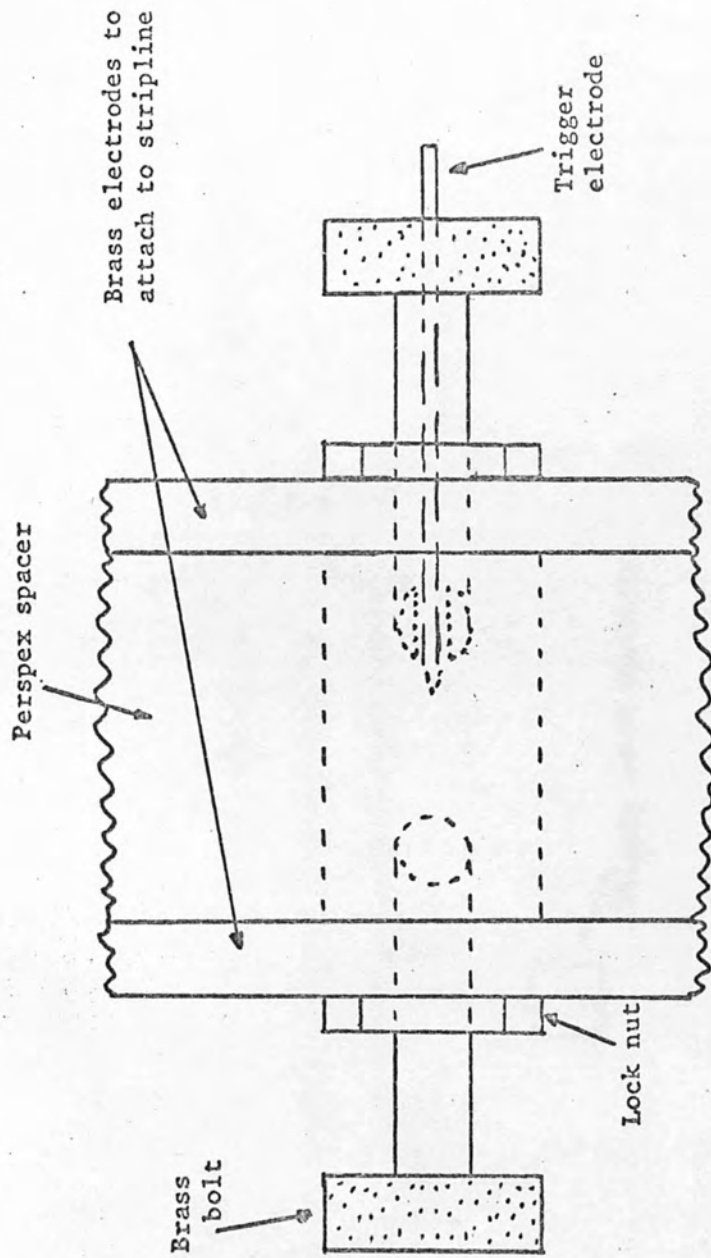


FIGURE 3.11: SINGLE SPARK GAP ARRANGEMENT

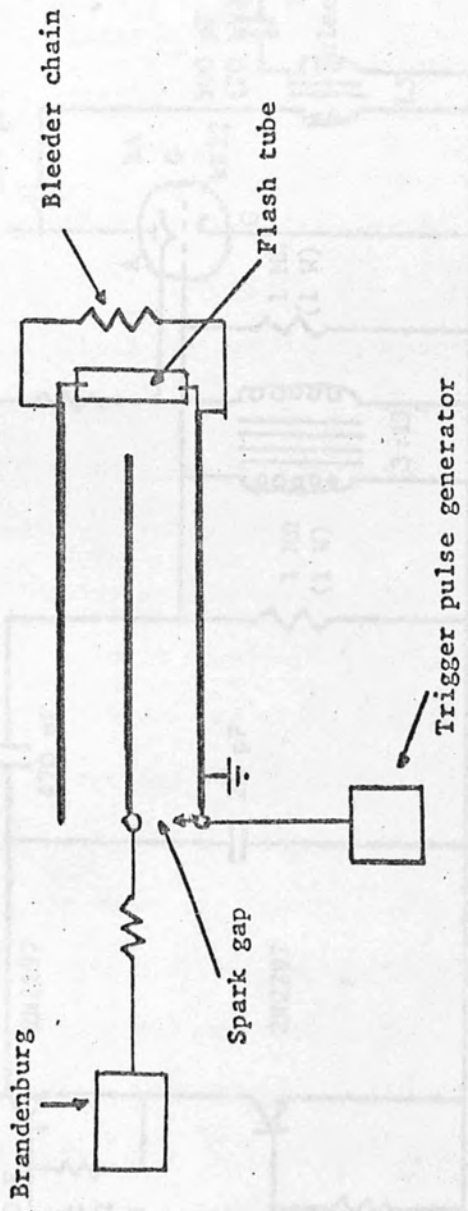


FIGURE 3.12a: SCHEMATIC DIAGRAM OF SYSTEM

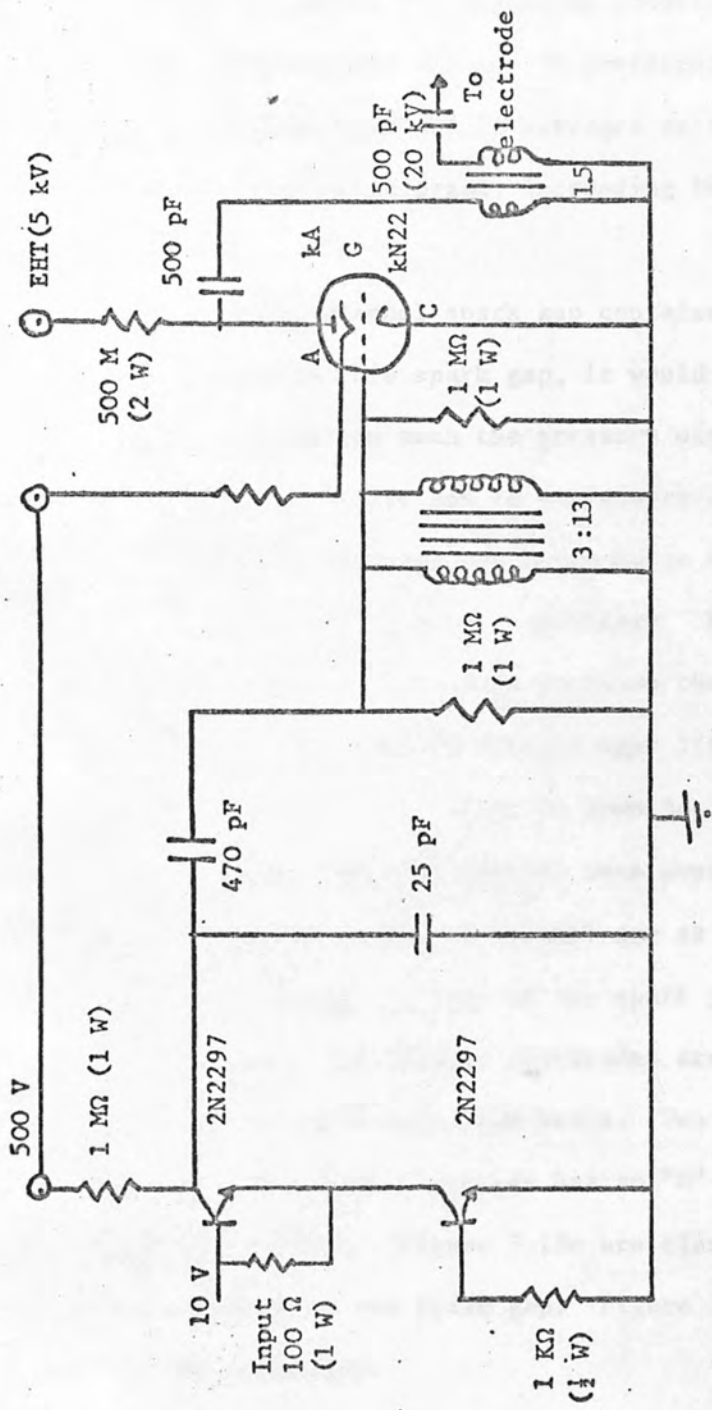


FIGURE 3.12b: TRIGGER PULSE GENERATOR

To achieve multi-channel operation, the gap between each pair of electrodes should be made equal as accurately as possible. Thus, altering the gap hold off voltage by increasing the space between the electrodes was no longer a viable proposition. Therefore we used the change of pressure inside the spark gap to adjust the breakdown potential. Industrial grade nitrogen was used to pressurise the gap in preference to argon - the other gas we tried. The voltage hold off of nitrogen decreased by a lesser amount per shot than that using argon, increasing the working life of the gap between overhauls.

The first multi-channel spark gap contained five electrode pairs. After about 200 shots with this spark gap, it would no longer hold off the required voltage no matter how much the pressure within the spark gap was increased. Evacuating the spark gap to a pressure of about a torr for approximately ten minutes restored the performance of the spark gap to within a few per cent of its original capability. However, as this had to be done fairly frequently we decided to increase the number of electrode pairs to 10. This gap had a considerably longer lifetime and was used for eighteen months without having to strip it down for cleaning. It was evacuated to about a torr for five minutes once every two weeks. The plans detailing the construction of the 10 channel gap as shown in Figure 3.13 a,b,c,d. Figure 3.13a shows the body of the spark gap made from perspex. Holes for main electrodes and trigger electrodes are shown. Figure 3.13b shows the main electrode unit made from brass. Two of these are made, one for each Blumlein plate. Each electrode has an "O" ring seal so that the spark gap can be pressurised. Figure 3.13c are clamping plates to hold the Blumlein sheets securely to the spark gap. Figure 3.13d shows the assembling arrangement for the spark gap.

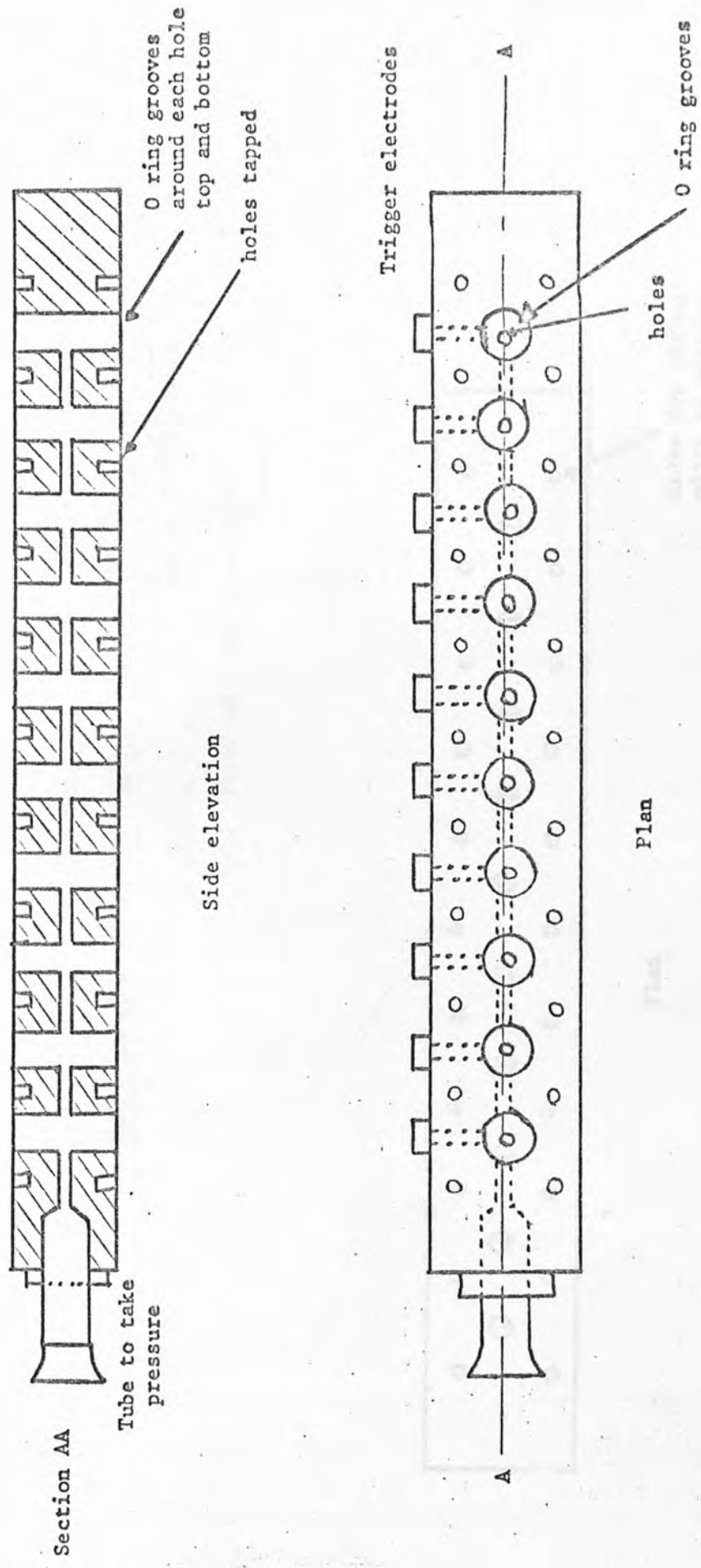


FIGURE 3.13a: MULTI-CHANNEL SPARK GAP

1/2 scale



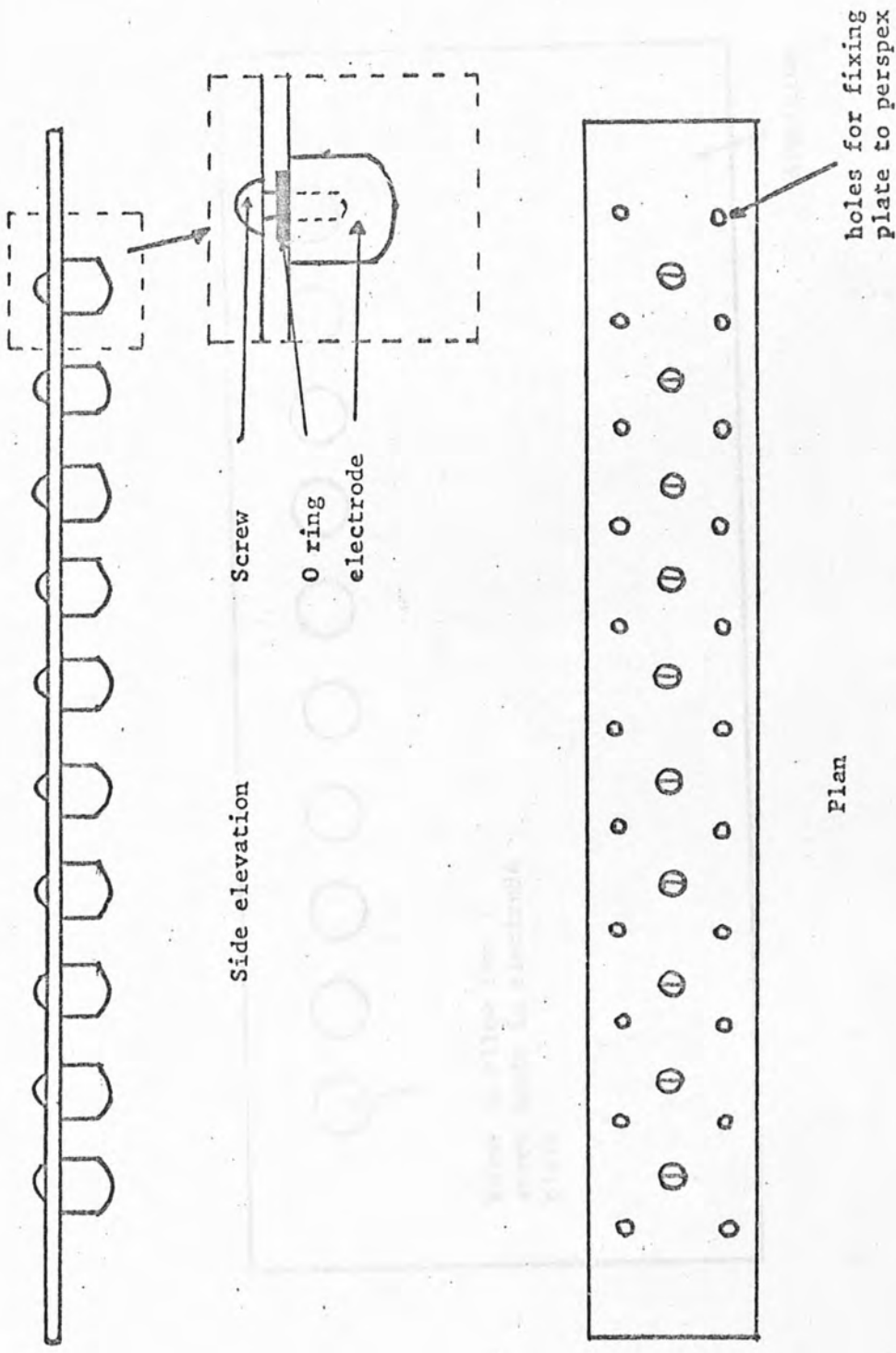


FIGURE 3.13b: BRASS PLATES INCORPORATING SPARK GAP ELECTRODES  $\frac{1}{4}$  scale

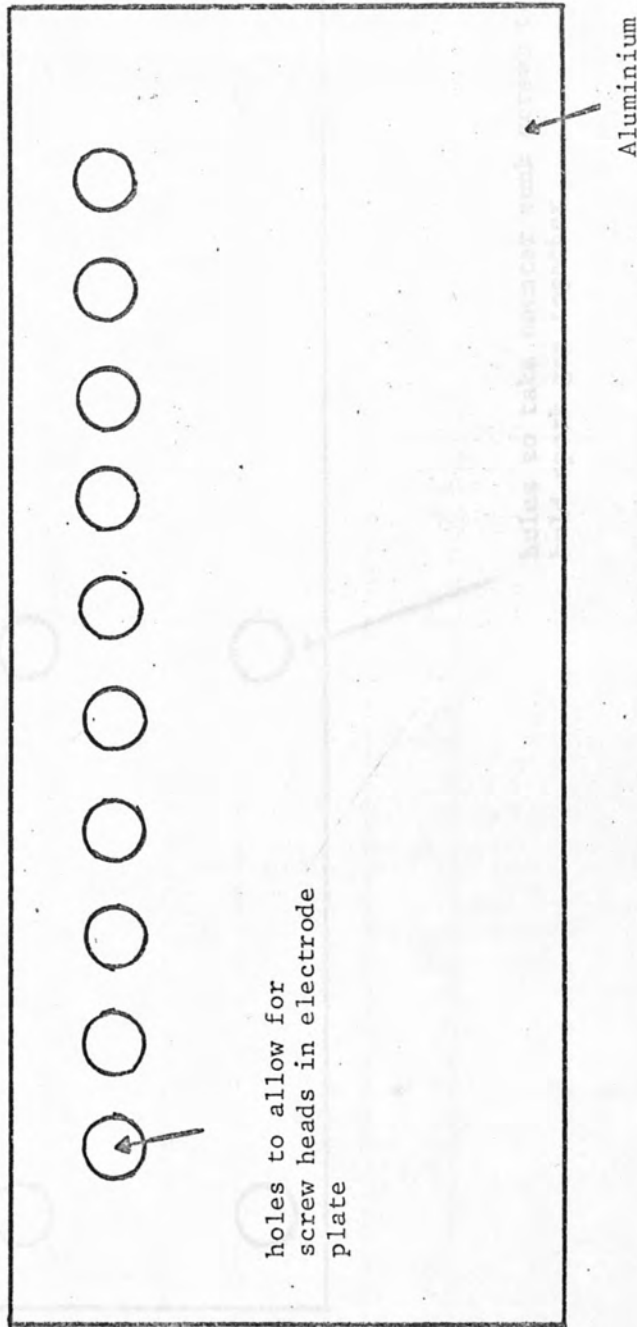


FIGURE 3.13c: PLATE TO GO ON TOP OF ELECTRODE PLATE

$\frac{1}{2}$  scale

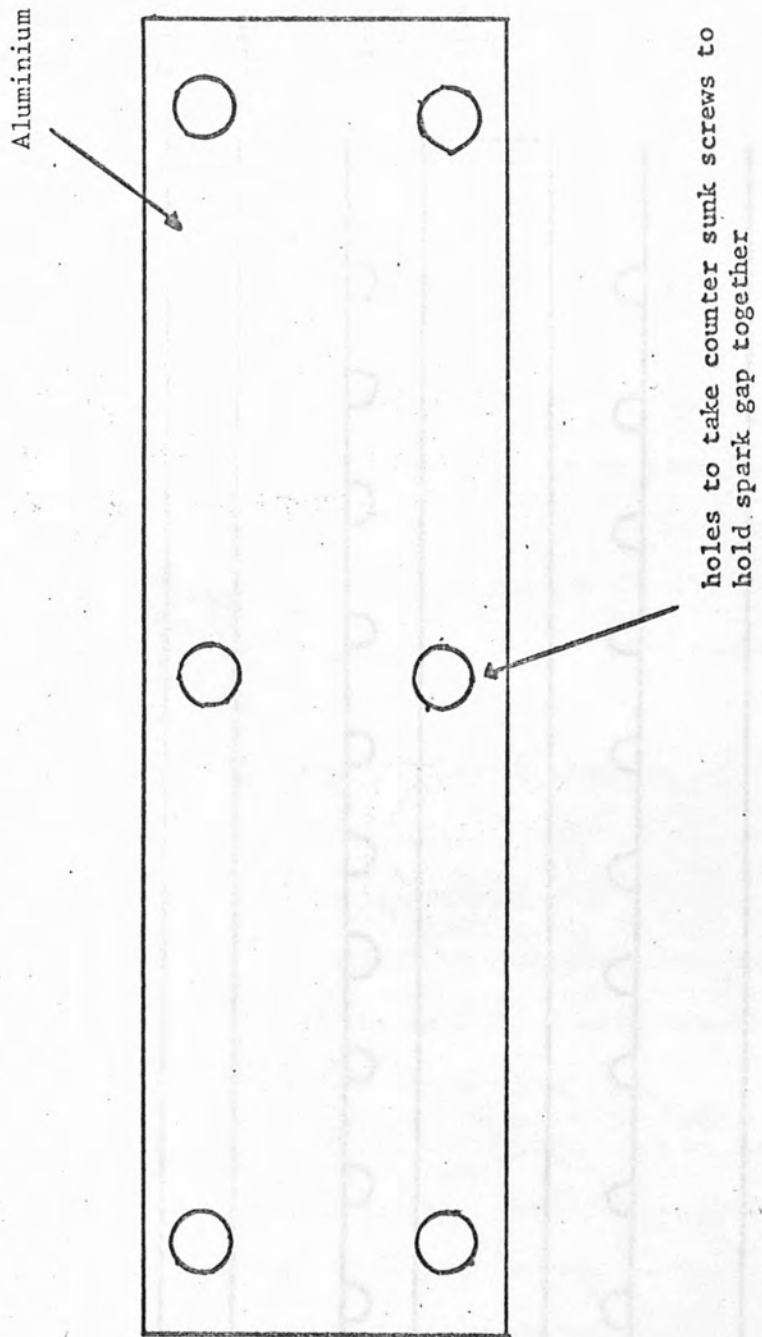


FIGURE 3.13 d: CLAMP ON PLATE

Clamping plate

Spacer plate

Electrode plate

Perspex with holes

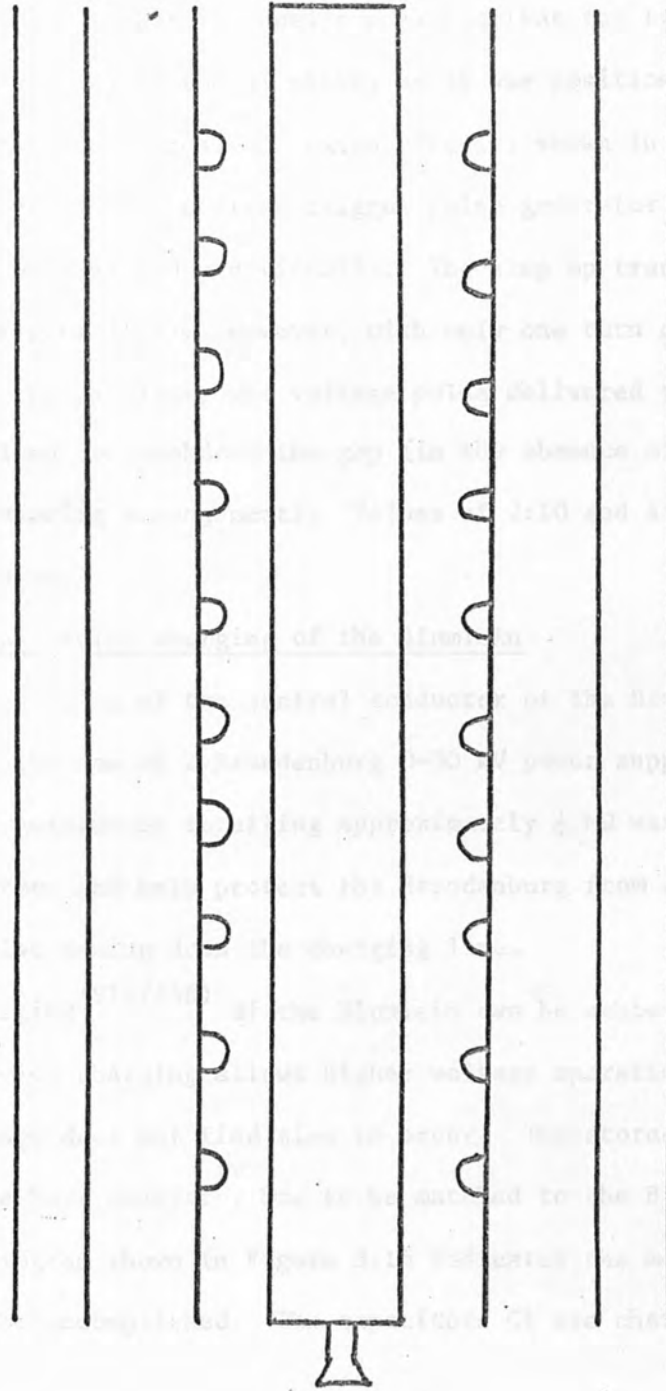


FIGURE 3.13e: ASSEMBLING ARRANGEMENT

Photograph, P1 shows a part of the 10 channel gap and photograph P2 shows the 5 channel gap in operation. The photographically integrated light output should be proportional to the energy deposited in the channel<sup>(60)</sup> showing, in photograph P2, that each gap was doing its fair share of the work.

The same trigger pulse generator as used on the earlier spark gap was used for the multi channel gap except that the trigger pin was biased to half the potential of the HT plate, as it was positioned half way between the HT and earth electrodes. An extra circuit, shown in Figure 3.14, was added to the output of the first trigger pulse generator so that the ten trigger pins could be fed individually. The step up transformer ratio was five to one (Figure 3.14). However, with only one turn on the primary and five turns on the secondary the voltage pulse delivered to the trigger electrodes failed to breakdown the gap (in the absence of any HT on the Blumlein and biasing arrangement). Values of 2:10 and 4:20 were, however, used successfully.

### 3.7 DC and Pulse charging of the Blumlein

DC charging of the central conductor of the Blumlein pulser was achieved with the use of a Brandenburg 0-30 kV power supply. A series of high voltage resistances totalling approximately  $\frac{1}{2}$  M $\Omega$  was used to limit the charging rate and help protect the Brandenburg from any reflected electrical pulse coming down the charging line.

Pulse charging<sup>(91)(146)</sup> of the Blumlein can be achieved using a Marx Generator. Pulse charging allows higher voltage operation of the system as corona damage does not find time to occur. The stored charge and pulsed voltage of the Marx Generator has to be matched to the Blumlein Capacitor. The circuit diagram shown in Figure 3.15 indicates the method by which pulse charging may be accomplished. The capacitors C1 are charged in parallel

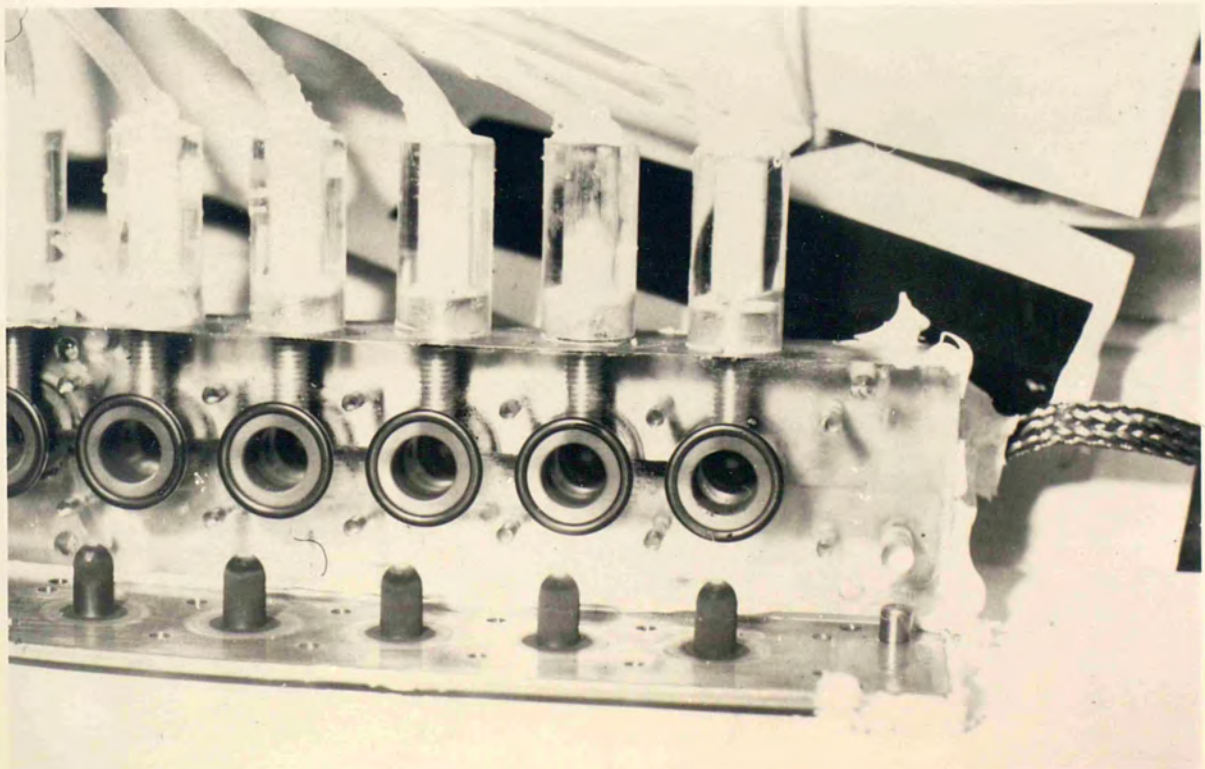
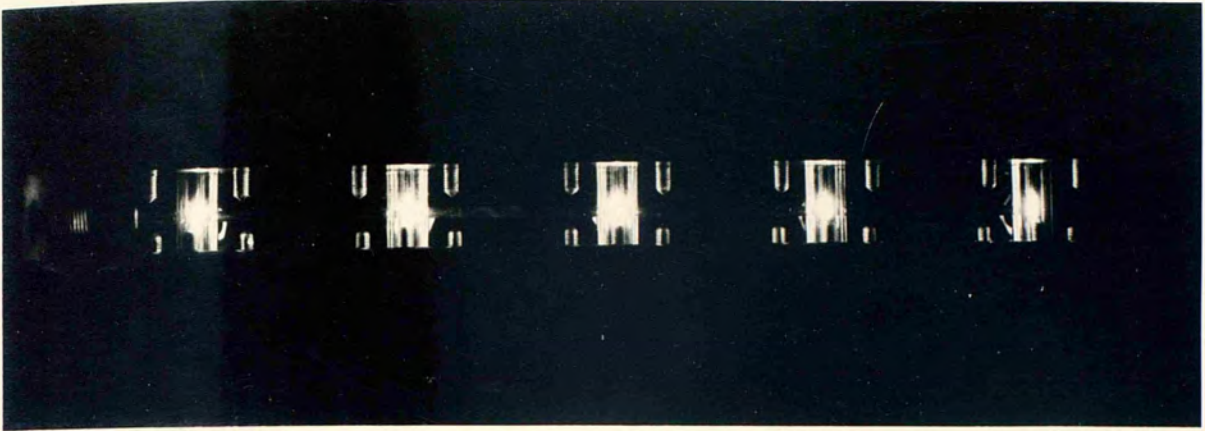
Photograph P2

The five channel spark gap in operation. The photographically light integrated output shows that each gap is passing approximately the same current.

Photograph P1

Part of the ten-channel spark gap. The electrodes are visible and the trigger wires are shown coming out of the top of the spark gap.





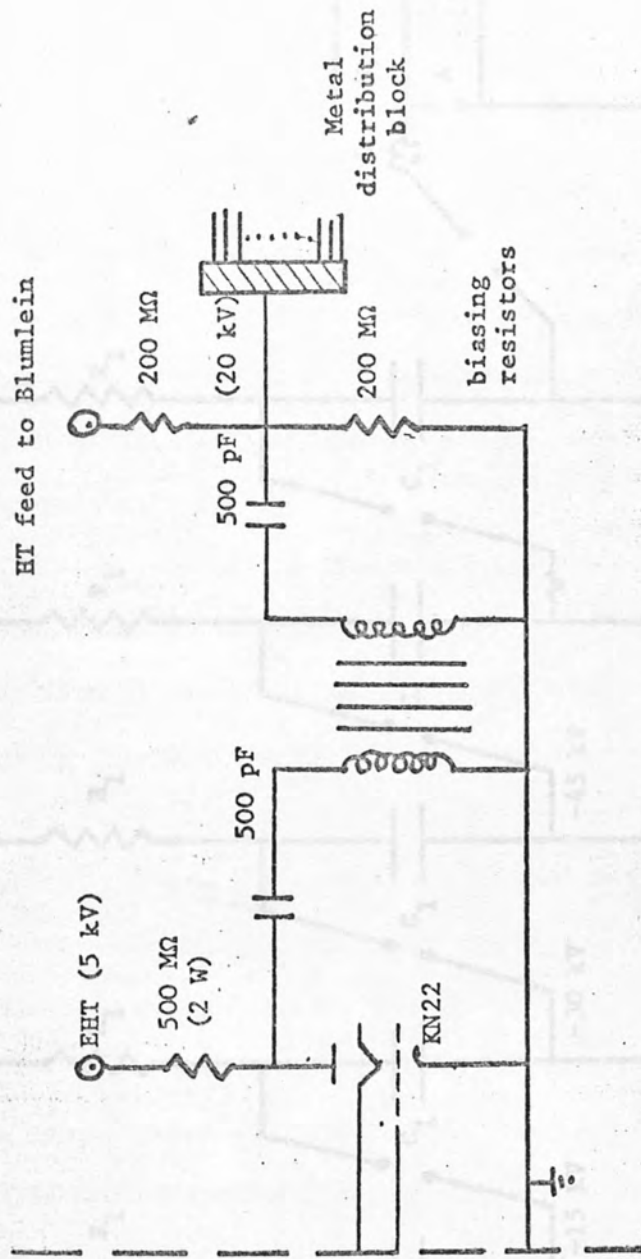


FIGURE 3.14: EXTRA CIRCUITRY ADDED TO TRIGGER PULSE GENERATOR FOR THE MULTI-CHANNEL SPARK GAP

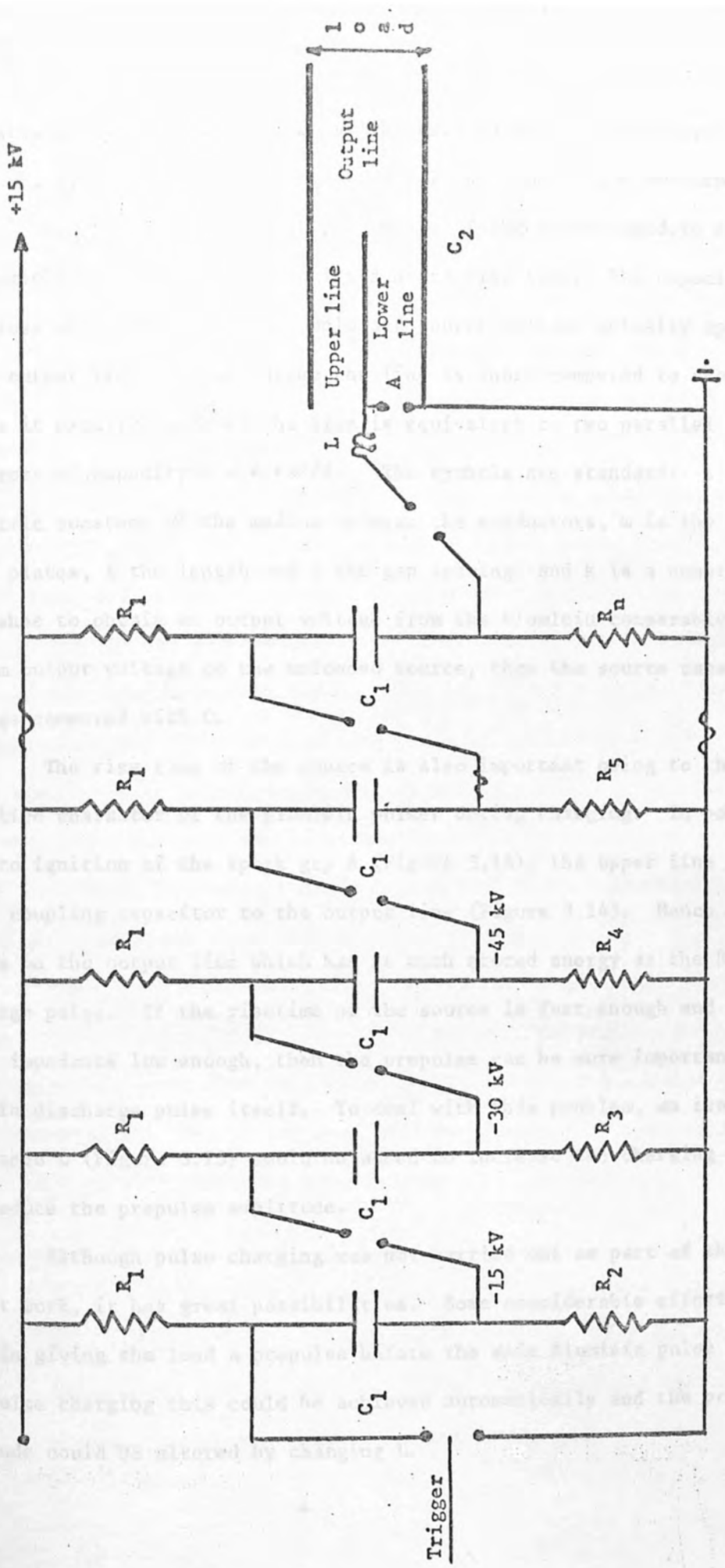


FIGURE 3.15: PULSE CHARGING-A BLUMLEIN SYSTEM USING A MARK GENERATOR

and discharged in series. Typical values used in such a system are  $C_1 \sim 2 \mu\text{F}$ ,  $R_1 \sim 10 \text{ M}\Omega$  and  $R_2, R_3 \dots R_n, 2 \text{ M}\Omega, 3 \text{ M}\Omega \dots n \text{ M}\Omega$  respectively.

The two most important parameters of the source used to charge the Blumlein pulser are its capacity and its rise time. The capacity determines what fraction of the unloaded source voltage actually appears at the output line. If we assume the line is short compared to the charging time as it usually is, then the line is equivalent to two parallel capacitors of capacity  $C = k \epsilon \omega \ell / d$ . The symbols are standard:  $\epsilon$  is the dielectric constant of the medium between the conductors,  $\omega$  is the width of the plates,  $\ell$  the length and  $d$  the gap spacing, and  $k$  is a constant. If one wishes to obtain an output voltage from the Blumlein comparable to the maximum output voltage of the unloaded source, then the source capacity must be large compared with  $C$ .

The rise time of the source is also important owing to the capacitive character of the Blumlein pulser during charging. In particular, prior to ignition of the spark gap A (Figure 3.14), the upper line looks like a coupling capacitor to the output line (Figure 3.14). Hence a prepulse appears on the output line which has as much stored energy as the Blumlein discharge pulse. If the risetime of the source is fast enough and the output impedance low enough, then the prepulse can be more important than the Blumlein discharge pulse itself. To deal with this problem, an isolation inductance  $L$  (Figure 3.15) could be added to increase the charging time and thus reduce the prepulse amplitude.

Although pulse charging was not carried out as part of this present work, it has great possibilities. Some considerable effort was spent in giving the load a prepulse before the main Blumlein pulse arrived. With pulse charging this could be achieved automatically and the prepulse amplitude could be altered by changing  $L$ .



## CHAPTER IV

### DESIGN OF APPARATUS USED IN EXPERIMENTS

#### 4.1 General description of linear and coaxial flashlamps

Figure 4.1 shows the basic design of the coaxial flashlamps used in the experiments. The general design of the lamps was fashioned according to those developed and used by Claesson and Lindquist<sup>(79)</sup> and also used by Sorokin et al<sup>(56)</sup>.

Various lengths, widths and annular gaps were used, each fashioned on the basic design shown in Figure 4.1. The walls of the flashlamp were made of fused silica of 1 mm thickness. The electrodes were made of brass and were glued to the quartz tubes with "torr seal". Figure 4.1 also shows the electrodes and the system for coupling the interior of the flashlamp to the vacuum system. The discharge took place between the brass ring electrodes in the annular space left between the two quartz tubes. In the inside of the inner tube a dye cell may be placed to absorb the flashlamp radiation and the outside of the outer tube is coated with Kodak white reflectance coating which reflects light back onto the dye cell.

The plasma discharge produced by the driving circuit used by Sorokin et al<sup>(56)</sup>, rarely, if ever filled the annular region. They found they required at least 3 mm wall thickness to prevent the impulse discharge from shattering it. Due to our more uniform discharge we were able to use tubes with 1 mm wall thickness successfully.

---

NOTE: The reason for this is that in a uniform discharge, the pressure acts radially in all directions (in a manner best absorbed by the quartz) whereas the arc discharge produces non uniform pressure waves which tend to shatter the quartz.

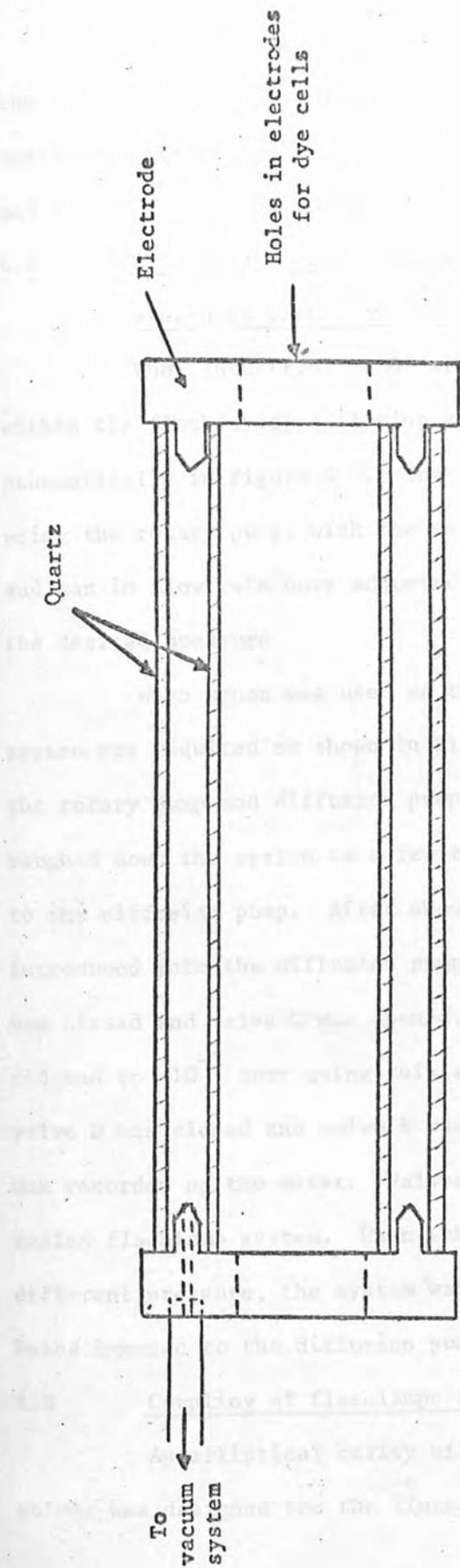


FIGURE 4.1 : SCHEMATIC DIAGRAM SHOWING GENERAL DESIGN OF COAXIAL FLASHLAMP

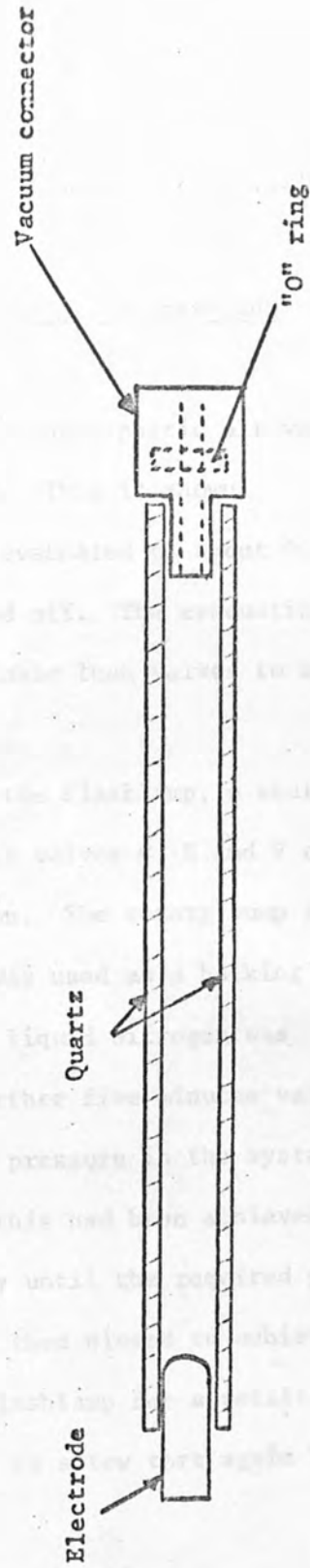


FIGURE 4.2: SCHEMATIC DIAGRAM SHOWING LINEAR FLASHLAMP



Figure 4.2 shows the type of linear flashlamp used. The wall of the flashtube was 1 mm thick made of fused quartz. Brass electrodes were again used, glued to the quartz with "torr seal". One electrode was hollow and fitted to a vacuum connector as shown.

#### 4.2 Experimental arrangements used for altering the gases and pressures within the flashlamps

When industrial grade argon, nitrogen or atmospheric air was used within the flashtubes, a flowing system was used. This is shown schematically in Figure 4.3. The flashlamp was evacuated to about 0.5 torr using the rotary pump, with the gas supply turned off. The evacuating rate and gas in flow rate were adjusted with controllable leak valves to achieve the desired pressure.

When xenon was used as the gas inside the flashlamp, a sealed system was required as shown in Figure 4.4. With valves C, E and F closed, the rotary pump and diffusion pump were turned on. The rotary pump then roughed down the system to a few torr and also was used as a backing pump to the diffusion pump. After about ten minutes liquid nitrogen was introduced into the diffusion pump. After a further five minutes valve A was closed and valve C was opened. The overall pressure in the system was reduced to  $10^{-5}$  torr using this system. Once this had been achieved, valve D was closed and valve E was opened gently until the required pressure was recorded on the meter. Valves E and G were then closed to achieve a sealed flashlamp system. When exhausting the flashlamp for a refill at a different pressure, the system was roughed down to a few torr again before being exposed to the diffusion pump.

#### 4.3 Coupling of flashlamps to the Blumlein pulser

An elliptical cavity with low inductance connections to the pulser was designed for the linear type flashlamp. The cavity could be

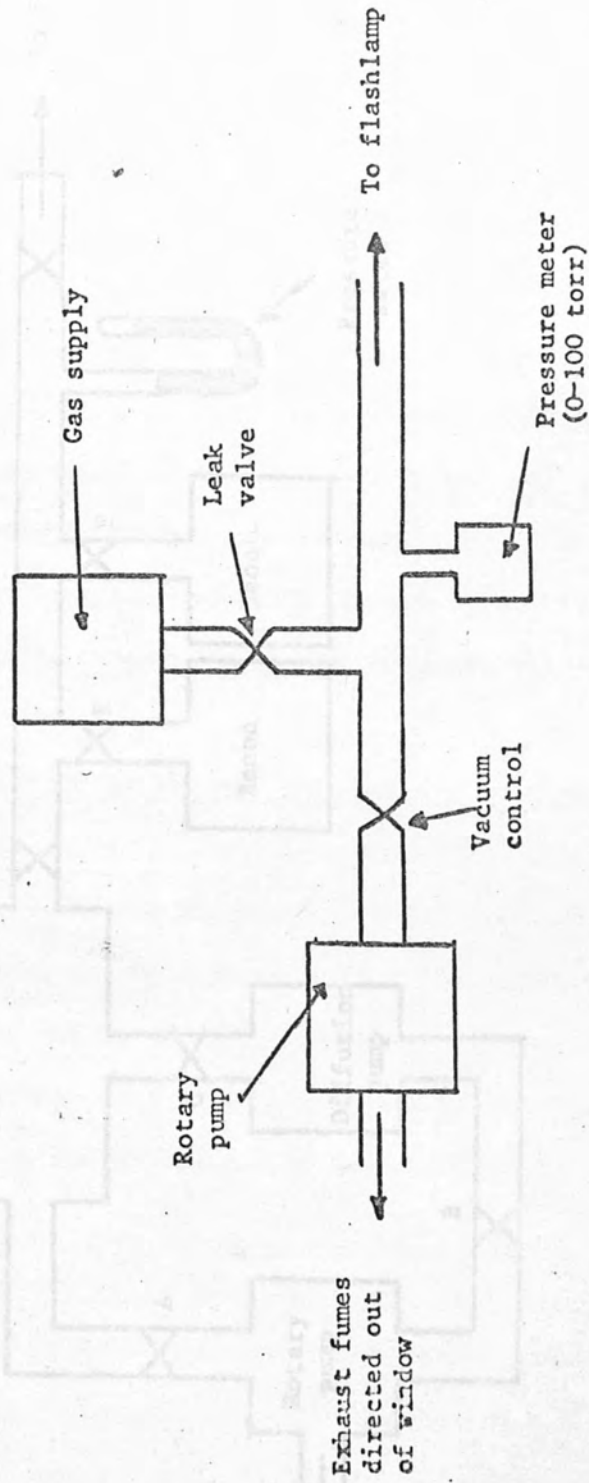


FIGURE 4.3: FLOW SYSTEM FOR FLASHTUBES WHEN INDUSTRIAL GRADE GASES USED

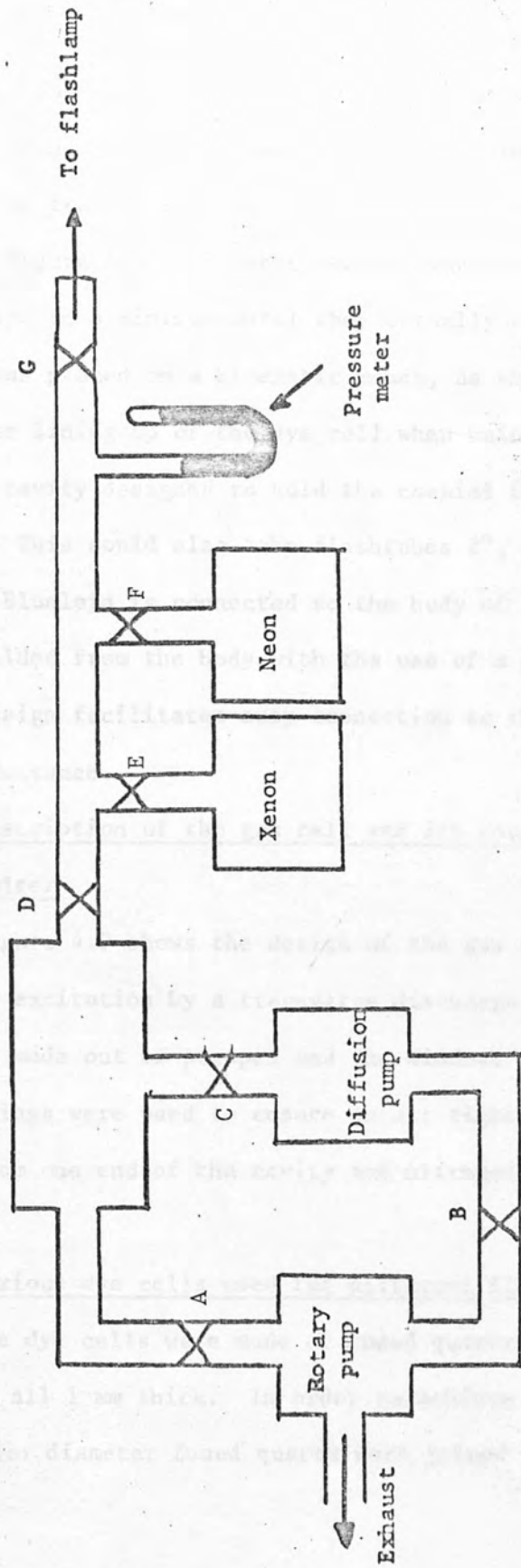


FIGURE 4.4: SEALED SYSTEM FOR USING XENON WITHIN FLASHLAMPS

adjusted to take flashlamps of 2", 4" or 6" in length and could also locate the dye cell accurately at the focus point not occupied by the flashlamp. P3 and P4 are photographs showing the design of the cavity. The earthy side of the transmission line was connected to the body of the cavity. The HT side of the transmission line was connected to one end of the flashlamp as shown in Figure 4.5. Distance between the conductors of the transmission line were kept to a minimum until they actually connected to the cavity. The cavity was placed on a kinematic mount, as shown in the photographs, to enable easier lining up of the dye cell when using a helium neon laser.

A cavity designed to hold the coaxial flashlamps is shown in Figure 4.6. This could also take flashtubes 2", 4" or 6" long. The earthy side of the Blumlein is connected to the body of the cavity, and the HT side is shielded from the body with the use of a perspex insert. Once again the design facilitates easy connection to the transmission line with minimum inductance.

#### 4.4 Description of the gas cell and its coupling to the Blumlein pulser

Figure 4.7 shows the design of the gas cell used to contain the nitrogen for excitation by a transverse discharge through the gas cell. The cell was made out of perspex and the windows were made of fused quartz. Rubber "O" rings were used to ensure an air tight cavity. The cell was evacuated from one end of the cavity and nitrogen was introduced at the other end.

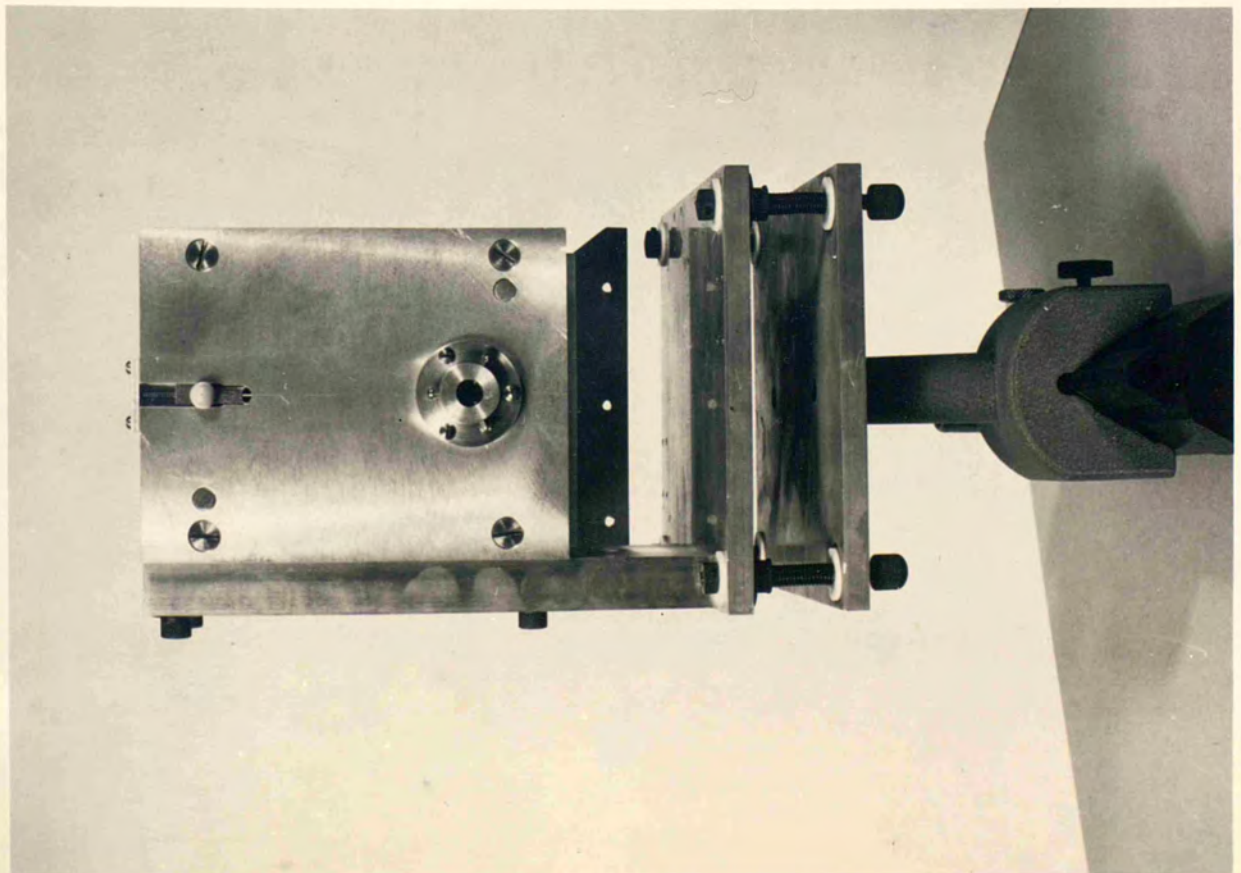
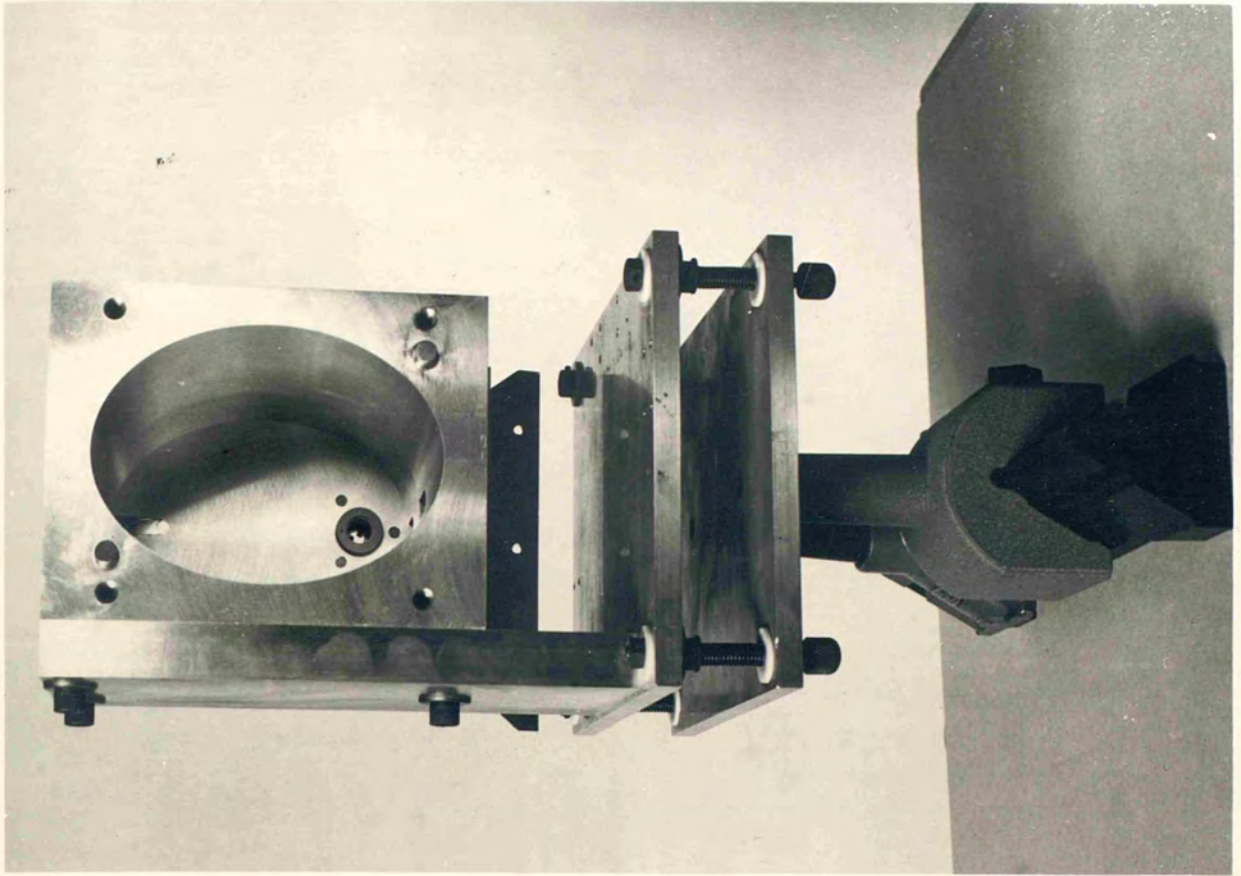
#### 4.5 Various dye cells used for different flashlamps and cavities

The dye cells were made of fused quartz of various diameters and lengths, but all 1 mm thick. In order to achieve a flow of the dye two side arms of smaller diameter fused quartz were joined to the main cell. One

PHOTOGRAPHS 3 AND 4

The elliptical cavity for the linear flashlamp and dye cell.







not to scale

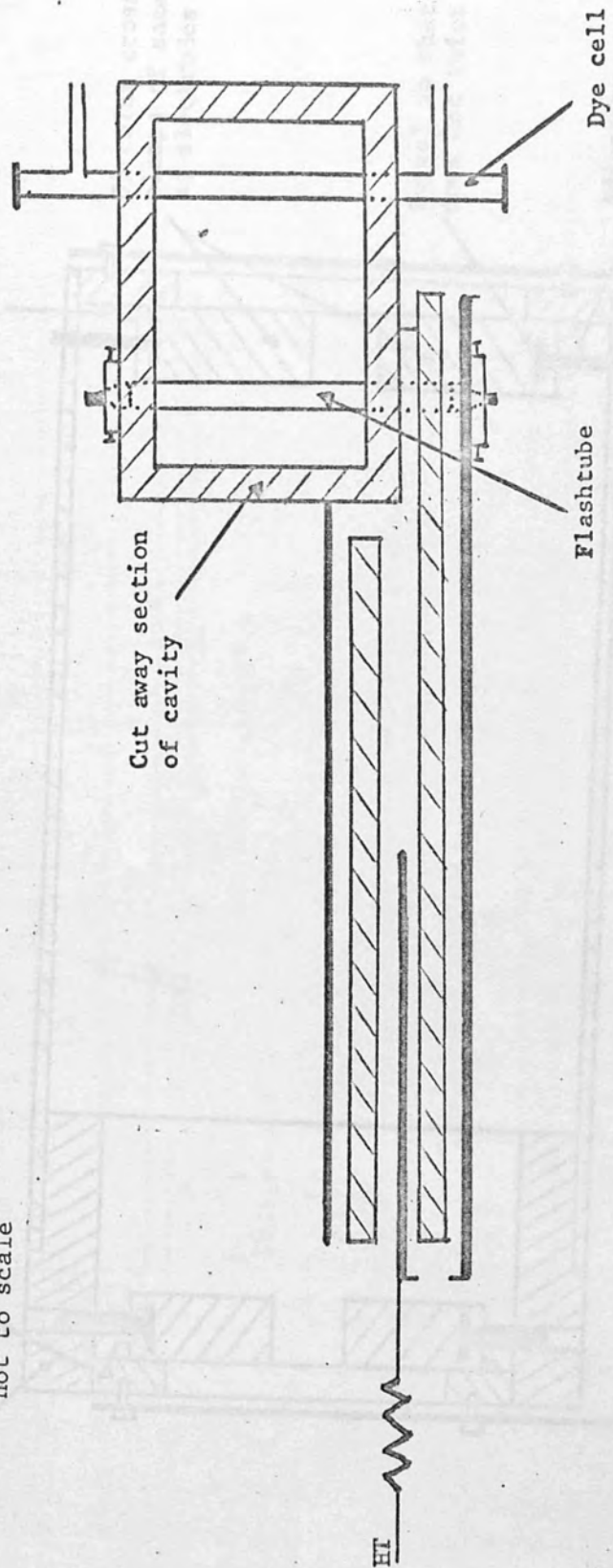


FIGURE 4.5: COUPLING THE CAVITY, FOR THE LINEAR FLASHTUBE, TO THE PULSER

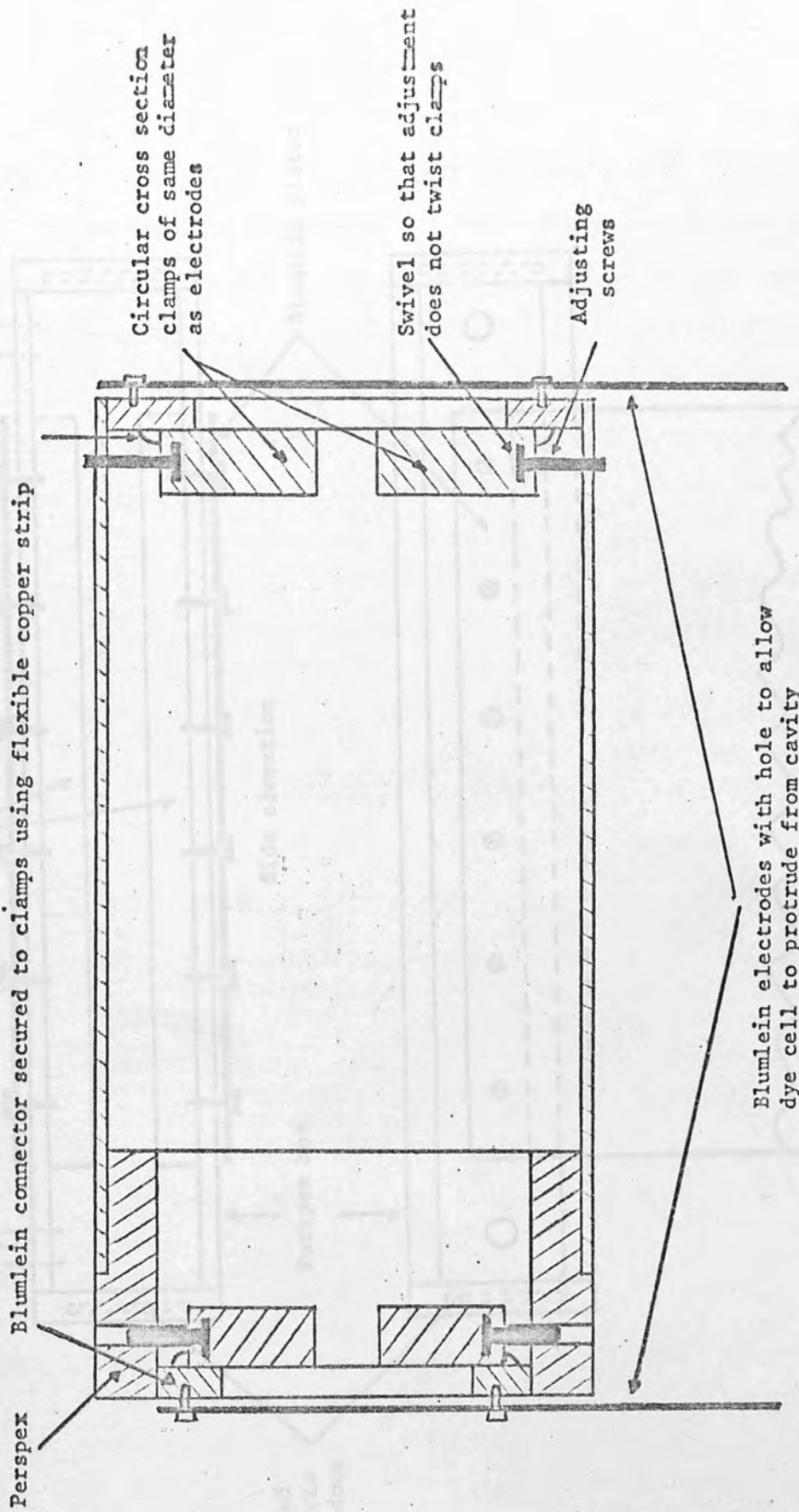
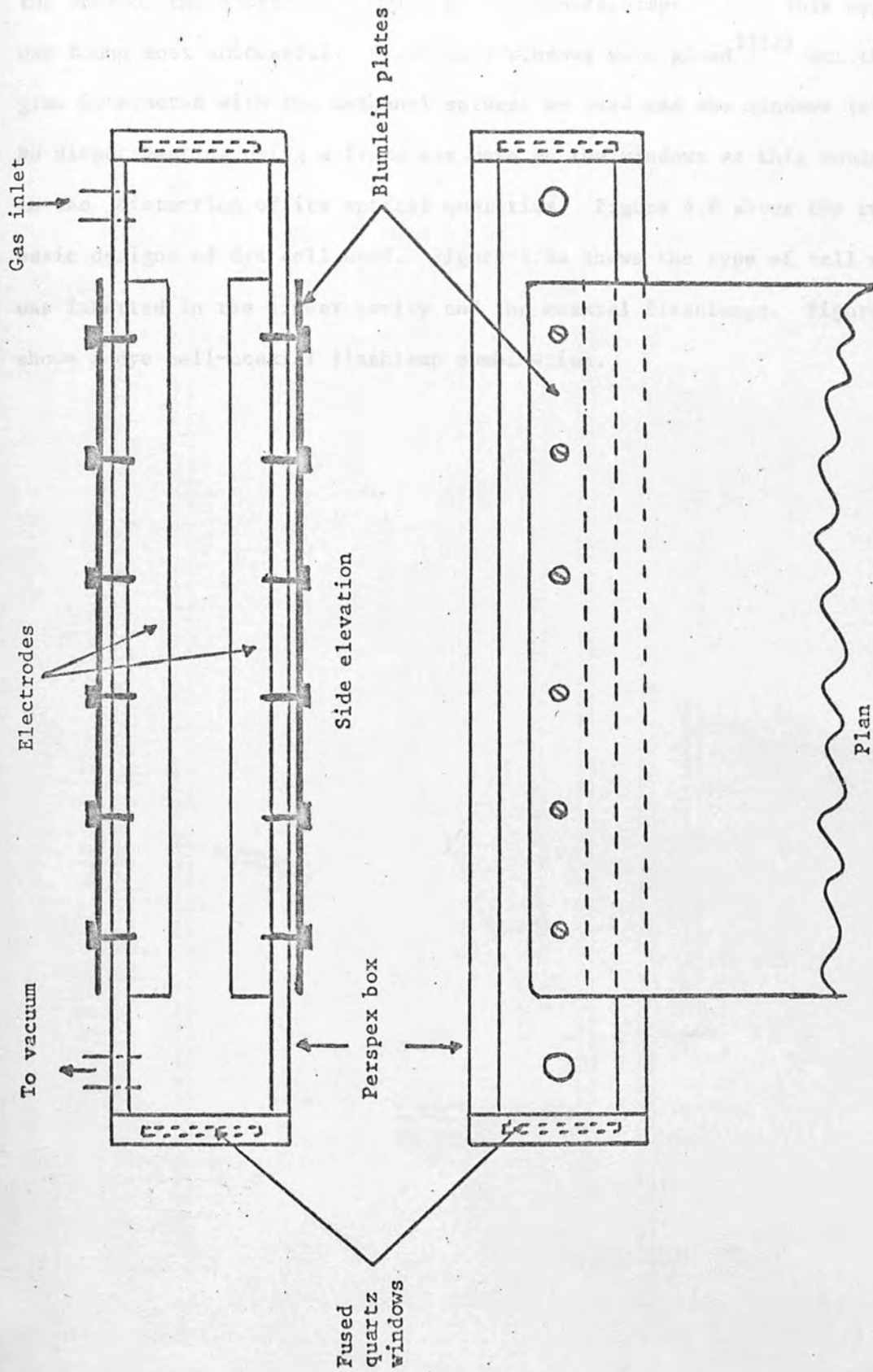


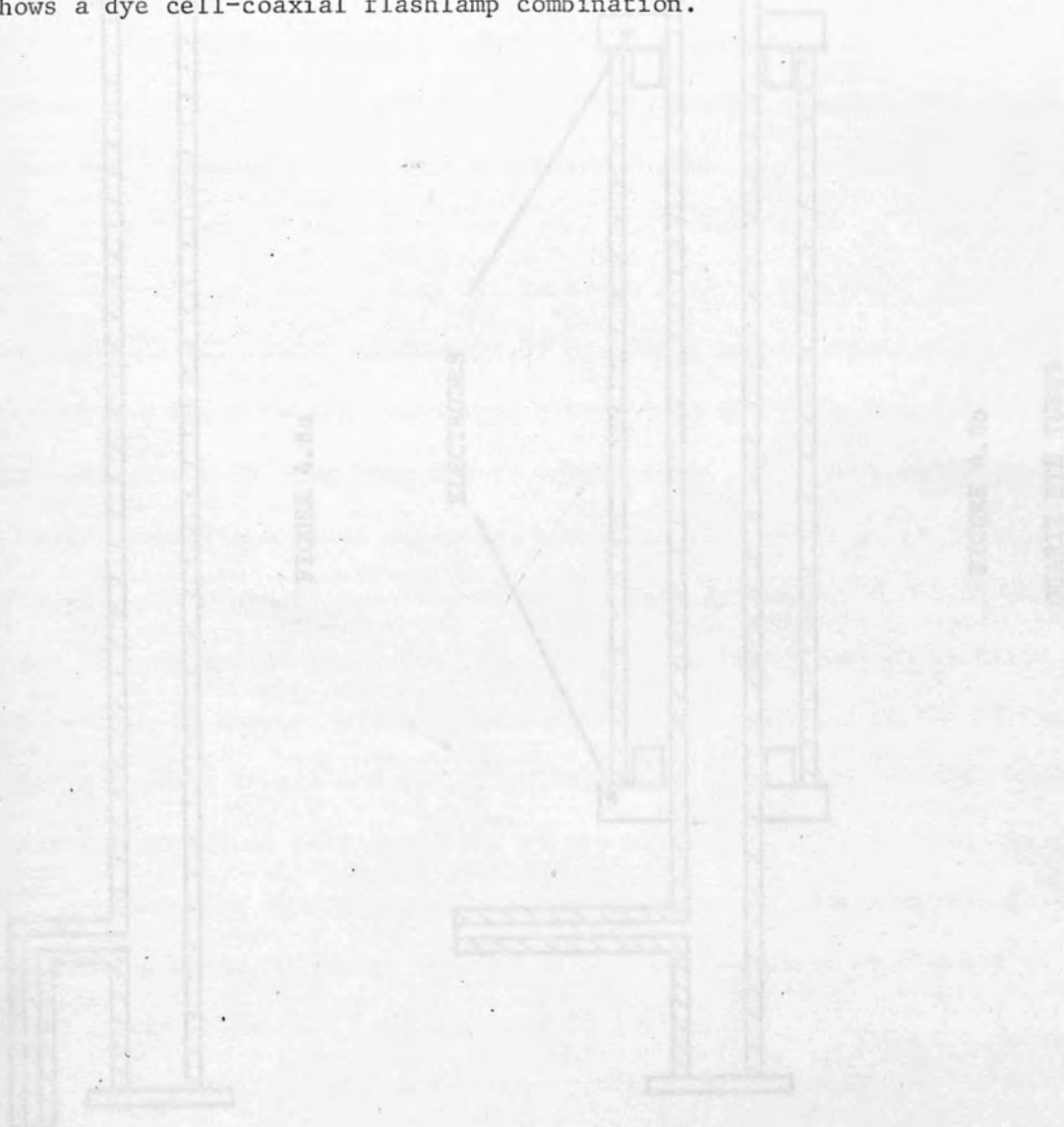
FIGURE 4.6: COAXIAL CAVITY IN CROSS SECTION



1 scale

FIGURE 4.7: THE GAS CELL

centimetre diameter quartz windows (spectrosil B quality) were fixed to the ends of the quartz tube using glass transfer tape<sup>(153)</sup>. This method was found most successful. Previously windows were glued<sup>(152)</sup> but this glue interacted with the methanol solvent we used and the windows fell off. No direct heating using a flame was used on the windows as this would result in the distortion of its optical qualities. Figure 4.8 shows the two basic designs of dye cell used. Figure 4.8a shows the type of cell which was inserted in the linear cavity and the coaxial flashlamps. Figure 4.8b shows a dye cell-coaxial flashlamp combination.



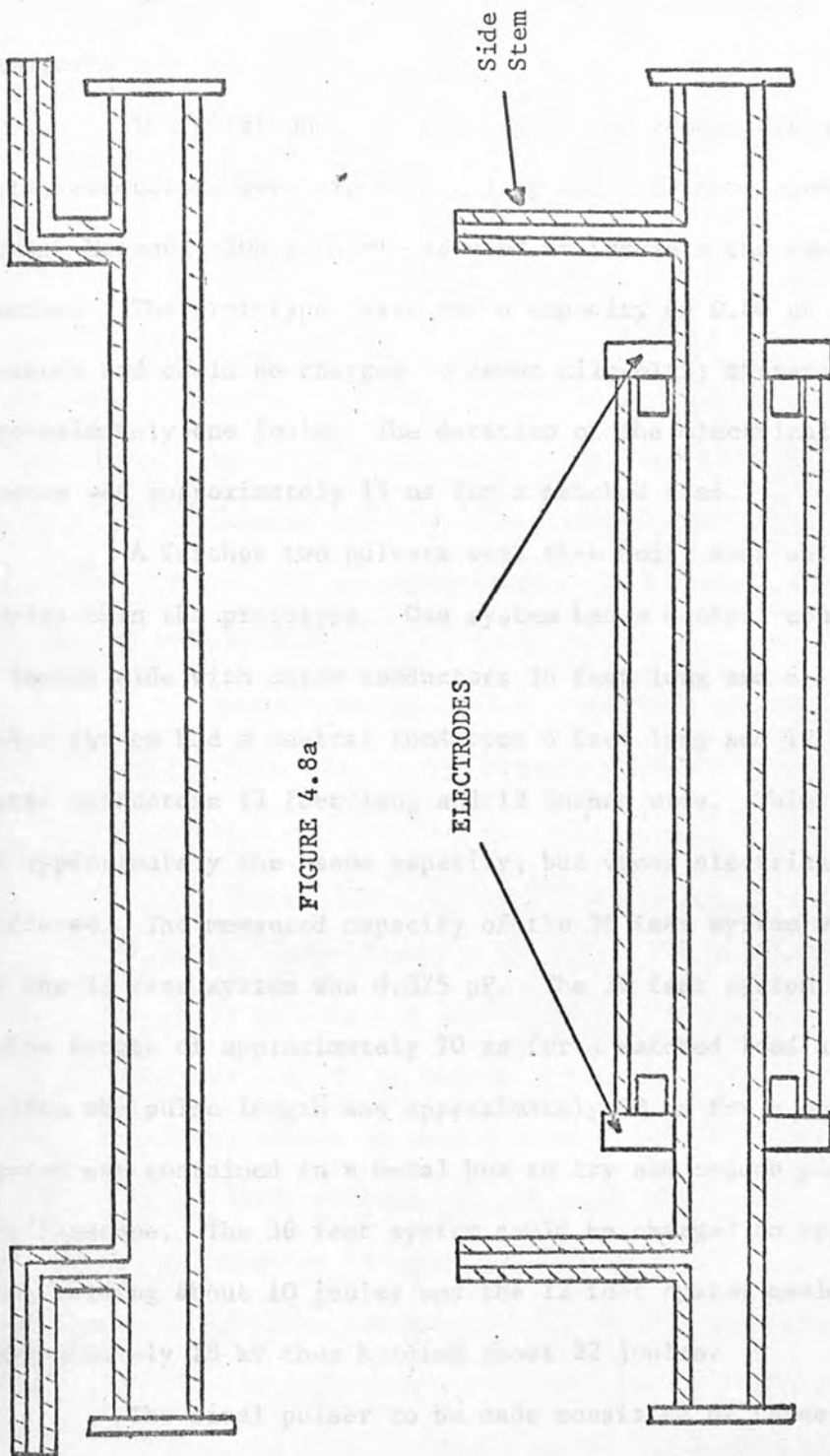


FIGURE 4.8a

FIGURE 4.8b

QUARTZ DYE TUBES

## CHAPTER V

### FLASHLAMP CHARACTERISTICS

#### 5.1 Introduction

Four Blumlein pulsers were built and their performances were evaluated.

The first one- the prototype- had conductors six inches wide. The outer conductors were eight feet long and the inner conductor was four feet long. Melanex  $\sim 200 \mu$  thick was used to insulate the conductors from one another. The prototype laser had a capacity of  $0.04 \mu\text{F}$  in each arm of the network and could be charged to seven kilovolts; therefore storing approximately one joule. The duration of the electrical pulse from this system was approximately 15 ns for a matched load.

A further two pulsers were then built each able to store more joules than the prototype. One system had a central conductor 18 feet long, 6 inches wide with outer conductors 36 feet long and 6 inches wide. The other system had a central conductor 6 feet long and 12 inches wide with outer conductors 12 feet long and 12 inches wide. This gave us two systems of approximately the same capacity, but whose electrical pulse lengths differed. The measured capacity of the 36 feet system was  $0.078 \mu\text{F}$  and that of the 12 feet system was  $0.075 \mu\text{F}$ . The 36 feet system had an electrical pulse length of approximately 70 ns for a matched load and in the 12 feet system the pulse length was approximately 20 ns for a matched load. Each system was contained in a metal box to try and reduce pick up noise on the oscilloscope. The 36 feet system could be charged to approximately 12 kV thus holding about 10 joules and the 12 feet system could be charged to approximately 18 kV thus holding about 22 joules.

The final pulser to be made consisted of three conductors of approximately the same length. They were 24 feet long and 12 inches wide. The capacity of the system was measured to be  $0.19 \mu\text{F}$  in each arm. The



electrical pulse length for this pulser was approximately 90 ns for a matched load. It could be charged to a maximum of about 16 kV storing approximately 50 joules.

With the 12 feet and 36 feet systems, the initial and reflected electrical pulses were each separated by an electrical pulse length for a matched load. With the 24 feet pulser, the initial and reflected electrical pulses were separated by only a few nanoseconds for a matched load.

For the experimental work on the flashlamps two oscilloscopes were used. Initially the Tektronix type 454 was used with a photomultiplier. (Wavelength range of photomultiplier was 1800-6000 Å). On the higher energy, 24 feet pulser and later experiments the Tektronix type 519 oscilloscope was used in conjunction with a diode. (Wavelength response of diode was 3000-8000 Å).

In all experiments (unless otherwise stated) the photodetector was placed at the normal to the flashlamp axis and pointed at the centre of the flashtube.

## 5.2 Analysis of results from the prototype pulser

The prototype Blumlein pulser can be regarded as giving an approximately 15 ns burst of electrons from the anode, then waiting approximately another 15 ns before the reflected pulse returns. The time taken for the electrons to travel from cathode to anode (a known distance) will yield the drift velocity of the electrons. For example, in photograph P5, the pulse risetime is approximately 40 ns. We can assume, for sufficiently high E/p, the movement of the electrons down the flashtube will be faithfully transmitted via light quanta being emitted from excited atoms, and that the peak intensity should occur just before the avalanching electrons hit the anode. Photograph P5 shows the light output from a

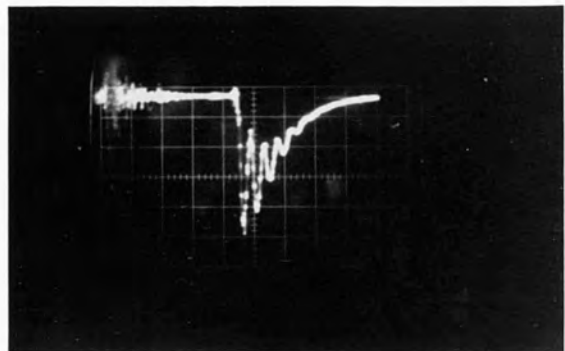
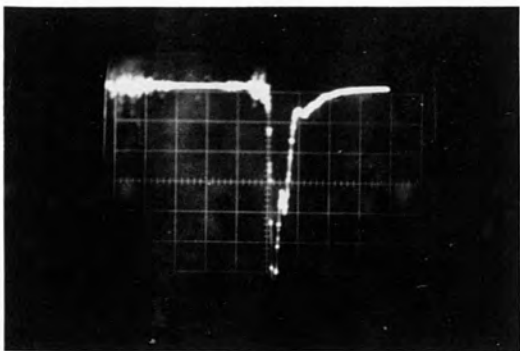
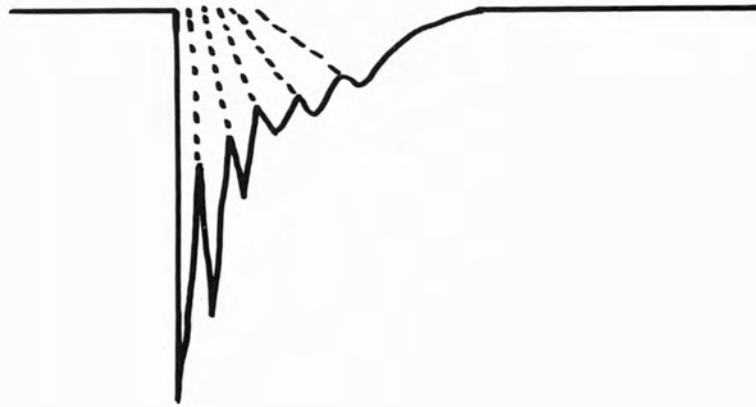


FIGURE 5.1

Schematic representation of photograph P6. The dotted lines extrapolated to the base line denote the electrical pulse separation.

FLASHLAMP OUTPUTS

PHOTOGRAPH P5

Blumlein voltage 12 kV. 14 cm long coaxial flashlamp filled with air at a pressure of 0.7 torr.  
Sweep speed 200 ns/div.

PHOTOGRAPH P6

Blumlein voltage 12 kV. 14 cm long coaxial flashlamp filled with air at a pressure of 8 torr.  
Sweep speed 200 ns/div.

14 cm long flashtube filled with air to a pressure of 0.7 torr. The Blumlein pulser delivered 12 kV across the flashlamp giving an  $E/p \approx 1200$  volts/cm torr in this case, and an electron drift velocity  $\sim 10^8$  cm s<sup>-1</sup>.

Photograph P6 shows the light output from the same flashlamp at a pressure of 8 torr ie an  $E/p \approx 110$ . The numerous peaks can be explained with the aid of Figure 5.1. Electrons generated for 15 ns by the rectangular shape pulse from the pulser liberates photons causing an increase of light output for this period of time. During the following 15 ns the electrons slow down producing fewer and fewer photons as the accelerating field does not exist. Due to the mismatch between pulser and flashtube, there exists a second electrical pulse which manifests itself across the flashtube for a further period of 15 ns. This pulse is not as rectangular as the initial pulse due to some absorption of the first pulse. This pulse causes electrons to accelerate again causing more collisions and releasing more photons. This situation continues until the pulser is discharged and in photograph P6 one can see six electrical pulses. The pulse with least reflections and most intense peak light output for this system corresponded to the flashtube with the lowest pressure fill (0.7 torr) and thus the highest  $E/p$  and electron drift velocity. Therefore the longer mean free path and greater  $E/p$  results in increased energy of the electrons which increases the number of photons produced due to collisions. Space charge effects could possibly reduce the number of electrons emitted from the cathode in the higher pressure, lower  $E/p$  case.

Although the light output was expected to be of longer duration than the voltage pulse across the tube, the fact that the half width of some of the light output pulses was about 200 ns for a voltage pulse of 15 ns duration implied a very poor impedance match between the Blumlein

pulser and flashtube. Only a very small fraction of the energy of the first and subsequent pulses (due to reflection) was deposited. If the initial impedance (resistive) of the flashlamp could be reduced then the peak intensity of the light output would become greater, the pulse duration would become less and possibly the rise time would become shorter. It was these facts which led us to try and ionise the gas in the flashtube before the arrival of the pulse from the Blumlein, and this form of preionisation was termed "keep alive".

This analysis has been simplified and qualitative. The larger the number of reflections, the longer the light output pulse will be due to the emission of electrons from the cathode. However, we cannot tell when the reflected pulse is too small to initiate further electrons from the cathode but still accelerate existing electrons in transit. These factors could influence the situation considerably, particularly for the longer Blumlein pulsers with large energies which supply longer more energetic pulses to the flash tube.

### 5.3 Analysis of the light output from flashlamps used in the different Blumlein pulsers

#### (a) Pulse shapes obtained with a linear flashtube

A linear flashlamp was first used with each of the Blumlein pulsers to establish their output characteristics. The flashtube was 9 cm long with an internal diameter of 6 mm, and was filled with air at various pressures.

The flashlamp output usually consisted of two light pulses for the 12 feet and 36 feet pulsers, and one light pulse for the 24 feet pulser.

A typical flashlamp output from the 36 feet system is shown in photograph P7. The sweep speed was 50 ns per division. In the upper two traces the flashlamp pressure was 0.39 torr whereas

PHOTOGRAPH P7

Flashlamp output from a 9 cm long linear flashlamp filled with air to pressures of

- (a) 0.35 torr
- (b) 0.35 torr
- (c) 10 torr
- (d) 10 torr

Sweep speed 50 ns/division Blumlein voltage 14 kV.

PHOTOGRAPH P8

Flashlamp output from a 9 cm long linear flashlamp filled with argon to pressures of

- (a) 5 torr
- (b) 6 torr
- (c) 7 torr
- (d) 8 torr

Sweep speed 100 ns/division Blumlein voltage 14 kV.

PHOTOGRAPH P9

Flashlamp output from a 9 cm long linear flashlamp filled with air to a pressure of 5 torr.

Sweep speed 100 ns/division Blumlein voltage 14 kV. Upper trace with UV filter. Lower trace without UV filter.

PHOTOGRAPH P11

Flashlamp output from a 14 cm long coaxial flashlamp filled with air to a pressure of 5 torr.

Sweep speed 200 ns/division Blumlein voltage 14 kV. Upper trace with UV filter. Lower trace without UV filter.

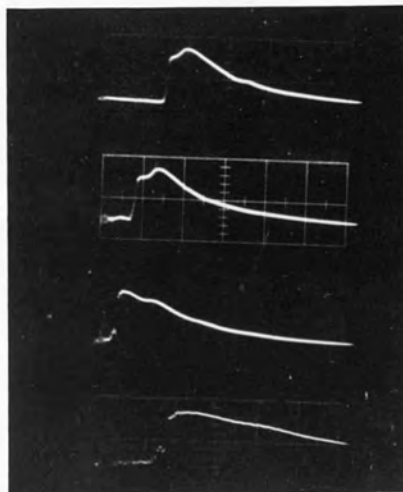
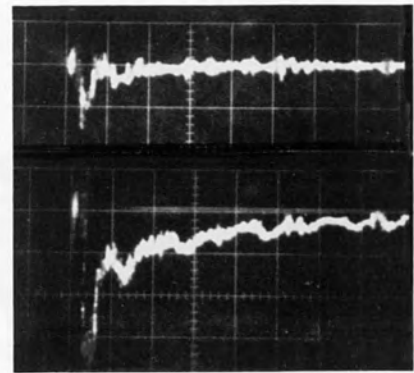
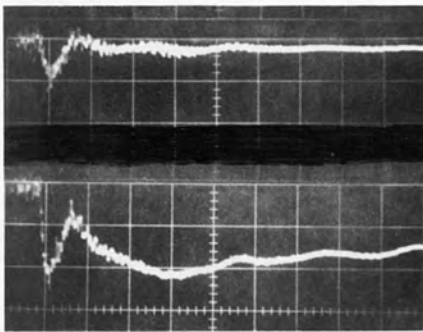
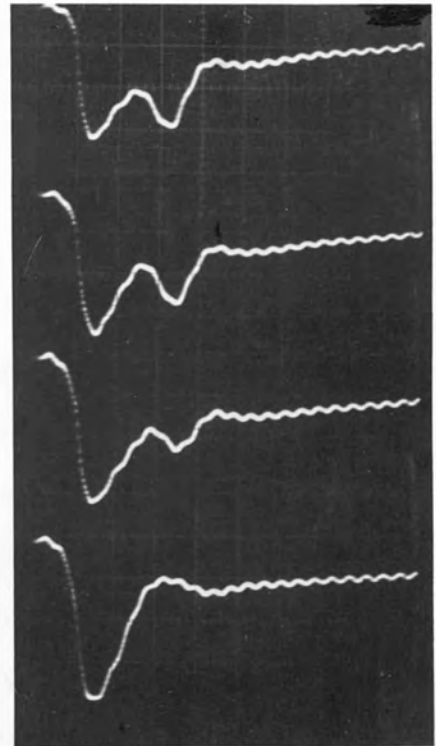
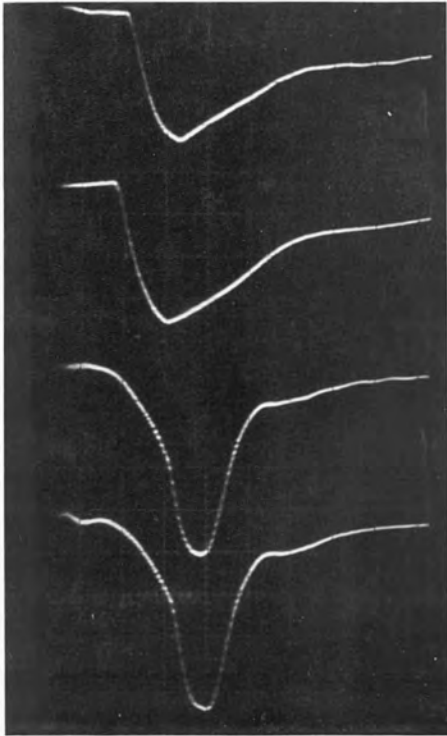
PHOTOGRAPH P10

Flashlamp output from a 9 cm long linear flashlamp filled to a pressures of

- (a) 85 torr - sweep speed 500 ns/division
- (b) 75 torr - " " " "
- (c) 65 torr - " " " "
- (d) 55 torr - " " " "

Blumlein voltage 15 kV





for the lower two traces, the pressure fill in the lamp was 10 torr. The results were repeated for each pressure to show the reproducibility of the results. Careful inspection of photograph P7 shows a second output pulse occurring near the tail of the initial output pulse. This double pulse effect becomes more pronounced when the flashlamp is filled with argon which we found to be more easily ionised. Also the presence of oxygen in the air filled flashlamps, may tend to reduce ionisation. Oxygen has a high electron attachment coefficient, thus there will be less free electrons available for use in the gas breakdown. Photograph P8, with a sweep speed of 100 ns per division, shows how variation in pressure, for constant input voltage, affects the intensity profile from the linear flashlamp filled with argon. The flashlamp pressures were 5, 6, 7, 8 torr respectively moving from the lower trace to the upper trace. We can see from this photograph that as the pressure increased, the mismatch between flashlamp and pulser increased and less energy was deposited in the initial pulse. This left more energy for the reflected pulse and the photograph shows how the second peak gains in intensity as the first peak loses. We found that flashlamps filled with argon struck more easily and could go to higher pressures without extinguishing compared with air filled flashlamps. The fact that argon was more easily ionised is shown by close examination of photographs P7 and P8. The time for ionisation before the fast increase of light output is longer for the air filled flashlamp (P7 lower two traces) than for the argon filled ones (P8).

In the 12 feet (20 ns) pulser, the double pulse effect was much more pronounced, even with air inside the flashtube. In fact, the second light pulse consists of 3 pulses joined together as shown in photograph P9 (lower trace). This shows the light output pulse for the linear flashlamp filled with air to a pressure of 5 torr. The sweep speed is 100 ns per division. The reason for the pronounced double pulse was due to the electrical pulse being only 20 ns long for the 12 feet pulser compared with the 70 ns long electrical pulse from the 36 feet pulser. The 36 feet pulser had more time to ionise and deposit more energy into the flashlamp in the initial pulse compared with the 12 feet pulser. Therefore it is to be expected that the reflected electrical pulse for the 12 feet system would contain more energy relative to the first pulse compared with the 36 feet pulser. This manifests itself in a larger second light output pulse from the flashlamp.

The 24 feet, 90 nanosecond pulser was able to store more energy than the other pulsers and the reflected electrical pulse followed the initial electrical pulse almost immediately. A typical pulse from this pulser with the linear flashtube is shown in photograph P10. A diode was used for the 24 feet system, to obtain a better signal to noise ratio, and the output is positive. The pulser was charged to 15 kV and the traces show the effect of increasing the air pressure within the flashtube. The pressures were 55, 65, 75, 85 torr, moving from the lower trace to the upper trace respectively. The top three traces were obtained with a sweep speed of 500 ns and the lower trace was 200 ns per division.

As expected there was no obvious double pulsing, although careful inspection of the single pulse shows structure due to the reflected electrical pulses.

These preliminary experiments showed that the 12 feet and 36 feet pulsers gave essentially the same sort of flashlamp output, but the 12 feet pulser was more useful for sorting out the fast processes occurring in a flashlamp compared with the slow ones. These two pulsers were used effectively to examine the effect of continuous preionisation on a flashtube reported in the next chapter. For the rest of the analysis, however, only the 12 feet pulser was used along with the higher energy, single light pulse, 24 feet pulser.

(b) Pulse shapes obtained from a coaxial flashtube

A 14 cm long coaxial flashlamp, of the basic design described in Chapter 4, was used in conjunction with the 12 feet and 24 feet pulsers. The flashlamp had an outside diameter of 2.5 cm, 1 mm thick fused quartz walls and an annular gap of 1.5 mm. Photographs showing the general pulse shape are included in this section and comparisons are made with the linear flashtube.

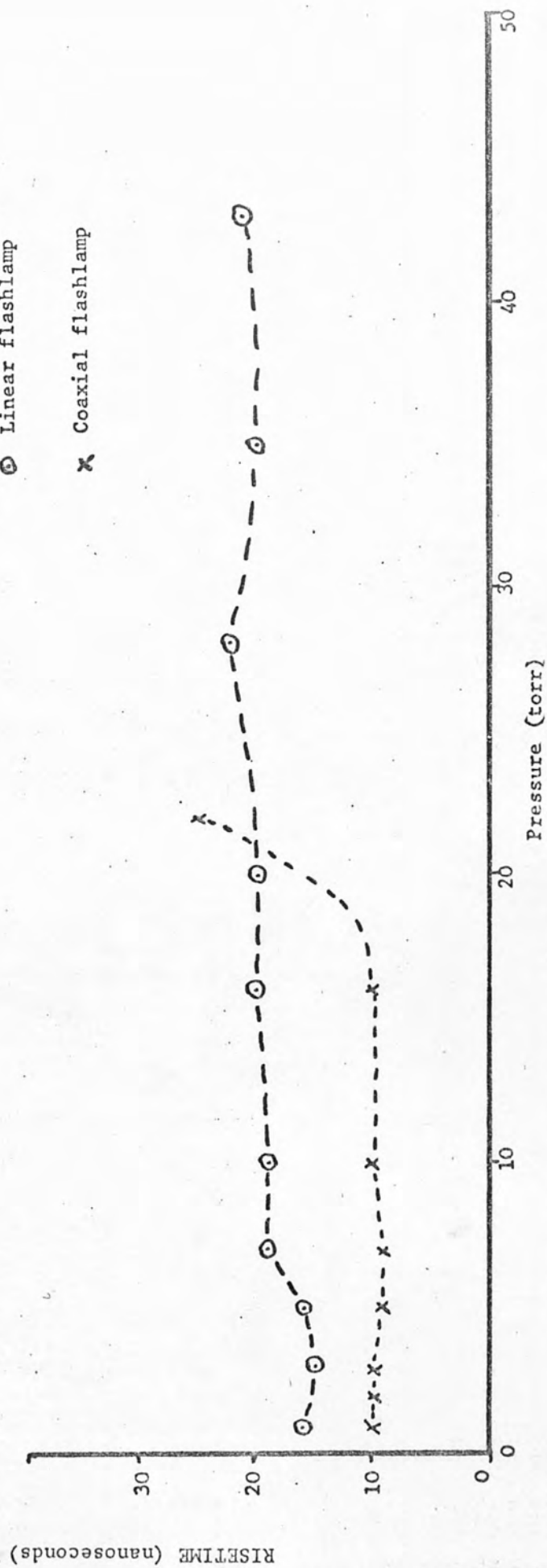
In the 12 feet system the light output pulses from the coaxial flashlamp were very similar to those obtained from the linear flashlamp except that the initial pulse was more intense than the second pulse for lower lamp fill pressures compared with the intensity ratio of first and second pulses from the linear flashtube. Photograph P11 (lower trace) shows the light output from the coaxial flashtube under identical voltage and pressure conditions (capacitor voltage 15 kV, air pressure of 5 torr within

the flashlamp) as that used with the linear flashlamp in obtaining photograph P10. Comparison of these two photographs show that more power is deposited into the first pulse and consequently less into the second pulse, for a coaxial flashtube compared with a linear flashtube for identical operating conditions. For higher pressures, however, we still obtain the reduction and then disappearance of the first pulse whilst the second pulse takes over. Photograph P12 shows the second pulse growing to the expense of the first pulse. The pressure at which this takes place is 22 torr for the coaxial flashlamp.

The pressure at which the flashtube would no longer strike was higher for the linear flashtube ( $\sim 45$  torr) compared with the coaxial flashtube ( $\sim 25$  torr).

The risetime of the initial pulse from the annular flashtube was, on average over the pressure range, around 10 ns where as the linear flashlamp had a risetime of around 20 ns as can be seen from graph 5.2.

The increased initial absorption of power and the faster risetimes obtained using the coaxial flashlamp could be due to the following reasons. The coaxial flashlamp with a uniform discharge has less inductance than a linear flashlamp. This would reduce the impedance of the flashlamp to the pulser simply due to design. The fast risetime may also be due to the availability of electrons from the tube walls, due to secondary emission from the walls, during the first high field period. The plasma has a much greater contact with the confining walls in a coaxial flashlamp compared with a linear flashlamp.



GRAPH 5.2: COMPARISON OF RISETIME OF FIRST LIGHT OUTPUT PULSE FOR COAXIAL AND LINEAR FLASHLAMP IN THE 12 ft SYSTEM



PHOTOGRAPH P12

Flashlamp output from a 14 cm long coaxial flashlamp filled to a pressure of 22 torr.

Sweep speed 200 ns/division  
Blumlein voltage 14 kV.

PHOTOGRAPH P13

Flashlamp output from a 14 cm long coaxial flashlamp filled to a pressure of

- (a) 50 torr
- (b) 45 torr
- (c) 40 torr
- (d) 35 torr
- (e) 30 torr

Sweep speed 200 ns/division  
Blumlein voltage 12 kV.

PHOTOGRAPH P16

Flashlamp output from a 2 inch linear flashlamp filled with xenon to a pressure of 50 torr.

Sweep speed 200 ns/division  
Blumlein voltage 12 kV.  
Lower trace viewed through safety glass.  
Upper trace obtained normally.

PHOTOGRAPH P14

Flashlamp output from a 2 inch linear flashlamp filled with argon to a pressure of

- (a) 50 torr
- (b) 27.5 torr
- (c) 12.5 torr
- (d) 2.5 torr
- (e) 1.5 torr

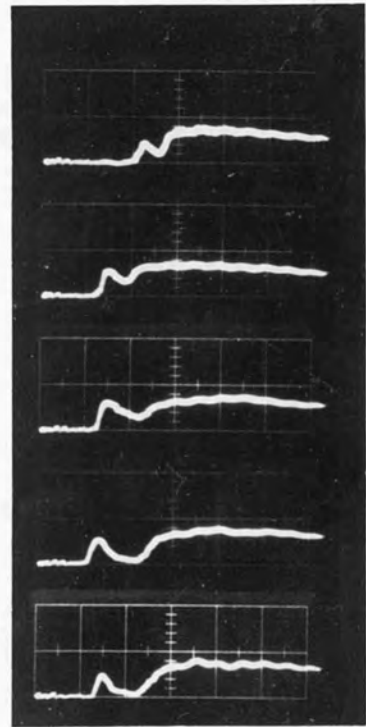
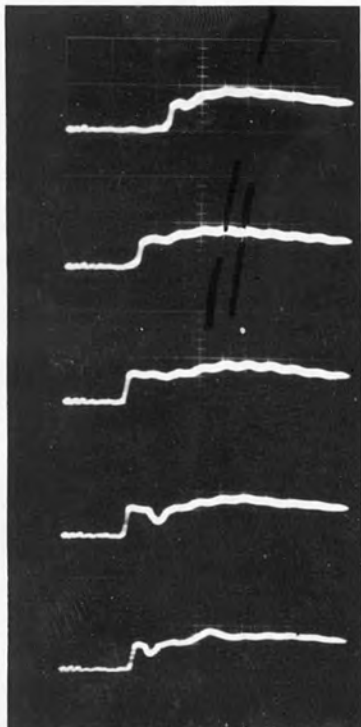
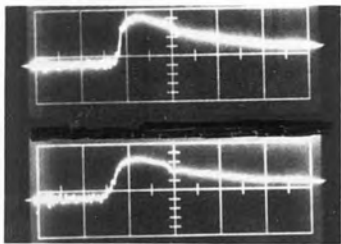
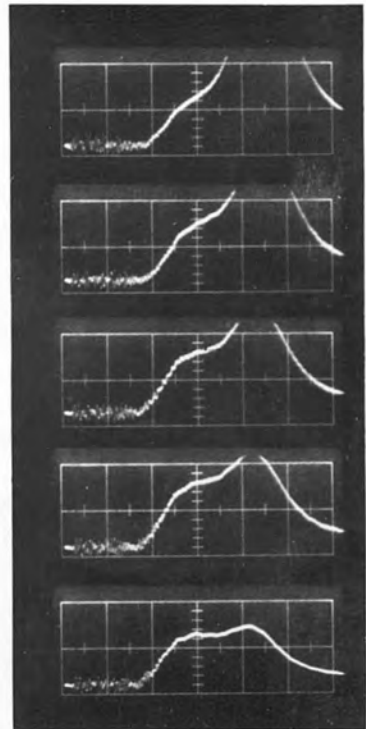
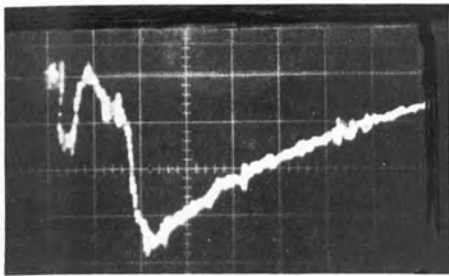
Sweep speed 100 ns/division  
Blumlein voltage 14 kV.

PHOTOGRAPH P15

Flashlamp output from a 2 inch linear flashlamp, with UV filter, filled with argon to a pressure of

- (a) 50 torr
- (b) 27.5 torr
- (c) 12.5 torr
- (d) 2.5 torr
- (e) 1.5 torr

Sweep speed 100 ns/division  
Blumlein voltage 14 kV.



In the 24 feet system, we note that the linear flashtube showed one light output pulse with some structure within this pulse due to the reflected electrical pulse. When the coaxial flashtube was used with the 24 feet pulser, this effect became more pronounced particularly for higher pressures. This can be seen in photograph P13. The pulser was charged to 12 kV and the pressure within the flashlamp was 30, 35, 40, 45, 50 torr from the lower to the upper trace respectively. The time base on the oscilloscope was set to 200 ns/division. We can see that the latter half of this light output pulse increases in amplitude over the initial half. We are thus obtaining a similar effect shown in the flashlamps in the 12 feet pulser. Here, however, the effect occurs in one flashlamp pulse due to the Blumlein configuration, whereas the pulses were separate in the 12 feet pulser. The reason the same effect was not observed in the linear flashlamp in this higher energy pulser system was probably due to saturation effects of the surface brightness of the flashlamp. This is analysed in more detail in Section 5.5, which covers flashlamps used in the 24 feet system in more detail.

Although the Blumlein pulsers have been described as 90 ns pulsers etc, this has been qualified with "for a matched load". When we consider non linear loads (such as flashlamps) and non coaxial connections between the strip line and flashlamp assemblies, the electrical pulse is considerably different from that expected for a matched load. Self inductance, variations in risetime and the effect of the spark gap used to trigger the pulser make the situation very complex indeed and extremely difficult to truly relate light output pulses from a flashtube to incoming electrical pulses from the pulser.

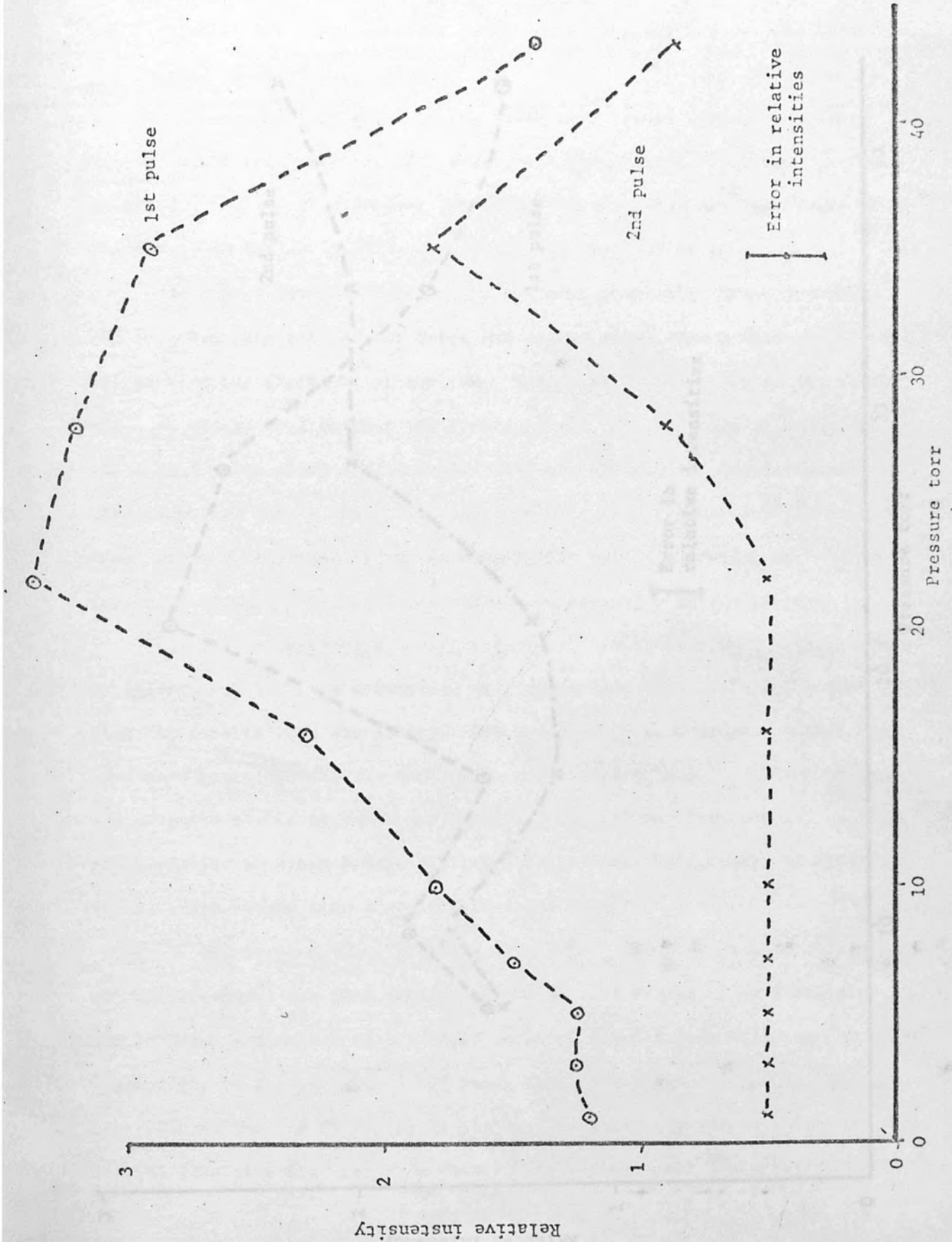
5.4 Flashlamp output in the wavelength range 3000-4000 Å compared with unrestricted spectral output

Light output in the wavelength range 3000-4000 Å from the 9 cm linear flashlamp in the 12 feet pulser was examined. The limited spectral range was obtained by putting a Kodak 18A ultra-violet filter in front of the photomultiplier. The filter had a pass band in the wavelength region 3000-4000 Å and in this region it decreased the light intensity recorded by approximately a half.

Graph 5.3 shows the relative intensities of the first and second pulse seen through the 18A filter as described above. The relative intensity of the first pulse builds up to a maximum at approximately 22 torr and then starts decreasing. At this point the second pulse begins to grow in intensity from its previous constant low level. At a pressure of 35 torr both pulses (first and second) in this wavelength region then decrease in amplitude as the pressure within the flashlamp is increased to the point where arcing takes place. (A small increase in the pressure (less than 5 torr) at which arcing takes place prevents the lamp from striking). The intensity profile, without the 18A filter in front of the photomultiplier, for the first and second pulses in exactly the same system is shown in graph 5.4. The profile follows a similar sort of pattern as in graph 5.3 with the first pulse being more intense than the second until a pressure of approximately 33 torr. This is the pressure just before the flashlamp starts obviously arcing. At this point the second pulse begins to grow more intense than the first pulse. Comparison with graph 5.3 indicates the spectral nature of the second pulse in the higher pressure regime is in the visible (greater than 4000 Å). Photograph P9 shows that most of the energy in the first pulse lies between 3000-4000 Å in the lower pressure regime. The

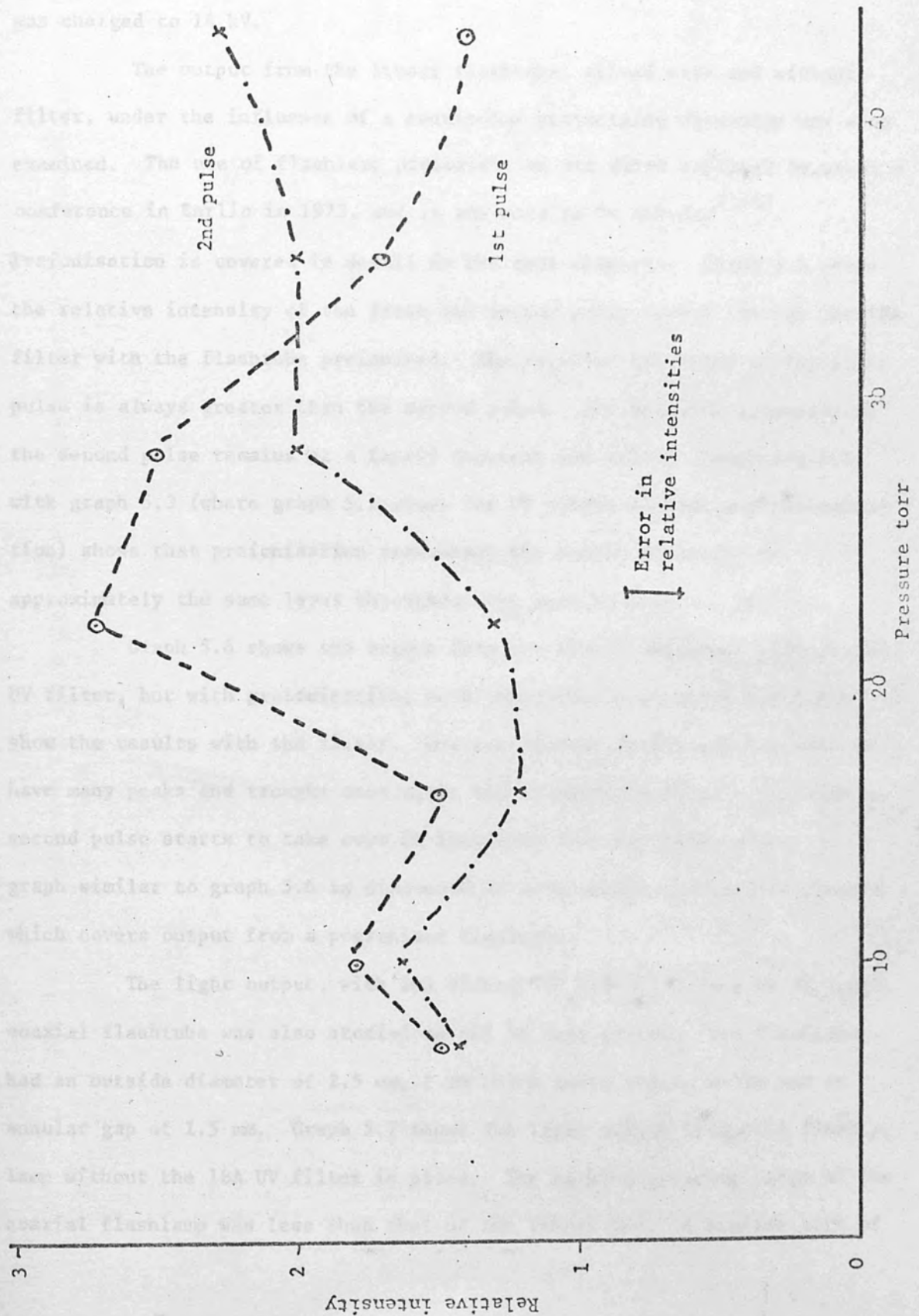
GRAPH 5.3: UV RESPONSE FOR THE DOUBLE PULSE AS A FUNCTION OF PRESSURE AT CONSTANT VOLTAGE; FOR A LINEAR FLASHTUBE IN THE 12 ft SYSTEM

FOR A LINEAR FLASHTUBE IN THE 12 ft SYSTEM.





GRAPH 5.4: VISIBLE RESPONSE FOR THE DOUBLE PULSE AS A FUNCTION OF PRESSURE AT CONSTANT VOLTAGE FOR A LINEAR FLASHTUBE IN THE 12 ft SYSTEM.





upper trace was obtained through the 18A filter, whereas the lower trace was without filter. The pressure in the flashlamp was 5 torr, and the pulser was charged to 14 kV.

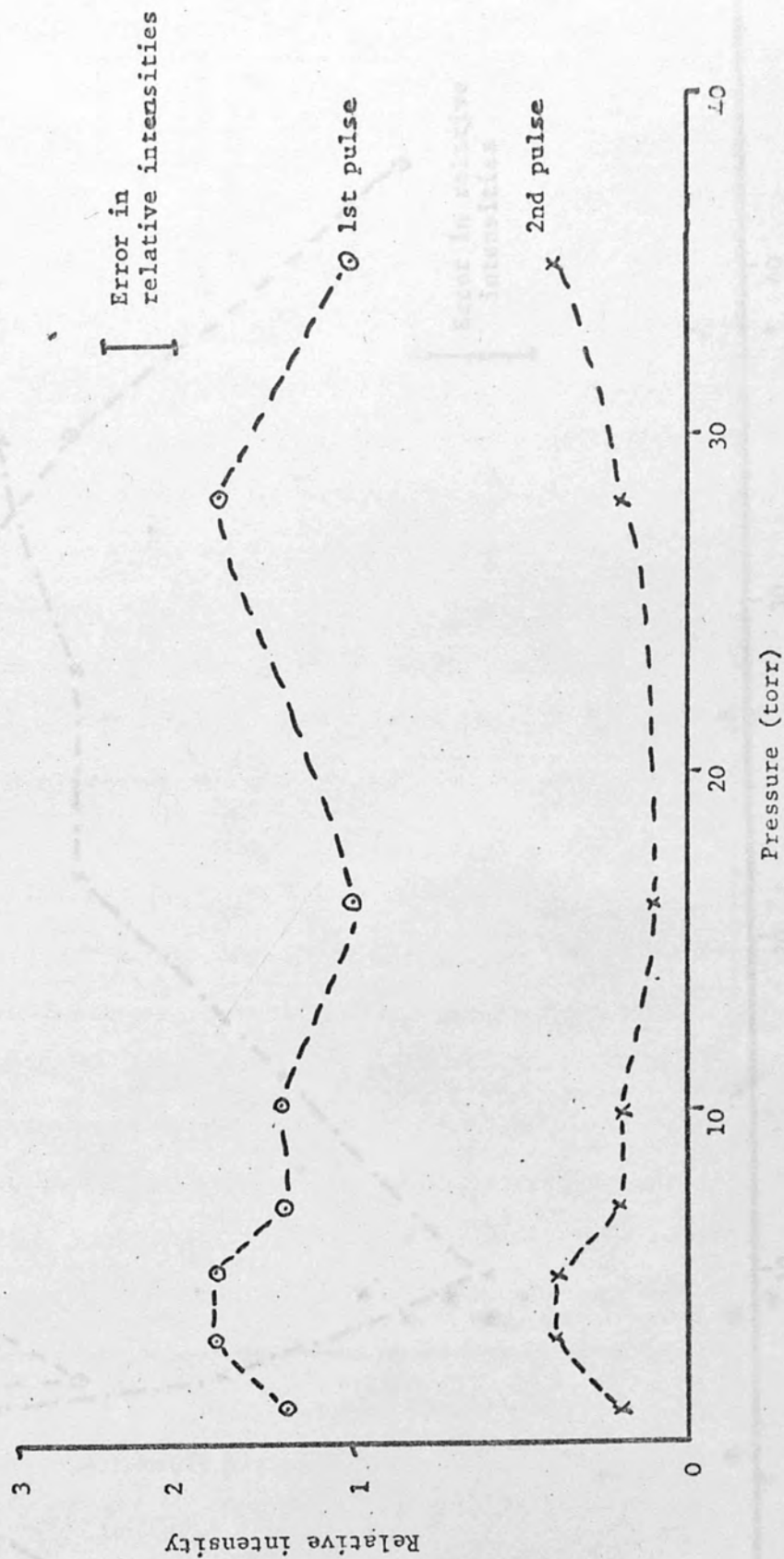
The output from the linear flashtube, viewed with and without filter, under the influence of a continuous preionising discharge was also examined. The use of flashlamp preionisation was first reported by us at a conference in Berlin in 1973, and is now used by Dr Schafer<sup>(155)</sup>.

(Preionisation is covered in detail in the next chapter). Graph 5.5 shows the relative intensity of the first and second pulse viewed through the 18A filter with the flashtube preionised. The relative intensity of the first pulse is always greater than the second pulse. The relative intensity of the second pulse remains at a fairly constant low value. Comparing 5.5 with graph 5.3 (where graph 5.3 shows the UV output without any preionisation) shows that preionisation tends to keep the output intensity at approximately the same level throughout the working pressure regime.

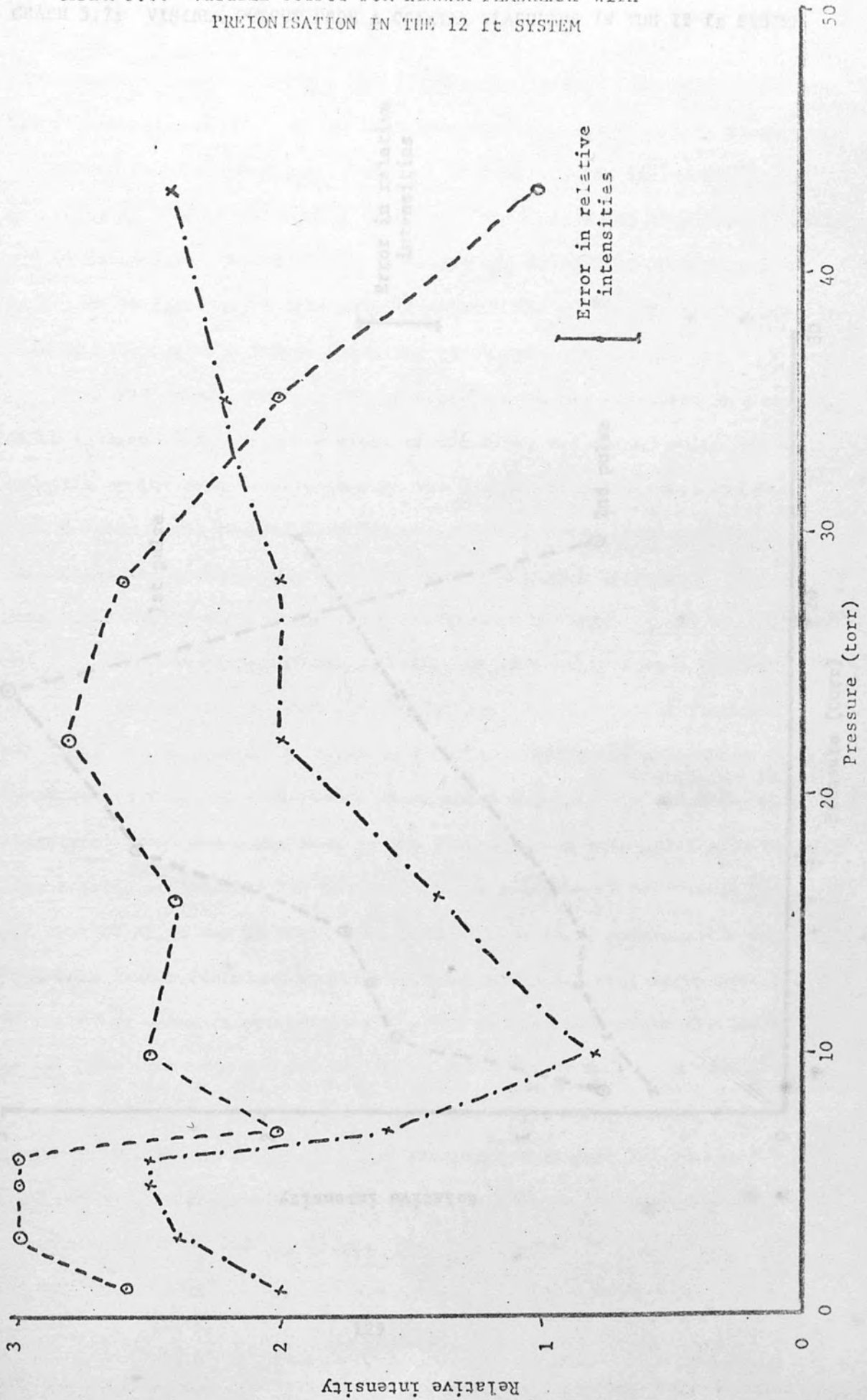
Graph 5.6 shows the output from the linear flashtube without the UV filter, but with preionisation, as a comparison with graph 5.5 which shows the results with the filter. One can observe from graph 5.6 that we have many peaks and troughs once again and at approximately 33 torr the second pulse starts to take over in intensity from the first pulse. A graph similar to graph 5.6 is discussed in more detail in the next chapter which covers output from a preionised flashtube.

The light output, with and without UV filter, from a 14 cm long coaxial flashtube was also studied on the 12 feet system. The flashtube had an outside diameter of 2.5 cm, 1 mm thick fused quartz walls and an annular gap of 1.5 mm. Graph 5.7 shows the light output from this flash lamp without the 18A UV filter in place. The working pressure range of the coaxial flashlamp was less than that of the linear one. A similar sort of

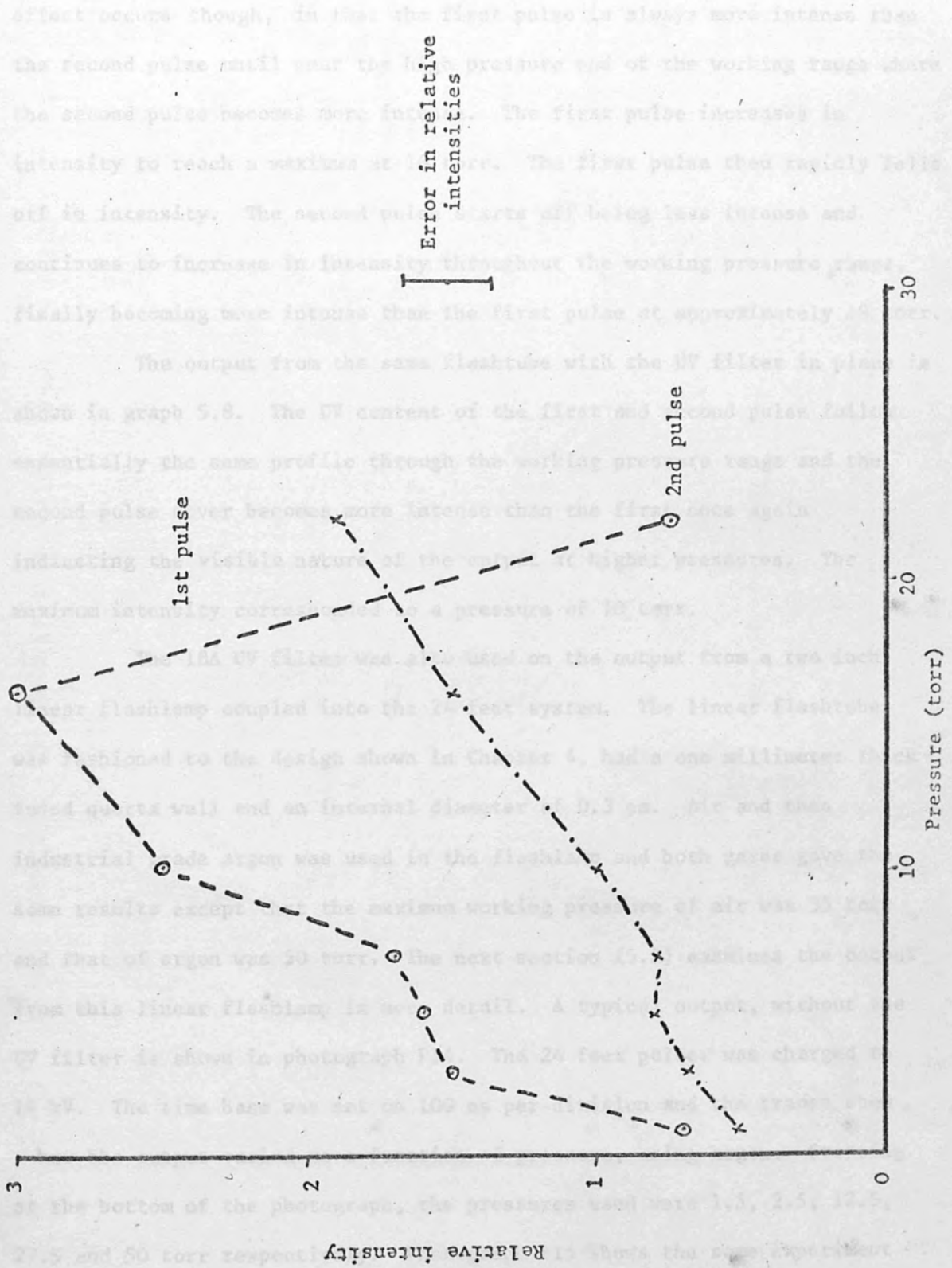
GRAPH 5.5: UV RESPONSE FOR THE DOUBLE PULSE WITH PREIONISATION FOR A LINEAR FLASHLAMP IN THE 12 ft SYSTEM



GRAPH 5.6: VISIBLE OUTPUT FOR LINEAR FLASHLAMP WITH  
PREIONISATION IN THE 12 ft SYSTEM



GRAPH 5.7: VISIBLE OUTPUT FROM A COAXIAL FLASHLAMP IN THE 12 ft SYSTEM



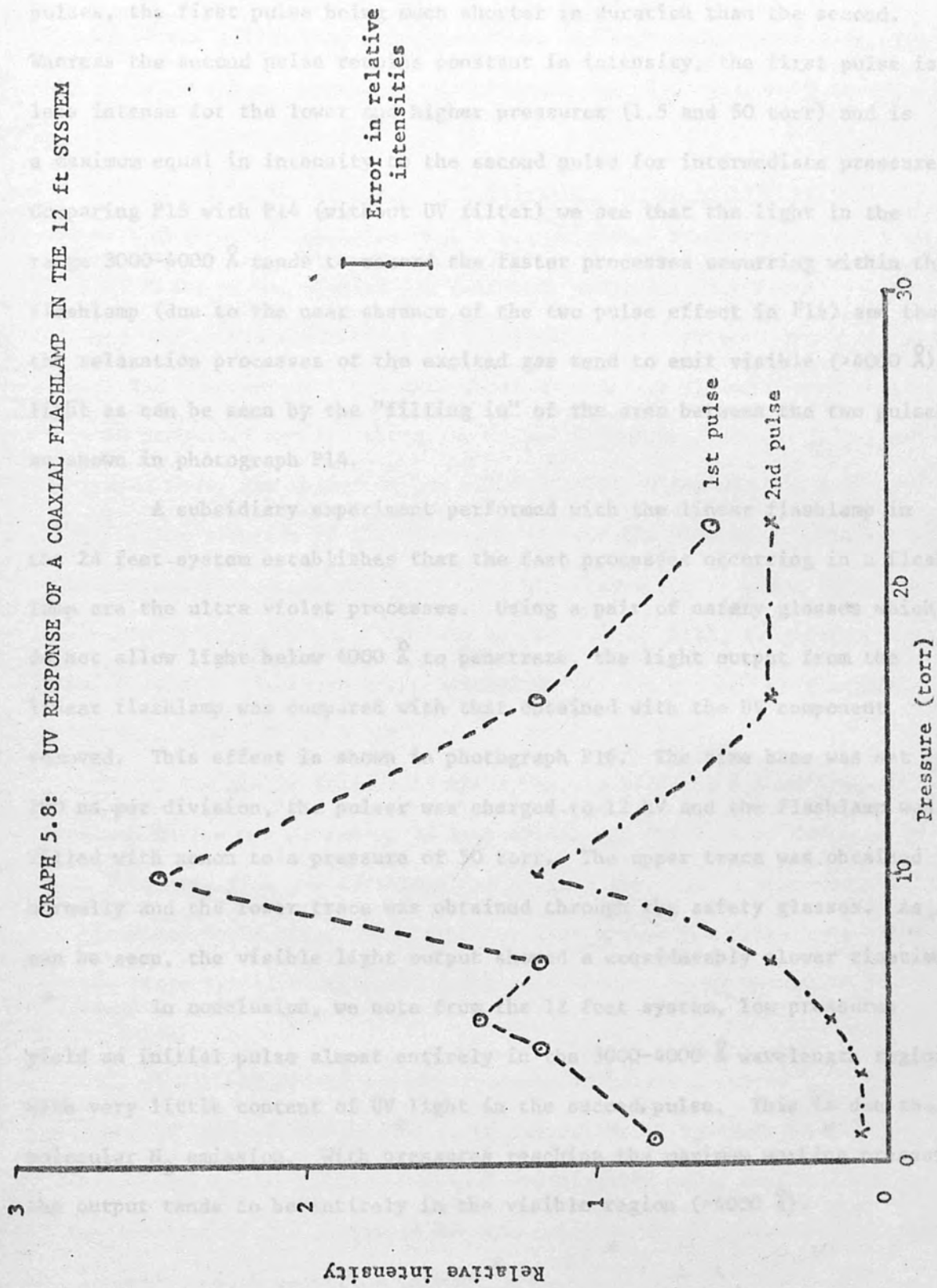


effect occurs though, in that the first pulse is always more intense than the second pulse until near the high pressure end of the working range where the second pulse becomes more intense. The first pulse increases in intensity to reach a maximum at 16 torr. The first pulse then rapidly falls off in intensity. The second pulse starts off being less intense and continues to increase in intensity throughout the working pressure range, finally becoming more intense than the first pulse at approximately 19 torr.

The output from the same flashtube with the UV filter in place is shown in graph 5.8. The UV content of the first and second pulse follow essentially the same profile through the working pressure range and the second pulse never becomes more intense than the first once again indicating the visible nature of the output at higher pressures. The maximum intensity corresponded to a pressure of 10 torr.

The 18A UV filter was also used on the output from a two inch linear flashlamp coupled into the 24 feet system. The linear flashtube was fashioned to the design shown in Chapter 4, had a one millimeter thick fused quartz wall and an internal diameter of 0.3 cm. Air and then industrial grade argon was used in the flashlamp and both gases gave the same results except that the maximum working pressure of air was 35 torr and that of argon was 50 torr. The next section (5.5) examines the output from this linear flashlamp in more detail. A typical output, without the UV filter is shown in photograph P14. The 24 feet pulser was charged to 14 kV. The time base was set on 100 ns per division and the traces show how the output varied as a function of pressure, using argon. Starting at the bottom of the photograph, the pressures used were 1.5, 2.5, 12.5, 27.5 and 50 torr respectively. Photograph P15 shows the same experiment recorded through an 18A UV filter. The output tends to separate into two

GRAPH 5.8: UV RESPONSE OF A COAXIAL FLASHLAMP IN THE 12 ft SYSTEM





pulses, the first pulse being much shorter in duration than the second. Whereas the second pulse remains constant in intensity, the first pulse is less intense for the lower and higher pressures (1.5 and 50 torr) and is a maximum equal in intensity to the second pulse for intermediate pressures. Comparing P15 with P14 (without UV filter) we see that the light in the range 3000-4000 Å tends to record the faster processes occurring within the flashlamp (due to the near absence of the two pulse effect in P14) and that the relaxation processes of the excited gas tend to emit visible (>4000 Å) light as can be seen by the "filling in" of the area between the two pulses as shown in photograph P14.

A subsidiary experiment performed with the linear flashlamp in the 24 feet system establishes that the fast processes occurring in a flashlamp are the ultra violet processes. Using a pair of safety glasses which do not allow light below 4000 Å to penetrate, the light output from the linear flashlamp was compared with that obtained with the UV component removed. This effect is shown in photograph P16. The time base was set to 200 ns per division, the pulser was charged to 12 kV and the flashlamp was filled with xenon to a pressure of 50 torr. The upper trace was obtained normally and the lower trace was obtained through the safety glasses. As can be seen, the visible light output showed a considerably slower risetime.

In conclusion, we note from the 12 feet system, low pressures yield an initial pulse almost entirely in the 3000-4000 Å wavelength region with very little content of UV light in the second pulse. This is due to molecular N<sub>2</sub> emission. With pressures reaching the maximum working pressure the output tends to be entirely in the visible region (>4000 Å).

In the higher energy 24 feet system, the single pulse obtained without filter splits into two pulses when viewed through the filter with each pulse having a considerable fraction of the light intensity in the spectral range 3000-4000 Å.

#### 5.5 Analysis of a short linear flashtube in the 24 feet system

The output intensity from a 6.4 cm linear flashtube with a 3 mm internal diameter was studied for different pressures at constant pulser voltages and constant pressures at different pulser voltages using air and argon. The risetime of the light output for the air filled flashlamp is shown in graph 5.9 and for the argon filled flashlamp in graph 5.10. As the graphs show, the change of gas within the flashlamp did not have any effect on the risetime of the light output from the flashtube. The results show that for both argon and air filled flashlamps the risetime is reduced as the over volting of the flashlamp is increased. Also, in general, the risetime tends to increase with increasing pressure within the flashlamps. (Shown in graphs 5.9 and 5.10).

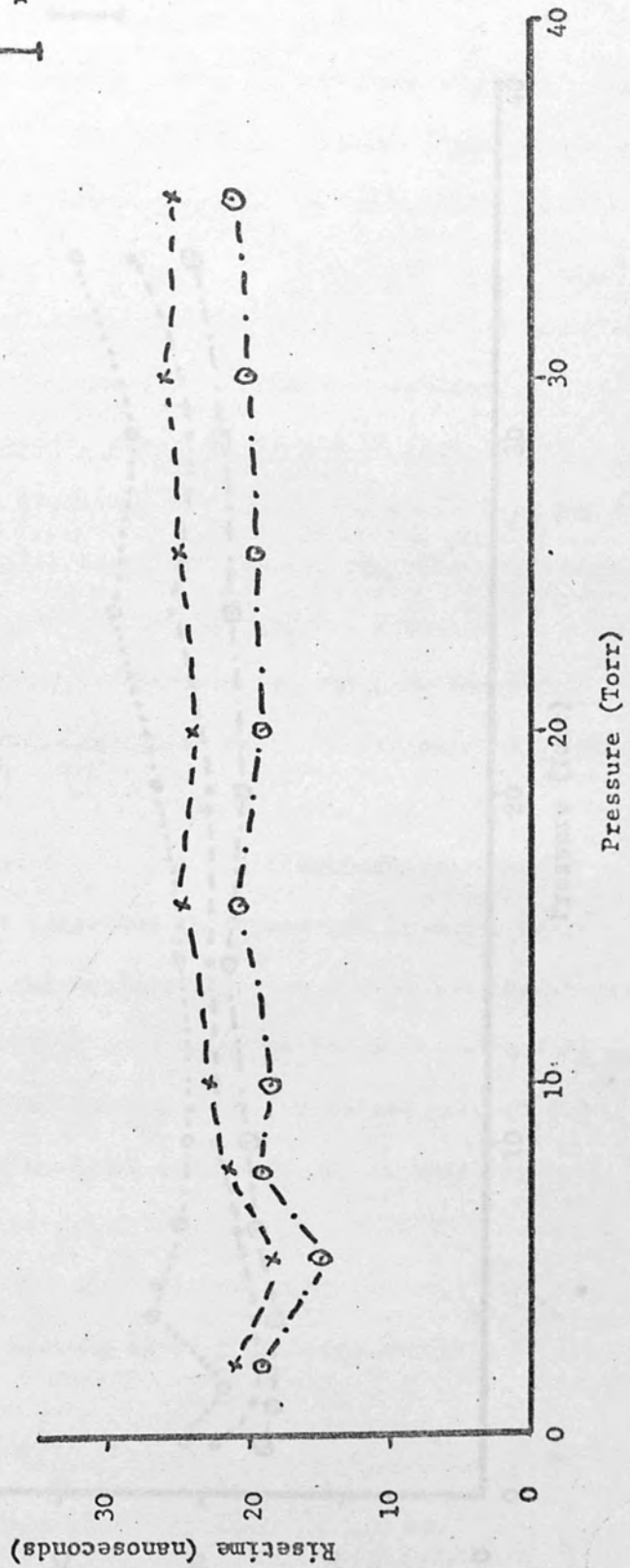
A noticeable feature of these results with the 6.4 cm linear flashlamp in the higher energy 24 feet system was the lack of increase in light intensity from the flashlamp for a given increase in pressure within the flashlamp, or a given increase in voltage across the flashlamp. (The voltage range was 12-16 kV which corresponds to an energy change of 30-50 joules).

A similar effect was observed by Furumoto and Ceccon<sup>(81)</sup> who explained it as a saturation effect of the surface brightness in the visible, ie the walls of the lamp cool the plasma's outer surface, and even if the interior of the plasma is hotter, the long wavelength radiation from the interior cannot penetrate through.

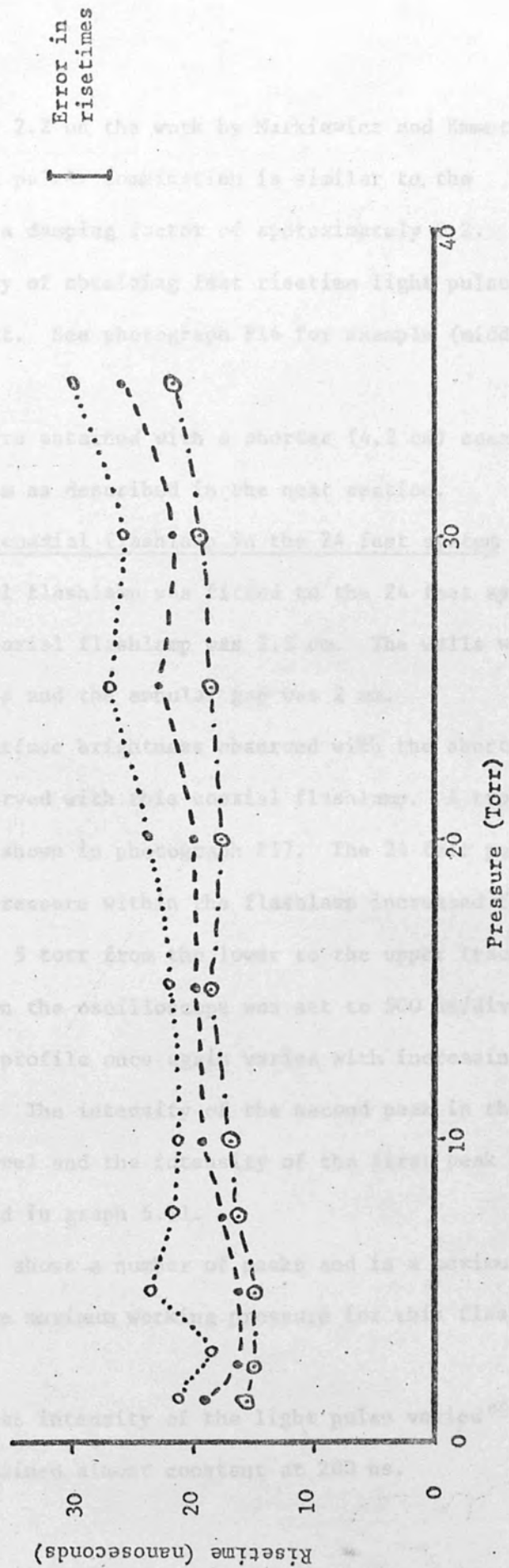
GRAPH 5.9: RISETIME AS A FUNCTION OF PRESSURE FOR DIFFERENT VOLTAGES ACROSS A AIR FILLED LINEAR FLASHLAMP IN THE 24 ft SYSTEM

○ 16 kV  
 × 12 kV

I  
 Error in  
 risetime



GRAPH 5.10: RISETIME AS A FUNCTION OF PRESSURE FOR DIFFERENT VOLTAGES ACROSS AN ARGON FILLED LINEAR FLASHLAMP IN THE 24 ft SYSTEM



Referring to Chapter 2.2 on the work by Markiewicz and Emmett<sup>(75)</sup>, the output from this flashtube pulser combination is similar to the computer print out indicating a damping factor of approximately 0.2. This combination is a convenient way of obtaining fast risetime light pulses of constant amplitude light output. See photograph P14 for example (middle trace).

Different results were obtained with a shorter (4.2 cm) coaxial flashlamp in the 24 feet system as described in the next section.

#### 5.6 Analysis of a short coaxial flashlamp in the 24 feet system

A 4.2 cm long coaxial flashlamp was fitted to the 24 feet system. The outside diameter of the coaxial flashlamp was 2.3 cm. The walls were made of 1 mm thick fused quartz and the annular gap was 2 mm.

The saturation of surface brightness observed with the short linear flashlamp, was not observed with this coaxial flashlamp. A typical output from this flashlamp is shown in photograph P17. The 24 feet pulser was charged to 14 kV and the pressure within the flashlamp increased from 30 torr to 50 torr in steps of 5 torr from the lower to the upper trace respectively. The time base on the oscilloscope was set to 500 ns/division. We can see that the intensity profile once again varies with increasing pressure within the flashlamp. The intensity of the second peak in the pulse remains at a constant level and the intensity of the first peak as a function of pressure is plotted in graph 5.11.

The output intensity shows a number of peaks and is a maximum at 50 torr. This pressure was the maximum working pressure for this flashlamp in this experiment.

Even though the output intensity of the light pulse varied considerably, the risetime remained almost constant at 200 ns.



PHOTOGRAPH P17

Flashlamp output from a 412 cm long coaxial flashlamp filled with air to pressures of

- (a) 50 torr
- (b) 45 torr
- (c) 40 torr
- (d) 35 torr
- (e) 30 torr

Sweep speed 500 ns/division  
Blumlein voltage 14 kV

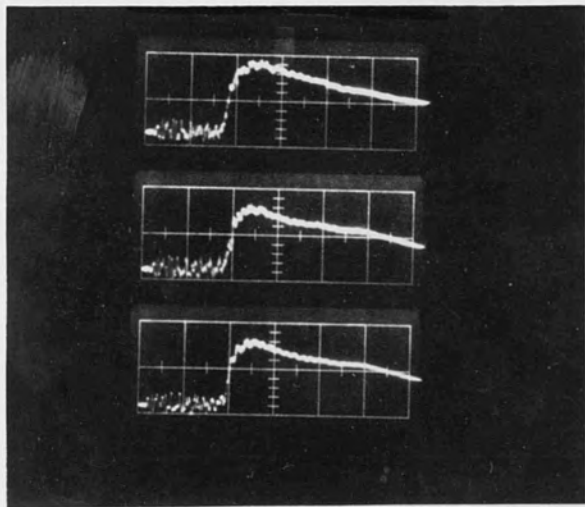
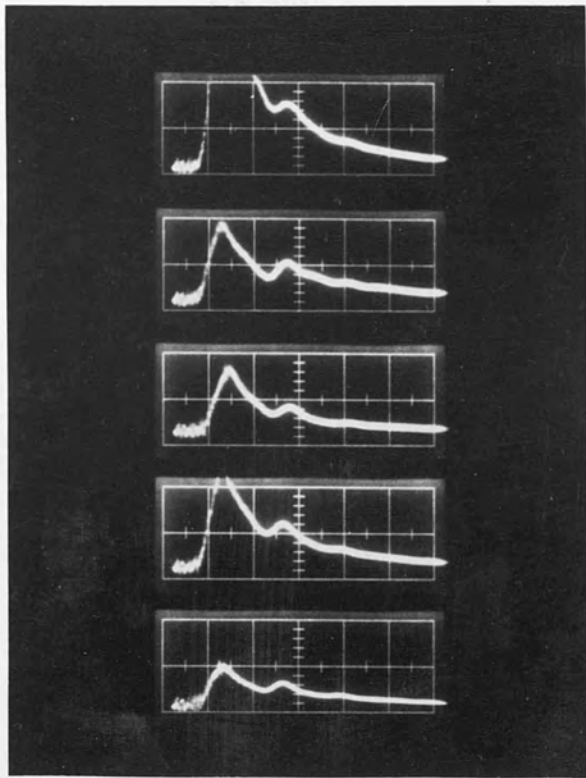
PHOTOGRAPH P18

Flashlamp output from a 412 cm long coaxial flashlamp filled with air to pressures of

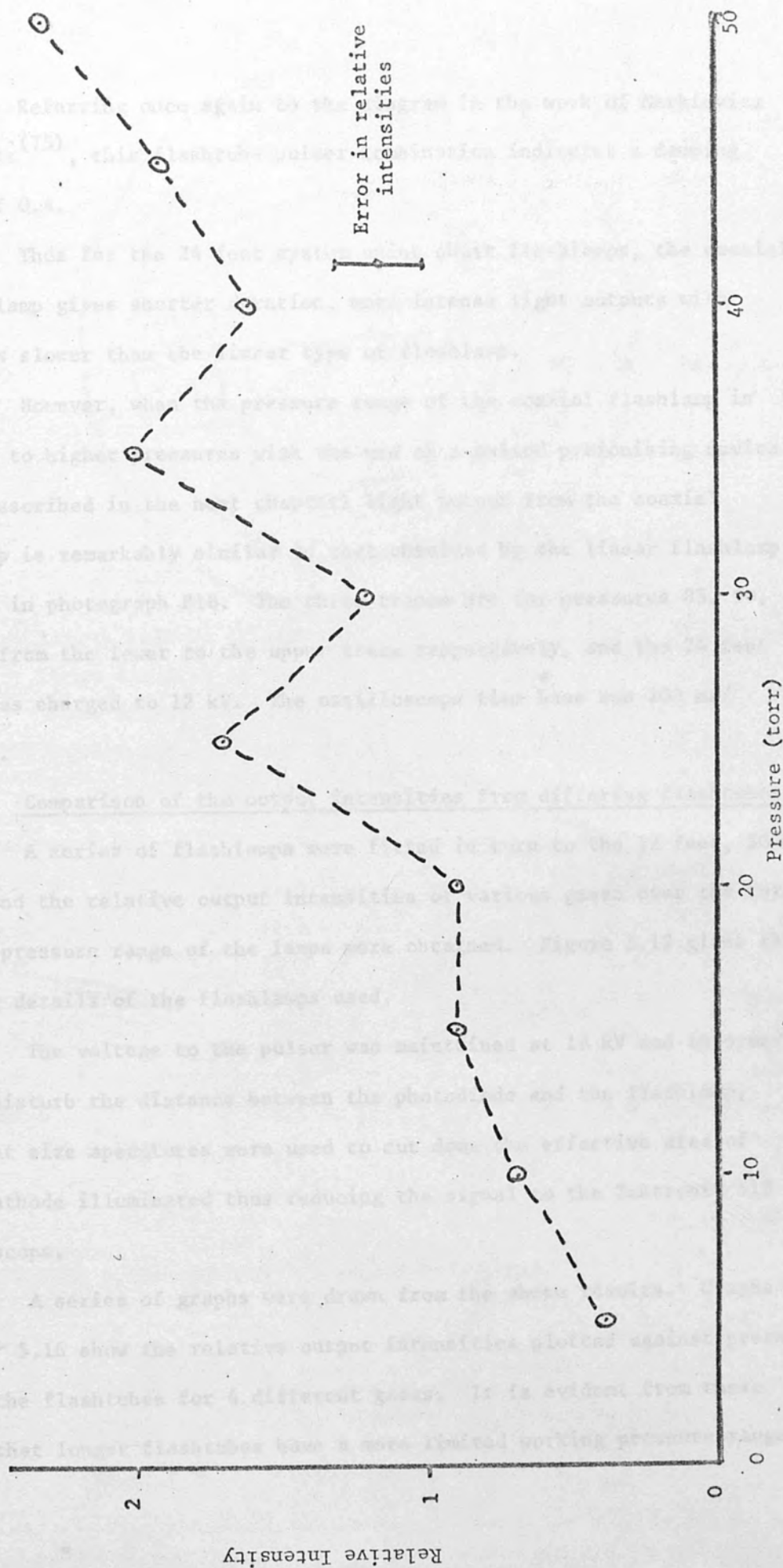
- (a) 95 torr
- (b) 90 torr
- (c) 85 torr

Sweep speed 200 ns/division  
Blumlein voltage 12 kV





GRAPH 5.11: OUTPUT INTENSITY FROM A 4.2 cm LONG COAXIAL FLASHTUBE IN THE 24 ft SYSTEM



Referring once again to the diagram in the work of Markiewicz and Emmett<sup>(75)</sup>, this flashtube pulser combination indicates a damping factor of 0.4.

Thus for the 24 feet system using short flashlamps, the coaxial type of lamp gives shorter duration, more intense light outputs with risetimes slower than the linear type of flashlamp.

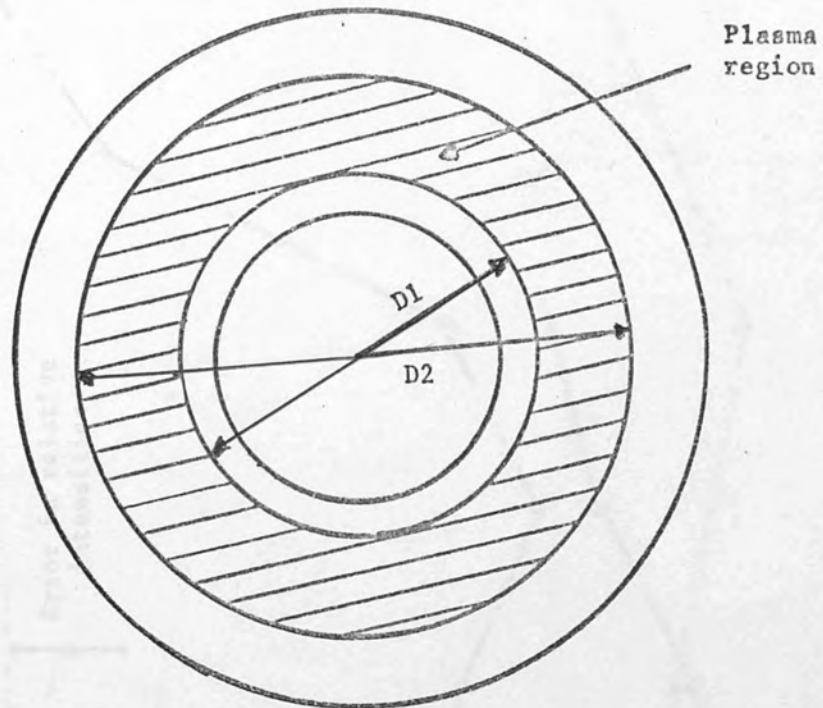
However, when the pressure range of the coaxial flashlamp is extended to higher pressures with the use of a pulsed preionising device (to be described in the next chapter) light output from the coaxial flashlamp is remarkably similar to that obtained by the linear flashlamp as shown in photograph P18. The three traces are for pressures 85, 90, 95 torr from the lower to the upper trace respectively, and the 24 feet pulser was charged to 12 kV. The oscilloscope time base was 200 ns/division.

#### 5.7 Comparison of the output intensities from differing flashtubes

A series of flashlamps were fitted in turn to the 12 feet, 20 ns pulser and the relative output intensities of various gases over the total working pressure range of the lamps were obtained. Figure 5.12 gives the relevant details of the flashlamps used.

The voltage to the pulser was maintained at 18 kV and in order not to disturb the distance between the photodiode and the flashlamp, different size apertures were used to cut down the effective area of photo cathode illuminated thus reducing the signal to the Tektronix 519 oscilloscope.

A series of graphs were drawn from the above results. Graphs 5.13 → 5.16 show the relative output intensities plotted against pressure within the flashtubes for 4 different gases. It is evident from these graphs that longer flashtubes have a more limited working pressure range

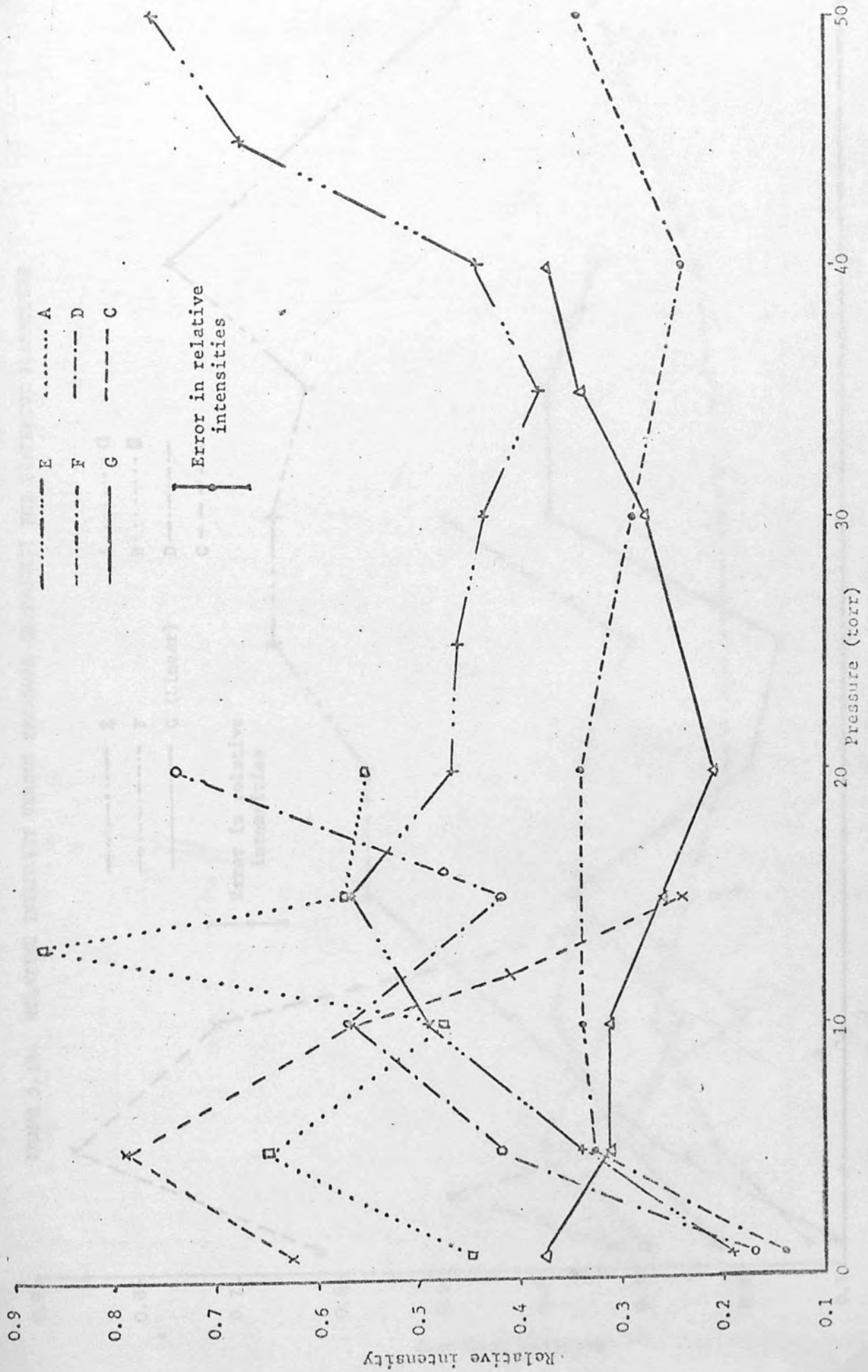


- L = Length between electrodes
- $D_1$  = Outer diameter of inner tube
- $D_2$  = Inner diameter of outer tube
- Y = Annular gap

Flashlamps	L(cm)	$D_1$ (cm)	$D_2$ (cm)	Y (cm)
Coax A	14.1	1.9	2.3	0.2
Coax B	14.1	1.7	2.1	0.2
Coax C	14.5	0.7	2.3	0.8
Coax D	8.8	2.4	2.7	0.15
Coax E	4.2	1.9	2.3	0.2
Coax F	4.2	0.6	1.2	0.3
Linear G	6.4	-	0.4	-

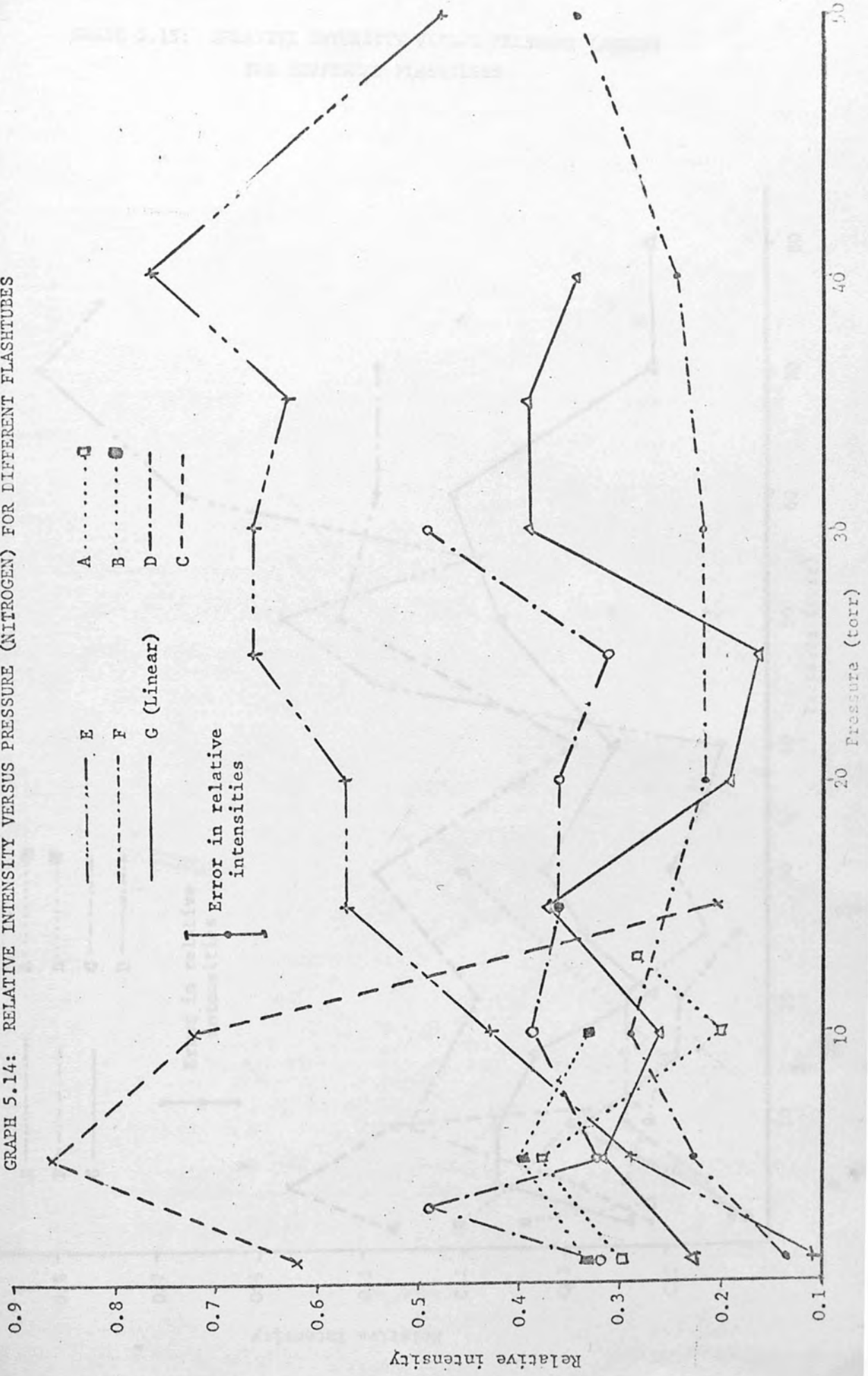
FIGURE 5.12: RELEVANT FLASHLAMP PARAMETERS

GRAPH 5.13: RELATIVE INTENSITY VERSUS PRESSURE (AIR) FOR DIFFERENT FLASHTUBES

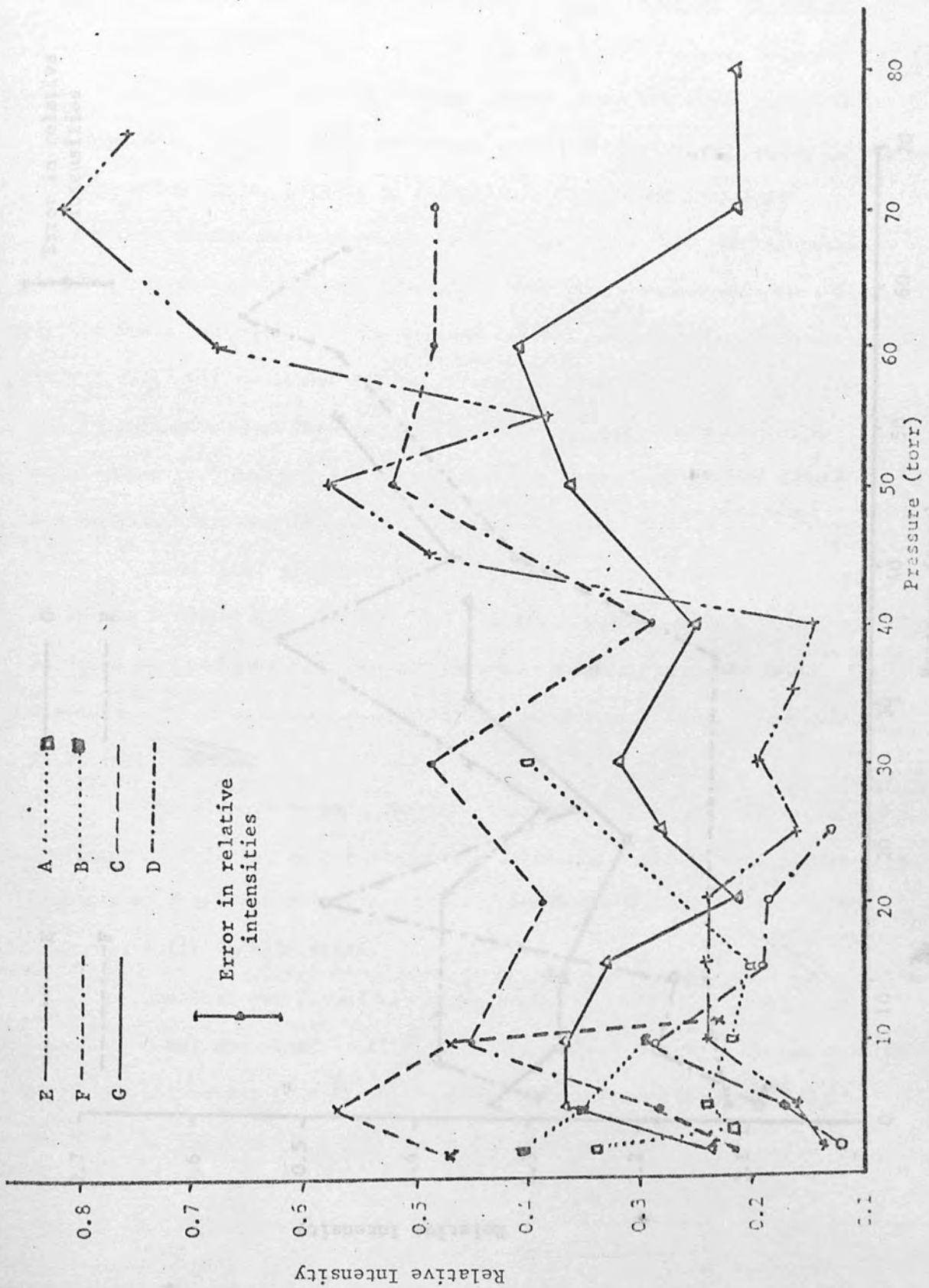




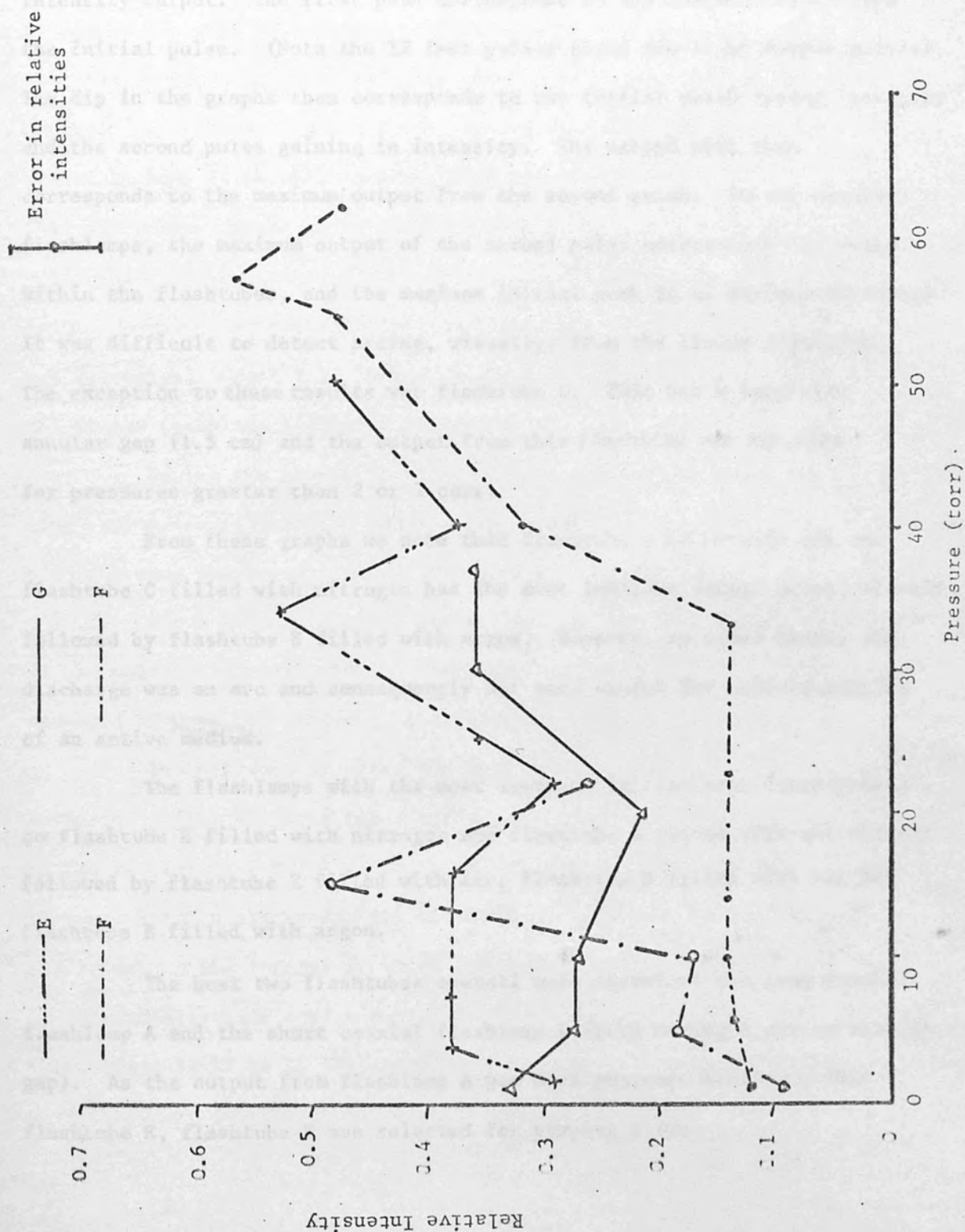
GRAPH 5.14: RELATIVE INTENSITY VERSUS PRESSURE (NITROGEN) FOR DIFFERENT FLASHTUBES



GRAPH 5.15: RELATIVE INTENSITY VERSUS PRESSURE (ARGON)  
FOR DIFFERENT FLASHTUBES:



GRAPH 5.16: RELATIVE INTENSITY VERSUS PRESSURE (XENON)  
FOR DIFFERENT FLASHTUBES



than the shorter flashtubes, and that narrow annular gap coaxial flashtubes are more luminous than the wide annular gap coaxial flashtubes and the linear flashtube. All the results show two major peaks in the relative intensity output. The first peak corresponds to the maximum output from the initial pulse. (Note the 12 feet pulser gives two light output pulses). The dip in the graphs then corresponds to the initial pulse losing intensity and the second pulse gaining in intensity. The second peak then corresponds to the maximum output from the second pulse. In the coaxial flashlamps, the maximum output of the second pulse corresponds to arcing within the flashtubes, and the maximum initial peak is of uniform discharge. It was difficult to detect arcing, visually, from the linear flashlamp. The exception to these results was flashtube C. This had a very wide annular gap (1.5 cm) and the output from this flashlamp was arc like for pressures greater than 2 or 3 torr.

From these graphs we note that flashtube A filled with air and flashtube C filled with nitrogen had the most luminous second pulse, closely followed by flashtube E filled with argon. However, as noted above, the discharge was an arc and consequently not very useful for uniform pumping of an active medium.

The flashlamps with the most luminous initial peak corresponded to flashtube E filled with nitrogen and flashtube A filled with air closely followed by flashtube E filled with air, flashtube D filled with air and flashtube E filled with argon.

The best two flashtubes overall were therefore the long coaxial flashlamp A and the short coaxial flashlamp E (both having a narrow annular gap). As the output from flashlamp A was more pressure sensitive than flashtube E, flashtube E was selected for pumping a dye.

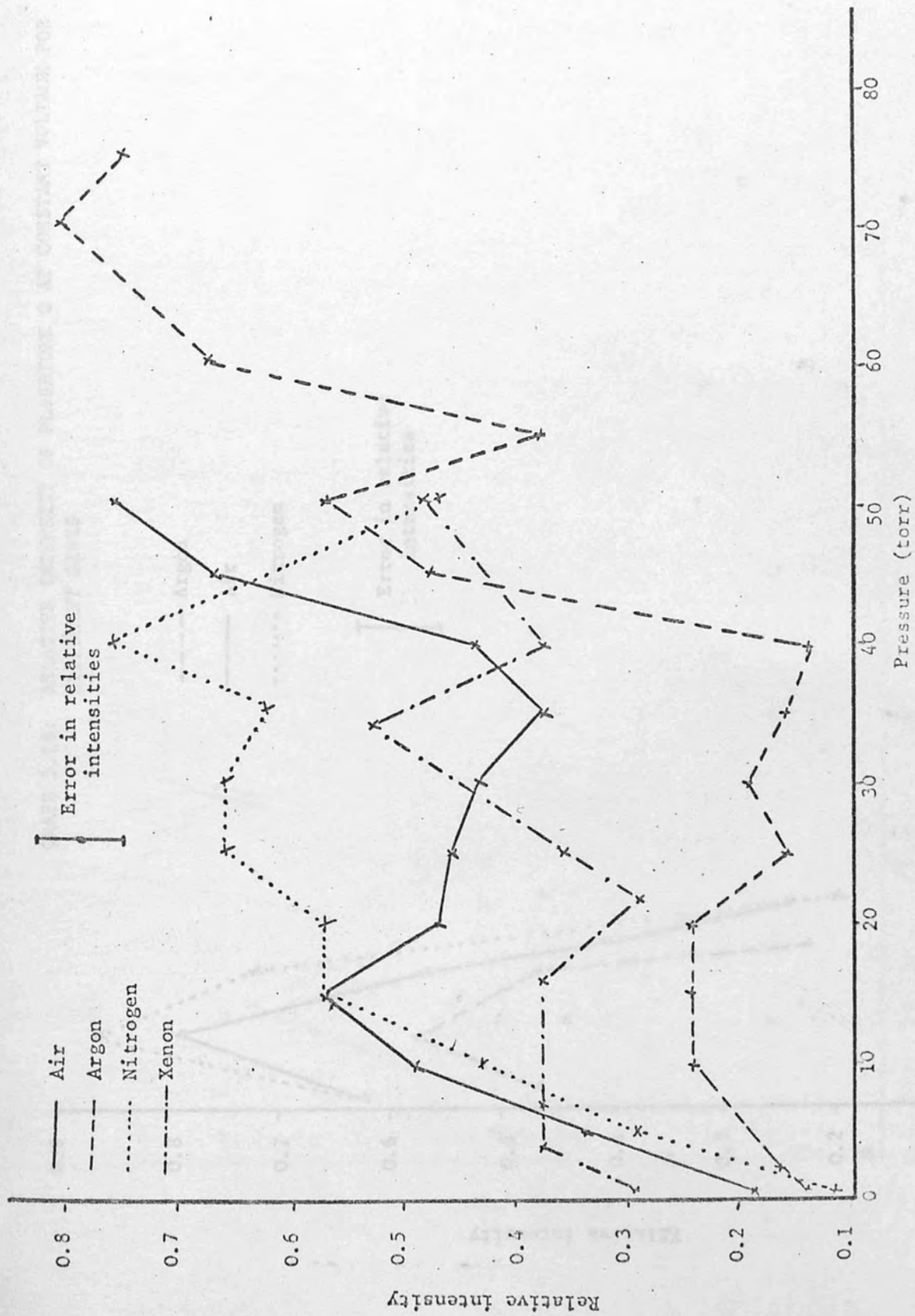
Graphs 5.17-5.22 were drawn to show the effect of different gases on the same flashtube more clearly. Each graph shows the relative intensity versus pressure for a number of gases within a given flashlamp. From these results we see that argon extends the working pressure of each flashtube and that it could be a useful gas to mix with other gases to give better flashlamp outputs. The results also show that no one gas was the best overall for a given flashlamp and that different gases performed better in some flashtubes compared with others. The notable exception to this was xenon. Xenon never showed itself to be a particularly luminous gas. This is surprising as many commercial flashlamps are filled with xenon. However, most commercial flashlamps are of the linear type with an arc discharge. Graph 5.22 in fact shows xenon becoming more luminous for the linear flashlamp at higher pressures.

During the change from the initial fast rising pulse to the second slow rising longer duration pulse, there exists a point where the two pulses have the same intensity. The double peak was critically pressure dependent ( $<1$  torr) for a given flashtube and a given voltage for the 12 feet system. If the potential applied to the flashlamp was increased, the double pulse occurred at a higher pressure, and the flashlamp pressure range was extended.

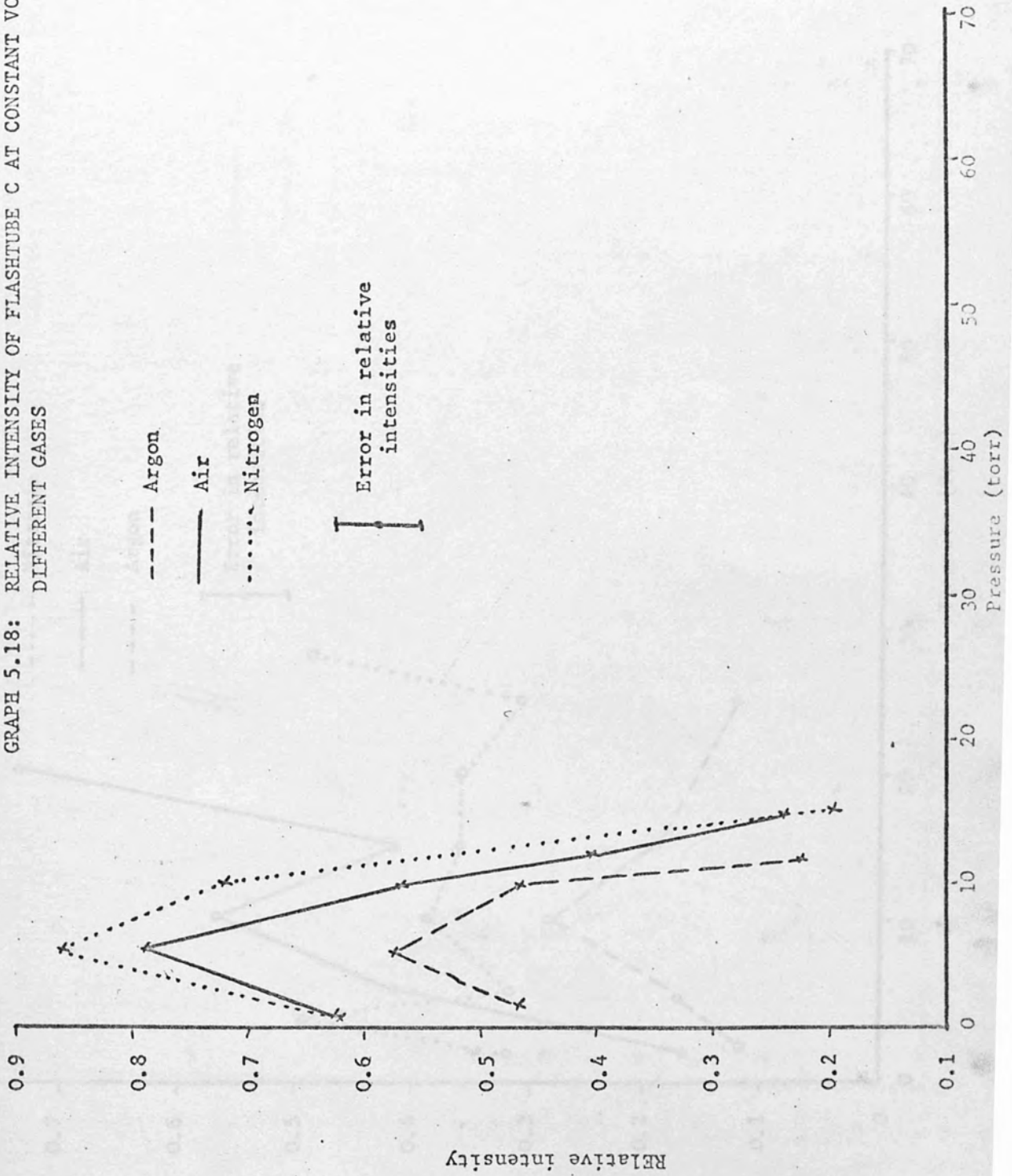
The pressure at which the double pulse occurred was noted for different pulser voltages for a series of coaxial flashlamps filled with air in the 12 feet pulser. A graph (5.23) was drawn with flashlamp pressure X distance between electrodes (as the ordinate) against voltage (as the abscissae) for the voltage at which the double pulse occurred in a given pressure X electrode (pd) separation. The voltage to the 12 feet pulser was varied from 12 kV to 20 kV, and within experimental error, straight lines were obtained; (see graph 5.23), for coaxial flashlamps A and B. The



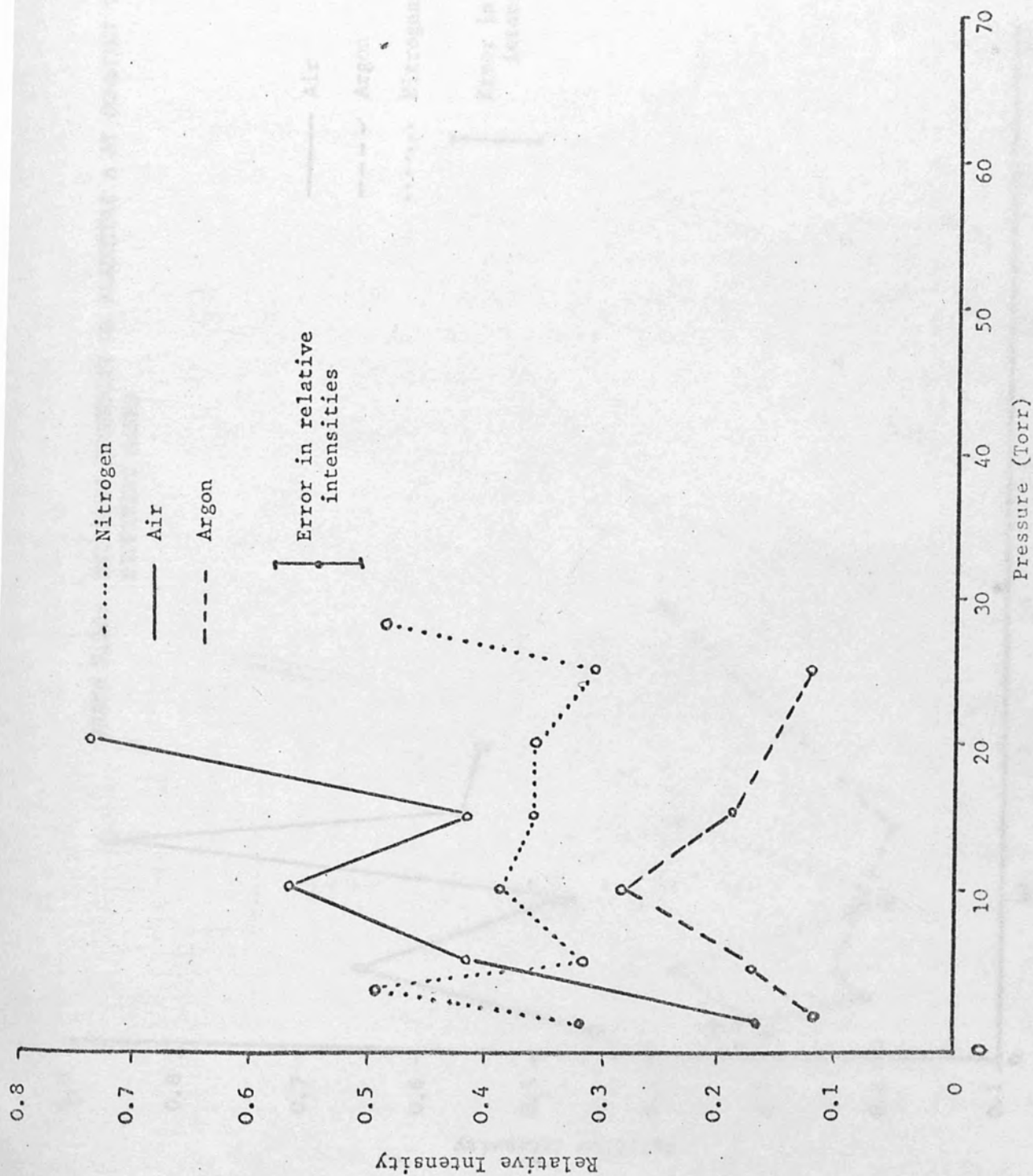
GRAPH 5.17: RELATIVE INTENSITY OF FLASHTUBE E AT CONSTANT VOLTAGE FOR DIFFERENT GASES.



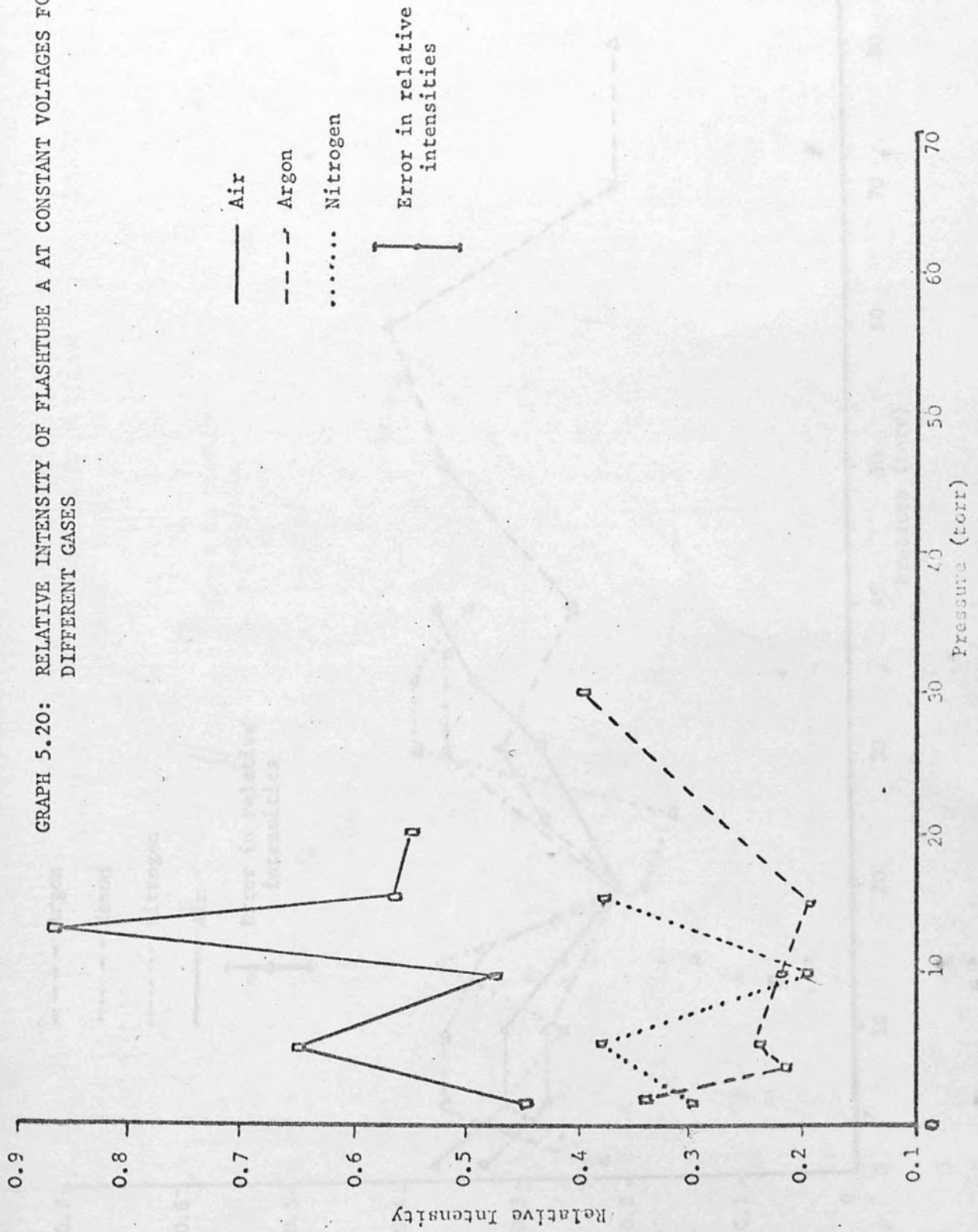
GRAPH 5.18: RELATIVE INTENSITY OF FLASHTUBE C AT CONSTANT VOLTAGE FOR DIFFERENT GASES



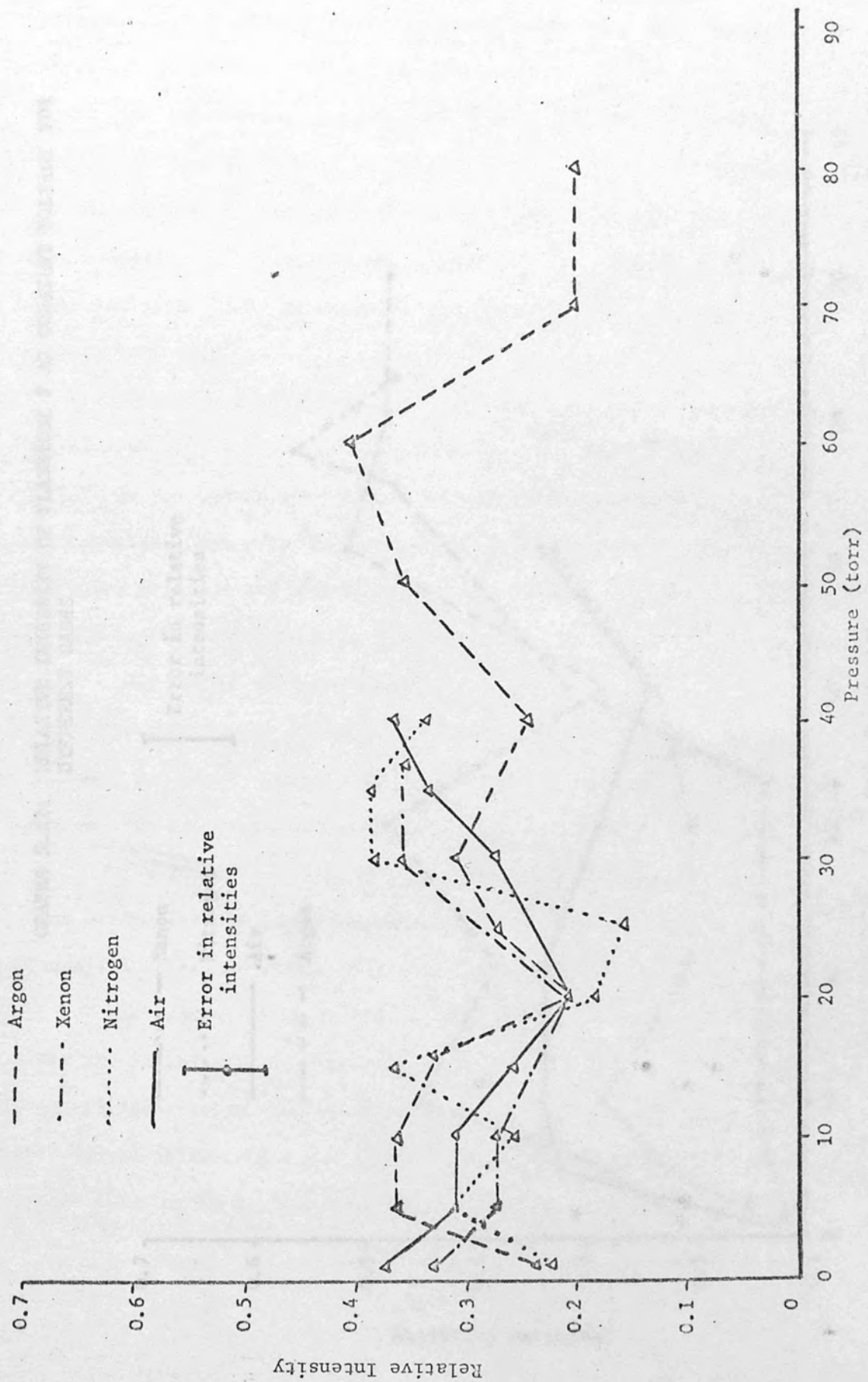
GRAPH 5.19: RELATIVE INTENSITY OF FLASHTUBE D AT CONSTANT VOLTAGE FOR DIFFERENT GASES



GRAPH 5.20: RELATIVE INTENSITY OF FLASHTUBE A AT CONSTANT VOLTAGES FOR DIFFERENT GASES

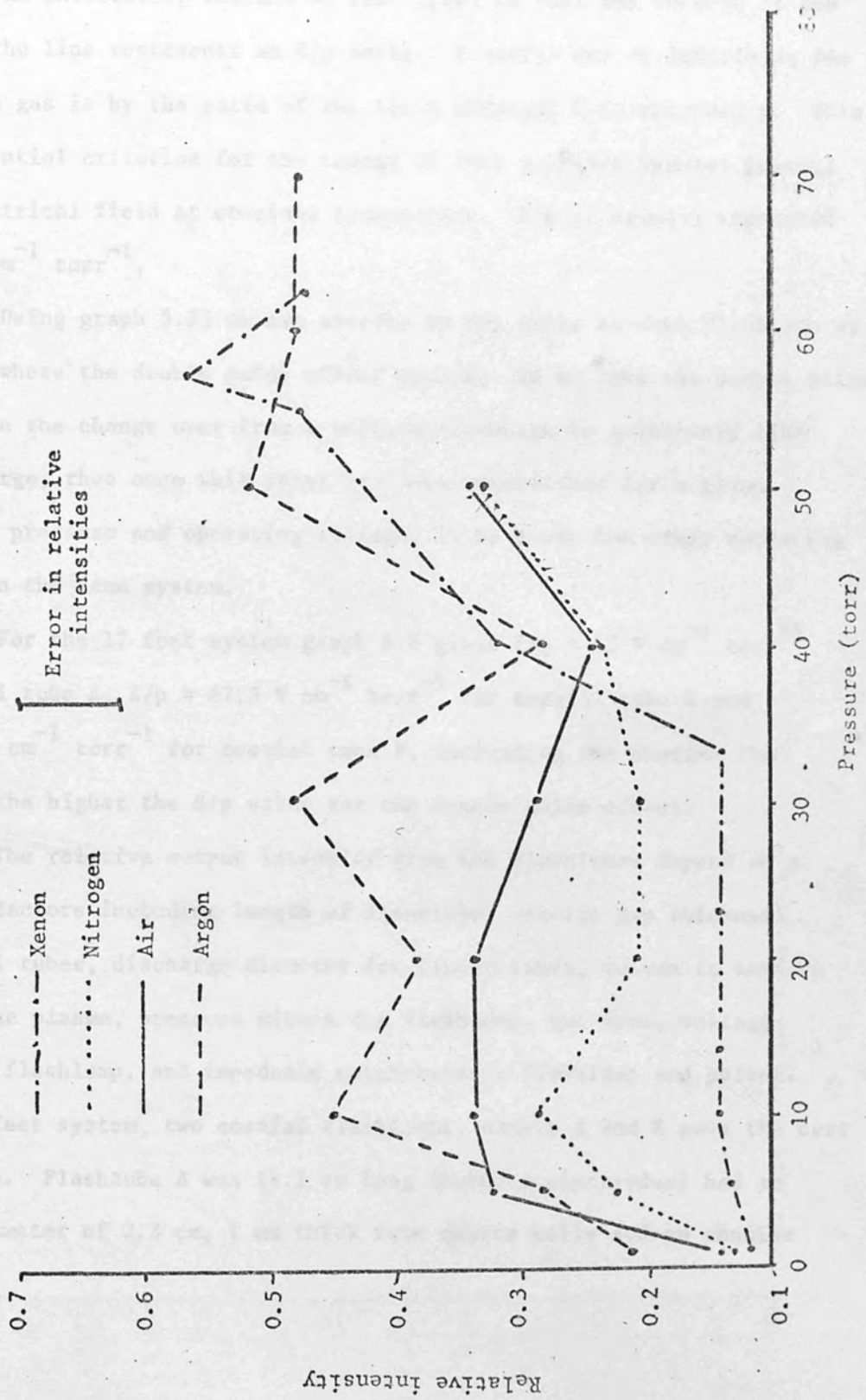


GRAPH 5.21: RELATIVE INTENSITY OF FLASHTUBE G AT CONSTANT VOLTAGES FOR DIFFERENT GASES





GRAPHS 5.22: RELATIVE INTENSITY OF FLASHTUBE F AT CONSTANT VOLTAGE FOR DIFFERENT GASES



shorter coaxial flashlamp F starts as a straight line and then tails off towards higher pd for lower pulser voltages.

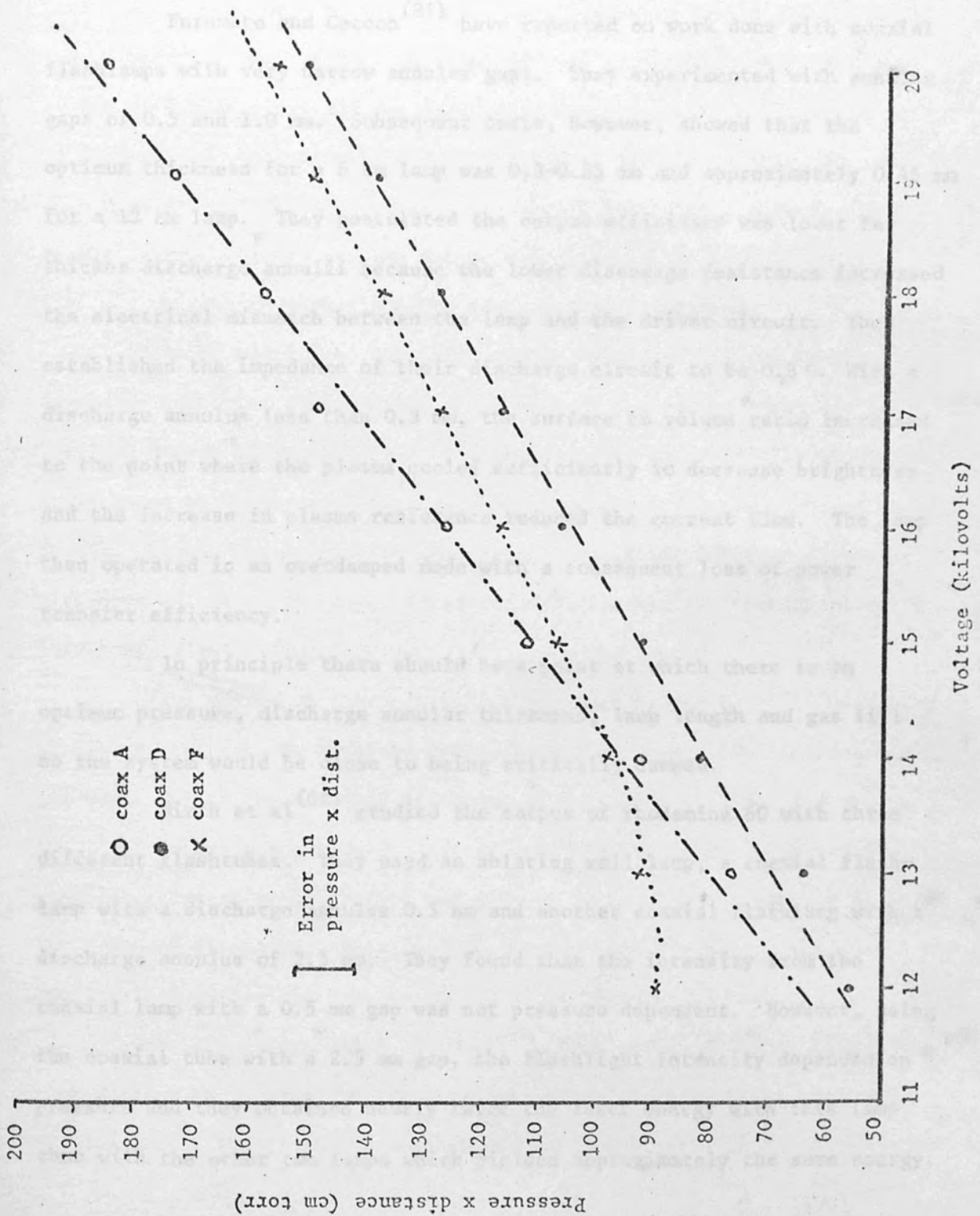
An interesting feature of this graph is that the inverse of the slope of the line represents an E/p value. A useful way of describing the state of a gas is by the ratio of the field strength E to pressure p. This is an essential criterion for the energy of ions acquired between impacts in an electrical field at constant temperature. E/p is usually expressed in volts  $\text{cm}^{-1} \text{ torr}^{-1}$ .

Using graph 5.23 we can ascribe an E/p value to each flashlamp at the point where the double pulse effect occurs. If we take the double pulse point to be the change over from a uniform discharge to a Townsend like arc discharge, then once this point has been established for a given flashtube, pressure and operating voltage, it is known for other operating voltages on the same system.

For the 12 feet system graph 6.6 gives  $E/p \approx 65 \text{ V cm}^{-1} \text{ torr}^{-1}$  for coaxial tube A,  $E/p \approx 87.5 \text{ V cm}^{-1} \text{ torr}^{-1}$  for coaxial tube D and  $E/p \approx 99 \text{ V cm}^{-1} \text{ torr}^{-1}$  for coaxial tube F, indicating the shorter the flashtube the higher the E/p value for the double pulse effect.

The relative output intensity from the flashtubes depend on a number of factors including length of flashtube, annular gap thickness for coaxial tubes, discharge diameter for linear tubes, volume to surface ratio of the plasma, pressure within the flashlamp, gas type, voltage across the flashlamp, and impedance match between flashlamp and pulser. In our 12 feet system, two coaxial flashlamps, namely A and E gave the best performance. Flashtube A was 14.1 cm long (between electrodes) had an outside diameter of 2.3 cm, 1 mm thick fuse quartz walls and an annular

GRAPH 5.23: GRAPH SHOWING PRESSURE x DISTANCE VERSUS VOLTAGE AT WHICH DOUBLE PEAK OCCURS FOR DIFFERENT COAXIAL FLASHLAMPS



gap of 1 mm. It performed well with air as the gas fill. Flashtube E was 4.2 cm long (between electrodes) had an outside diameter of 2.3 cm 1 mm thick fused quartz walls and an annular gap of 1 mm. Its performance was good for all gases studied. (Air, nitrogen, argon and xenon). Other coaxial tubes with narrower or wider annular gaps did not perform so well.

Furumoto and Ceccon<sup>(81)</sup> have reported on work done with coaxial flashlamps with very narrow annular gaps. They experimented with annular gaps of 0.5 and 1.0 mm. Subsequent tests, however, showed that the optimum thickness for a 6 cm lamp was 0.3-0.35 mm and approximately 0.45 mm for a 12 cm lamp. They postulated the output efficiency was lower for thicker discharge annulii because the lower discharge resistance increased the electrical mismatch between the lamp and the driver circuit. They established the impedance of their discharge circuit to be  $0.3 \Omega$ . With a discharge annulus less than 0.3 mm, the surface to volume ratio increased to the point where the plasma cooled sufficiently to decrease brightness and the increase in plasma resistance reduced the current flow. The lamp then operated in an overdamped mode with a consequent loss of power transfer efficiency.

In principle there should be a point at which there is an optimum pressure, discharge annular thickness, lamp length and gas fill so the system would be close to being critically damped.

Hirth et al<sup>(62)</sup> studied the output of rhodamine 6G with three different flashtubes. They used an ablating wall lamp, a coaxial flashlamp with a discharge annulus 0.5 mm and another coaxial flashlamp with a discharge annulus of 2.5 mm. They found that the intensity from the coaxial lamp with a 0.5 mm gap was not pressure dependent. However, using the coaxial tube with a 2.5 mm gap, the flashlight intensity depended on pressure and they obtained nearly twice the laser energy with this lamp than with the other two lamps which yielded approximately the same energy.



It is interesting to note here that in the published literature on dye lasers pumped by flashlamps, an E/p figure around  $50 \text{ V cm}^{-1} \text{ torr}^{-1}$  is used most often. For the 12 feet pulser, the lowest E/p value obtained was for the argon filled flashlamp and this was around  $60 \text{ V cm}^{-1} \text{ torr}^{-1}$ . Lower E/p values could be more easily obtained using the 24 feet 90 nano-second pulser. (The greater capacity of this pulser allowed flashlamps to run at higher pressures for less voltage across them). Therefore the 24 feet pulser was destined for dye laser work and the 12 feet, 20 nano-second pulser was destined to pump a gas cell filled with nitrogen to enable us to obtain a nitrogen pumped dye laser.

#### 5.8 Discharge mechanisms for fast coaxial flashlamps

In an electrical discharge at low values of E/p the Townsend discharge mechanism predominates. The primary ionisation mechanism is electron impact ionisation, and the current grows exponentially with time. These types of trace were obtained when the coaxial flashlamps arced in our system. Due to the filamentary discharge, the circuit inductance remains high even in a coaxial geometry and current risetime and consequently light output risetime is long.

The discharge characteristics obtained by Furumoto<sup>(81)</sup> were very similar to the ones we obtained before arcing occurred. The characteristics are quite unlike the Townsend discharge characteristics discussed above. The light output trace showed a lot of hash and its rising edge had a gradient greatest at initiation and did not increase exponentially as in the Townsend discharge. Also, unlike the Townsend discharge, the output was completely reproducible even to the point of reproducing hash.

In the recent years Raethers<sup>(94)</sup> Kanalaufbau or Kanal Theory has been applied to explain the rapid radial growth of an electron avalanche. In this model, the electrons accelerated in an impressed field across a gas



start an avalanche similar to a Townsend discharge. At high fields and high current amplification rates the external field is soon modified by space charge effects. The plasma is distorted by the external field into a dipole, and local fields greater than the external applied field are produced. Meanwhile high energy UV photons are being released by collisions and recombinations within the plasma cloud. The photons emanating from the plasma ionise the neutral gas surrounding the plasma, and the electronic products of the ionisation are rapidly accelerated toward the head of the plasma cloud, suffering ionising collisions on the way. Each of the secondary channels can likewise repeat the process.

In the analysis of Kanalaufbau, investigators used uniform fields, or slight modification of uniform fields. In addition currents were kept low for diagnostic purposes, so that self and mutual inductances as well as magnetic field effects could be ignored. The fast flashlamp, on the other hand, is primarily a high current process, and self inductance is a dominant parameter. The high current discharges consequently develops high magnetic fields which cannot be ignored. Despite the difference, the Kanal theory modified to include the presence of magnetic field effects was used by Furumoto and Ceccon<sup>(81)</sup> to qualitatively explain the process observed during the discharge of the coaxial flashlamp.

In the fast, coaxial lamp the discharge starts in a manner described above for the Kanal theory. However, the discharge is confined to the narrow annular channel between the two walls so any blooming of the streamer tends to fill the discharge volume quickly. This process is aided by the magnetic field generated by the outer current sheet which tends to channel electrons azimuthally towards regions of low or no current density. The azimuthal magnetic field tends to uniformly distribute the plasma current sheet. Due to this uniform distribution, the self inductance of

the lamp can easily decrease by an order of magnitude from the value given by a single filament. The current can then rise rapidly because of the decrease in inductance of the lamp and the increased current increases Kanal formation. The stored energy in the capacitor can be rapidly depleted in this self-propagating process. The current pulse is not expected to be simple exponential and the characteristic toe of a Townsend discharge current is not observed. The hash observed by Furumoto and Ceccon on the current traces were ascribed to the successors or more exactly photo-successors as described by Raether<sup>(94)</sup>.

## CHAPTER VI

### PREIONISATION

#### 6.1 Gas breakdown at radio frequencies

Radiation is absorbed in the radio frequency region by the same fundamental process as at all other wavelengths - ie the separation of the energy levels concerned is equal to one quantum of the incident radiation - but the energy of quanta at these frequencies is very small, and is only about a ten millionth of an electron volt. The small splittings necessary to produce absorption in the radio frequency region are those normally associated with the hyperfine structure of electronic spectra, and correspond to the different orientations of the nuclear moments in an applied field. In atomic spectra these energy level splittings produce small changes in the total energy of the electronic transition, and are thus responsible for the hyper fine structure, whereas, in the radio frequency region, it is the transitions between these individual energy levels themselves that produce the absorption spectra. This type of absorption, however, would not cause breakdown and ionisation in a gas.

When radio frequency and microwave frequencies are used, the electric field oscillates so rapidly that the force on an electron changes direction before the electron can travel very far<sup>(92)</sup>. This means that electrons are not swept out of the discharge areas as they are when lower frequencies are used. Electrons that leave the discharge area do so by the process of diffusion. Electrons can also be lost to the system within the body of the discharge by recombination or attachment. There will be relatively few electrons of very high energy striking the walls of the container. For this reason the production of secondary electrons at the walls need not be considered; all electrons are produced within the body of the discharge by field ionisation.

Consider this process in detail by following a single electron which we assume has practically zero energy. The electric field accelerates it for a short time until the field changes direction or the electron collides with an atom. The collision, in general, will result in a change in the direction of motion of the electron but will cause little loss in speed (elastic collision). On average a fraction  $2m/M$  of the energy is transferred to the atom, where  $m$  and  $M$  are the masses of the electron and atom respectively. After collision the electron is accelerated by the electric field for another brief interval. The energy of the electron increases and decreases by small steps, the increases depending on the electric field applied and, in general, adding up to more than the decreases. When the electron has reached a kinetic energy greater than the lowest excitation energy of the atom, there will be a finite chance that the next collision will be inelastic and will result in a change in the internal energy of the atom and loss of most of the energy to the electron. Unless the state so excited in the atom is metastable, the atom will immediately change to the ground state giving off its characteristic radiation. If the electric field is high enough, some of the electrons will not collide inelastically until they have more than the ionisation energy. There will then be a chance that a collision will produce a second electron and a positive ion. When the electric field is large enough, such collisions will happen so often that the production rate will become greater than the loss rate and breakdown will occur.

## 6.2 Continuous rf excitation of a flashtube

In order to realise the full benefit of the novel design of the Blumlein system, it is necessary to match the flashtube to the impedance of the line. For this purpose we require a moderately dense plasma in the flashtube prior to and during the arrival of the main stripline electrical



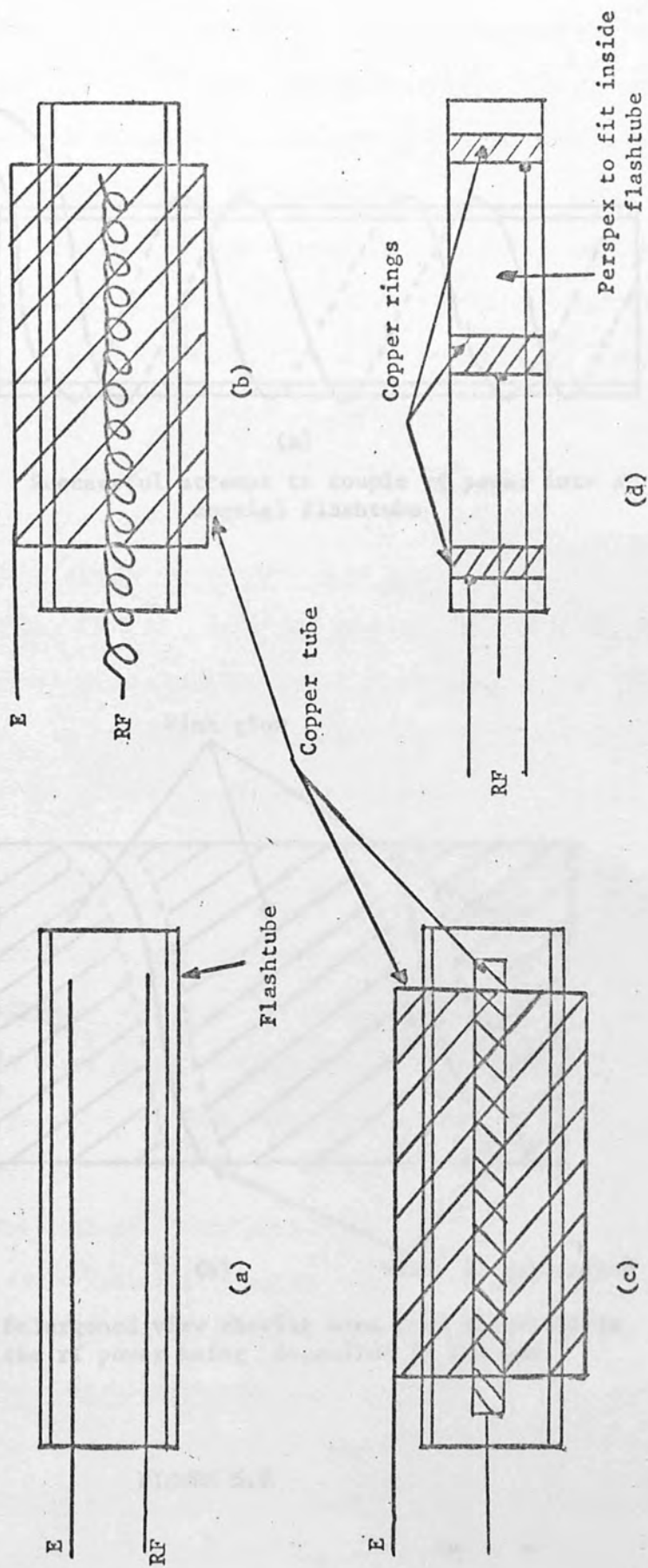
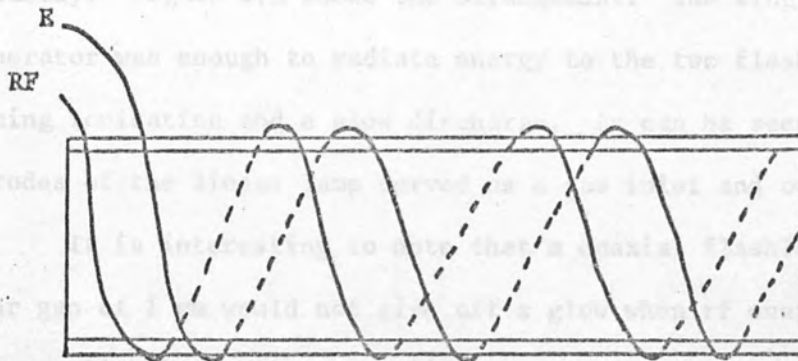


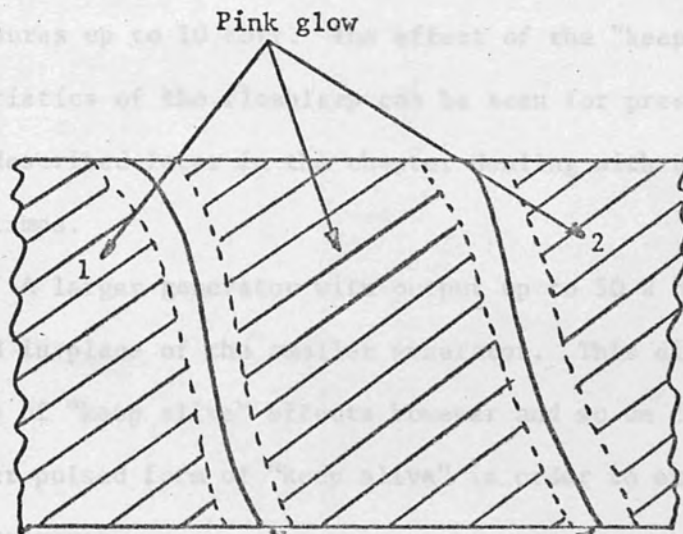
FIGURE 6.1: UNSUCCESSFUL ATTEMPTS TO ACHIEVE COUPLING OF RF POWER INTO A COAXIAL FLASHTUBE





(a)

Successful attempt to couple rf power into a coaxial flashtube



(b)

Wire (5 amp mains)

Enlarged view showing area that glows due to the rf power being deposited in the gas.

FIGURE 6.2

The radio frequency power could be coupled to linear flashtubes more easily. Figure 6.3 shows the arrangement. The single wire from the rf generator was enough to radiate energy to the two flashlamp electrodes producing ionisation and a glow discharge. As can be seen, one of the electrodes of the linear lamp served as a gas inlet and outlet.

It is interesting to note that a coaxial flashlamp with an annular gap of 1 mm would not give off a glow when rf energy was applied whereas a slightly larger gap -  $1\frac{1}{2}$  mm caused no trouble. This was probably due to the cooling of any would-be plasma due to the large surface to volume region allowed to the discharge.

### 6.3 Limitations of continuous rf preionisation

Using 15 W of continuous rf produced a uniform pinkish glow up to 5 torr pressure within the N<sub>2</sub> filled flashlamp. An arc like glow persisted for pressures up to 10 torr. The effect of the "keep alive" on the output characteristics of the flashlamp can be seen for pressures up to 16 torr as will be described later in the chapter dealing with output characteristics of flashlamps.

A larger generator with output up to 50 W of continuous rf power was tried in place of the smaller generator. This did not greatly extend the range of "keep alive" effects however and so we decided to develop a high power pulsed form of "keep alive" in order to extend its range to higher pressures.

The failure of the continuous rf discharge at higher pressures was due to extra inelastic electron collisions preventing the electrons achieving the required velocity, and hence energy, to produce ionisation.

### 6.4 Pulsed preionisation of a flashlamp

To obtain the pulse required for "keep alive" another modification was added to the end of the basic trigger pulse generator as shown in Figure 6.4. The complete electrical set up is shown schematically in

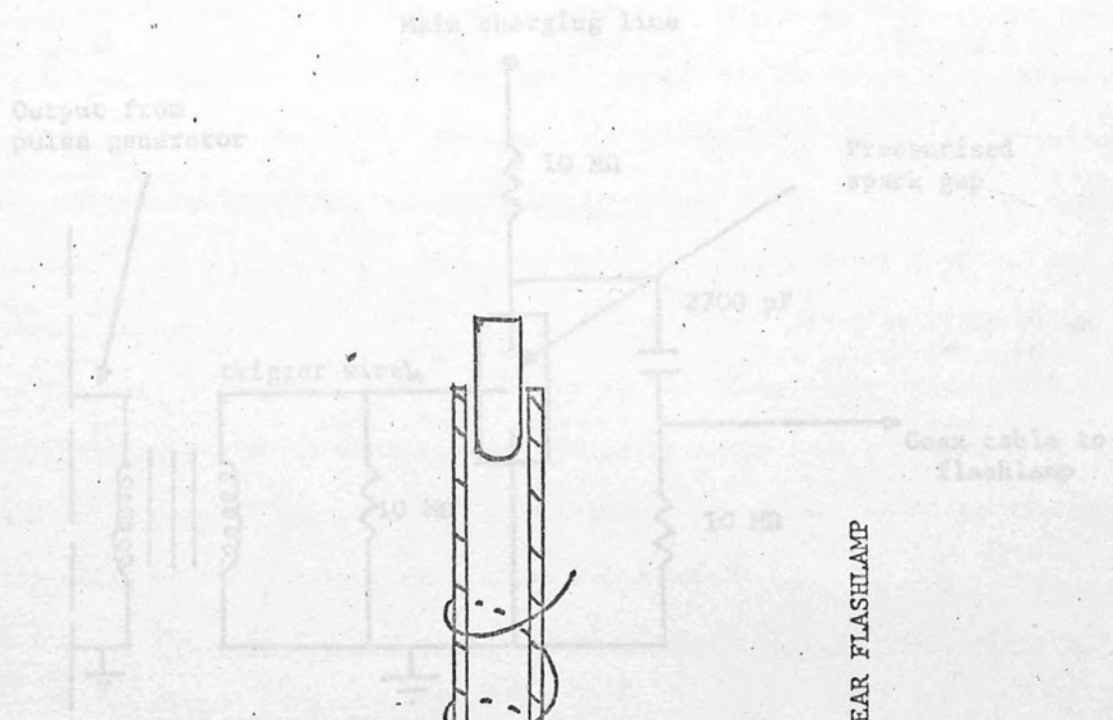
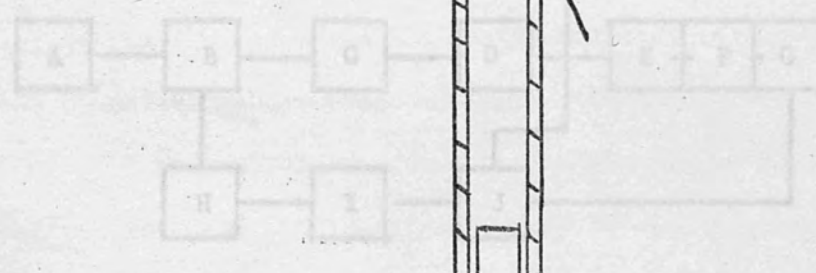


FIGURE 6.4: MAIN CHARGING LINE TO TRIGGER PULSE GENERATOR TO OPERATE KEEP ALIVE PULSE



- A - Push button
- B - 10 V trigger pulse
- C - Delay box
- D - Trigger pulse generator
- E - Multi channel spark gap
- F - Minicore pulser
- G - Flashlamp
- H - Delay box
- I - Trigger pulse generator
- J - Keep alive pulse generator
- K - Brandenburg high voltage power supply

FIGURE 6.3: COUPLING RF POWER INTO A LINEAR FLASHLAMP

FIGURE 6.5

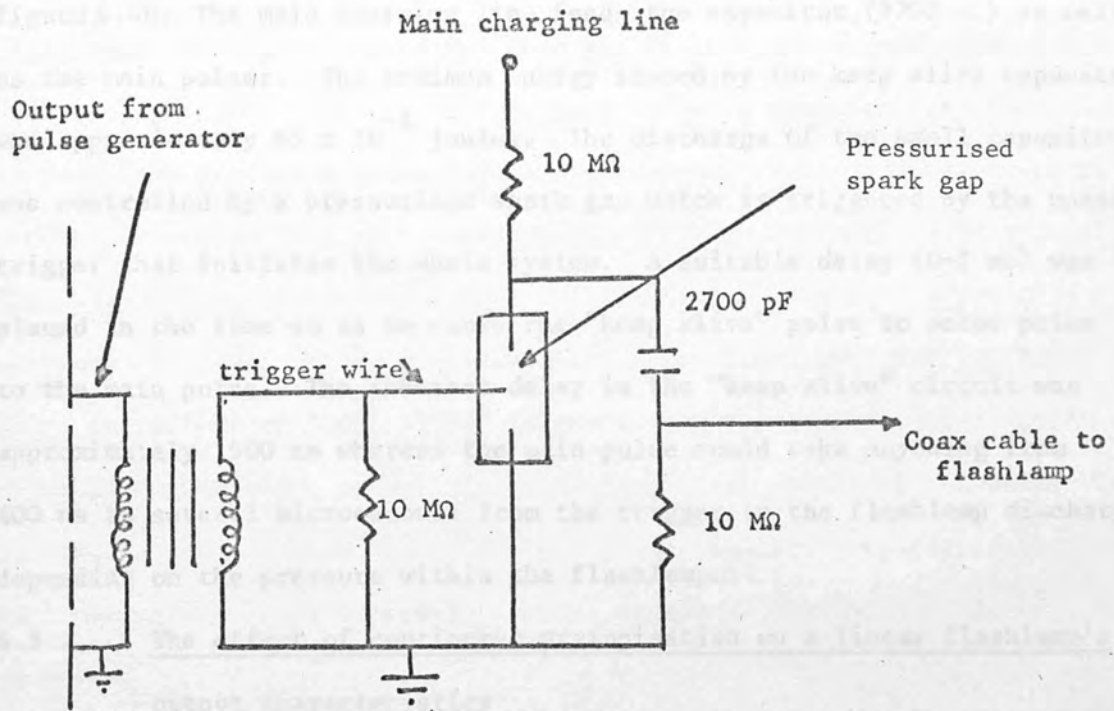
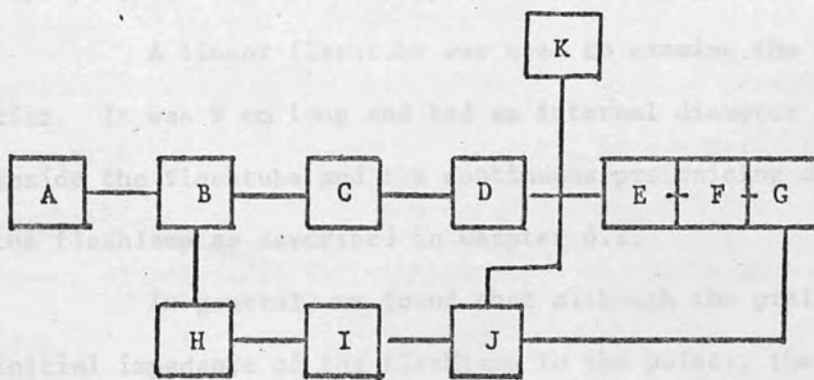


FIGURE 6.4: MODIFICATION TO TRIGGER PULSE GENERATOR TO OBTAIN A KEEP ALIVE PULSE



- |                             |   |
|-----------------------------|---|
| A - Push button             | G - Flashlamp                             |
| B - 10 V trigger pulse      | H - Delay box                             |
| C - Delay box               | I - Trigger pulse generator               |
| D - Trigger pulse generator | J - Keep alive pulse generator            |
| E - Multi channel spark gap | K - Brandenburg high voltage power supply |
| F - Blumlein pulser         |   |

FIGURE 6.5



Figure 6.4b. The main charging line feeds the capacitor (2700 pF) as well as the main pulser. The maximum energy stored by the keep alive capacitor was approximately  $45 \times 10^{-2}$  joules. The discharge of the small capacitor was controlled by a pressurised spark gap which is triggered by the master trigger that initiates the whole system. A suitable delay (0-1 ms) was placed in the line so as to cause the "keep alive" pulse to occur prior to the main pulse. The inherent delay in the "keep alive" circuit was approximately 1500 ns whereas the main pulse could take anything from 400 ns to several microseconds from the trigger to the flashlamp discharge depending on the pressure within the flashlamp.

#### 6.5 The effect of continuous preionisation on a linear flashlamp's output characteristics

The effect of preionisation on the output characteristics of a flashtube was slightly different for the differing Blumlein pulsers employed, and for the two types of flashlamp (coaxial and linear).

A linear flashtube was used to examine the effects of preionisation. It was 9 cm long and had an internal diameter of 6 mm. Air was used inside the flashtube and the continuous preionising device was connected to the flashlamp as described in Chapter 6.2.

In general, we found that although the preionisation lowered the initial impedance of the flashlamp to the pulser, the impedance was still too high for efficient transfer of power and a large proportion of the energy in the front edge of the pulse was still reflected back into the line. The over volting of the flashtube, due to the pulse from the Blumlein, ionised the gas inside the flashlamp still further, however, very rapidly lowering the impedance of the lamp. For a pulse of long enough duration, the continued overvolting will finally cause the impedance of the lamp to adjust itself to the best matching condition although the process itself



might be oscillatory. Therefore, once the initial ionisation period is completed, the transfer of power into the flashtube is maximised. If the overvolting of the flashtube is not very large, a comparatively long time is needed to produce a dense enough plasma required for matched operation, especially without any preionisation. Photograph P19 shows such a condition. This was obtained from the 36 feet pulser charged to 9 kV. Argon at a pressure of 8 torr was used within the linear flashlamp. The top trace shows the effect of "keep alive" as compared with the lower trace which was obtained without keep alive, all other conditions remaining the same. Thus we see the preionisation helps to reduce the time for complete ionisation by reducing the initial mismatch, which increases the initial absorption of power.

At large overvolting conditions, the pulse risetime in the flash lamp can be very rapid even without any keep alive. This can be seen from photograph P20, obtained from the 36 feet system charged to 12 kV. The time scale is 50 ns per division and the top two traces are with keep alive whereas the bottom two are without. Flashlamp pressure was 10 torr.

When the 12 feet system was used, it was noticeable that the double pulse effect (visible in photographs P19 and P20) became more pronounced - (see photograph P21 for example which shows the output from linear flash lamp filled to 5 torr. The sweep speed was 100 ns per division). This was due to the difference of electrical pulse length between the two systems. For the 12 feet system the electrical pulse length was approximately 20 ns for a matched load whereas the 36 feet system had an electrical pulse length of approximately 70 ns for a matched load. Thus the 36 feet system was able to deposit more energy into the flashlamp in the first pulse, than the 12 feet system, as was mentioned in Chapter 5.

PHOTOGRAPH P19

Flashlamp output from a 9 cm long linear flashlamp filled with argon to a pressure of 8 torr.

Sweep speed 50 ns/division  
Blumlein voltage 9 kV

Sweep speed 50 ns/division  
Blumlein voltage 9 kV

Upper trace with keep alive.  
Lower trace without keep alive.

PHOTOGRAPH P20

Flashlamp output from a 9 cm long linear flashlamp filled with nitrogen to a pressure of 10 torr.

Sweep speed (a) 100 ns/div  
(b) 50 ns/div  
(c) 100 ns/div  
(d) 50 ns/div

Blumlein voltage 12 kV

Upper two traces with keep alive.  
Lower two traces without keep alive.

PHOTOGRAPH P21

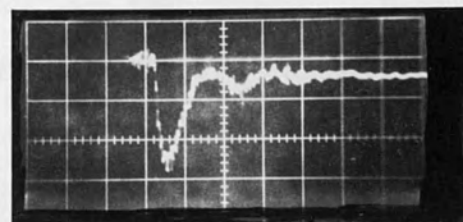
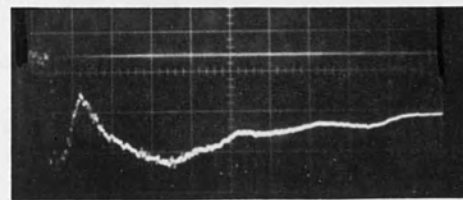
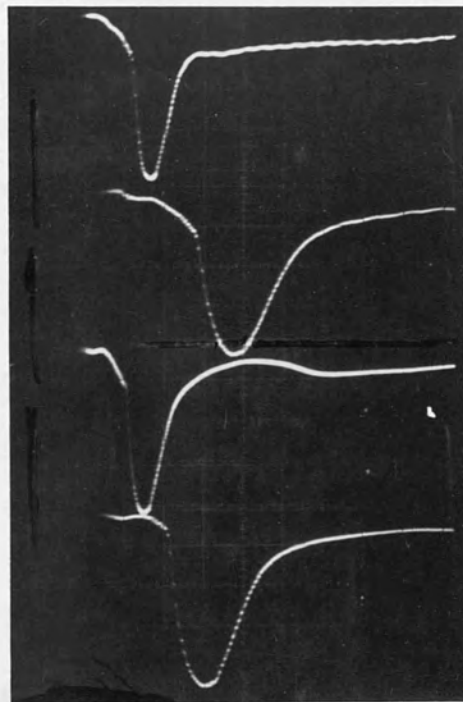
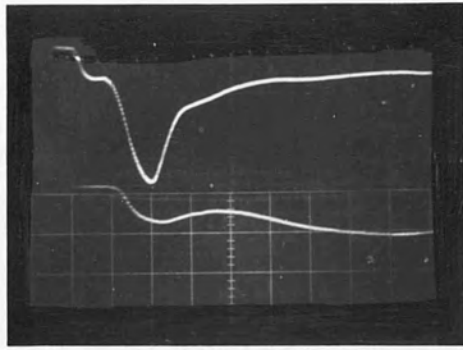
Flashlamp output from a 9 cm long linear flashlamp filled with nitrogen to a pressure of 5 torr.

Sweep speed 100 ns/div  
Blumlein voltage 14 kV

PHOTOGRAPH P22

Flashlamp output from a 9 cm long linear flashlamp with keep alive, filled with nitrogen to a pressure of 10 torr.

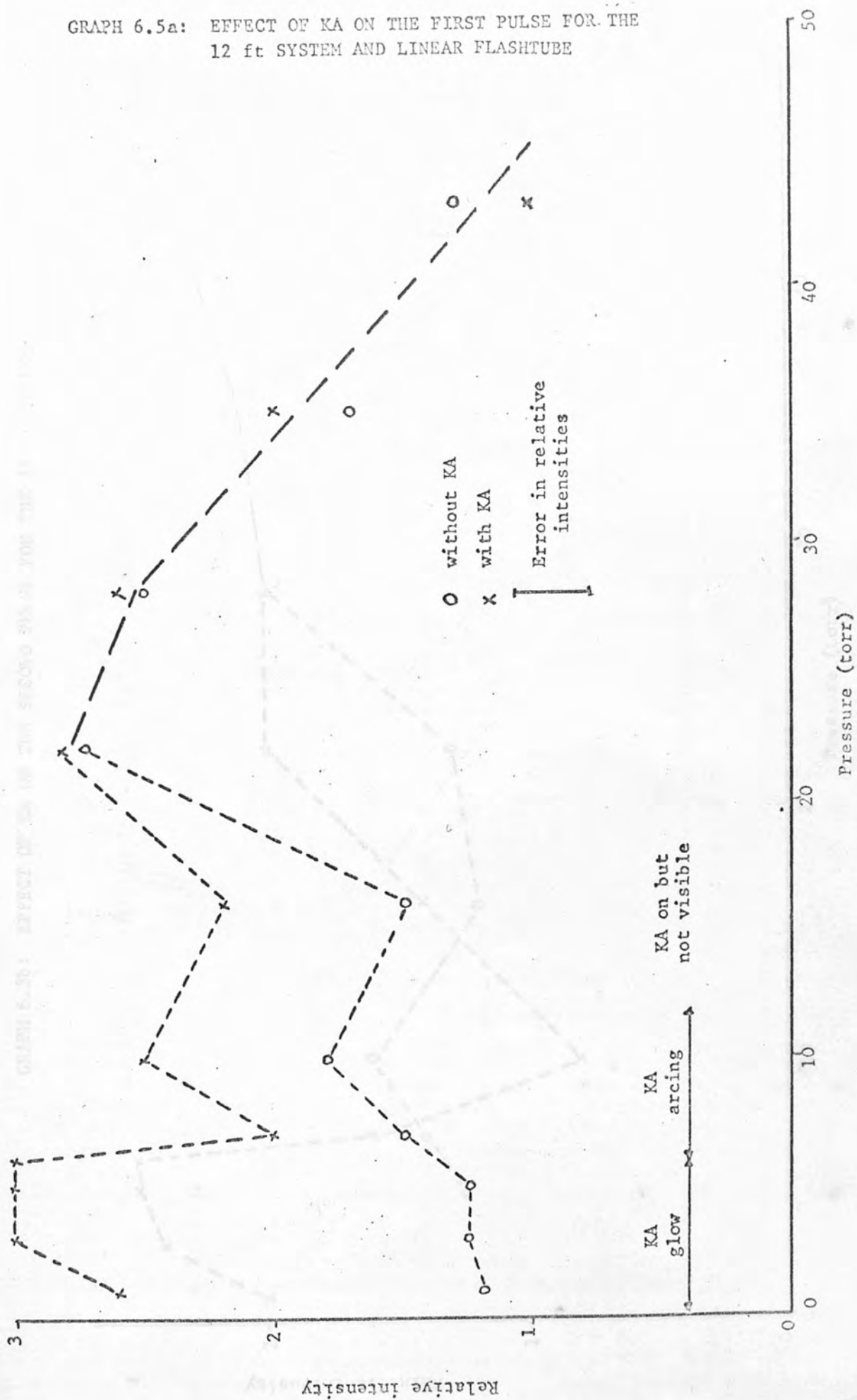
Sweep speed 50 ns/div  
Blumlein voltage 14 kV



When the keep alive was used on the 12 feet system, the amount of energy deposited into the initial pulse grew and consequently the second pulse got smaller. Compare photograph P21 with P22. In photograph P22 the keep alive was used. (Pressure in lamp was 10 torr and sweep speed was 50 ns per division). Results showing the relative intensities of the first and second pulses as a function of pressure, at fixed voltage, with and without keep alive, for the 12 feet system are shown in graphs 6.5(a) and 6.5(b). Graph 6.5(a) shows that for pressures up to 6 torr, the light output from the linear flashtube during the first pulse has been more than doubled. Due to this, the risetime of the first pulse is slightly longer with keep alive than without keep alive as can be seen from graph 6.5(c). (Graph 6.5(c) shows the risetime of the first pulse in the 12 feet system, with and without keep alive). Referring back to graph 6.5(a) we see that from 6 torr to 20 torr the keep alive does not have so much effect on the light output, and beyond 20 torr the effect is negligible. (This was due to the preionisation decreasing with increasing pressure as was mentioned in Chapter 6.3).

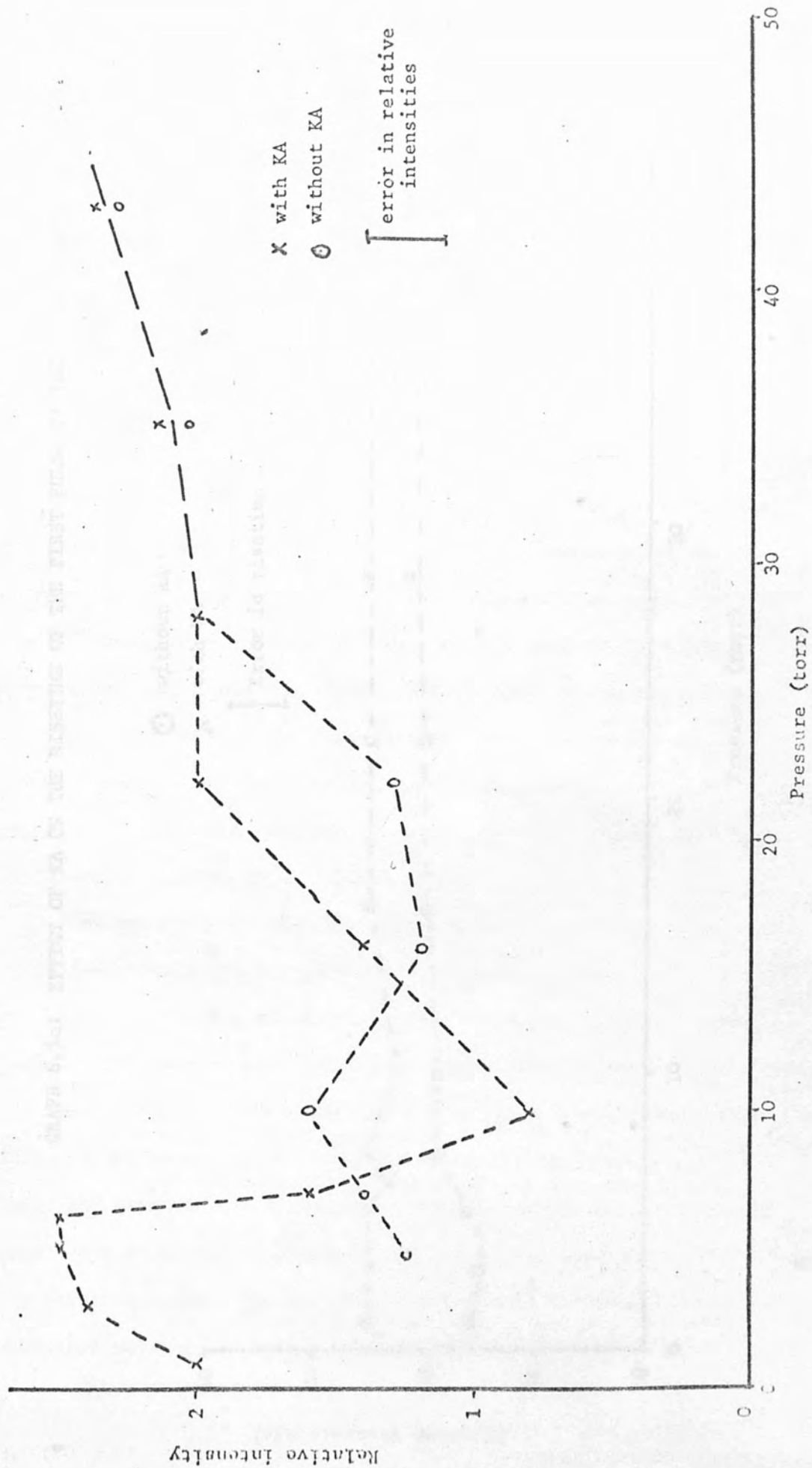
Thus we see that for its effective range (1-20 torr) the keep alive reduces the initial impedance of the flashtube to the pulser effectively enough to deposit more energy into the initial pulse across the flashtube, as one would be able to achieve without keep alive. With reference to graph 6.5(b), we see that the relative intensity of the second pulse with keep alive does reduce to a level below that obtained without keep alive for a flashlamp pressure of 10 torr. For lower pressure (1-7 torr), however, the intensity of the second pulse obtained with keep alive is greater than that obtained without keep alive. This implies that for this pressure range the impedance of the flashlamp compared with the pulser was in such a mismatched condition that effective energy deposition

GRAPH 6.5a: EFFECT OF KA ON THE FIRST PULSE FOR THE 12 ft SYSTEM AND LINEAR FLASHTUBE

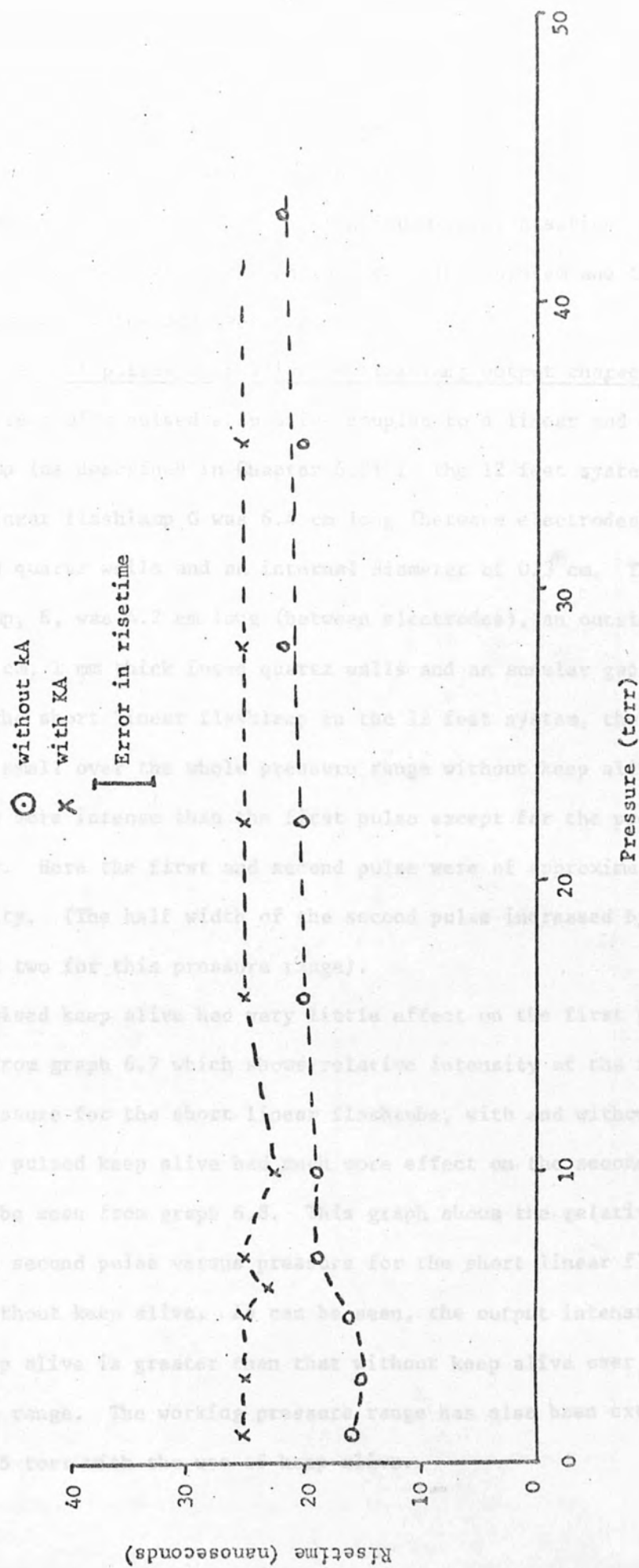




GRAPH 6.5b: EFFECT OF KA ON THE SECOND PULSE FOR THE 12 ft SYSTEM



GRAPH 6.5c: EFFECT OF KA ON THE RISETIME OF THE FIRST PULSE OF THE 12 ft SYSTEM



was prohibited even after two electrical pulses, without keep alive, and that with keep alive closer matching was achieved.

Due to the limited range of the continuous preionisation, a pulsed "keep alive" system was next used in the 12 feet system and the results are described in the next section.

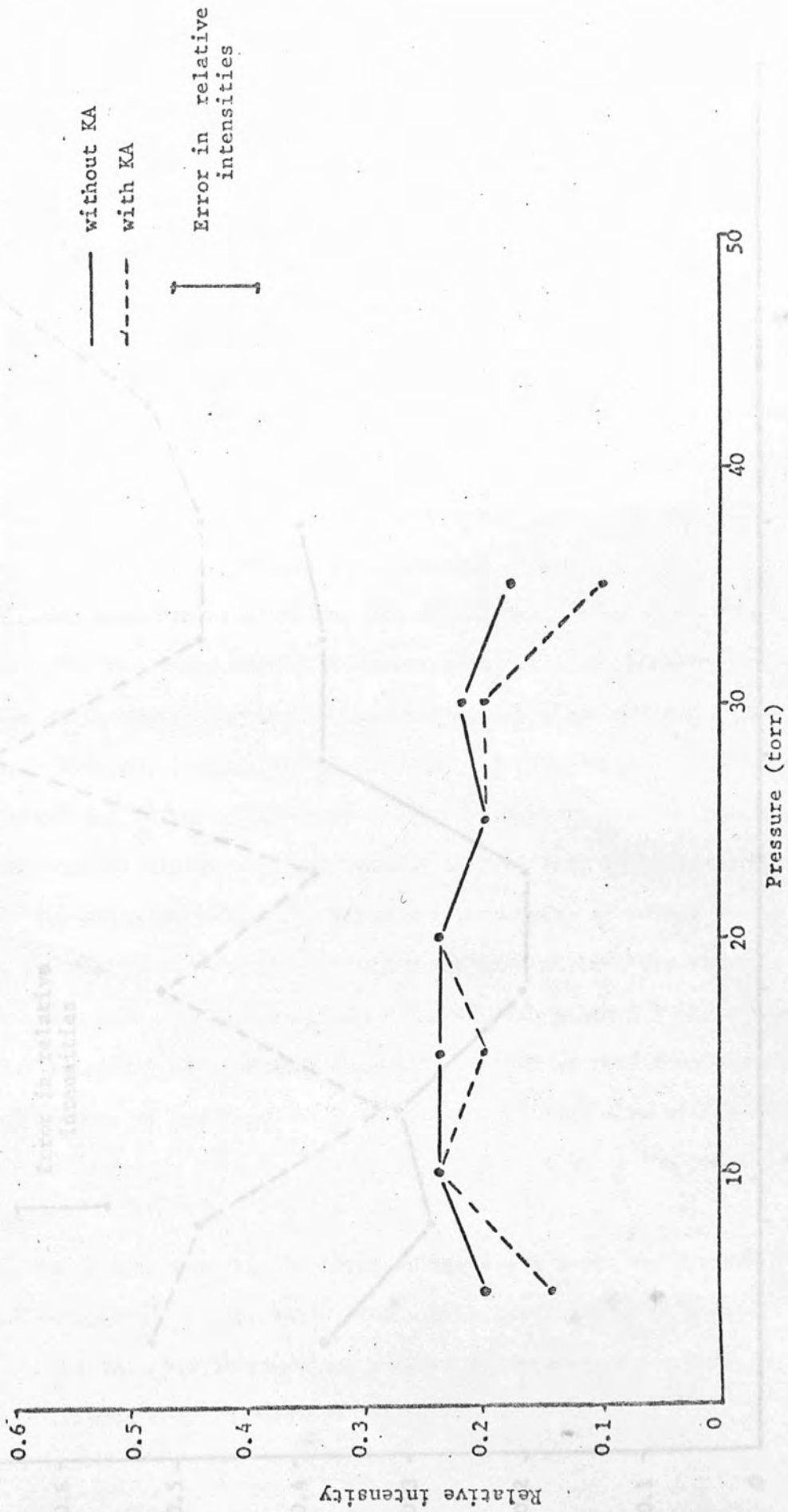
#### 6.6 The effect of pulses keep alive on flashlamp output characteristics

The effect of a pulsed keep alive coupled to a linear and a coaxial flashlamp (as described in Chapter 6.2) in the 12 feet system was studied. The linear flashlamp G was 6.4 cm long (between electrodes), had 1 mm thick fused quartz walls and an internal diameter of 0.3 cm. The coaxial flashlamp, E, was 4.2 cm long (between electrodes), an outside diameter of 2.3 cm, 1 mm thick fused quartz walls and an annular gap of 1 mm.

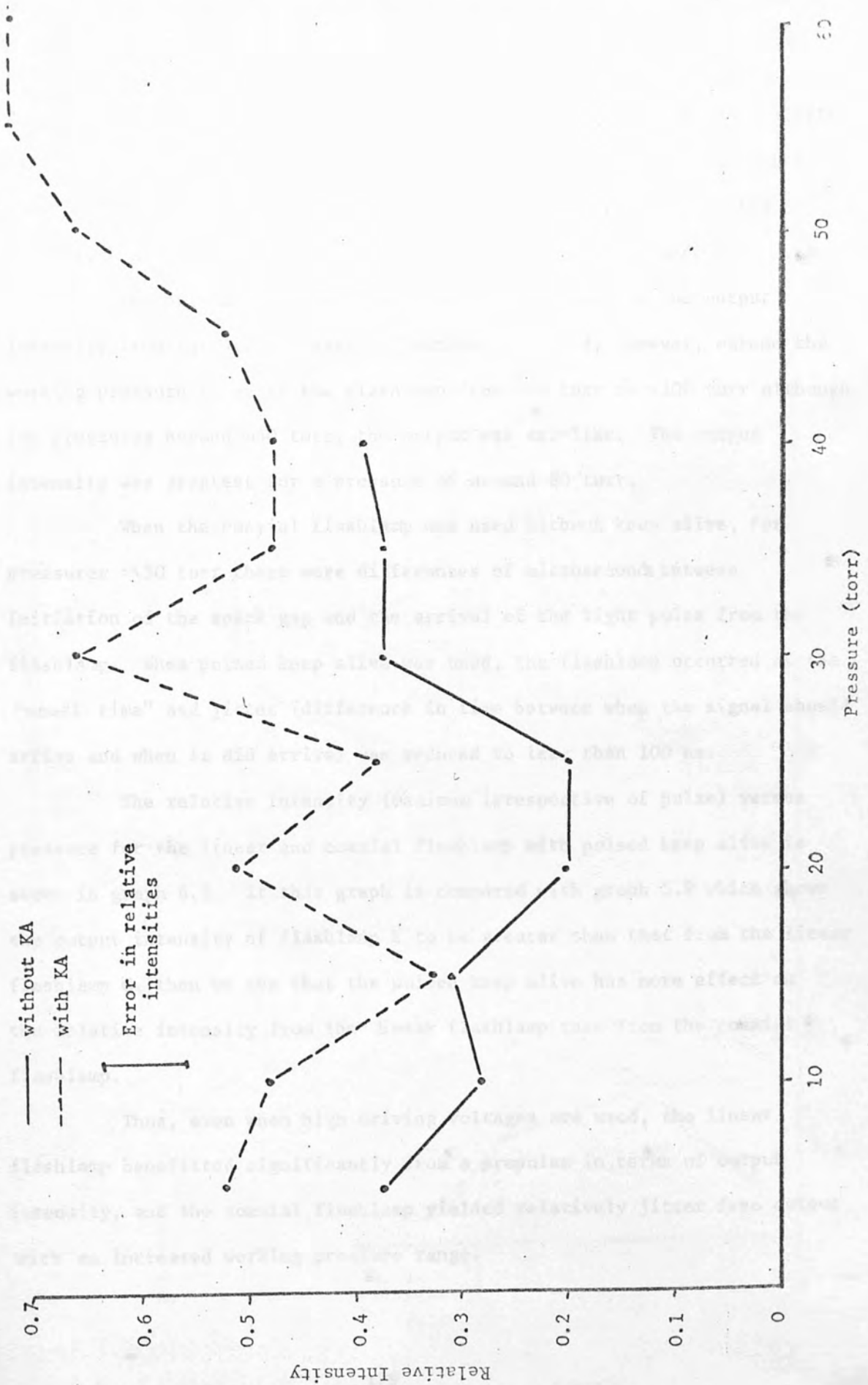
With the short linear flashlamp in the 12 feet system, the first light pulse was small over the whole pressure range without keep alive. The second pulse was more intense than the first pulse except for the pressure range 20-25 torr. Here the first and second pulse were of approximately the same intensity. (The half width of the second pulse increased by more than a factor of two for this pressure range).

The pulsed keep alive had very little effect on the first pulse as can be seen from graph 6.7 which shows relative intensity of the first pulse versus pressure for the short linear flashtube, with and without keep alive. The pulsed keep alive had much more effect on the second pulse, however, as can be seen from graph 6.8. This graph shows the relative intensity of the second pulse versus pressure for the short linear flash tube with and without keep alive. As can be seen, the output intensity using pulsed keep alive is greater than that without keep alive over the working pressure range. The working pressure range has also been extended from ~45 torr ~65 torr with the use of keep alive.

GRAPH 6.7: RELATIVE INTENSITY VERSUS PRESSURE (AIR) FOR LINEAR FLASHTUBE G (1st PULSE) IN THE 12 ft SYSTEM WITH AND WITHOUT KEEP ALIVE



GRAPH 6.8: RELATIVE INTENSITY VERSUS PRESSURE (AIR) FOR LINEAR FLASHTUBE G (2nd PULSE) IN THE 12 ft SYSTEM WITH AND WITHOUT KEEP ALIVE





The output from the 4.2 cm coaxial flashlamp in the 12 feet system differed from that obtained with the long coaxial flashlamp described earlier. Up to around 25 torr, the output consisted of a single fast rising pulse ( 20 ns risetime). Between 25 and 30 torr this pulse showed the double peak effect (as described in Chapter 5.7). Beyond 30 torr, a slower risetime longer duration pulse was obtained.

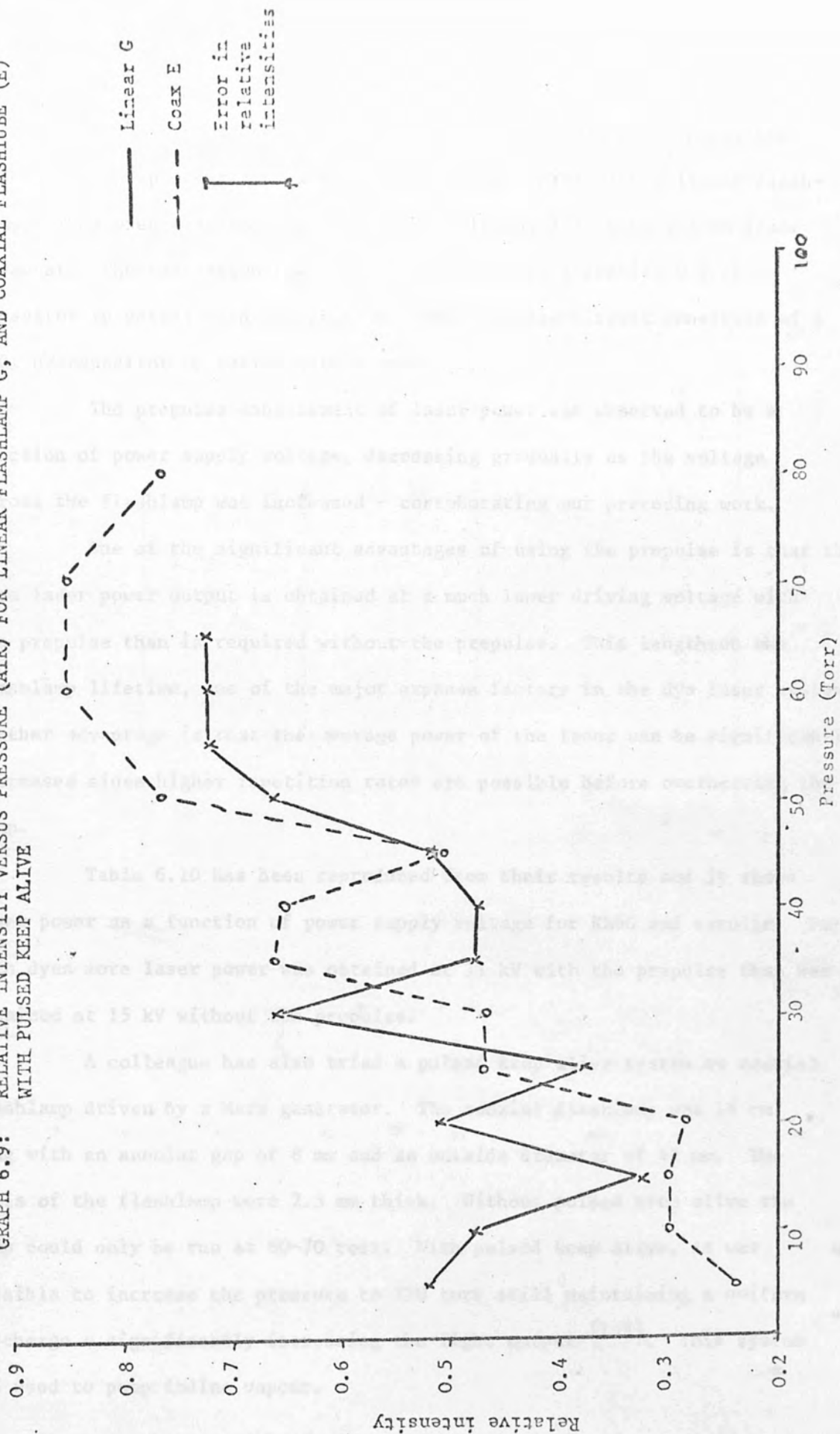
The pulsed keep alive had very little effect on the output intensity from the 4.2 cm coaxial flashlamp. It did, however, extend the working pressure range of the flashlamp from  $\sim 60$  torr to  $\sim 100$  torr although for pressures beyond  $\sim 40$  torr, the output was arc-like. The output intensity was greatest for a pressure of around 80 torr.

When the coaxial flashlamp was used without keep alive, for pressures  $> \sim 50$  torr there were differences of microseconds between initiation of the spark gap and the arrival of the light pulse from the flashlamp. When pulsed keep alive was used, the flashlamp occurred at the "usual time" and jitter (difference in time between when the signal should arrive and when it did arrive) was reduced to less than 100 ns.

The relative intensity (maximum irrespective of pulse) versus pressure for the linear and coaxial flashlamp with pulsed keep alive is shown in graph 6.9. If this graph is compared with graph 5.9 which shows the output intensity of flashlamp E to be greater than that from the linear flashlamp G, then we see that the pulsed keep alive has more effect on the relative intensity from the linear flashlamp than from the coaxial flashlamp.

Thus, even when high driving voltages are used, the linear flashlamp benefitted significantly from a prepulse in terms of output intensity, and the coaxial flashlamp yielded relatively jitter free output with an increased working pressure range.

GRAPH 6.9: RELATIVE INTENSITY VERSUS PRESSURE (AIR) FOR LINEAR FLASHLAMP G, AND COAXIAL FLASHTUBE (E) WITH PULSED KEEP ALIVE



## 6.7 The effect of pulsed keep alive on laser output

A paper published recently by Ornstein and Derr<sup>(93)</sup> shows how effective a prepulse can be when pumping organic dyes with a linear flashlamp. They used a 10 cm long xenon filled linear lamp with a 3 mm inner diameter. The main discharge circuit consisted of a coaxial 0.2  $\mu\text{F}$  capacitor in series with a thyatron. The prepulse circuit consisted of a 0.01  $\mu\text{F}$  capacitor in series with a spark gap.

The prepulse enhancement of laser power was observed to be a function of power supply voltage, decreasing gradually as the voltage across the flashlamp was increased - corroborating our preceding work.

One of the significant advantages of using the prepulse is that the same laser power output is obtained at a much lower driving voltage with the prepulse than is required without the prepulse. This lengthens the flashlamp lifetime, one of the major expense factors in the dye laser system. Another advantage is that the average power of the laser can be significantly increased since higher repetition rates are possible before overheating the lamp.

Table 6.10 has been reproduced from their results and it shows laser power as a function of power supply voltage for Rh6G and esculin. For both dyes more laser power was obtained at 11 kV with the prepulse than was obtained at 15 kV without the prepulse.

A colleague has also tried a pulsed keep alive system on coaxial flashlamp driven by a Marx generator. The coaxial flashlamp was 18 cm long with an annular gap of 8 mm and an outside diameter of 47 mm. The walls of the flashlamp were 2.5 mm thick. Without pulsed keep alive the lamp could only be run at 60-70 torr. With pulsed keep alive, it was possible to increase the pressure to 220 torr still maintaining a uniform discharge - significantly increasing the light output<sup>(154)</sup>. This system was used to pump iodine vapour.

TABLE 6.10

PREPLUSE ENHANCEMENT OF LASER POWER VS FLASHLAMP VOLTAGE

Flashlamp Voltage (kV)	Rhodamine 6G ( $\lambda = 5940 \text{ \AA}$ ) Laser Power (kW)		Esculin ( $\lambda = 4690 \text{ \AA}$ ) Laser Power (kW)	
	Without Prepulse	With Prepulse	Without Prepulse	With Prepulse
8	0.9	1.60	...	...
9	1.25	5.25	...	...
10	2.75	8.9	...	...
11	4.9	12.4	0.12	2.5
12	6.4	16.3	0.31	2.8
13	7.75	17.9	0.81	5.6
14	9.5	18.1	1.25	7.3
15	11.75	18.6	1.50	10.0

## CHAPTER VII

### SPECTRAL ANALYSIS

#### 7.1 Introduction

According to the quantum theory, no radiation can be emitted from an atom unless it receives energy at least equal to that necessary to raise the electron from the lowest to the second lowest orbit. Corresponding to this energy is the first critical potential, or resonance potential of the atom,  $V$ . It follows that if  $v$  is the velocity of the electron required to do this, we have  $mv^2/2 = V_e = hv$  where  $\nu$  is the frequency of the resonance line. If a gas is bombarded with electrons with just this energy, the optical electron in the atoms can be raised to the first excited level and after a short time ( $\sim 10^{-18}$  s) falls back to the normal state, a spectral line being emitted in the process. Only a single line will be emitted. When the velocities of the incident electrons are increased a second line is emitted. With still higher velocities, a third line, then a fourth etc, will in turn be radiated, until, when the ionisation potential is reached the whole of the arc spectrum will be given out<sup>(143)</sup>.

A continuous spectrum is, in general, obtained from solids and liquids. In these states of matter the atoms and molecules are close together, and electron orbital changes in a particular atom are influenced by neighbouring atoms to such an extent that radiations of all different wavelengths are emitted. In a gas the atoms are far apart and are able to emit definite frequencies until the gas is at a fairly high pressure. The lines then become broadened because of the more frequent collisions and other effects. This broadening increases with pressure, so that finally the lines merge into a continuous spectrum as the gas approaches the liquid state<sup>(144)</sup>.



There exists many types of radiation from a plasma, but the important types when considering pulsed discharge lamps are excitation (line) radiation, recombination radiation and bremsstrahlung radiation.

Excitation or line radiation is due to a transition between any two bound energy levels, ie  $E_m - E_n = h\nu_{mn}$  (see Figure 7.1). There is an infinite array of energy levels and transitions are permissible providing they obey selection rules. I shall include band spectra under this heading. Band spectra are obtained from molecules and consist of a series of bands each sharp at one end but "fading" at the other end. Careful examination reveals that the bands are made up of numerous fine lines very close to each other corresponding to vibrational and rotational levels superimposed on every electronic energy level.

The recombination radiation is considered to be of the electronic volume type. This is due to a transition from a free energy level to a bound energy level. Suppose we have a positive (ie free) energy level shown as x in Figure 7.1. This level is of energy  $\frac{1}{2}mv^2$ . If this electron was captured by an ion such that the electron made a transition down to  $E_j$  say, then the energy radiated is

$$h\nu_{vj} = \frac{1}{2}mv^2 + E_\infty - E_j$$

and since the upper levels are continuous, the radiation emitted is of a continuum nature.

Bremsstrahlung radiation is one type of transition between two unbound or free energy levels. (Other types being cyclotron radiation and cerenkov radiation). Classically, the electromagnetic theory predicts that an accelerated electric charge will radiate electromagnetic waves, whereas we could also look upon the radiation as being due to the coulomb interaction between particles under acceleration. If an electron in a free

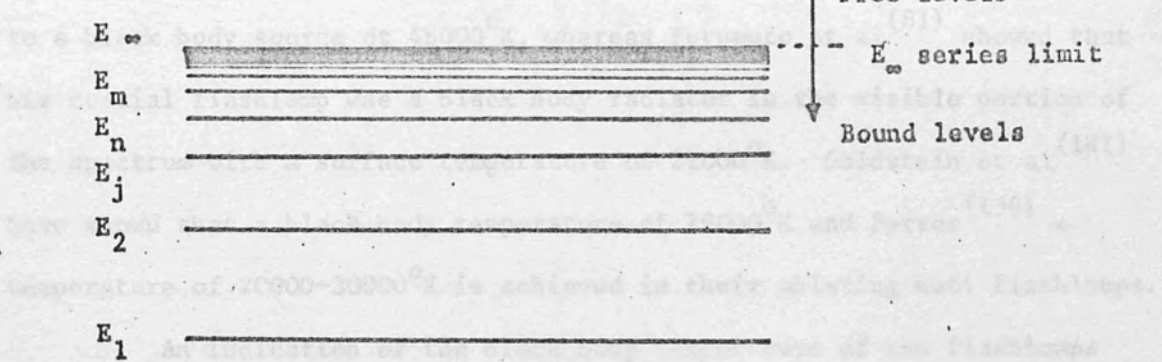
state is deflected by an ion (for example) such that the electron ends up in a different continuum state (usually of lower energy) than we obtain from stationary radiation.

### Experimental work

The mechanism of light production by the discharge in a flashtube is usually regarded as black body radiation from the hot plasma.

(138)-(141) with the spectral distribution resembling that of a continuum, ranging from the ultra-violet to the infra red, with superimposed lines.

Forokin et al (56) estimated his coaxial



temperature of 20000-30000°K is achieved in their pulsed flashtubes. An illustration of the energy levels of the plasmas can be obtained from the part-part spectrum of the discharge. The radiating area of the flashtube, and the use of the... (142) assuming an electrical to radiant power conversion of 10%.

FIGURE 7.1: POSSIBLE ENERGY LEVELS

For 10 ns pulses in these flashtubes, Forokin et al (138) found the spectral intensity of the gas discharge... (138) the radiation characteristics... (139) they obtained 10 ns duration pulses (0.5 to 100 ns range) using electrical energies from 100-500 joules.

state is deflected by an ion (for example) such that the electron ends up in a different continuum state (usually of lower energy) then we obtain Bremsstrahlung radiation.

## 7.2 Experimental work

The mechanism of light production by the discharge in a flashlamp is usually regarded as black body continuum radiation from the hot plasma, (138)-(141), with the spectral distribution consisting of a continuum, ranging from the ultra violet to the infra red, with superimposed lines<sup>(79)</sup>.

Sorokin et al<sup>(56)</sup> estimated his coaxial flashlamp approximated to a black body source at 48000°K, whereas Furumoto et al<sup>(81)</sup> showed that his coaxial flashlamp was a black body radiator in the visible portion of the spectrum with a surface temperature of 21000°K. Goldstein et al<sup>(141)</sup> have shown that a black body temperature of 19000°K and Ferrar<sup>(139)</sup> a temperature of 20000-30000°K is achieved in their ablating wall flashlamps.

An indication of the black body temperature of the flashlamps can be obtained from the peak power deposition into the flashlamp, the radiating area of the flashlamp, and the use of the Stefan-Boltzmann law<sup>(142)</sup> assuming an electrical to radiant power conversion of 100%.

The total amount of light emitted by the lamp at a particular wavelength depends on the average black body temperature maintained during the plasma heating period in which energy is supplied electrically to the plasma, and during the cooling period or after-glow<sup>(138)</sup>.

For 10  $\mu$ s pulses in linear flashtubes, Baker et al<sup>(138)</sup> found the exact details of the gas fill were not very important in determining the radiation characteristics once the high temperature plasma had formed. They obtained 10  $\mu$ s duration pulses (in the 250-300 nm region) using electrical energies from 100-500 joules.

The pulses from our flashtubes were of much shorter time duration and the electrical energies used were <50 joules. Under these circumstances we found the radiation characteristics to vary with voltage across the flashtube and pressure within the flashtube.

The light output from various flashlamps including both linear and coaxial types was analysed using a time integrated Hilger Watts spectrometer which utilises a fused quartz prism. The slit width used varied from 20-50  $\mu\text{m}$  and Kodak plates type HP3 were used for recording the spectrum.

A brief overall look at the spectral plates before going into detail show that for a given voltage, low pressures give pronounced band structure, from the coaxial type flashlamps, mostly in the ultra violet portion of the spectrum. The spectral output from the linear flashlamp differs considerably from the spectra of the coaxial flashlamps at low gas pressures. As the pressure is increased spectral lines appear in the visible region of the spectrum for both the linear and coaxial flashlamps. For higher pressures, continuum radiation with structure superimposed is visible from the linear flashtube and the shorter coaxial flashtubes (where the pressure can be increased enough). Continuum radiation is more easily obtained from linear rather than coaxial flashlamps.

Plates PL1 and PL2 compare the output from a linear flashlamp for the same range of pressures for two different pulser voltages. Apart from plate PL2 being far more intense than plate PL1, (only exposed to 3 flashlamp shots in plate PL2 compared with 9 flashlamp exposures in plate PL1), it also shows a very good example of self reversal. This is produced by absorption in the cooler outer layers of the source. Comparing plates PL1 and PL2 shows this effect clearly.

Practically identical results were obtained when industrial grade argon replaced the nitrogen within the linear flashlamp other conditions

PLATE PL1

The spectral output from a linear flashlamp filled with nitrogen. The Blumlein voltage was 12 kV. The plate shows Hg lines and then spectral outputs corresponding to lamp pressures of 1.5, 2.5, 5, 10, 15, 25, 35 torr respectively. The flashlamp was triggered nine times for each exposure.



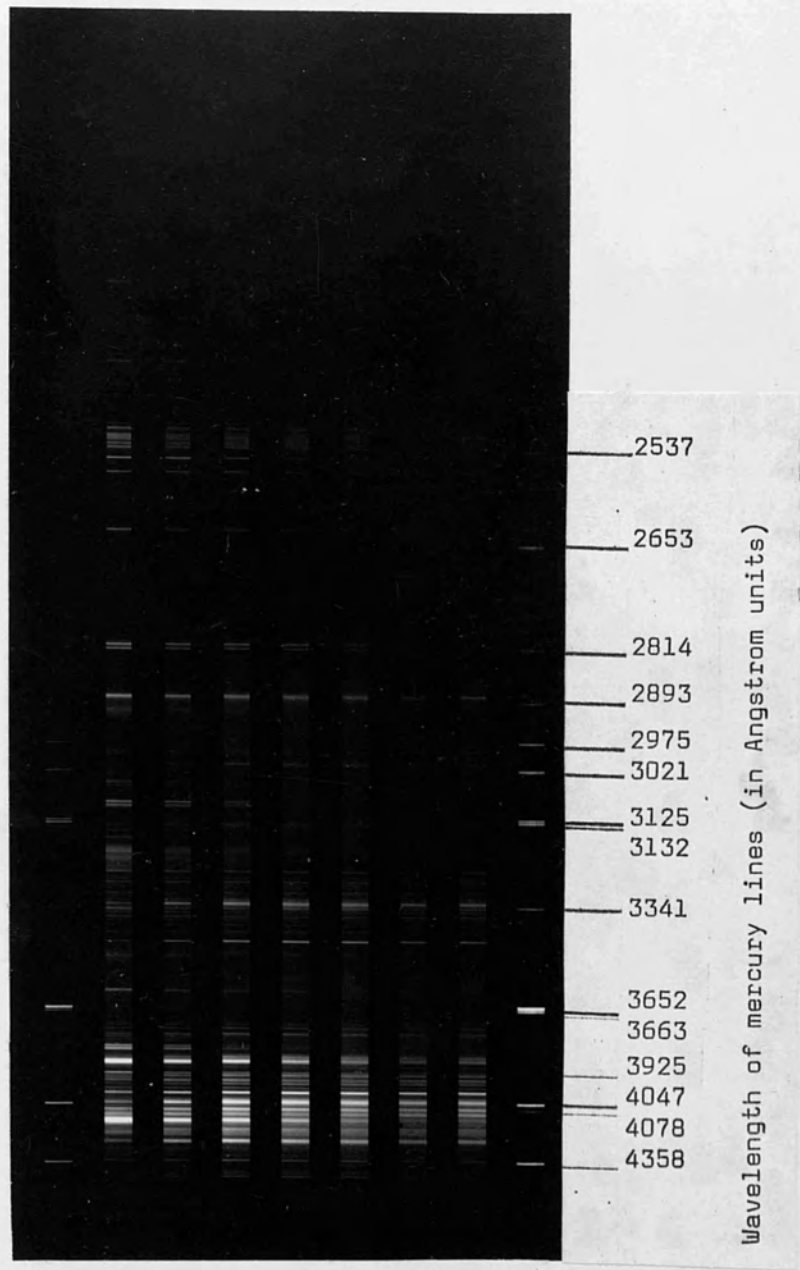
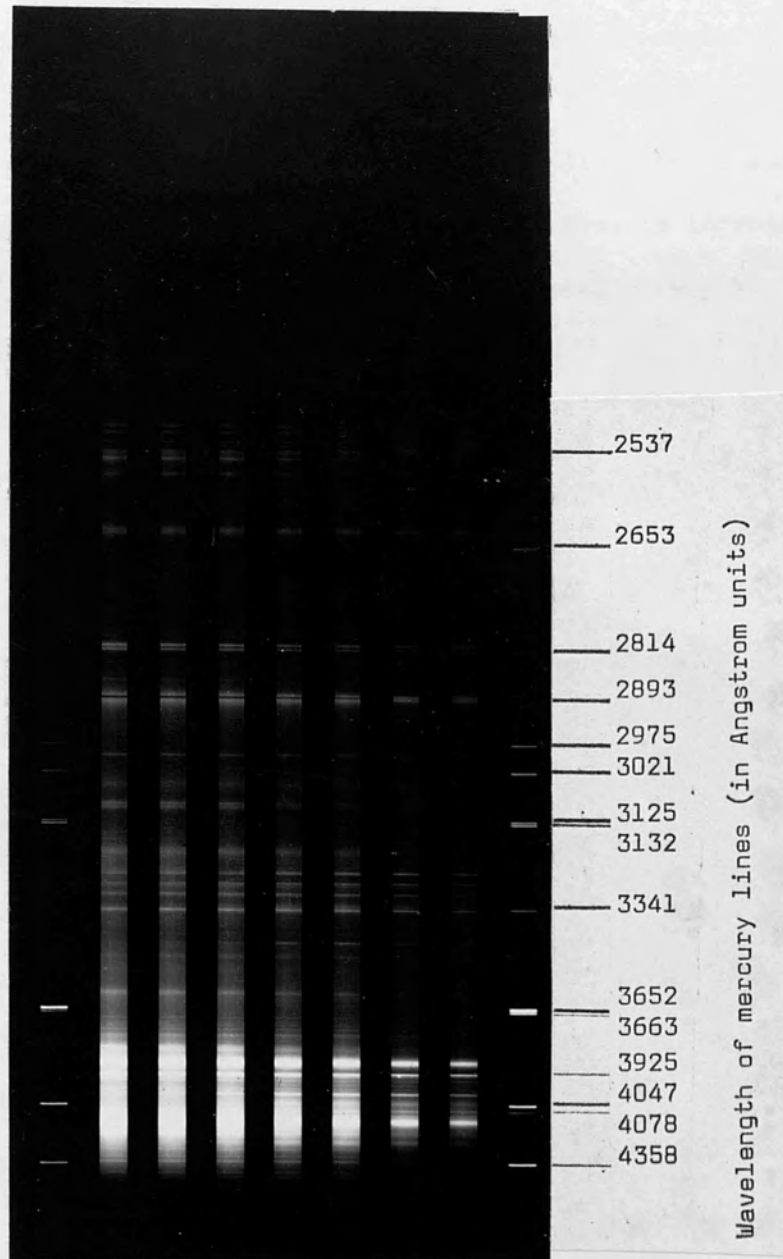


PLATE PL2

The spectral output from a linear flashlamp filled with nitrogen. The Blumlein voltage was 18 kV. The plate shows Hg lines and then spectral outputs corresponding to lamp pressures of 1.5, 2.5, 5, 10, 15, 25, 35 torr respectively. The flashlamp was triggered three times for each exposure.



being unchanged, the main difference being a more intense spectrum from the argon filled lamp compared with the nitrogen filled lamp. (This is expected - note results shown on graph 5.21 showing output intensity from the linear flashlamp for different gas fills).

Plate PL3 shows the spectrum of a linear flashtube containing air at 20 torr. Four band systems are present: the bands of NO (2300-2700 Å), negative nitrogen bands ( $N_2^+$ , 2900-5000 Å) second positive nitrogen bands ( $N_2$ , 5500-7000 Å). Plate PL4 shows the absence of visible output for low pressures (~5 torr) within coaxial flashtube B, and how the visible spectral lines appear again as the pressure is increased (~10 torr). (This confirms the results on flashtubes, using the 18A filter, analysed in the last Chapter).

Plate PL5 is a typical spectral output for the shorter coaxial flashtube where a higher pressure range was achieved. The coaxial flash tube was filled with air for a pressure range 1-70 torr for this plate.

From plate PL5, and Figure 7.2 which shows the absorption and emission bands for rhodamine 6G and POPOP, it is obvious that a pressure in excess of 50 torr is required for this coaxial tube to efficiently pump the rhodamine dye. For dyes like POPOP, however, (absorption band 275-400 nm) low pressure fills are preferable.

It is interesting to note the work done by Baker and King<sup>(138)</sup> on UV emission from a linear flashlamp. They established that xenon filled flashlamps were appreciably more efficient than low pressure ablating wall flashlamps at producing light in the 250-300 nm region when microsecond duration excitation pulses were used, the efficiency being independent of pressure above 50 torr of xenon. The loss in efficiency in the ablating wall region appears to be due to a large part of the input energy causing wall heating, resulting in a threshold input energy

PLATE PL3

Spectral output from a linear flashlamp. Blumlein voltage 18 kV. The plate shows Hg lines and the spectral corresponds to five flashlamp exposures for the following conditions:

Gas type	Pressure (torr)
Air	5
Air	20
Argon	5
Argon	20
Nitrogen	5
Nitrogen	20



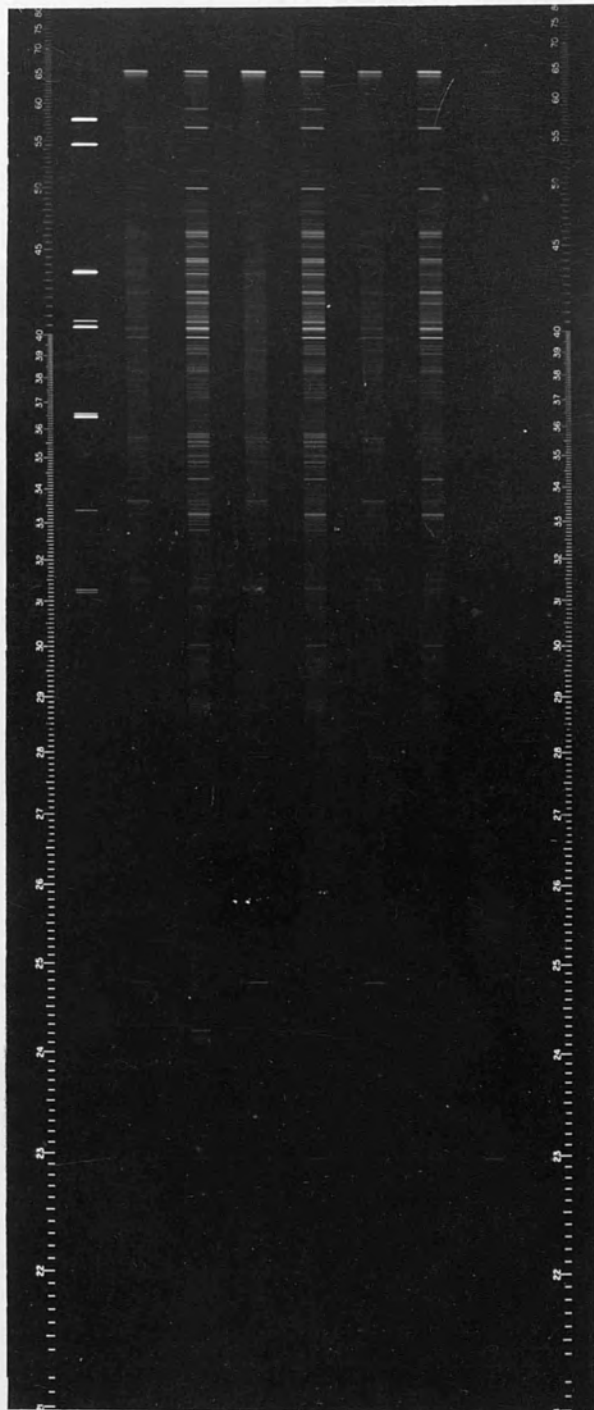


PLATE PL4

Spectral output from coaxial flashtube B. Blumlein voltage 18 kV. The plate shows Hg lines and the spectra corresponds to fifteen flashlamp exposures for the following conditions:

Gas type	Pressure (torr)
Air	2
Air	10
Nitrogen	1
Nitrogen	5
Nitrogen	10
Argon	1
Argon	5
Argon	10

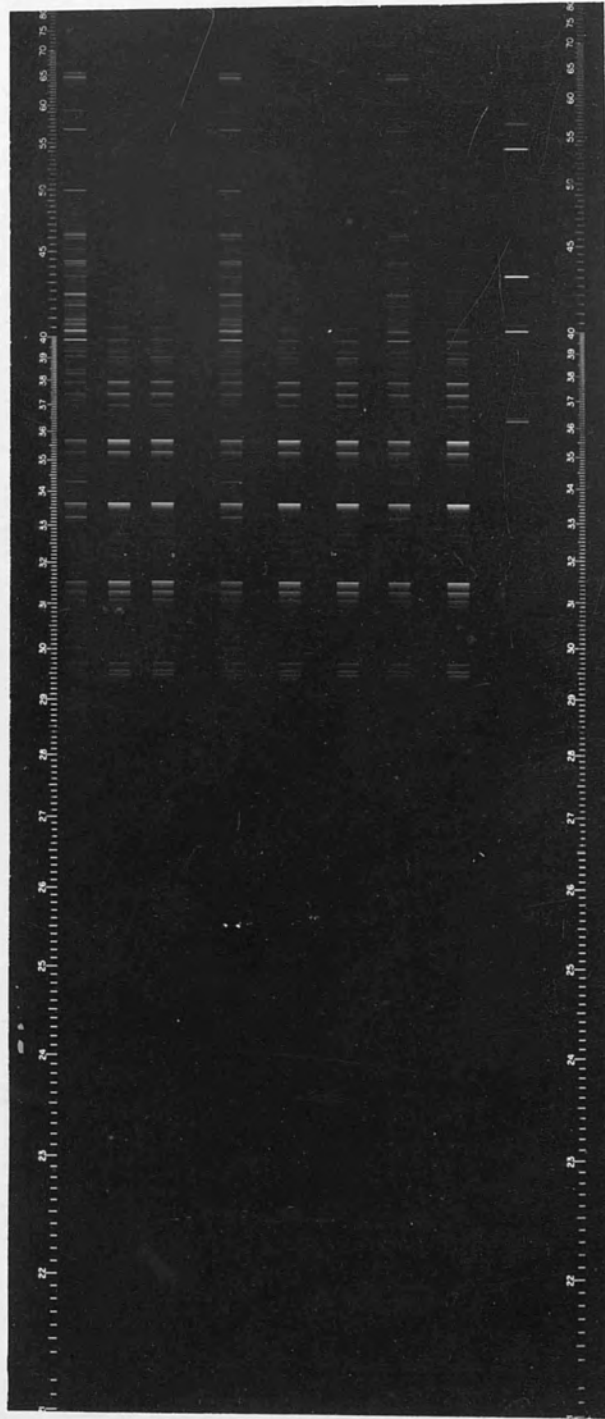
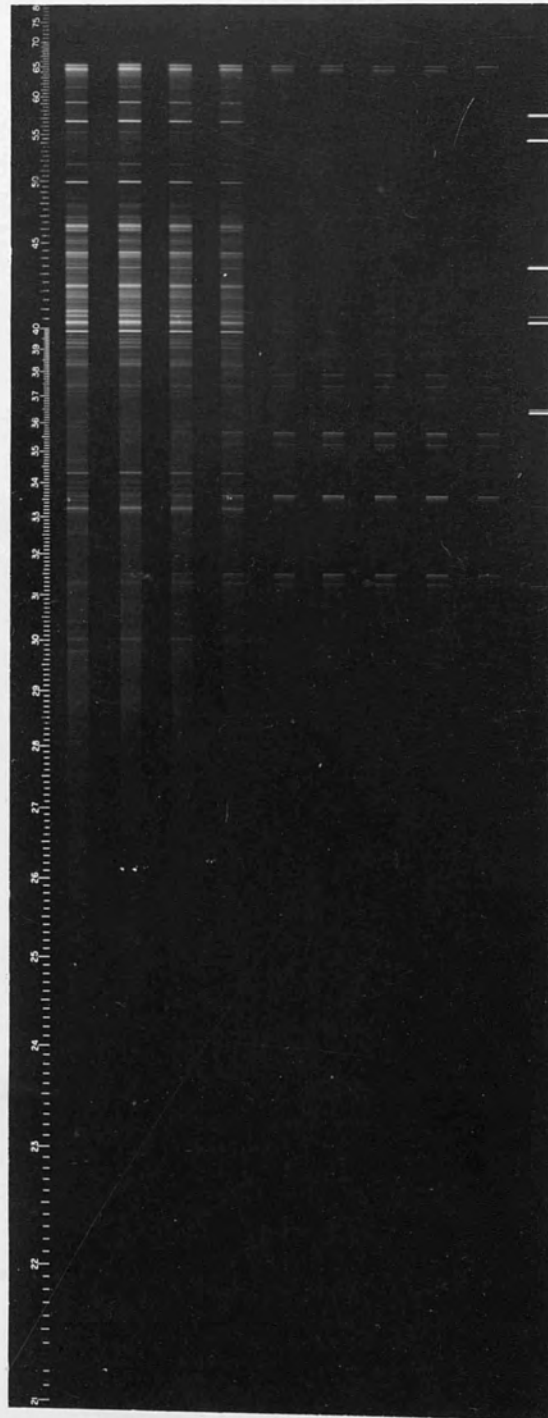


PLATE PL5

The spectral output from coaxial flashtube G filled with argon. The Blumlein voltage was 18 kV. The plate shows Hg lines and then spectral outputs corresponding to lamp pressures of 1, 5, 10, 20, 30, 40, 50, 60, 70 torr respectively. The flashlamp was triggered five times for each exposure.

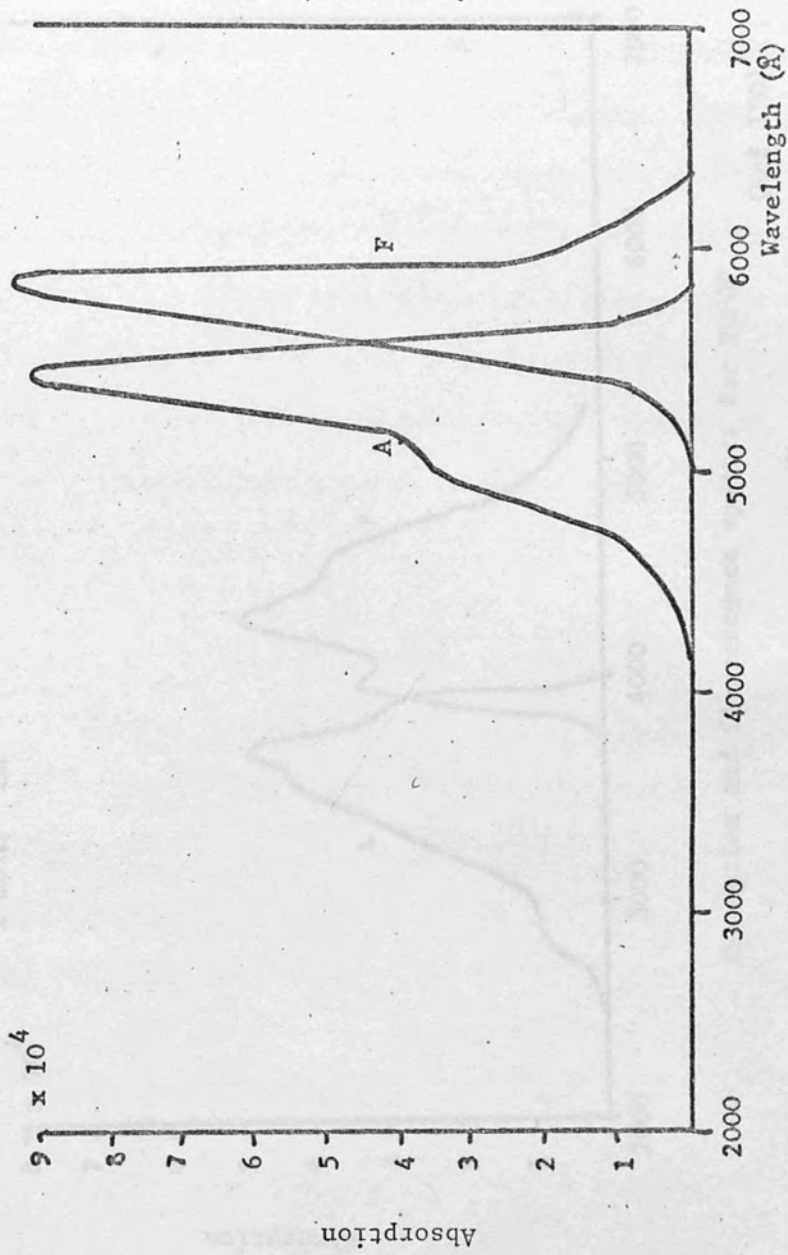




Molar extinction coeff.

$\epsilon \text{ mole}^{-1} \text{ cm}^{-1}$

$\times 10^4$



Fluorescence  
(Relative Intensity)

Absorption and fluorescence spectra for Rhodamine 6G

FIGURE 7.2a

below which UV production is very inefficient. By using the shortest duration current pulses, less heat flows into the body of the tube wall takes place during the wall ablation process, reducing the threshold energy and making the overall efficiency of the high pressure lamp filled flashing under similar operating conditions. However, with the shortest discharge current pulse generation, the ion mode operation still remains less efficient than the glow mode. For the point of view of maintaining the optical path length and the peak UV power, which maintains a good lamp life, it is better to use a glow mode operation with a pulse width of about 100 ns and a pulse rate of 100 Hz.

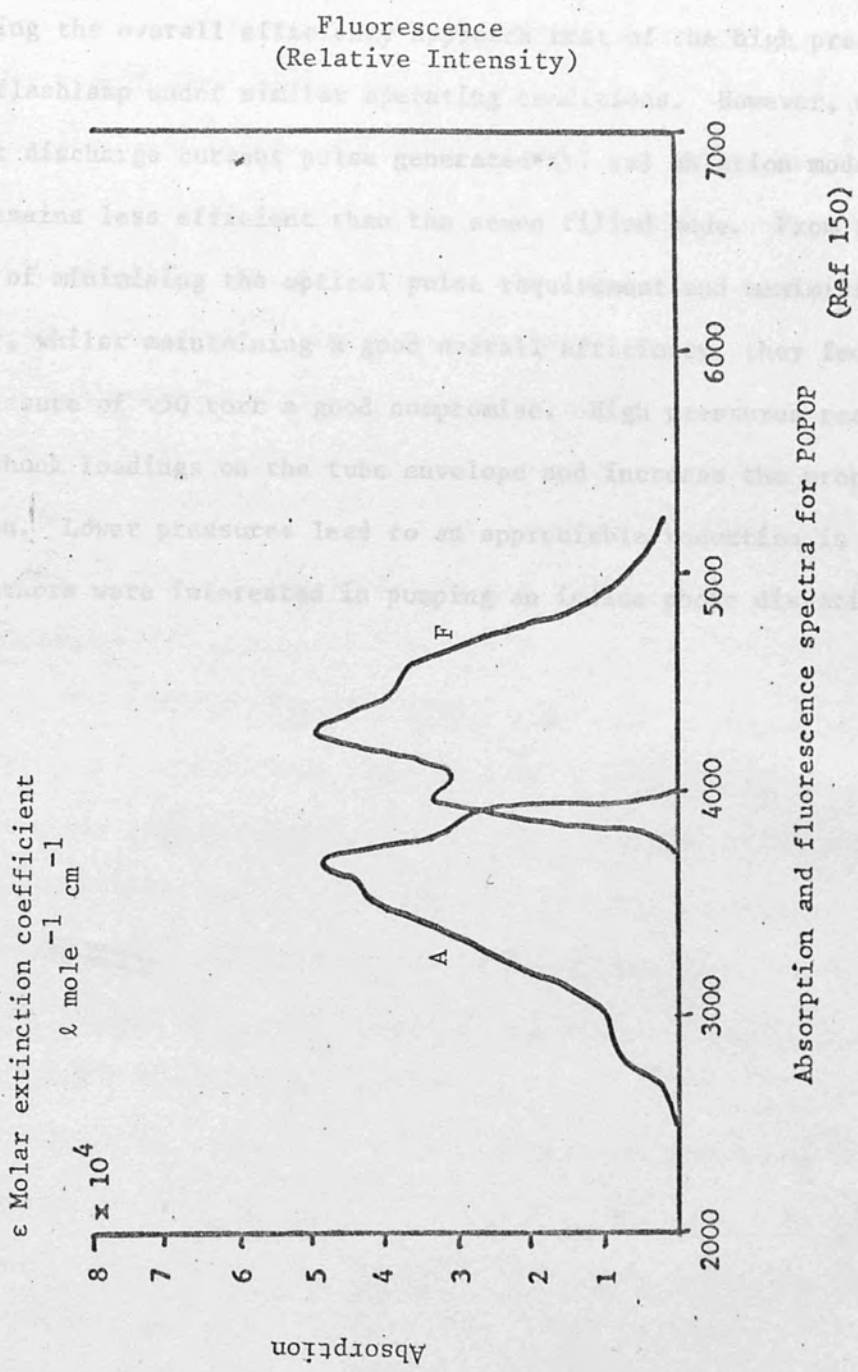


FIGURE 7.2 b

below which UV production is very inefficient. By using the shortest duration current pulses, less heat flow into the body of the tube wall takes place during the wall ablation process, reducing the threshold energy and making the overall efficiency approach that of the high pressure xenon filled flashlamp under similar operating conditions. However, with the shortest discharge current pulse generated ( $\sim 1 \mu\text{s}$ ) ablation mode operation still remains less efficient than the xenon filled mode. From the point of view of minimising the optical pulse requirement and maximising the peak UV power, whilst maintaining a good overall efficiency, they found a xenon fill pressure of  $\sim 50$  torr a good compromise. High pressures result in much higher shock loadings on the tube envelope and increase the probability of explosion. Lower pressures lead to an appreciable reduction in efficiency. These authors were interested in pumping an iodine photo dissociation laser.

## CHAPTER VIII

### THE NITROGEN LASER

#### 8.1 Introduction

In 1963, Heard<sup>(95)</sup> reported laser action in the second positive band system of molecular nitrogen at  $3371 \text{ \AA}$  using a fast rising, high voltage discharge. Leonard<sup>(96)</sup> and Gerry<sup>(97)</sup> were the first to use transverse excitation of the  $\text{N}_2$  laser to obtain high output power, and they predicted that higher output powers ( $\sim \text{MW}$ ) could be obtained by using faster excitation mechanisms. Shipman<sup>(82)</sup> confirmed this using a low inductance pulser system, triggered by six dielectric switches in such a manner as to produce a travelling wave of excitation along the laser tube. Since this time several workers<sup>(83)(89)(98-104)</sup> have obtained stimulated emission using discharges of high current densities established with an extremely fast initial rise.

The nitrogen laser is a very good optical pumping source of excitation for organic dyes. Most dyes have some absorption around the  $3371 \text{ \AA}$  output line of nitrogen and the fast risetime short duration pulse of high power from the  $\text{N}_2$  laser negates quenching mechanisms. Any prospective dye for use with a flashlamp should be tested for lasing by pumping it with a  $\text{N}_2$  pulse. If the  $\text{N}_2$  laser does not produce stimulated emission in the dye then a flashlamp will not.

Numerous laser dyes, operating from the near ultra violet through the visible spectrum and into the near infra red, can be pumped very efficiently with the nitrogen laser<sup>(105-112)</sup>, and strikingly large tuning ranges<sup>(113-115)</sup> are possible.

## 8.2 The inversion criterion

If we populate the  $C^3\pi_u$  level of  $N_2$  in a time which is short enough with respect to its natural radiative lifetime ( $\approx 40$  ns)<sup>(116)</sup>, it is possible to establish a population inversion between the  $C^3\pi_u$  and  $B^3\pi_g$  levels of the second positive system of  $N_2$  to obtain stimulated emission<sup>(117)</sup>. The  $B^3\pi_g$  level has a lifetime 5-8  $\mu$ s. Therefore, we may consider the  $N_2$  laser at 3371 Å as a three level laser<sup>(117)</sup>. The ground state (1) being considered as  $X^1\Sigma_g^+$ , the low level (2) being  $B^3\pi_g$  and the high level (3) being  $C^3\pi_u$ . Figure 8.1 shows the potential energies of the nitrogen molecule for the first and second bands. (See Appendix V).

Consideration of the rate equations for the nitrogen laser reveals the requirement for rapid excitation. Let  $N_1$ ,  $N_2$  and  $N_3$  be the population densities of levels 1, 2 and 3 respectively. Let  $X_{ij}$  be the collision excitation rate with electrons from level  $i$  to level  $j$  with  $i < j$ , and  $Y_{ji}$  the collision de-excitation rate from level  $j \rightarrow i$ . Let  $\tau_{ji}$  be the radiative lifetime from  $j$  to  $i$  and  $R_{ji}^i$  be the induced emission rate which includes the linewidth, the Einstein coefficient  $B$ , and the energy density. The rate equations are then<sup>(117)</sup>

$$\frac{dN_3}{dt} = X_{13} N_1 + X_{23} N_2 - \left( Y_{31} + Y_{32} + \tau_{31}^{-1} + \tau_{32}^{-1} \right) N_3 - R_{32}^i \left[ N_3 - \left( \frac{g_3}{g_2} \right) N_2 \right]$$

$$\frac{dN_2}{dt} = X_{12} N_1 + \left( \tau_{32}^{-1} + Y_{32} \right) N_3 - \left( \tau_{21}^{-1} + Y_{21} + X_{23} \right) N_2 + R_{32}^i \left[ N_3 - \left( \frac{g_3}{g_2} \right) N_2 \right]$$

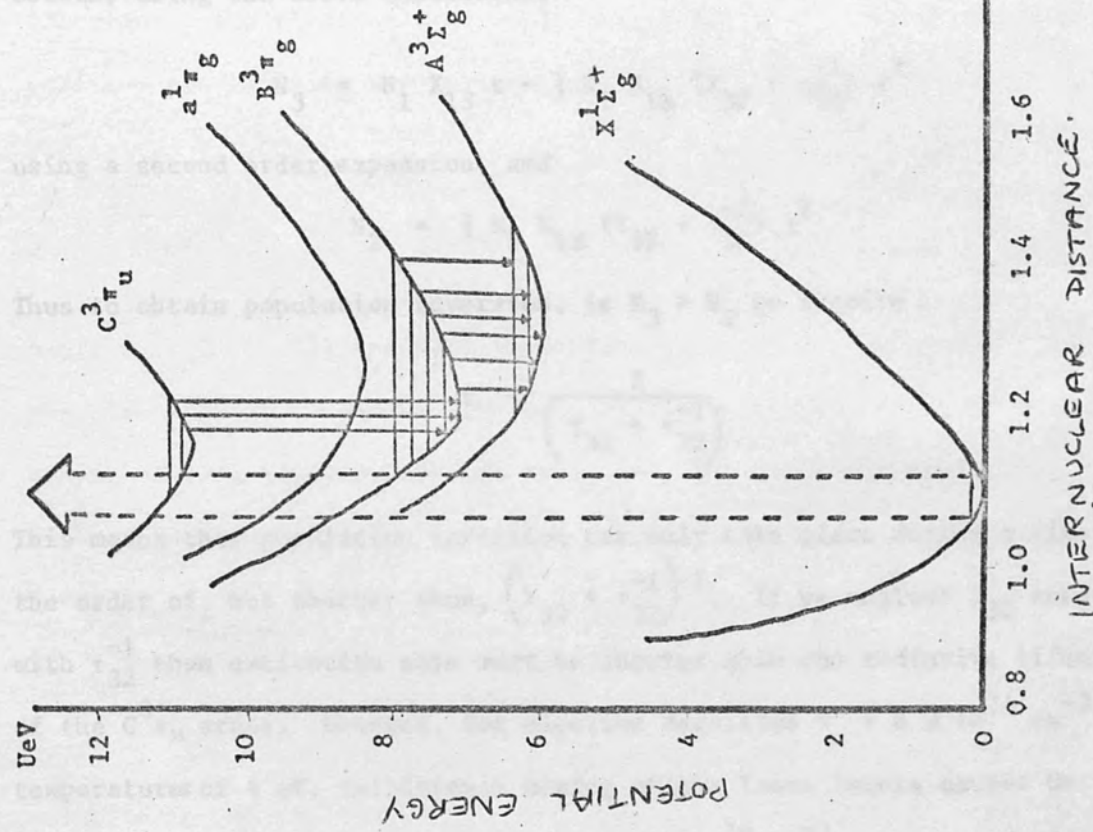
$$\frac{dN_1}{dt} = - \left( X_{12} + X_{13} \right) N_1 + \left( \tau_{21}^{-1} + Y_{21} \right) N_2 + \left( \tau_{31}^{-1} + Y_{31} \right) N_3$$



where  $g_1$  and  $g_2$  are the statistical weights of the high and low laser levels respectively.

The induced emission and absorption rates are neglected along with the de-excitation rate through collisions from the laser level to the ground state.

Assuming that  $A_{21}$  and the pumping rates are negligible, we obtain, using the above condition,



INTERNUCLEAR DISTANCE.

FIGURE 8.1: POTENTIAL CURVES OF THE N<sub>2</sub> MOLECULE: THE TRANSITIONS SHOWN ARE ACTIVE IN THE LASER EMISSION

where  $g_3$  and  $g_2$  are the statistical weights of the high and low laser levels respectively.

The induced emission and absorption rates are neglected along with the de-excitation rate through collision from the laser level to the ground state (117)(118). Since the C state is metastable we may put

$\tau_{31} \gg \tau_{32}$ . In accordance with the Franck Condon principle we may assume  $X_{13} > X_{12}$ . We may also assume  $\tau_{21} > \tau_{32}$  (since  $\tau_{32} \approx 40$  ns and  $\tau_{21} \approx 10$   $\mu$ s).

Assuming that  $N_1$  and the pumping rates are constants then we obtain, using the above conditions,

$$N_3 = N_1 X_{13} t - \frac{1}{2} N_1 X_{13} (Y_{32} + \tau_{32}^{-1}) t^2$$

using a second order expansion, and

$$N_2 = \frac{1}{2} N_1 X_{13} (Y_{32} + \tau_{32}^{-1}) t^2$$

Thus to obtain population inversion, ie  $N_3 > N_2$  we require

$$t < \sqrt{\frac{2}{Y_{32} + \tau_{32}^{-1}}}$$

This means that population inversion can only take place during a time of the order of, but shorter than,  $(Y_{32} + \tau_{32}^{-1})^{-1/2}$ . If we neglect  $Y_{32}$  compared with  $\tau_{32}^{-1}$  then excitation rate must be shorter than the radiative lifetime of the  $C^3\pi_u$  state. However, for electron densities  $N_e > 6 \times 10^{14} \text{ cm}^{-3}$  at temperatures of 4 eV, collisional mixing of the laser levels cannot be ignored. This means  $Y_{32} > \tau_{32}^{-1}$  for  $N_e > 6 \times 10^{14} \text{ cm}^{-3}$  and the inversion duration is shortened. We now see that more efficient pumping would be obtained by exciting nitrogen in a time shorter than 40 ns.

### 8.3 Dependence of laser power density on various parameters

Ali<sup>(119)</sup> considered the case of the nitrogen molecule as a lasing system, coupled to an electric circuit consisting of a capacitor with a capacitance  $C$  charged originally to some voltage  $V_o$ , a fixed external resistance  $R_e$  and inductance  $L$ . The lasing medium, as part of the electric circuit, acts as a variable resistance  $R(t)$  which is the sum of the plasma resistance (ion-electron collisions) and the resistance due to electron neutral collisions. In this case, however, the latter is the most important. The electrons are ohmic heated and lose their energies by exciting and ionising the molecules. The circuit equation used by Ali<sup>(119)</sup> was

$$L \frac{dI}{dt} + R_T I = V_o - \int_0^t \left( I \frac{dt'}{C} \right)$$

where  $R_T = R_e + R(t)$  and  $R(t)$  is obtained from the mobility data<sup>(120)</sup> for the electrons in nitrogen. The rate equations, including electron impact mixing of laser levels, coupled to the circuit equation were solved under saturation approximations<sup>(97)</sup>. The saturation assumption advanced by Gerry is

$$N_3 - N_2 \ll N_3 \text{ and } N_3 \approx N_2 = N$$

The calculations of the saturated power output were solved numerically for two different approaches in which energy is supplied to the system.

One, a fast rising current discharge (risetime  $\sim 3$  ns) and decaying slowly (method A), and the other a sine wave current discharge with a period large compared to the laser lifetime (method B). The saturated power output for A was about 50 times larger than for method B.

On the other hand the pulse half width was narrower by a factor of two. From a physical stand point we see that more electrons are created at a faster rate and are hotter for method A than that for method B. Thus Ali considered method A to have high potentiality in terms of the power output and this was corroborated by Shipman's<sup>(82)</sup> results.

The effects of excitation of the vibrational levels and collisional mixing cause a considerable amount of electron energy to be lost in the vibrational levels - narrowing the power pulse appreciably. This is because the electrons have cooled down to  $\sim 4$  eV after 2 ns from the onset of the discharge, where the rate of energy loss to the vibrational levels predominates any other loss rates (this is true for the electron temperature range of  $T_e < 6$  eV). This implies however, that electron impact excitation of the upper laser level has been curtailed. From Ali's theory collisional mixing also causes narrowing (or the shut off) of the power pulse and some reduction in the peak power. Utilising experimental data in his equations, Ali considered the rate of collisional de-excitation to exceed the rate of radiative decay at  $N_e > 6 \times 10^{14} \text{ cm}^{-3}$ .

Thus, the first requirement is to minimise circuit inductance. The faster the current rises, ie the smaller the circuit inductance, the higher the peak power density and the shorter the width of the pulse becomes. This arises for high currents with fast risetimes since the ionisation rate is higher and the electrons have relatively more energy during the time period 0-2 ns. The laser power density is basically proportional to the rate of excitation of the upper laser level which is a function of electron density and temperature. This means power density increases with increase in  $N_e$  and  $T_e$  and also the hotter the electrons the less the energy that is lost to the excitation of ground state vibrational levels. For  $T_e < 4$  eV, the rate of energy loss by electrons in

the excitation of ground state vibrational levels is greater than other rate processes, ie ionisation of molecule and excitation of upper laser level. These rates are essential to a higher laser power density so that the efficiency of a nitrogen laser depends on having the electron temperature above 4 eV.

The laser power density and duration are dependent on the pressure in the laser cavity. The peak power density increases and arrives earlier as the gas pressure increases whilst the pulse duration decreases. The energy density has an optimum value at a pressure 25-30 torr<sup>(96)(82)</sup>. As the gas pressure increases beyond 30 torr the electrons are cooler leading to less excitation to the upper laser level; the electrons lose their energies mostly in exciting the vibrational levels of the ground state.

Increasing the capacitor voltage  $V_0$ , increases the laser power density. This is due to the intense electric fields giving higher  $E/p$  values. Higher  $E/p$  values imply higher electron drift velocities and higher electron densities and these in turn imply higher currents.

The narrowing of the laser pulse depends on several factors. The laser line  $3371 \text{ \AA}$  has a lower level which is long lived compared with the radiative lifetime,  $\tau_{32}$ . In itself, this limits the duration of the laser pulse to a time  $t < \tau_{32}$ . With increasing laser density the induced emission rate predominates over the spontaneous emission term. The effective lifetime is practically the inverse of the induced emission rate, so that pulse narrowing would be expected.



#### 8.4 Calculating the optimum E/p value

It is possible to calculate the E/p value required for optimum efficiency of the nitrogen laser.<sup>(118)</sup> Cartwright<sup>(121)</sup> has calculated the total cross sections for the excitation of the seven lowest triplet electronic states of nitrogen as a function of the electron energy from  $v'' = 0$  of the ground state (Figure 8.2). The diagram indicates that the electrons should have an energy of 14 eV in order to provoke the highest population inversion between  $C^3\pi_u$  and  $B^3\pi_g$  levels. (In fact, as the curve is not symmetrical on each side of the maximum and the electrons are not mono-energetic, it is better to take a value of about 16 eV)<sup>(118)</sup>.

The mean free path,  $\lambda$ , of the electrons at 16 eV in  $N_2$  as a function of pressure is<sup>(118)</sup>

$$\lambda = (\sigma N)^{-1}$$

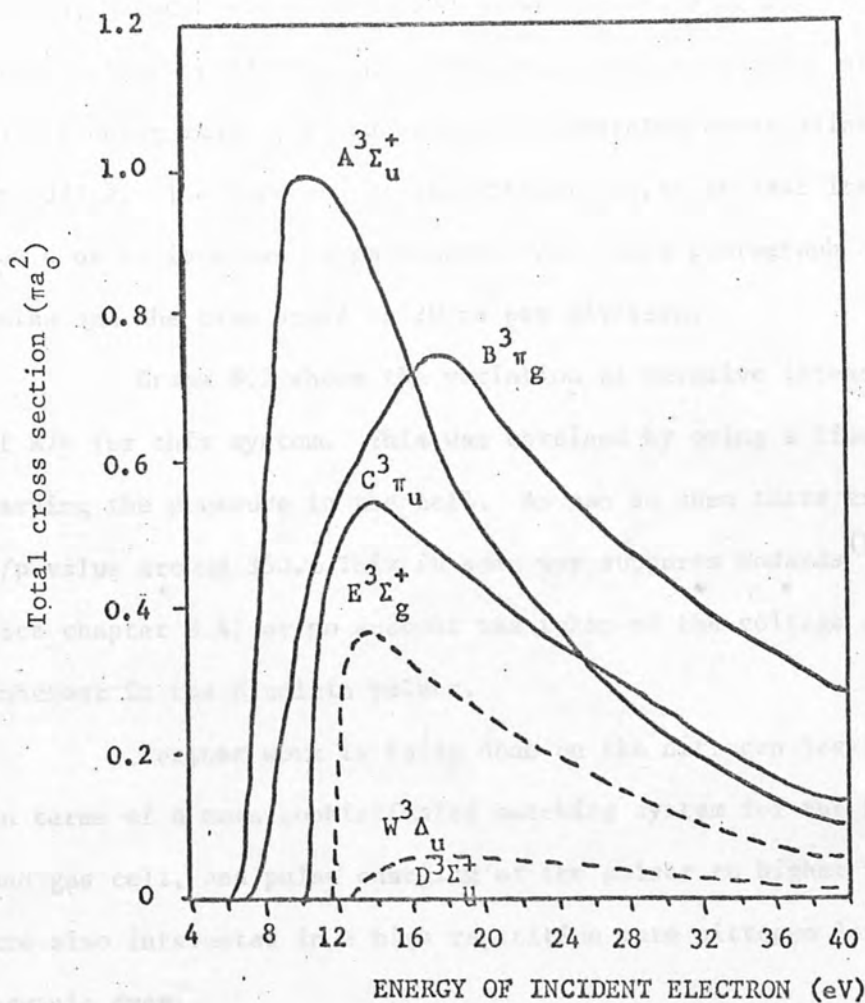
where  $\sigma$  is the total cross section and  $N$  is the number of molecules per unit volume and per torr. Here, then,  $\sigma$  is the sum of the cross sections at 16 eV to excite  $N_2$  to the various electronic states.

The formulae is valid for a mono-energetic beam of electrons. As this is not the case here, the value obtained will be a minimum one due to the electron acceleration and cross section variation.

According to Figure 8.2,  $\sigma \approx 5 \pi a_0^2$  where  $a_0$  is the first Bohr radius of the hydrogen atom. This yields  $\lambda = 0.064 \text{ cm}$ <sup>(118)</sup> for one torr. The maximum field  $E$  that gives an energy of 16 eV to the electrons at a pressure of one torr is  $E = 16/\lambda$ , which gives a value of  $E/p \approx 250 \text{ V cm}^{-1} \text{ torr}^{-1}$ .

#### 8.5 Experimental results

The 12 feet, 20 ns pulser was used to obtain nitrogen laser pulses. This pulser and the cell used to contain the nitrogen was described in Chapter IV. At one end of the 45 cm cell was placed a 98%



Total cross sections for excitation of the seven lowest triplet electronic states of  $N_2$  from  $v'' = 0$  of the ground state as a function of the incident electron energy. The cross sections for the  $A^3\Sigma$  and  $C^3\Pi$  states shown here have been reduced by factors of  $^u3.5$  and  $^u2.0$  respectively.

FIGURE 8.2

reflecting aluminium mirror. When air at a pressure of 25 torr was used in the cell, the output from the system was entirely in the ultra violet region, between 4000 Å and 2500 Å, without showing any pronounced superfluorescence at 3371 Å. However, when industrial grade nitrogen was used, in a flowing manner, we successfully generated superradiant radiation at 3371 Å. The duration of the optical output at half its peak amplitude was 6 ns as is shown in photograph P23. This photograph shows a typical pulse and the time scale is 20 ns per division.

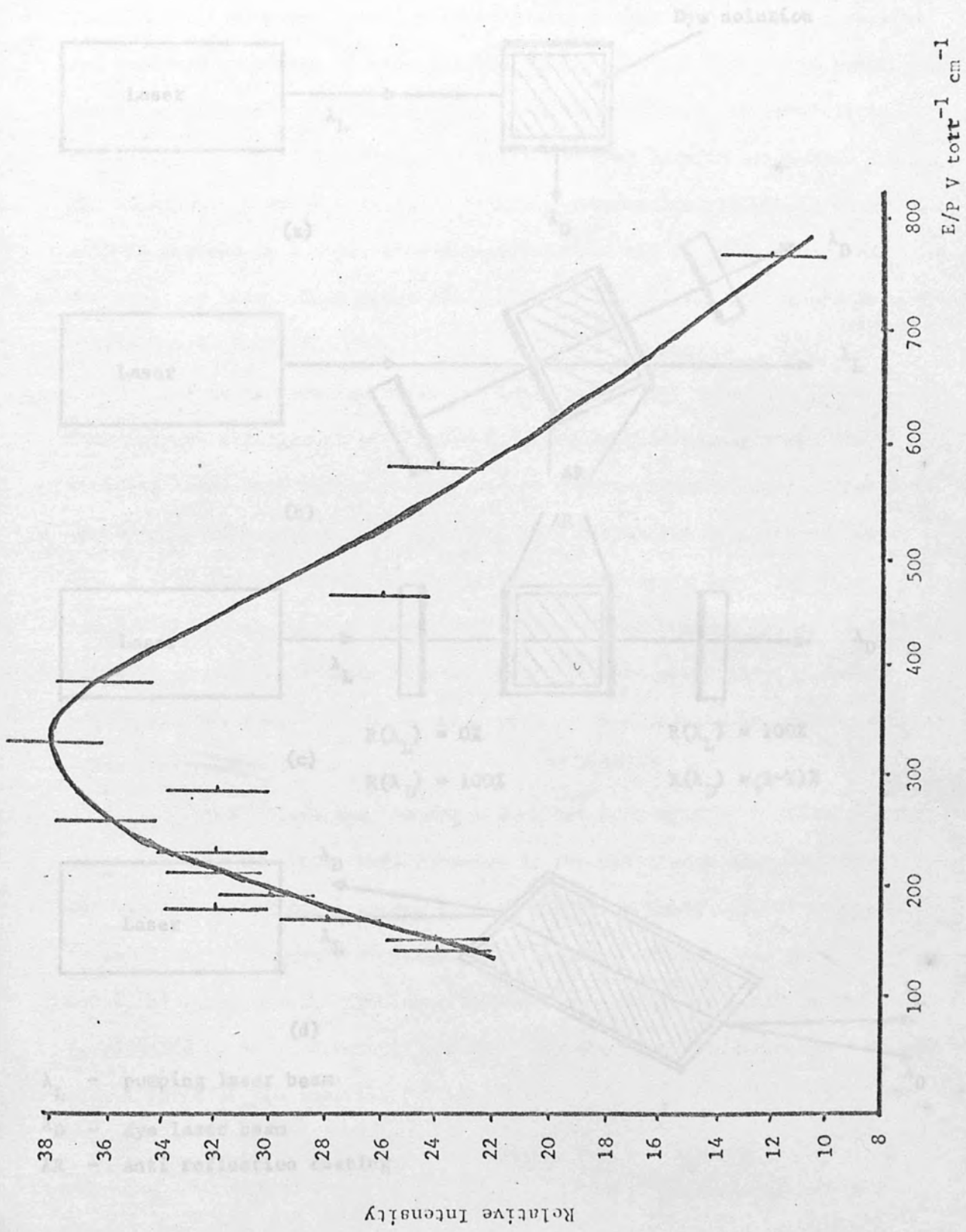
Graph 8.3 shows the variation of relative intensity as a function of  $E/p$  for this system. This was obtained by using a fixed voltage and varying the pressure in the cell. As can be seen there exists an optimum  $E/p$  value around 350. This in some way supports Godards<sup>(118)</sup> postulation (see chapter 8.4) as no account was taken of the voltage doubling effect inherent in the Blumlein pulser.

Further work is being done on the nitrogen laser by my colleagues in terms of a more sophisticated matching system for the Blumlein pulser and gas cell, and pulse charging of the pulser to higher voltages. They are also interested in a high repetition rate nitrogen laser for pumping organic dyes.

#### 8.6 Resonator configurations for laser pump dye lasers

A simple dye laser structure was used in many of the early investigations. It is still useful for exploratory studies of new dyes<sup>(35)</sup>. It consists of a square spectro-photometer cuvette filled with the dye solution (Figure 8.4) which is excited by the beam from a suitable laser. As shown in the figure, the resonator is formed by the two glass air interfaces of the polished sides of the cuvette (heavy lines in Figure 8.4(a)) and the exciting laser and dye laser beams are at right angles.

FIGURE 8.3: VARIATION OF RELATIVE INTENSITY OF N<sub>2</sub> LASER OUTPUT WITH E/P V torr<sup>-1</sup> cm<sup>-1</sup>



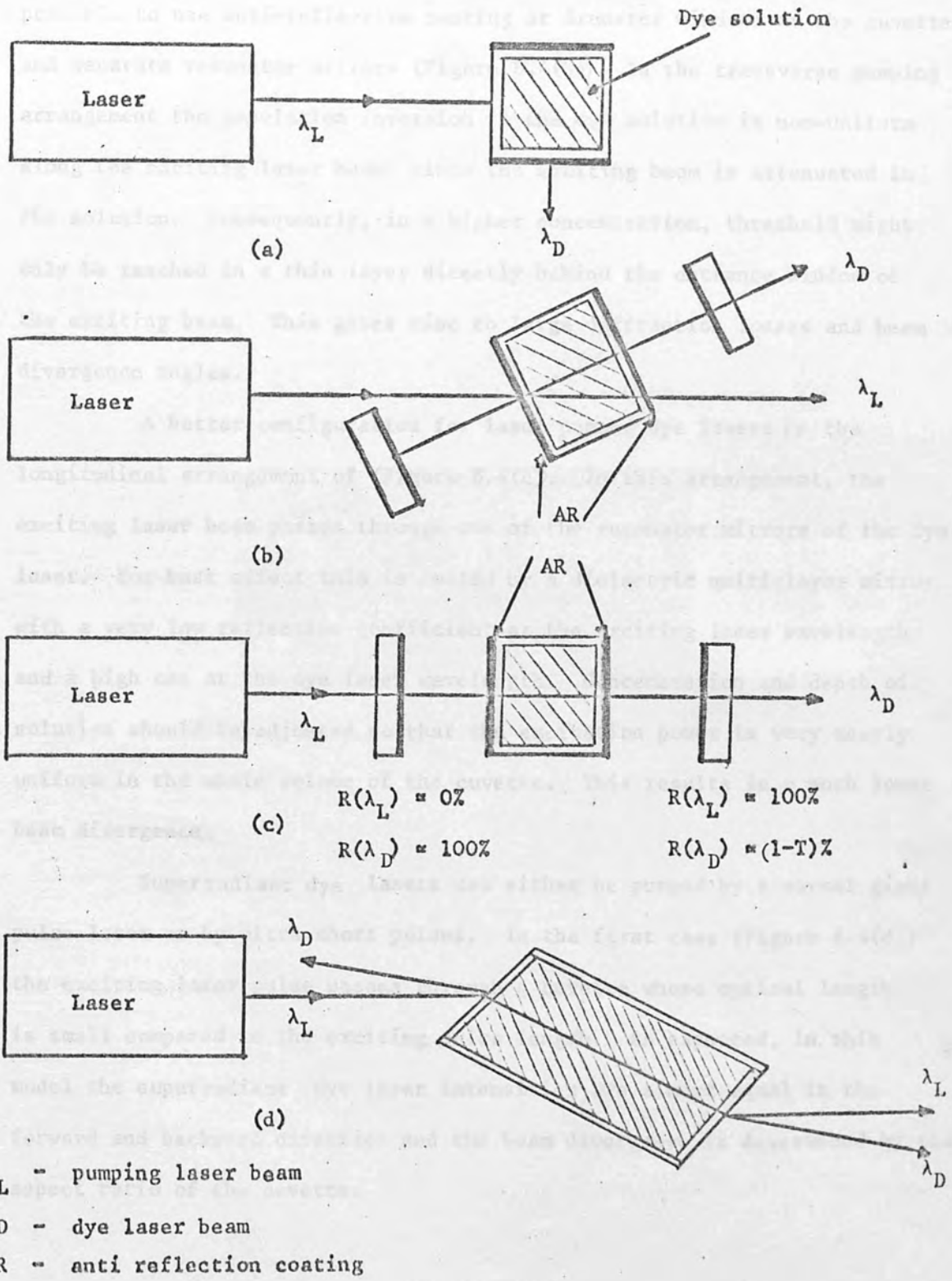


FIGURE 8.4: RESONATOR CONFIGURATIONS FOR LASER PUMP DYE LASERS

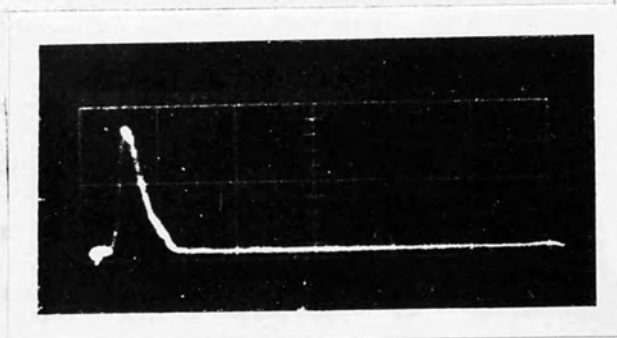


Reflective coatings on the windows consisting of suitable metallic or multiple dielectric layers enhance the Q of the resonator. It is also possible to use anti-reflective coating or Brewster windows at the cuvette and separate resonator mirrors (Figure 8.4(b)). In the transverse pumping arrangement the population inversion in the dye solution is non-uniform along the exciting laser beam, since the exciting beam is attenuated in the solution. Consequently, in a higher concentration, threshold might only be reached in a thin layer directly behind the entrance window of the exciting beam. This gives rise to large diffraction losses and beam divergence angles.

A better configuration for laser pumped dye lasers is the longitudinal arrangement of (Figure 8.4(c)). In this arrangement, the exciting laser beam passes through one of the resonator mirrors of the dye laser. For best effect this is coated by a dielectric multi-layer mirror with a very low reflection coefficient at the exciting laser wavelength and a high one at the dye laser wavelength. Concentration and depth of solution should be adjusted so that the excitation power is very nearly uniform in the whole volume of the cuvette. This results in a much lower beam divergence.

Superradiant dye lasers can either be pumped by a normal giant pulse laser or by ultra short pulses. In the first case (Figure 8.4(d)) the exciting laser pulse passes through a cuvette whose optical length is small compared to the exciting pulse length. As expected, in this model the superradiant dye laser intensities are almost equal in the forward and backward direction and the beam divergence is determined by the aspect ratio of the cuvette.

Pump lasers which have been used so far with one or other of these arrangements include argon-ion (514 nm), neodymium (1.06  $\mu\text{m}$ ) and its harmonics (532 nm, 354 nm and 266 nm), ruby (694 nm) and its harmonic (347 nm), nitrogen (337 nm) and other dye lasers.



PHOTOGRAPH P23

Nitrogen laser output pulse. Oscilloscope time base was set to 20 ns/div and the half-width of the pulse is 6 ns.

## CHAPTER IX

### ORGANIC DYE OUTPUTS

#### 9.1 Introduction

The use of a long flashlamp (as suggested by Holzrichter et al)<sup>(76)</sup> makes the use of an equally long dye cuvette advisable. This in turn makes a flow system almost mandatory, because in a long cuvette even small thermal gradients can severely degrade the resonator characteristics. If the repetition rate of the pump pulse is increased above about one shot per minute, the heat generated via radiationless transitions in the dye molecules and energy transfer to the solvent can cause Schlieren in the cuvette which deteriorates the dye laser outputs<sup>(35)</sup>. A flow system would ensure a fresh solution for every shot negating the above deterioration.

The dye flow in the cuvette of a flashlamp pumped dye laser may be longitudinal or transverse. In both cases the flow should be high enough to be in the turbulent regime. This rapidly mixes the liquid and hence reduces thermal gradients due to non uniform pump light absorption in the cuvette. It is important, however, not to have any bubbles greater than 50  $\mu$  within the cuvette<sup>(122)</sup> as this seriously depletes the lasers performance. Any "O" ring seals or hoses connecting the cuvette with the circulating pump should consist of silicone rubber for use with methanol or ethanol solvents. Commercial rubber "O" rings and clear plastic hoses usually give off absorbing or quenching fillers and plasticisers<sup>(35)</sup> and hence should not be used.

For the solvents like dimethyl-formamide or dimethyl-sulfoxide, teflon coatings are required on "O" rings and hoses. A similar choice of materials is required with the pump and the reservoir of the dye solution. Magnetically coupled centrifugal or toothed wheel pumps made of teflon and stainless steel are well suited for this application. Membrane pumps, on

the other hand, lead to less reproducible results because of the pulsation in the flow rate.

The efficiency of a dye laser is a function of a great number of parameters: energy and risetime of the driver circuit, reflectivity of the cavity mirrors, dye concentration, dye cell size and flashtube design. In this section I shall look more closely at dye cell concentration and dye cell size.

A theoretical paper by Blit et al<sup>(123)</sup> considers the distribution of absorbed pump power in flashlamp pumped dye lasers. Their calculation takes into account both the geometrical parameters (diameter of the dye tube and wall thickness) and the relevant physical parameters, such as the indices of refraction of the tube material and dye solution, dye concentration, absorption spectrum of the dye and emission spectrum of the flash.

They assume the dye solution is contained in a cylindrical tube made of material which is transparent to the pumping light (See Figure 9.1). The medium outside has an index of refraction  $n_0$  assumed constant with respect to the wavelength of the pump radiation since variations over the relevant range are small. The tube has an inner radius  $R$  and an external radius  $R_1$ , and its length is much larger than its diameter, so that end effects are neglected. The calculation is performed for a coaxial configuration which consists of two coaxial tubes. The inner tube contains the dye solution, and the flash occurs in the volume between the two cylinders. The authors state the results should also be valid for configurations of the closed wrap type, in which a number of flashlamps surround the dye tube<sup>(124)</sup> so that cylindrical symmetry is maintained. The authors assume the flashlamp to be at a high enough temperature so that its emission behaves as black body radiation. The index of refraction of the tube material is considered to be  $n_1$ , and the calculation allows for

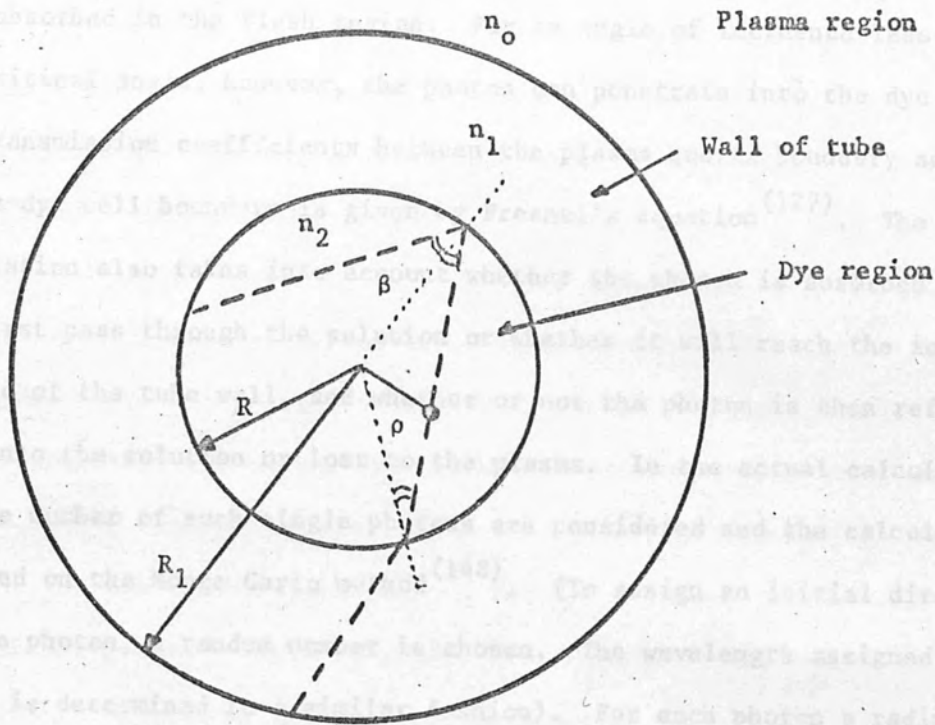


**FIGURE 9.1: CROSS SECTION OF FLASHLAMP DYE CELL ARRANGEMENT**  
**ALL SYMBOLS ARE DEFINED IN THE TEXT**



partial reflection at the plasma, quartz interface. The index of refraction of the solution is  $n_2$ , and in many practical situations  $n_1 > n_2$  (eg quartz tube and a dye solution in water or ethanol). In such cases a critical angle exists and it is possible a photon will not penetrate the solution. This photon will zig-zag inside the tube wall and eventually be reabsorbed in the flash region. For an angle of incidence less than the critical angle, however, the photon can penetrate into the dye solution. The transmission coefficients between the plasma quartz boundary and the quartz-dye cell boundary is given by Fresnel's equation<sup>(127)</sup>. The calculation also takes into account whether the photon is absorbed during its first pass through the solution or whether it will reach the inner surface of the tube wall, and whether or not the photon is then reflected back into the solution or lost to the plasma. In the actual calculation, a large number of such single photons are considered and the calculation is based on the Monte Carlo method<sup>(148)</sup>. (To assign an initial direction for the photon, a random number is chosen. The wavelength assigned to the photon is determined in a similar fashion). For each photon a radius  $\rho$  is obtained, at which it is absorbed.

The authors then divide  $R$  into  $N$  intervals and defining  $\rho_i = i (R/N)$ , ( $0 < i < N$ ) they obtain  $N$  numbers,  $N_i$  which give the number of photons absorbed between  $\rho_{i-1}$  and  $\rho_i$ . The fraction of the total pump energy, which is absorbed, is found by dividing  $\sum_i N_i$  by the total number of photons sampled. The absorbed pump energy per unit volume is therefore proportional to  $W_i = N_i / \bar{\rho}_i$

where

$$\bar{\rho}_i = \frac{1}{2(\rho_{i-1} + \rho_i)}$$

A histogram of  $\omega_i$  will give the absorption profile desired, ie the pump energy absorbed per unit volume as a function of the distance from the axis of the dye tube.

The above procedure is quite general and can be applied to any dye for which the physical parameters are known. The application of the calculation to rhodamine 6G in ethanol is discussed. As expected, the absorption profile as a function of  $\rho/R$  depends on the product of the inner radius of the dye tube ( $R$ ) and the concentration ( $N_o$ ), and not on each of these alone. Values of  $N_o R$  between  $3 \times 10^{17} \text{ cm}^{-2}$  and  $3 \times 10^{15} \text{ cm}^{-2}$ , which are typical values used ( $10^{-3}$ - $10^{-5} \text{ ml}^{-1}$  for  $2R = 1 \text{ cm}$ ) in Rh 6G lasers, were chosen. Another parameter which affects the profile is the ratio  $R_1/R$ , and values between 1.1 and 1.5 were investigated. The black body temperature of the flash was chosen at a number of values between 20000 and 30000<sup>o</sup>K, which are typical for fast discharge flashlamps used to pump dye lasers. The absorption cross section for Rh 6G at wavelengths above 600 nm is practically zero. Since UV radiation causes photo-dissociation, this radiation is frequently filtered out in practice<sup>(128)</sup>. Blit and Ganiel therefore sampled only photons in the wavelength range 230-600 nm. For each calculation  $2 \times 10^5$  photons were sampled and the interval (0,R) divided into 50 segments. This was found to yield satisfactory statistics. Some typical results are reproduced in Figures 9.2 and 9.3. It was found that no significant change in the absorption profile occurs for black body temperatures between 20000<sup>o</sup>K and 30000<sup>o</sup>K. This is not surprising, since at all temperatures in this range the peak emission occurs at wavelengths well below the lowest wavelength of the photons sampled.

As can be seen from Figure 9.2, the absorption profile depends rather critically on the product  $N_o R$ . If a homogeneous profile is desired,

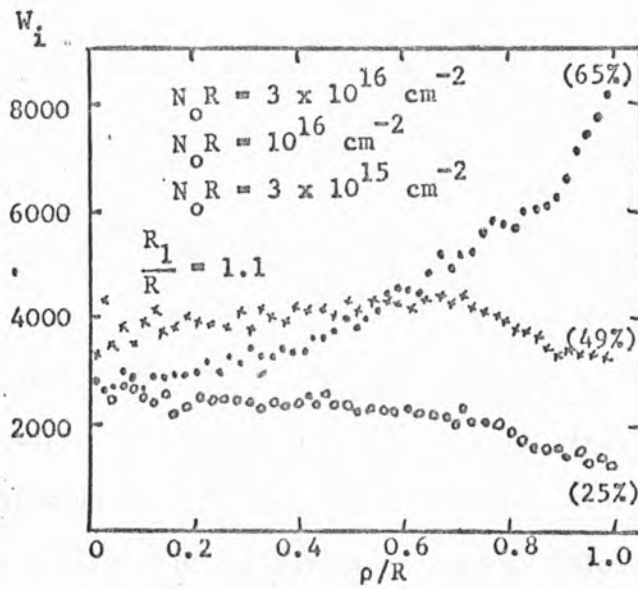


FIGURE 9.2: CALCULATED ABSORPTION PROFILES FOR Rh 6G, FOR THREE VALUES OF  $N_0 R$ . THE PERCENTAGE OF THE TOTAL NUMBER OF SAMPLED PHOTONS, WHICH WERE ABSORBED IN THE DYE SOLUTION, IS GIVEN IN EACH CASE

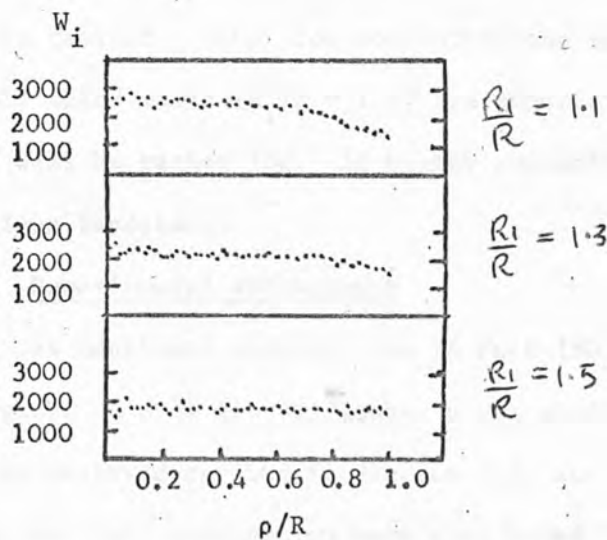


FIGURE 9.3: CALCULATED ABSORPTION PROFILES SHOWING THE EFFECT OF WALL THICKNESS OF THE TUBE, FOR A LOW CONCENTRATION SOLUTION ( $N_0 R = 3 \times 10^{15} \text{ cm}^{-2}$ )

then in Rh 6G the optimum value is about  $3 \times 10^{15} \text{ cm}^{-2}$  ( $\sim 1.7 \times 10^{-5} \text{ m/l}$  for  $R = 0.5 \text{ cm}$ ). However, at this concentration only about 30% of the sampled photons are absorbed in the dye solution. At higher concentrations, the total absorption increases, but the absorption profile becomes very inhomogeneous. At  $N_0 R = 3 \times 10^{16} \text{ cm}^{-2}$ , already 65% of the sample photons are absorbed, but the energy per unit volume at the edge of the tube is about three times larger than on the tube axis. This trend will be even more pronounced at higher concentrations. Too high concentrations therefore render a large part of the dye solution useless, since most of the excitation will then occur at an annular region close to the tube wall.

The effect of wall thickness on the pumping profile is demonstrated in Figure 9.3, where the authors plot some pumping profiles for  $N_0 R = 3 \times 10^{15} \text{ cm}^{-1}$  at a number of values of  $R_1/R$ . At higher values of  $R_1/R$  the absorption at the edge ( $\rho/R \sim 1$ ) increases at the expense of the absorption further into the solution ( $\rho/R < 1$ ). If a homogeneous pumping profile is desired, rather low concentrations ( $N_0 R = 3 \times 10^{15} \text{ cm}^{-2}$ ) and relatively thick walls ( $R_1/R = 1.5$ ) are superior. Overall efficiency, however, will be rather low. At higher concentrations, the effect of  $R/R_1$  becomes less important.

## 9.2 Experimental arrangement

As mentioned earlier, the 24 feet (90 ns) pulser was used for the dye work. A 6 cm linear flashtube was used in conjunction with the elliptical cavity described in Section 4.3, and a coaxial and triaxial flashlamp dye cell combination were also tried. The coaxial flashlamp-dye cell combination was the type where the inner wall of the flashlamp was also the outer wall of the dye cell. Such a design is shown in Section 4.3. The tri-axial configuration consisted of a coaxial flashlamp

with a dye cell inserted within the inner tube. Dye cells used inside the coaxial flashlamp and in the elliptical cavity are shown in section 4.5.

The dye used in these preliminary experiments was rhodamine 6G and the solvent used was methanol (ultra grade). The dye was circulated using a peristaltic pump, which, due to our fast pulses and slow repetition rate, did not seem to have an adverse effect on the output from the dye. We did not use a filter system for removing bubbles and this meant that the time between shots needed to be long to remove the bubbles caused by the flashlamp discharge<sup>(62)</sup> inducing shock waves. No triplet quenching additives were used but the dye in the reservoir was in contact with the laboratory air at atmospheric pressure (before the system was sealed for circulating purposes).

Broad-band aluminium reflectors were used and these were obtained from our own evaporation plant. The mirrors assumed to be totally reflecting, reflected about 98% of the light from a helium-neon laser (6328 Å) and the partially reflecting mirrors used were typically 60% reflecting with transmission around 25% and thus loss around 15% at 6328 Å.

The inside of the linear flashlamp elliptical cavity contained an aluminium coated steel shim approximately 1/2000" thick. The exterior of the coaxial flashlamps were coated in white reflectance made by Kodak. This reflected 99.9% of the incident light upon it.

In these preliminary investigations, no prepulse enhancement was used.



### 9.3 Flashtube coupling to the active media

Using the linear flashlamp in conjunction with the elliptical cavity we did not manage to obtain any lasing action. Although the output from the linear flashlamp was not so intense as that from the coaxial flashlamp the most probable reason for the lack of lasing action was the poor coupling between the linear flashlamp and the dye cell.

Although the two inch coaxial flashlamp (E) was the most luminous, the coupling of the pump light into the dye cuvette was not as efficient as the coaxial flashtube - dye cell combination (F). Referring to the introduction at the beginning of this chapter we see this is most likely to be due further probability of pump light being reflected from the dye cell. Lasing action was achieved using coaxial flashtube (E) but the electrical energy input required for lasing action was greater than that required by the coaxial flashtube - dye cell combination (F). In this combination, only one quartz wall separates the active media from the flashtube plasma thus increasing absorption of the plasma photons by the active media.

Although the lower threshold conditions were obtained for coaxial system (F) this is not necessarily the better of the two types of system. Hirth et al<sup>(62)</sup> reported a serious limitation of the energy and of the pulse repetition rate of coaxial flashlamp excited dye lasers due to the ultrasonic wave initiated by the electrical discharge which propagates through the dye cell during the laser emission. Ewanizky and Wright<sup>(129)</sup> and Blit, Fisher and Ganiel<sup>(130)</sup> have also observed this effect and the latter authors suggest ways of removing the shock wave effect. They suggest infra red absorption by the dye as being responsible for the shock wave formation in the liquid. Two ways are suggested to remove the

shock effects. The first is to use a pyrex dye cell (which has strong absorption in the infra-red) or use a triaxial system and use distilled water, for example, between the interior of the flashlamp and the exterior of the dye cell. The infra-red radiation from the flashlamp is completely absorbed in the water surrounding the lamps and does not reach the dye solution. This arrangement has the additional advantage that the pump light can be filtered by various additives to the water, and pump light normally outside the absorption band of the dye can possibly be converted into radiation in the right wavelength by the additives.

#### 9.4 Lasing action from rhodamine 6G in methanol

Lasing action from rhodamine 6G in methanol was first achieved using coaxial flashlamp (E) which had an arc channel 1.5 mm wide and 4.2 cm long. Industrial grade argon at a pressure of 90-100 torr was used in the flashlamp. Photograph P24 (sweep speed 200 ns/division) was obtained using a photodiode (HL62) 18 inches away from, and in line with, the laser cavity. The traces show fluorescence and finally lasing output as the electrical energy to the pluser is increased. The top trace was obtained for 20 joules electrical input (10 kV) and the lasing action appeared for electrical input of 32 joules (13 kV). The cavity had aluminium coated windows of 98% and 60% reflectivity. Transmission through the partially reflecting mirror was about 25%. The flashlamp was wrapped with aluminium foil and taped to prevent breakdown from the electrodes.

Another important factor influencing stimulated emission from the system was the distance between the end of the dye cell and the reflecting mirror. In our case, if this gap was two centimeters or more no lasing action was observed. Due to the dye tube design and the mirror mount assembly we could not decrease this distance below one centimeter. A dye tube whose end windows were the cavity mirrors would vastly improve the efficiency of the system.

PHOTOGRAPH P24

Output from Rhodamine 6G in methanol as the voltage to the flashlamp is increased from

- (a) 10 kV - fluorescence
- (b) 11 kV - fluorescence
- (c) 12 kV - fluorescence
- (d) 13 kV - lasing threshold

Sweep speed 200 ns/div.

PHOTOGRAPH P25

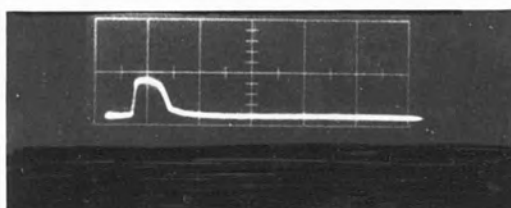
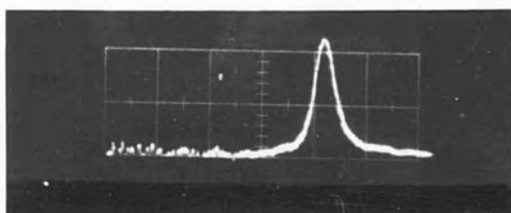
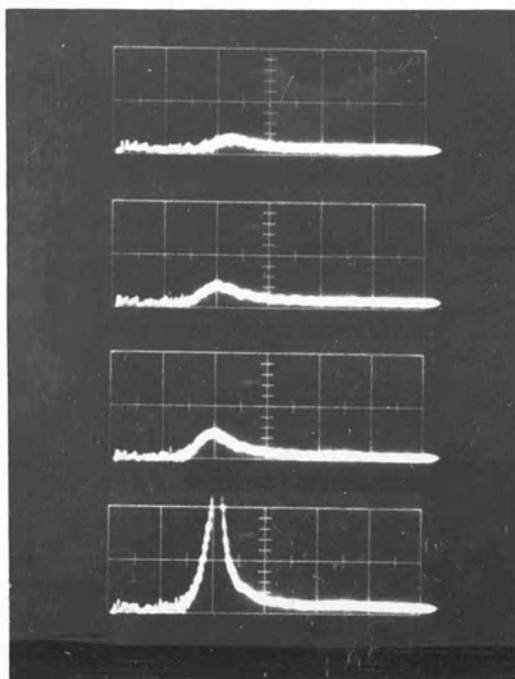
Output from Rhodamine 6G in methanol for an electric input of 24 joules.

Sweep speed 100 ns/div.

PHOTOGRAPH P26

Output from Rhodamine 6G in methanol for an electric input of 40 joules.

Sweep speed 100 ns/div.



A laser pulse, close to threshold, from the flashlamp dye cell combination (F) is shown in photograph P25 (sweep speed 100 ns/division). This was obtained with 24 joules of electrical energy. Photograph P26 shows the type of pulses obtained for 40 joules of electrical output. The concentration of Rh 6G in methanol was  $1 \times 10^{-5}$  m/l. Visual observation of the spatial profile obtained by looking at the output impinging on a piece of cardboard showed a homogeneous profile (in agreement with theory of section 8.1). Output energy of these pulses was approximately 0.2 milli-joules as measured on an ITL laser calorimeter. The time scale on photograph P26 is 100 ns per division, thus we have  $\sim 2.5$  kW output.

The life of the flashlamps used in obtaining the preliminary results were fairly limited, as they cracked after around 20 shots. This was due to arcing within the flashlamp. Pulse charging to higher voltages or the use of "keep alive" could cure this problem.

#### 9.5 Discussion

The first cw dye laser action was achieved in mid 1970<sup>(63)</sup> using rhodamine 6G in a solution of water and Triton-X-100. Water has a very low temperature coefficient of refractive index and the Triton-X-100 was added as a deaggregating agent to prevent the formation of dimers in the water solution. This is necessary as the aggregates invariably absorb at the laser wavelength. The soap additive has the further advantage that it acts as an efficient triplet state quenching agent as well. The cw dye laser is<sup>(63)(131)</sup> usually pumped by cw argon ion beam focussed onto a small dye cell through which dye is flowing  $\sim 200$  cm s<sup>-1</sup>.

The construction of a stable narrow band dye laser using a nitrogen laser as a pump source<sup>(105)</sup> producing high pulse repetition rates together with the short pulse length and high intensity open numerous



promising applications in non-linear spectroscopy. Moreover, the fast risetime eliminates the problem of triplet state absorption and provides low thresholds. Numerous laser dyes, operating from the near ultra violet through the visible spectrum and into the near infra red, can be pumped efficiently with the nitrogen laser<sup>(105-112)</sup>.

Laser action in flashlamp pumped dye solutions was first reported by Sorokin and Lankard in 1967<sup>(26)</sup>.

The early investigations into the characteristics of organic dye lasers put great emphasis on the role of the triplet states in quenching the laser action. Sorokin and co-workers<sup>(56)</sup> presented a detailed analysis of these effects, concluding that rise times below  $\sim 1 \mu\text{s}$  are needed for the flashlamp pumping pulse, if lasing is to be achieved in xanthene type dyes. Accordingly they built a fast risetime ( $\sim 300 \text{ ns}$ ) flashlamp system. A typical feature encountered in their experiments was that the lasing action was terminated before the pumping pulse decreased back to the threshold value. Schmidt and Schafer<sup>(27)</sup> found this effect even more pronounced in their experiments. This phenomenon of early termination was initially attributed to accumulation of dye molecules in the long lived triplet states, causing quenching of the laser action by triplet state losses.

In later experiments, however,<sup>(49)</sup> it was found that under certain conditions the risetime requirements for the pump pulse can be substantially relaxed. Snavely and Schafer<sup>(49)</sup> used oxygen saturated solutions of rhodamine 6G in methanol and obtained long pulses ( $\sim 100 \mu\text{s}$ ) of laser light.

The phenomenon of early termination of the lasing action still appeared and was explained in this case by thermal lensing effects that

distort the optical cavity<sup>(49,55)</sup>. These effects have been shown<sup>(49,55)</sup> to take place after 20-30  $\mu$ s, explaining the experimental results (40-50  $\mu$ s pulse widths) quite well. More recently, however, Pappalardo et al<sup>(132)(51)</sup> investigated the effect of adding cyclo-octatetraene (COT) as a triplet quenching (TQ) agent to Rh6G solutions in ethanol. These investigators were able to obtain laser pulses that did not show the early termination effect, by using either high enough ( $3.5 \times 10^{-2}$  m/l) concentrations of COT or by filtering the UV radiation out of the spectrum at lower COT concentration. Their results in obtaining long laser pulses (up to 650  $\mu$ s) point toward the absence of thermal effects suggested by Snavely<sup>(55)</sup>. Long pulse dye laser emission was also reported by Marling et al<sup>(48)(50)</sup> in dyes other than Rh6G, again by adding TQ agents to the laser solution. An important consideration in improving the efficiency of flashlamp pumped dye lasers is the elimination of the early termination effect mentioned earlier. In the cases where this difficulty has been overcome<sup>(132)</sup>, the pumping pulses were relatively long with rather slow risetimes - typically a few hundreds of joules were discharged in hundreds of microseconds. Huth et al<sup>(57)</sup> pointed out that very large pump rates were required for efficient operation due to the high saturation intensity for dye lasers. With high power, high energy laser pulses another early termination manifested itself<sup>(62,129,130)</sup>. Propagation of ultrasonic waves initiated by the flashlamp discharge limited the pulse duration to the time required for the shock wave to reach the axis of the dye cell. (Shock velocity was measured to be  $\sim 1600$  ms<sup>-1</sup>),<sup>(62)(130)</sup> Blit et al<sup>(130)</sup> suggested infra-red absorption by the dye as being responsible for shock wave formation and showed that one could once again obtain long pulses, even for high powers, if one filtered out the infra-red component from the flashtubes.

Energies of 12 J,<sup>(124)</sup> 32 J<sup>(133)</sup> and 110 J<sup>(128)</sup> have been reported for flashlamp pumped dye lasers, and enhanced output powers can be obtained by using a prepulse delivered to the flashlamp before the main pulse arrives.

On the shorter time scale, mode locking of a dye laser may be achieved by pumping with a mode locked system<sup>(134)</sup> (gain modulation), or by using a saturable absorber in the conventional way<sup>(135)(136)</sup>.

The organic dye solution laser is at the present time the most versatile continuously tunable source of coherent light. The most practical methods of tuning dye lasers are (1) changing the dye and (2) introducing a frequency selective element into the cavity.

The dye laser has numerous potential applications as a tunable coherent light source in physics, chemistry, photo-biology and in communications and display systems.

One of the pulsed lasers was used to pump a gas cell. When air at a pressure of 25 Torr was used within the cell, the output from the system was entirely in the ultra violet region between 4000 and 4300 Å, without showing any pronounced super fluorescence at 3371 Å. However, when industrial grade nitrogen was used in a flow system, we successfully generated superfluorescent emission at 3371 Å. The duration of the optical output of this cell was approximately 10 ns.

## CONCLUSIONS

In this thesis, the criteria for efficient optical excitation of a liquid was considered. The properties of strip line pulsers were considered in detail and a series of original pulse generators were developed and evaluated. These strip line pulse generators were used to excite specially designed coaxial and linear flashlamps.

A continuous and a pulsed preionising device was developed and shown to have significant effect on the output characteristics of a flashlamp particularly when low overvolting of the flashlamp was used. The continuous preionisation reduced the risetime and increased the light output from a flashlamp. The pulsed preionisation was found to increase the working pressure of the flashlamp and to reduce the "jitter" in the arrival of the light pulse. The use of a preionising device was first reported by us in a conference in Berlin in 1973. Schafer has adopted preionisation for his flashlamps since that time. More recently Ornstein and Derr have used a prepulse which enabled them to get more laser power using a main driving voltage of 11 kV than they obtained using 15 kV without a prepulse. The ultra violet (3000-4000 Å) light output from linear and coaxial flashlamps was studied and with our flashlamp-pulsers combination it was possible to obtain short duration pulses with risetimes less than 15 ns. This was reported at the 11th International Congress on High Speed Photography (1975).

One of the pulsers was used to pump a gas cell. When air at a pressure of 25 torr was used within the cell, the output from the system was entirely in the ultra violet region between 4000 and 2500 Å, without showing any pronounced super fluorescence at 3371 Å. However, when industrial grade nitrogen was used, in a flow system, we successfully generated superradiant emission at 3371 Å. The duration of the optical output at half its peak amplitude was 6 ns.

Preliminary experiments on exciting rhodamine 6G in methanol using a coaxial flashlamp dye cell combination were carried out. Laser pulses of energy 0.2 mJ were obtained. The total pulse width was less than 100 ns. This corresponds to an optical power in the yellow of 2 kW.

Further work on this project should be directed towards a more comprehensive study of exciting a variety of dyes including, especially, dyes with absorption bands in the ultra violet. Work has already begun on pumping an iodine vapour using a coaxial flashlamp with pulsed preionisation, and on a repetitively pulsed nitrogen laser using a modified Blumlein pulser. The pumping of gases (eg oxygen) using electron beams or gas discharges is becoming popular (particularly in the US) owing to their promise in the fields of nuclear fusion and isotope separation.



## APPENDIX I

### THE BEER-LAMBERT ABSORPTION LAW (137)

The absorption of a mono-chromatic beam of light by a homogeneous absorbing system is described by the combined Beer-Lambert Law. One form of the law is:

$$\frac{I}{I_0} = 10^{-\epsilon CL}$$

where  $I_0$  = the light energy (or number of quanta) of strictly mono-chromatic light incident per unit of time at the front of a column of a single absorbing species of concentration  $C$  moles/litre.

$I$  = the energy per unit time transmitted through the column of material  $L$  cm in length and

$\epsilon$  = (litre/mole-cm) is the molar extinction coefficient and is a constant for a given pure absorbing species at a given wavelength and is a measure of the probability that the quantum - molecule interaction will lead to absorption of the quantum.

NOTE:  $\epsilon$  is also called the molar absorptivity, the molar absorbancy index, and the absorption coefficient. The use of the base of natural logarithms is often made in formulating the absorption law.

$$\frac{I}{I_0} = e^{-\alpha CL}$$

where  $\alpha = 2.303\epsilon$  = the absorption coefficient. However, the form of the law used in dye laser literature (Snively<sup>(55)</sup>) is

$$I = I_0 e^{-\epsilon NL}$$

where  $N$  is the concentration expressed as  $N$  molecules  $\text{cm}^{-3}$  and  $\epsilon$  is the molecular decadic extinction coefficient and has dimensions of  $\text{cm}^2$ , and is also known as the absorption cross section for a single dye molecule.

## APPENDIX II

### OXYGEN QUENCHING OF TRIPLET STATES

The population of the triplet state,  $N_T$ , can decay back to the ground state through a variety of processes in fluid solution. Three important processes are represented by the terms on the right hand side of (1)

$$-\frac{dN_T}{dt} = \left[ K_p + K_{O_2} [O_2] + K_{TT} N_T \right] N_T \quad \dots (1)$$

where  $N_T$  is the concentration of triplets,  $[O_2]$  is the concentration of oxygen and  $K_p$  is the rate arising from phosphorescent decay,  $K_{O_2} [O_2]$  is the deactivation rate from collisions between dye molecules in the triplet state and oxygen molecules.  $K_{TT} N_T$  is the rate dependent on collisions between two excited molecules in the triplet state.

The radiative transition from the excited triplet state to the singlet ground state is forbidden, and therefore  $K_p$  is relatively small ( $K_p \sim 200 \text{ s}^{-1}$ ). Quenching reactions are known to be diffusion controlled, and the rate of reaction is determined by the frequency of collisions. This frequency is, in general, inversely proportional to the solvent viscosity<sup>(66)</sup>. Typical values of  $K_{O_2}$  and  $[O_2]$  are  $10^9 \text{ l/(m-s)}$  and  $10^{-3} \text{ m/l}$  respectively. Thus the non-radiative quenching rate is approximately four orders of magnitude larger than radiative decay. Triplet-triplet quenching will depend on the number of triplets generated, but for typical cases this quenching rate will be several orders of magnitude smaller than the rate for oxygen quenching.

To calculate the concentration of dissolved oxygen, one needs the solubilities that can be defined in terms of the Ostwald coefficient.

The Ostwald coefficient,  $\ell$ , is defined as the ratio of the volume of gas,  $V_g$ , absorbed at any partial pressure and temperature by the volume of liquid,  $V_l$  ie

$$\ell = \frac{V_g}{V_l} \quad \dots (2)$$

The number of moles of gas absorbed is

$$n = \frac{P_g V_g}{RT} \quad \dots (3)$$

where  $P_g$  is the partial pressure of the gas,  $R = 0.0821 \text{ l-atm/m-k}$  is the universal gas constant, and  $T$  is the absolute temperature. Using (2) and (3) the molarity of dissolved gas is

$$\frac{n}{V_l} = \frac{P_g \ell}{RT} \quad \text{or using } P_g = 0.21 \text{ atm}$$

$$\frac{n}{V_l} = (8.5 \times 10^{-3}) \ell \text{ m/l}$$

### APPENDIX III

#### PROPERTIES OF THE STRIP LINE

The strip line is a true transmission line having distributed parameters along which the discharge wave front travels at the velocity of light in the dielectric which separates the strip, ie  $C_0/n$ .

Strip lines may take several forms the simplest of which is shown in Figure A1. The properties of striplines do not differ significantly from transmission lines with circular cross section.

In carrying out the analysis of a transmission line it is assumed that each element of length  $\Delta x$  may be treated as if equivalent to the circuit shown in Figure A2 with fixed values of R, L, C and G in the limit as  $\Delta x$  is made to approach zero. As usual

R = resistance per unit length

L = inductance per unit length

C = capacitance per unit length

G = transverse conductance per unit length

For the strip line used in the present work  $R_1$  and  $L_1$  can be assumed to be equal respectively to  $R_2$  and  $L_2$ .

Since  $\Delta x$  is small, the currents and the potential difference at the point  $x = \Delta x$  may be expressed in terms of the currents and potential differences at the point  $x$  by means of Maclaurins expansion

$$I_{x+\Delta x} = I_x + \left(\frac{dI}{dx}\right)_x \Delta x + \left(\frac{d^2 I}{dx^2}\right)_x \frac{(\Delta x)^2}{2} + \dots \quad \dots (1)$$

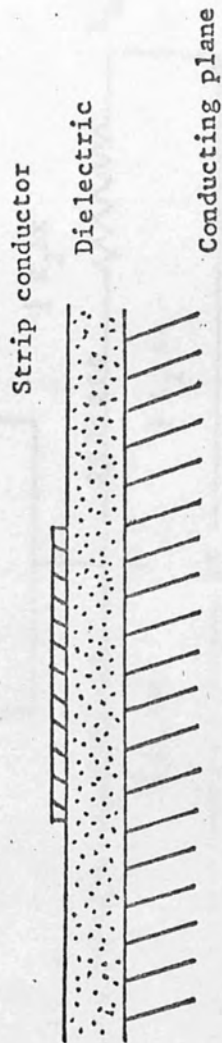
$$V_{x+\Delta x} = V_x + \left(\frac{dV}{dx}\right)_x \Delta x + \left(\frac{d^2 V}{dx^2}\right)_x \frac{(\Delta x)^2}{2} + \dots \quad \dots (2)$$



Dielectric

Strip conductor

(a)



Strip conductor

Dielectric

Conducting plane

(b)

FIGURE A.1: VARIOUS FORMS OF STRIPLINE



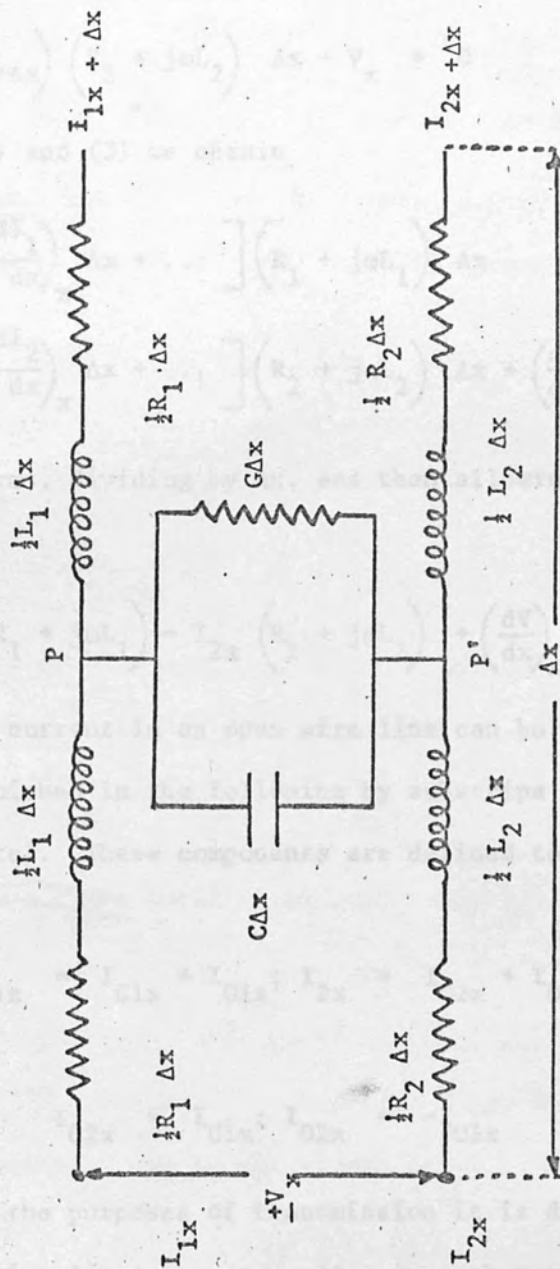


FIGURE A.2: EQUIVALENT CIRCUIT FOR A TRANSMISSION LINE

Applying Kirchoff's emf law around the rectangle formed by the input and output terminals of the section, we obtain

$$\frac{1}{2} \left( I_{1x} + I_{1x+\Delta x} \right) \left( R_1 + j\omega L_1 \right) \Delta x + V_{x+\Delta x} - \frac{1}{2} \left( I_{2x} + I_{2x+\Delta x} \right) \left( R_2 + j\omega L_2 \right) \Delta x - V_x = 0 \quad \dots (3)$$

Using (1), (2) and (3) we obtain

$$\frac{1}{2} \left[ 2I_{1x} + \left( \frac{dI_1}{dx} \right)_x \Delta x + \dots \right] \left( R_1 + j\omega L_1 \right) \Delta x - \frac{1}{2} \left[ 2I_{2x} + \left( \frac{dI_2}{dx} \right)_x \Delta x + \dots \right] \left( R_2 + j\omega L_2 \right) \Delta x + \left( \frac{dV}{dx} \right)_x \Delta x + \dots = 0 \quad \dots (4a)$$

Collecting terms, dividing by  $\Delta x$ , and then allowing  $\Delta x$  to approach zero and we obtain

$$I_{1x} \left( R_1 + j\omega L_1 \right) - I_{2x} \left( R_2 + j\omega L_2 \right) + \left( \frac{dV}{dx} \right)_x = 0 \quad \dots (4b)$$

The current in an open wire line can be resolved into two components, to be distinguished in the following by subscripts C (for co-directional) and O (for opposite). These components are defined to satisfy the following relations

$$I_{1x} = I_{C1x} + I_{O1x}; \quad I_{2x} = I_{C2x} + I_{O2x} \quad \dots (5a)$$

$$I_{C2x} = I_{C1x}; \quad I_{O2x} = -I_{O1x} \quad \dots (5b)$$

For the purposes of transmission it is desirable to drive and arrange open-wire lines symmetrically in such a manner that

$$I_{Cx} = 0; \quad I_{O2x} = I_{O1x} = -I_x \quad \dots (6)$$

Open wires that satisfy (6) are balanced.

For practical purposes (6) is always satisfied for the currents on the inner conductor and on the inner surface of the outer conductor of a coaxial line. Antenna currents, if they exist on a coaxial line, are on the outer surface of the outer conductor.

Putting

$$R \equiv R_1 + R_2, L \equiv L_1 + L_2 \text{ and } Z = R + j\omega L \quad \dots (7)$$

where R, L and Z are the total resistance, inductance and impedance per loop unit length. Using (6) and (7), (4b) becomes

$$ZI_x = - \left( \frac{dV}{dx} \right)_x \quad \dots (8)$$

The voltage across PP' is  $\frac{1}{2} (V_x + V_{x+\Delta x})$ . Thus using Kirchoffs current law

$$I_{1x} = I_{1x+\Delta x} + \frac{1}{2} (V_x + V_{x+\Delta x}) (G + j\omega C) \Delta x \quad \dots (9)$$

Using (1), (2) and (9) and dividing by  $\Delta x$  before allowing this to approach zero, we obtain

$$y V_x = - \left( \frac{dI}{dx} \right)_x \quad \dots (10)$$

where y stands for the total shunt admittance per unit length

$$y \equiv G + j\omega C \quad \dots (11)$$

The first-order differential equations (8) and (10) are the transmission line equations. The variables can be separated, and the equations replaced by two of the second order.

$$- Z \left( \frac{dI}{dx} \right)_x = \left( \frac{d^2 V}{dx^2} \right)_x = yZ V_x \quad \dots (12)$$

$$- y \left( \frac{dV}{dx} \right)_x = \left( \frac{d^2 I}{dx^2} \right)_x = yZ I_x \quad \dots (13)$$

It is convenient to define a quantity  $\gamma$ , known as the complex propagation constant as follows

$$\gamma^2 \equiv yZ = (G + j\omega C)(R + j\omega L) \quad \dots (14)$$

The real and imaginary parts of  $\gamma$  are  $\alpha$  and  $\beta$ . Thus

$$\gamma = \alpha + j\beta$$

$\alpha$  = attenuation constant (per unit length)

$\beta$  = phase constant (nepers per unit length)

The general solution of (12) is

$$V = A \exp(-\gamma x) + B \exp(\gamma x) \quad \dots (15a)$$

or

$$V = a \cosh \gamma x + b \sinh \gamma x \quad \dots (15b)$$

Rewriting (13)

$$I = -\frac{1}{(R + j\omega L)} \frac{dV}{dx}$$

and substituting into (15a) we obtain

$$I = \frac{\gamma}{(R + j\omega L)} \left[ A \exp(-\gamma x) - B \exp(\gamma x) \right]$$

$$= \sqrt{\frac{(G + j\omega C)}{(R + j\omega L)}} \left\{ A \exp(-\gamma x) - B \exp(\gamma x) \right\} \quad \dots (16)$$

where we have used (14).

The factor

$$\sqrt{\left(\frac{R + j\omega L}{G + j\omega C}\right)}$$

has dimensions of impedance and is called the characteristic impedance of the line. It is denoted by  $Z_0$ . Thus

$$Z_0 = \sqrt{\left(\frac{R + j\omega L}{G + j\omega C}\right)} \quad \dots (17)$$

At frequencies greater than about  $10^7 \text{ s}^{-1}$   $\omega L \gg R$  and  $\omega C \gg G$ .

Hence

$$Z_0 \approx \sqrt{\frac{L}{C}} \quad \dots (18)$$

which is a real quantity independent of frequency.

From equation (14) we can write the propagation constant thus

$$\gamma = \alpha + j\beta = \sqrt{\{(R + j\omega L)(G + j\omega C)\}}$$

$$\text{Now} \quad (\alpha^2 - \beta^2) = RG - \omega^2 LC \quad \dots (19)$$

$$2\alpha\beta = \omega(LG + CR) \quad \dots (20)$$

Squaring and adding yields

$$(\alpha^2 + \beta^2)^2 = (RG - \omega^2 LC)^2 + \omega^2 (LG + CR)^2 \quad \dots (21)$$

Hence from (19) and (21)

$$\alpha^2 = \frac{1}{2} \left\{ \sqrt{[R^2 + \omega^2 L^2]} (G^2 + \omega^2 C^2) + (RG - \omega^2 LC) \right\} \quad \dots (22a)$$

$$\beta^2 = \frac{1}{2} \left\{ \sqrt{[R^2 + \omega^2 L^2]} (G^2 + \omega^2 C^2) - (RG - \omega^2 LC) \right\} \quad \dots (22b)$$

$\alpha$  is zero if  $R = G = 0$

at high frequency  $\beta \approx \omega \sqrt{LC}$



Hence the phase velocity is

$$v_p = \frac{1}{\sqrt{LC}} = \frac{C_0}{\sqrt{\epsilon_r}}$$

where  $C_0$  is the velocity of electromagnetic waves in vacuo, and  $\epsilon_r$  is the relative permittivity of the dielectric.

For a line having  $LG = RC$ , then from (22a) and (22b)

$$\alpha = \sqrt{RG} \quad \dots (23a)$$

$$\beta = \omega \sqrt{LC} \quad \dots (23b)$$

and the velocity of propagation is

$$v = \frac{1}{\sqrt{LC}} \quad \dots (23c)$$

ie the attenuation and the velocity of propagation are independent of frequency, and the line is distortionless.

#### REFLECTION COEFFICIENT AND STANDING WAVES

From (12) we can put

$$\frac{d^2V}{dx^2} = (R + j\omega L)(G + j\omega C)V = \gamma^2 V \quad \dots (24)$$

A general solution of which is

$$V = A \exp(-\gamma x) + B \exp(\gamma x)$$

From (15) and (16) we have

$$I = \frac{1}{Z_0} \left[ A \exp(-\gamma x) - B \exp(\gamma x) \right] \quad \dots (25)$$

From (24) and (25) we can obtain an expression from the impedance  $Z_x$ , at any point, defined as

$$Z_x = \frac{V}{I} = Z_o \left[ \frac{A \exp(-\gamma x) + B \exp(\gamma x)}{A \exp(-\gamma x) - B \exp(\gamma x)} \right]$$

Hence if we consider a line of length  $l$  terminated with an impedance  $Z_T$  where

$$Z_T = |Z_T| \exp(\gamma \sigma_T) \quad \text{then}$$

$$\frac{Z_T}{Z_o} = \frac{A \exp(-\gamma l) + B \exp(\gamma l)}{A \exp(-\gamma l) - B \exp(\gamma l)} \quad \text{or}$$

$$\frac{Z_T - Z_o}{Z_T + Z_o} = \frac{B \exp(\gamma l)}{A \exp(-\gamma l)} \quad \dots (26)$$

Since  $B \exp(\gamma l)$  represents the reflected wave at the termination and  $A \exp(-\gamma l)$  represents the forward wave, then the ratio of these two quantities is called the (voltage) reflection coefficient at the termination. Let this be denoted  $k_T$ , then

$$k_T = \frac{B \exp(\gamma l)}{A \exp(-\gamma l)}$$

which may be written

$$k_T = K_T \exp(\gamma \phi_T) \quad \dots (27)$$

From (26) we see that

$$k_T = \frac{Z_T - Z_o}{Z_T + Z_o} \quad \dots (28)$$

In (27)  $K_T$  is the ratio of the amplitudes of the reflected and forward waves at the point of reflection, and  $\phi_T$  is the phase change which occurs on reflection.

There are three cases of special interest:

(a) if  $Z_T = Z_o$ , then  $k_T = 0$ . There is no reflected wave and all the power is absorbed in the pure resistance  $Z_T$ . The line is said to be matched or properly terminated.

(b) if  $Z_T = 0$ , corresponding to a short circuit, then  $k_T = -1$  and the reflected voltage wave is of the same amplitude as the incident one but of opposite sign.

(c) if  $Z_T \rightarrow \infty$ , as in the case where the line is open circuited,  $k_T = 1$  and reflection of the voltage wave occurs without change in phase.

Since the phase of the backward component of current is reversed relative to that of the corresponding voltage component, the current reflection coefficient is written

$$-\frac{Z_T - Z_o}{Z_T + Z_o}$$

Consequently, the current reflection coefficient is +1 for a short circuit and -1 for an open circuited line.

APPENDIX IV

STEFAN - BOLTZMANN LAW

The rate of emission of energy per unit area of a surface is its emissive power, E. From some of the early measurements on emissive powers, Stefan pointed out that these powers, and hence the intensity of radiation emitted by a given body at different temperatures, appeared to be proportional to the fourth power of the absolute temperature of the emitter. Subsequently Boltzmann showed by thermodynamic reasoning that this result should be accurately true for a black body, for which therefore

$$E = \sigma T^4$$

where  $\sigma$  is a constant, referred to as Stefan's constant and

$$\sigma = 5.70 \times 10^{-5} \text{ erg cm}^{-2} \text{ s}^{-1} \text{ deg}^{-4}.$$

APPENDIX V  
SPECTROSCOPIC NOTATION <sup>(149)</sup>

An electronic state is characterised by the component of the orbital angular momentum of the electrons in the direction of the molecular axis in terms of the quantum number  $\Lambda$ , total electron spin  $S$ , and symmetry properties of the state.

States with  $\Lambda = 0, 1, 2, 3 \dots$  are denoted by the Greek letters  $\Sigma, \pi, \Delta, \dots$ . The component of the spin in the direction of the molecular axis can assume  $2S + 1$  values, with a corresponding splitting of each term or energy level. The multiplicity  $2S + 1$  of the term is shown by a super script at the left eg

$${}^3\Sigma, {}^2\pi \text{ (} S = 1, S = \frac{1}{2} \text{ resp.)}$$

Upon reflection in a plane in which the molecular axis lies, the axial component of the orbital angular momentum of the electron changes sign (because it is a pseudo - or polar vector); corresponding to this fact, the terms with non zero orbital angular momentum are doubly degenerate. More precisely, these terms are split into two as a result of the interaction between the rotation of the molecule and the motion of the electrons. This phenomenon is called  $\Lambda$  -type doubling ("lambda" - type doubling). If, however,  $\Lambda = 0$ , the reflection does not change the electron energy at all; the wave function is multiplied by either +1 or -1. This symmetry of the  $\Sigma$  terms is shown by a super script at the right:  $\Sigma^+, \Sigma^-$ .

If the molecule consists of identical atoms, then still another symmetry property appears, namely, the energy is invariant with respect to a simultaneous change in sign of the coordinates of all electrons and nuclei. The wave function is in this case multiplied by either +1 or -1, which is denoted by the subscripts  $g$  and  $u$  on the right, for example,  $\Sigma_g, \Sigma_u$ . As a rule, the ground state of diatomic molecules is completely



symmetrical and the ground term is  $^1 \Sigma_g^+$ . Exceptions are the  $O_2$  molecule, whose ground term is  $^3 \Sigma_g^-$ , and the NO molecule, whose ground term is  $^2 \pi$ .

Allowed transitions between different electronic states (dipole transitions with emission or absorption of light) are subject to certain selection rules. These rules depend on the type of coupling between the orbital motion of the electrons, their spin, and the rotation of the molecule. The following are the selection rules for the many important cases:  $\Delta \Lambda = 0, \pm 1$ ; the multiplicity  $2S + 1$  remains unchanged; transitions  $\Sigma^+ \leftrightarrow \Sigma^-$  and transition  $g \rightarrow g$  or  $u \rightarrow u$  are forbidden (the two last rules are independent of the type of coupling).

## REFERENCES

1. J P Gorden, H J Zeiger and C H Townes. Phys Rev 99, 1264-1274 (1955).
2. A L Schawlow and C H Townes, Phys Rev 112, 1940-1949 (1958).
3. T H Maiman, Brit Commun and Electr 7, 674-5 (1960).
4. T H Maiman, Nature, 187, 493-4 (1960).
5. A Javan, W R<sup>o</sup> Bennett Jr, D R Herriot, Phys Rev Lett 6, 106-110 (1961).
6. N G Basov, O N Krokhin, Zh ek sper teor Fiz (USSR) 39, 1770-80 (1960). In Russian.
7. P P Sorokin and M J Stevenson, Phys Rev Lett 5, 557-9 (1960).
8. P P Sorokin and M J Stevenson, Advances in Quantum Electronics. Ed: J R Singer, Columbia Univ Press, New York (P65-76) (1961).
9. P P Sorokin and M J Stevenson, IBM, J Res Dev 5, 56-58 (1961).
10. R N Hall et al, Phys Rev Lett 9, 366-68 (1962).
11. M J Nathen et al, App Phys Lett 1, 62-4 (1962).
12. T M Quist et al, App Phys Lett 1, 91-92, (1962).
13. N E Wolff and R J Pressley, App Phys Lett 2, 152-4 (1963).
14. A Lempicki and H Samelson, Phys Lett 4, 133-5 (1963).
15. A Lempicki and A Heller, Appl Phys Lett 9, 108 (1966).
16. E J Schimitschek, J Appl Phys 39, 6120 (1968).
17. E G Brock et al, J Chem Phys, 35, 759-60 (1960).
18. S G Rautian and I I Sobel'mann, Opt Spectry 10, 65-6 (1961).
19. D L Stockman, W R Mallory and K F Tittel, Proc IEEE 52, 318-9 (1964).
20. D L Stockman "Proceedings of the 1964 ONR Conf on Organic Lasers" (1964).
21. P P Sorokin and J R Lankard, IBM Journal of Res and Dev 10, 162-3 (1966).
22. P P Sorokin et al, IBM J Res Dev 10, 401.
23. E F Schafer, W Schmidt and J Volze, App Phys Lett 9, 306-9 (1966).

24. M L Spaeth and D P Bortfield, App Phys Lett 9, 179-81 (1966).
25. P P Sorokin et al, IBM J Res Dev 11, 130-48 (1967)
26. P P Sorokin et al, IBM J Res Dev 11, 148 (1967).
27. W Schmidt and F P Schafer, Z Naturforsch, 22a, 1563-66 (1967).
28. For example: Electrophotonics.
29. M Bass, T F Deutch and M J Weber, "Lasers" 3, 269 (Morcel Dekber) (1971).
30. C H Hutchinson and B W Magnum, J Chem Phys 32, 1261 (1960).
31. P K Callagher, J Chem Phys 43, 1742 (1965).
32. A Heller, J Am Chem Soc 88, 2058 (1966).
33. A Heller, Physics Today 20, 34 (1967).
34. D Andreou, Ph D Thesis (1973) (Univ London).
35. F P Schafer, "Liquid Lasers". Laser handbook edited by F T Arecci and E O Schulz-Du Bois, North Holland, Pub Co pp 369-423 (1972).
36. H Winston and R A Gudmundsen, Appl Opt 3, 143, (1964).
37. G H C New, Alta Frequenza No. 10. Vol XL1 pp 706-710 (1972).
38. B H Soffer and B B McFarland, App Phys Lett 10, 226 (1967).
39. H Kuhn, Progress in the Chemistry of Organic Natural Products (D Zechmeister ed; Springer-Verlag; Wien) Vol XVI and XVII.
40. H Kuhn, Chimia 9, 237 (1955).
41. N J Turro, Molecular Photochemistry, W A Bengamin Inc p24 (1965).
42. S J Strickler and R A Berg, J Chem Phys 37, 304 (1962).
43. C A Parker "Photoluminescence of Solutions" Elsevier Amsterdam (1968).
44. D J Morantz, B G White and A J C Wright, Phys Rev Lett 8, 23 (1962).
45. D J Morantz, Proceedings of the Symposium on Optical Lasers. (Polytechnic Press; Brooklyn) (1963).
46. F P Schafer, W Schmidt, J Volze and K Marth, Ber Bunsenges Physik Chemie 72, 328 (1968).

47. W Schmidt and F P Schafer, Z Naturforsch 22a, 1563, (1967).
48. J B Marling, D W Gregg and L Wood, App Phys Lett 17, 527 (1970).
49. B B Snavely, F P Schafer, Phys Lett 28A, 728 (1969).
50. J B Marling, D W Gregg, S J Thomas, IEEE J Quant Electron QE6, 570 (1970).
51. R Pappalardo, H Samelson, A Lampicki, App Phys Lett 16, 267 (1970).
52. M Bass, T F Deutch, M J Weber, App Phys Lett 13, 120 (1968).
53. M J Weber, M Bass, IEEE J Quant Electron. QE5, 175 (1969).
54. B B Snavely, O G Peterson. IEEE J Quant Electron. QE4, 540 (1968).
55. B B Snavely, Proc IEEE 57, 1374 (1969).
56. P P Sorokin, J R Lankard, V L Moruzzi, E C Hammond, J Chem Phys 48, 4726 (1968).
57. B G Huth, M R Kagan, IBM J Res and Dev 278 (1971).
58. O De Witte, R Signore, J Gauss, Revue Technique, Thompson - CSF 4, 284 (1972).
59. P Flamant, Y H Meyer, Optics Commun 7, 146 (1973).
60. G Burns, A H El Chicking "Laser rate equations (4-level rate equations at high temperatures)" IBM Research Note. Available on request from the Library at IBM. T J Watson Research Centre, Yorktown Heights, New York.
61. R A Keller, IEEE J Quant Electron. QE6, 411 (1970).
62. A Hirth, K Vollrath, J P Fouasser, Opt Commun 9, 139 (1973).
63. O G Peterson, S A Tuccio, B B Snavely, App Phys Lett 17, 245 (1970).
64. R Torg, W B Tiffany, App Phys Lett 15, 302 (1969).
65. W Koechner, Laser focus 6, 37 (1970)
66. Progress in Reaction Kinetics Ed: G Porter, Vol 4, 251 (1967) Pergamon Press.
67. W Kohrmann, Zeitschrift fur Naturforschung 19a, 926 (1964).
68. J S Townsend, Electricity in Gases, Oxford (1915).
69. J J Thompson, Conduction of Electricity through Gases. Vol 2 Cambridge 3rd Ed. 1933.

70. L B Loeb, Proc Phys Sco 60, 561 (1948).
71. W Rogowshi, Archiv fur Electrotechnik 20, 99 (1918), and summarised in Electrical Breakdown in Gases. J A Rees, MacMillian (1973).
72. H Raether, Archiv fur Electrotechnik 34, 49 (1970).
73. J M Meek, Phys Rev 57, 722 (1940).
74. J H Goncz, J App Phys 36, 342 (1965).
75. J P Markiewicz, J L Emmett. IEEE J Quant Electron. QE2, 707 (1966).
76. J F Holzrichter, M S and A L Schawlow, Annals New York Academy of Sciences P703 (1969)
77. F Aussenegg, J Schubert, Phys Lett 30A, 488 (1969).
78. M E Mack, App Phys Lett 19, 108 (1971).
79. S Claesson, L Lindquist, Arkiv Kemi 12, 1 (1958).
80. P P Sorokin, J R Lankard, IBM J Res Dev, 11, 130 (1967).
81. H W Furumoto, H L Ceccon, App Optics 8, 1613 (1969).
82. J D Shipman Jr, App Phys Lett 10, 3 (1967).
83. J G Small, R Ashori, Rev Sci Inst 43, 1205 (1972).
84. Andersson, E B Hans, Physica Scripta 4, 215 (1971).
85. Yu A Yanait, G A Abakumov, C I Kromskii, A J Simonov, V V Fadeer, R V Khokhior, JETP Lett 13, 438 (1971).
86. A D Blumlein, UK patent spec 589, 217 (1947).
87. See Appendix III
88. K J R Wilkinson, J Inst Elec Engineers (London) 93, Part 111A, 1090 (1946).
89. M Geller, D E Altman, T A De Temple, App Oct 7, 2232 (1968).
90. J C Martin, Internal Note at AWRE.
91. S Majumdar - Private Communication.
92. A D MacDonald, Microwave Breakdown in Gases, J Wiley & Sons (1966).
93. M H Ornstein, V E Derr, App Opt 13, 2100 (1974).
94. H Raether, Electron Avalanches and Breakdown in Gases, Butterworths (1964).



95. H Heard, Nature 200, 667 (1963).
96. D A Leonard, Appl Phys Lett 7, 4 (1965).
97. E T Gerry, Appl Phys Lett 10, 3 (1965).
98. D Basting, F P Schafer, D Steyer, Opto Electronics 4, 43 (1972).
99. N R Nillson, O Steinwall, C K Subramanian, L Hoberg, Physica Scripta 1, 153 (1970).
100. V F Tarasenko, Yu I Bychkov, Inst & Exp Tech 16, 221 (1973).
101. V F Tarasenko, Yu A Kurbatou, Yu I Bychkov, Sov J Quant Electron 2, 155 (1972).
102. H E B Anderssen, S A Borgstrom, Opto Electron 6, 225 (1974).
103. J P Girardeau-Montant, M Roumy, J Hamelin, L Avan, C R Acad Sci B 273, 725 (1971).
104. P Goujon, M Clerc, Journal De Chimie Physique 71, 206 (1974).
105. T W Hansch, App Opt 11, 895 (1972).
106. J A Meyer, C L Johnson, E Kierstead, R D Sharma, I Itzkan Appl Phys Lett 16, 3 (1970).
107. G Capelle, D Phillips, App Opt 9, 2742 (1970).
108. H P Broida, S C Haydon, App Phys Lett 16, 143 (1970).
109. G Capelle, D Phillips, App Opt, 9, 517 (1970).
110. J R Lankard, R J Von Gutfield, IEEE J Quant Electron QE-5, 625 (1969).
111. C E Moeller, C M Verber, A H Adelman, App Phys Lett 18, 278 (1971).
112. C Lin, IEEE J Quant Electron, QE-11, 61, (1975).
113. C V Shank, A Diens, A M Trozzolo, J A Meyer, App Phys Lett 16, 405, (1970).
114. A Diens, C V Shank, A M Trozzolo, App Phys Lett 17, 189, (1970).
115. R J Von Gutfield, B Welber, E E Tynan, IEEE J Quant Electron QE5, 532 (1970).
116. M Jeunehomme, J Chem Phys 51, 1692 (1969).  
M Jeunehomme, J Chem Phys 44, 2672 (1966).

117. A W Ali, A C Kolb, A D Anderson, App Opt 6, 2115 (1967).
118. B Godard, IEEE J Quant Electron QE10, 147 (1974).
119. A W Ali, App Opt 8, 893 (1969).
120. S C Brown "Basic Data of Plasma Physics" J Wiley & Sons (1959).
121. D C Cartwright, Phys Rev A 2, 1331 (1970).
122. J Bunkenburg, Rev Sci Inst 43, 1611 (1972).
123. S Blit, U Ganiel, Opt and Quant Electron 7, 87 (1975).
124. P Anliker, M Gassman, H Weber, Opt Commun 5, 137 (1972).
125. J L Emmett, A L Shawlow, E H Weinberg, J App Phys 35, 2601 (1964).
126. C M Ferrar, Rev Sci Inst 40, 1436 (1969).
127. M Born, E Wolf, "Principles of Optics" Pergamon Press (1965).
128. F N Baltakov, B A Barikhin, V G Kornilov, S A Miknov, A R Rubinov, L V Sukhanov, Sov Phys-Tech Phys 17, 1161 (1973).
129. T F Ewanizky, R H Wright Jr, H H Theissing, App Phys Lett, 22 520 (1973).
130. S Blit, A Fisher, U Ganiel, App Optics 13, 335 (1974).
131. C V Shank, J Edighoffer, A Dienes, E P Ippen, Opt Commun 7, 176, (1973).
132. R Pappalardo, H Samelson, A Lampicki, IEEE J Quant Electron QE6, 716 (1970).
133. V A Alekseev, I V Antonov, Sov J Quant Electron 1, 643 (1972).
134. D J Bradley, A J F Durrant, Phys Lett 27A, 73 (1968).
135. W Schmidt, F P Schafer, Phys Lett 26A, 558 (1968).
136. D J Bradley, A J F Durrant, F O'Neil, B Sutherland, Phys Lett 30A, 535 (1969).
137. Calvert, Pitts "Photochemistry" J Wiley & Sons (1966).
138. H J Baker, T A King, J Phys E 8, 219 (1975).
139. C R Ferrar, Rev Sci Inst 40, 1436 (1969).
140. J L Emmett, A L Schawlow, E H Weinberg, J App Phys 35, 2601 (1964).
141. R Goldstein, F N Mastrup, IEEE J Quant Electron QE3, 521 (1967).

142. See Appendix IV.
143. S Tolansky, "Introduction to Atomic Physics Longmans p214 (1963).
144. F A Jenkins, H E White "Fundamentals of Optics" McGraw Hill p443 (1950).
145. L B Loeb "Fundamental processes of electrical discharge in Gases" John Wiley & Sons p144 (1939).
146. J H Crouch, W S Risk, Rev Sci Inst 43, 632 (1972).
147. R W Smith, P F Liao, C V Shank, C Lin, P J Maloney, Appl Phys Lett 25, 144-6 (1974).
148. G W Brown "Monte Carlo Methods" Chapter 12 in Modern Maths for the Engineer. Ed: E F Beckenbach, McGraw Hill (1965).
149. Ya B Zeldovich, Yu P Raizer "Physics of Shock Waves and High Temperature Hydrodynamic Phenomena" Ed: W D Hayes, R F Probstein. Academic Press (1966), p306.
150. J B Birks, Koch-Light Labs Ltd "Solutes and Solvents for Liquid Scintillation Counting (1972).
151. R W Smith, P F Liao, C V Shank, C Lin, P J Maloney, IEEE J Quant Electron QE11, 84-9 (1975).
152. M Green, R Mason, J Phys E 6, 62 (1973).
153. R Mason "Use of glass transfer tapes for optical sealing in laser cells" (To be published).
154. C Raptis (Private Communication).
155. S Majumdar (Private Communication).

#### ACKNOWLEDGEMENTS

I would like to acknowledge the guidance and able supervision of Dr S Majumdar and Dr V I Little during the course of this work and to thank them for their constant encouragement. I would also like to thank my colleagues and the technical staff at Royal Holloway College for the help they have given me.

I am grateful to the Science Research Council for a financial award enabling me to carry out this work and to Royal Holloway College for the opportunity to use their extensive facilities. My thanks also to Miss T Lascaris for deciphering my hand writing and typing the manuscript.

Finally my appreciation and thanks to my parents and to my wife without whose support and encouragement I would have not had an academic career.